LEONARDO MORO CARISTE

PAPEL DA INTEGRINA LFA-1 E DO RECEPTOR DE QUIMIOCINA CX3CR1 NA DIFERENCIAÇÃO E ATIVAÇÃO DE LINFÓCITOS T CD8+ DURANTE A INFECÇÃO EXPERIMENTAL PELO *TRYPANOSOMA CRUZI*.

Tese apresentada à Universidade Federal de São Paulo para obtenção do Título de Doutor no Programa de Pós-graduação de Bioprodutos e Bioprocessos.

SANTOS

2022

LEONARDO MORO CARISTE

PAPEL DA INTEGRINA LFA-1 E DO RECEPTOR DE QUIMIOCINA CX3CR1 NA DIFERENCIAÇÃO E ATIVAÇÃO DE LINFÓCITOS T CD8+ DURANTE A INFECÇÃO EXPERIMENTAL PELO *TRYPANOSOMA CRUZI*.

Tese apresentada à Universidade Federal de São Paulo para obtenção do Título de Doutor no Programa de Pós-graduação de Bioprodutos e Bioprocessos.

Orientador: Prof. Dr. José Ronnie Carvalho de Vasconcelos

SANTOS

2022

Ficha catalográfica elaborada por sistema automatizado
com os dados fornecidos pelo(a) autor(a)

Cariste, Leonardo Moro.
C277p PAPEL DA INTEGRINA LFA-1 E DO RECEPTOR DE QUIMIOCINA CX3CR1 NA DIFERENCIAÇÃO E ATIVAÇÃO DE LINFÓCITOS T CD8+ DURANTE A INFECÇÃO PELO TRYPANOSOMA CRUZI.. / Leonardo Moro Cariste; Orientador José Ronnie Carvalho de Vasconcelos; Coorientador . -- Santos, 2022.
184 p. ; 30cm

Tese (Doutorado - Pós-Graduação em Bioprodutos e Bioprocessos) -- Instituto Saúde e Sociedade, Universidade Federal de São Paulo, 2022.

1. Trypanosoma cruzi. 2. Integrinas. 3. Quimiocinas. 4. LFA-1. 5. CX3CR1. I. Vasconcelos, José Ronnie Carvalho de, Orient. II. Título.

CDD 660.6

LEONARDO MORO CARISTE

PAPEL DA INTEGRINA LFA-1 E DO RECEPTOR DE QUIMIOCINA CX3CR1 NA DIFERENCIAÇÃO E ATIVAÇÃO DE LINFÓCITOS T CD8+ DURANTE A INFECÇÃO EXPERIMENTAL PELO *TRYPANOSOMA CRUZI*.

PRESIDENTE DA BANCA

Prof. Dr. José Ronnie Carvalho de Vasconcelos

BANCA EXAMINADORA

Prof. Dr. Eduardo Lani Volpe da Silveira

Prof. Drª. Joseli Lannes Vieira

Prof. Dr. Marcos Leoni Gazzarini Dutra

Prof. Dr. Rafael Ribeiro Almeida

SUPLENTES DA BANCA EXAMINADORA

Drª. Barbara Ferri Moraschi

Prof. Drª. Flávia Andressa Mazzuco Pidone

UNIVERSIDADE FEDERAL DE SÃO PAULO
***CAMPUS* BAIXADA SANTISTA**
PÓS-GRADUAÇÃO BIOPRODUTOS E BIOPROCESSOS
DOUTORADO ACADÊMICO
DEPARTAMENTO DE BIOCIÊNCIAS

CHEFE DO DEPARTAMENTO
Prof. Dr. Daniel Araki Ribeiro

COORDENADOR DO CURSO DE PÓS-GRADUAÇÃO
Prof. Drª Ana Claudia Muniz Renno

“Sem o passo inicial, ninguém vence as distâncias.”

Joanna de Ângelis

DEDICATÓRIA

Ao Pedro Moro, *in memorian*

AGRADECIMENTOS

Inicialmente gostaria de agradecer a Deus e todos os mentores de luz, que me abençoaram, auxiliaram e ampararam para chegar até aqui.

Aos meus pais, Rolando Jr. e Patrícia, por estarem do meu lado durante todo o tempo, me incentivando, me apoiando, acreditando no meu potencial, por todo amor do mundo, sem vocês não seria possível, amo vocês e minha eterna gratidão.

A minha irmã, Lizandra sem você minha infância seria vazia e minhas histórias menos emocionantes, obrigado por toda ajuda, conselhos e desabafos.

Aos meus familiares Nelson, Rosana, Guilherme e Gabriel por sempre estarem presentes nessa caminhada.

A minha namorada Bianca, são anos com amor, carinho, risadas, ausência, companheirismo, muito trabalho e todas as vezes que eu caia, lá estava você com sua mão estendida para me levantar, obrigado por tornar esse caminho mais leve. Te amo.

Aos meus amigos de infância César e Caldeira.

Ao meu orientador Prof. José Ronnie, pela oportunidade de trabalhar em seus laboratórios desde a minha iniciação científica; por ter confiado a mim esse projeto, por todos os ensinamentos, discussões, publicações de artigos, idas à bancada e amizade. Você é uma inspiração!

A todos os meus colegas de laboratório. Liana, agradeço por toda paciência e auxílio para o desenvolvimento desta tese. Isaú, sua ajuda foi fundamental para a execução dos experimentos, além das risadas no laboratório. Letícia, por todas as suas

histórias hilárias, que transformaram a tensão da bancada em momentos de alegria. Flavinha, por todas as discussões de biologia molecular e incentivo. Camila, pelo ensino de diversas técnicas. Barbara, que é a “zica” dos experimentos.

Aos colegas dos demais laboratórios do 3º andar da UNIFESP *campus* Baixada Santista.

Aos técnicos e funcionários, por todo cuidado e os auxílios, em especial a Betty (CTCMol – UNIFESP São Paulo).

A banca examinadora por toda discussão científica.

A todos os professores que participaram da minha formação desde o ensino básico até a pós-graduação.

Aos camundongos utilizados nesse projeto.

A equipe do xenodiagnóstico do Instituto Dante Pazzanese de Cardiologia, Angela e Cris por sempre estarem dispostas e nos conceder os parasitos.

As agências de fomento FAPESP, INCTV, CAPES e CNPq por todo auxílio financeiro e tornarem a pesquisa uma realidade.

Á todos que contribuíram para essa tese de alguma forma muito obrigado.

Trabalho realizado no Laboratório de Imunologia Molecular e Vacinas Recombinantes no Edifício acadêmico I da Universidade Federal de São Paulo *campus* Baixada Santista e sob orientação do Prof. Dr. José Ronnie Carvalho de Vasconcelos. Projeto financiado pela CAPES, CNPq e FAPESP (mestrado **2017/11499-7** e doutorado direto **2019/17994-5**).

RESUMO

Os linfócitos T CD8+ são cruciais no controle de infecções por patógenos intracelulares como *Trypanosoma cruzi*. As moléculas de quimiocinas e integrinas são essenciais para a migração dos linfócitos T. No entanto, são escassos o papel dessas moléculas durante a infecção pelo *T. cruzi*. Os receptores de quimiocinas CX3CR1 e CXCR3 são moléculas altamente expressas na superfície dos linfócitos T CD8+ durante a infecção por patógenos intracelulares, como *T. cruzi*, e são importantes na ativação e diferenciação dessas células. A integrina LFA-1 também possui papel na ativação e diferenciação dos linfócitos em células de memória, uma vez que é extremamente importante no estabelecimento do contato dos linfócitos com as células apresentadoras de antígenos. Portanto nosso objetivo foi analisar as moléculas CX3CR1, CXCR3 e LFA-1 no controle da infecção, ativação, migração e diferenciação dos linfócitos T CD8. Nossos resultados demonstram que o bloqueio do CXCR3 e/ou LFA-1 levou a um aumento na carga parasitária sanguínea e tecidual além de tornar os camundongos da linhagem C57BL/6 suscetíveis à infecção pelo *T. cruzi*. Além disso, o bloqueio da integrina LFA-1 diminui a função efetora, citotoxicidade e migração das células T CD8+ quando comparados ao grupo infectado. Essa diminuição da função efetora também foi observada em camundongos da linhagem OT-I quando infectados com a cepa Y-OVA e tratados com anti-LFA-1. Ainda, observamos que o bloqueio do LFA-1 altera o fenótipo das células T CD8+, uma vez que os animais infectados têm um fenótipo de células T efetoras, já os tratados com LFA-1 se assemelham ao fenótipo de células naive. Também observamos que receptor de quimiocina CX3CR1 é altamente expresso nas células T CD8, porém sua ausência não comprometeu a sobrevivência e secreção de IFN-γ pelas células T CD8. Em conjunto, nossos dados demonstram que o LFA-1 e CXCR3 tem um papel crítico na imunidade protetora dos animais, além disso o LFA-1 exerce um papel extremamente importante nas células T CD8 auxiliando na sua migração, diferenciação e execução da sua função efetora, permitindo assim novos estudos para vacinas direcionais, com o intuito do aumento da proteção e resposta celular.

Palavras-chave: LFA-1, CXCR3, CX3CR1, integrinas, quimiocinas, células T CD8+, *Trypanosoma cruzi*.

ABSTRACT

CD8+ T lymphocytes are crucial in the control of infections by intracellular pathogens such as Trypanosoma cruzi. Chemokine and integrin molecules are essential for the migration of T lymphocytes. However, the role of these molecules during T. cruzi infection is scarce. In addition, the role of these molecules in the activation and differentiation of CD8 + T lymphocytes during viral and bacterial infections has now been reported. However, the role of these molecules during *T. cruzi* infection is unclear. Interestingly, CX3CR1 and CXCR3 chemokine receptors are highly expressed on the surface of CD8+ T lymphocytes during infection by intracellular pathogens, such as *T. cruzi*, and are important in the activation and differentiation of these cells. LFA-1 integrin also plays a role in the activation and differentiation of lymphocytes in memory cells since it is extremely important in establishing contact of lymphocytes with antigen-presenting cells. Therefore, our objective was to analyze the molecules CX3CR1, CXCR3 and LFA-1 in the control of infection, activation, migration, and differentiation of CD8 T lymphocytes. Our results demonstrate that blocking CXCR3 and/or LFA-1 led to an increase in blood and tissue parasitism, in addition making C57BL/6 mice susceptible to *T. cruzi* infection. In addition, blocking LFA-1 integrin decreases effector function, cytotoxicity, and migration of CD8+ T cells when compared to the infected group. This reduction of effector function was also observed in OT-I mice, when infected with the Y-OVA strain and treated with anti-LFA-1. Furthermore, we observed that blocking LFA-1 alters the phenotype of CD8+ T cells, since infected animals had an effector T cell phenotype, whereas those treated with LFA-1 resemble the naive cell phenotype. We also observed that the chemokine receptor CX3CR1 is highly expressed on CD8 T cells, but its absence did not compromise the survival and secretion of IFN-γ by CD8 T cells. Together, our data demonstrate that LFA-1 and CXCR3 play a critical role in the protective immunity of animals, thus allowing new studies for directional vaccines, with the aim of increasing cellular protection and response.

Key words: LFA-1, CXCR3, CX3CR1, integrins, chemokines, CD8+ T cells, *Trypanosoma cruzi*

LISTA DE FIGURAS

LISTA DE TABELAS

LISTA DE ABREVIATURAS E SIGLAS

2-ME – 2-Mercaptoetanol

ANOVA – Análise de Variância

APC – Células apresentadoras de antígeno

ASP-2 – Proteína da superfície de amastigota-2 do inglês *Amastigote surface proteins-2*

ATP – Adenosina trifosfato

BIOEX – Biotério de experimentação

BSA – Albumina do soro bovino

Cam. – Moléculas de adesão celular do inglês *Cell Adhesion Molecules*

CTCMol – Centro de Terapia Celular e Molecular

D.P – Desvio Padrão

DAB – 3,3'-diaminobenzidina

DAG – Diacilglicerol

DEPC – Dietil pirocarbonato

DNA - Ácido Desoxirribonucleico

EDTA – Ácido etilenodiamino tetraacético do inglês *Ethylenediamine tetraacetic acid*

ELISA- Ensaio de imunoabsorção enzimática do inglês *Enzyme Linked Immuno Sorbent Assay*

GFP- Proteína de fluorescência verde do inglês *Green fluorescent protein*

HCl – Ácido clorídrico

HE – Hematoxilina e eosina

HSD – Diferença significante honesta do inglês *honestly significant diference*

ICAM – Molécula de adesão intercelular do inglês *Intercellular Adhesion Molecule*

ICS – Marcação intracelular do inglês *intracellular staining*

IFN – Interferon

IgG – Imunoglobulina G

IL – Interleucina

IP3 – Inositol trifosfato

JAK – Janus quinase

K.O – Geneticamente deficiente em células do inglês *Knock out*

LCMV – Vírus da coriomeningite linfocítica do inglês *Lymphocytic choriomeningitis vírus*

LFA-1 – Antígeno associado a função linfocitária -1 do inglês *lymphocyte function-associated antigen-1*

MAP – Proteína-quinases ativadas por mitógenos do inglês *Mitogen Activated Protein Kinases*

MFI – Média de intensidade de fluorescência

MHC – Complexo de histocompatiblidade do inglês major histocompatibility complex

MIG – Monocina induzida pôr gama do inglês *monokine induced by gamma*

N.S – Não significante

NaCl – Cloreto de sódio

NEAA – Solução de aminoácidos não-essenciais do inglês *Non-essential Amino Acid Solution*

NK – Células NK do inglês *Natural killer*

NKT – Célunas NKT do inglês *Natural killer T*

Pa8 – Peptídeo

PAMP – Padrões moleculares associados a patógenos do inglês *pathogen associated molecular patter*

PBS – Salina tamponada com fosfato do inglês *Phosphate Buffered Saline*

PCR – Reação de cadeia polimerase do inglês *Polymerase chain reaction*

pH – Potencial hidrogeniônico

PI3 – Fosfatidilinositol 3-quinases

PLC – Fosfolipase C do inglês Phospholipase C

RPMI – Meio de cultura do inglês *Roswell Park Memorial Institute*

SDS – Dodecil sulfato de sódio

SFC – Células formadoras de spots

Src – Proteína quinase não receptora

STAT – Transdutor de sinal e ativador de transcrição do inglês *signal transducer and activator of transcription*

T. cruzi – Trypanossoma cruzi

T-bet – Fator de transcrição

TCM – Células T de memória central do inglês *Central Memory T Cells*

TCR – Receptor de células T do inglês *T cells receptor*

TE – Células T efetoras

TEM – Células T efetoras de memória do inglês *Effector Memory T Cells*

TGF – Fator transformador de crescimento do inglês *transforming growth fatcor*

Th – Células T auxiliar do inglês *T helper*

TLR – Receptor do tipo Toll do inglês *Toll like receptor*

TNF – Fator de necrose tumoral

TRIS – Trisaminometano

UNG – Uracila-N-glicosilase do inglês *uracil-N-glycosylase*

VLA4 – Antígeno de expressão tardia do inglês Very Late Antigen-4

WHO – Organização Mundial de Saúde do inglês *World Health Organization*

SUMÁRIO

1 INTRODUÇÃO

1.1 Doença de Chagas

A Doença de Chagas causada pelo parasito intracelular *Trypanosoma cruzi*, continua sendo um grave problema de saúde pública, onde cerca de 6 a 7 milhões de pessoas estão infectadas, ocasionando aproximadamente 7.000 mortes anualmente (WHO, 2017). Apesar das infecções ocorrerem principalmente em áreas endêmicas da América Latina, vem sendo reportado um aumento do número de casos fora dessas áreas, como na Europa, América do Norte, Japão e Austrália, devido ao fluxo migratório das pessoas portadoras da doença (VIRGILIO et al., 2014). A infecção pode ocorrer através das fezes contaminadas com as formas tripomastigotas metaciclícas do *Trypanosoma cruzi*, que são infectantes e são depositadas pelo inseto hematófago da família *Triatominae*, logo após o repasto sanguíneo. A contaminação também pode ocorrer pela via oral, logo após a ingestão de alimentos contaminados com as fezes do inseto contendo as formas tripomastigostas e também pela transmissão congênita (WHO, 2017). No Brasil, especificamente na região norte do país a maior forma de contaminação é a via oral, uma vez que nessa região possui um alto consumo da fruta açaí, sendo um risco a fruta não higienizada adequadamente (FERREIRA; BRANQUINHO; LEITE, 2014).

No ano de 2020 a perspectiva para o Brasil é de cerca de 3,2 milhões de infectados, sendo ao longo dos anos entre 1999 até atualmente registra-se uma redução no índice de mortalidade, com exceção da região Nordeste, que apresenta uma tendência crescente de infecção.(MELO *et al*., 2012) Nesse caso, a doença é classificada como uma das 18 doenças tropicais negligenciadas (DTN) identificadas pela Organização Mundial da Saúde (OMS), que se referem a infecções causadas por doenças infecciosas e parasitárias com alta morbidade e mortalidade causadas por um grupo de doenças que afetam principalmente, as populações mais pobres e vulneráveis respondem por mais de 12% da carga global de doenças (WHO, 2017; VICTORIA *et al*.,2003; BRASIL 2014; MENDONÇA *et al*.,2020).

1.2 Ciclo Biológico do *Trypanosoma cruzi*

O ciclo de vida do *Trypanosoma cruzi* (**Figura 1**) é do tipo heteróxeno, sendo necessário dois hospedeiros para realizar o ciclo completo da doença de chagas. O ciclo se inicia com o vetor *triatomineo* realizando a hematofagia em mamíferos (humanos, roedores, marsupiais, canídeos) infectados, assim ingere as formas tripomastigotas sanguíneas. Na porção média do intestino do vetor o parasito se diferencia em epimastigota, onde se multiplicará por fissão binária e sequencialmente se diferenciam para forma tripomastigota metacíclico na porção final do intestino. Nos mamíferos, durante a hematofagia o inseto defeca na pele do hospedeiro, as fezes contendo a forma infectante podem entrar em contato através da ferida ocasionada pela picada. Em seguida ocorre a penetração de tripomastigotas metacíclicas em qualquer célula do hospedeiro próximo a inoculação evoluindo para forma amastigota intracelular, sendo assim, as amastigotas crescem exponencialmente por divisão binária se diferenciando em tripomastigotas, após o rompimento das células infectadas são liberadas na corrente sanguínea as formas tripomastigotas sanguíneas que podem circular e invadir novas células ou infectar o vetor. (REEY, 2010; CDC, 2019; COURA, 2013).

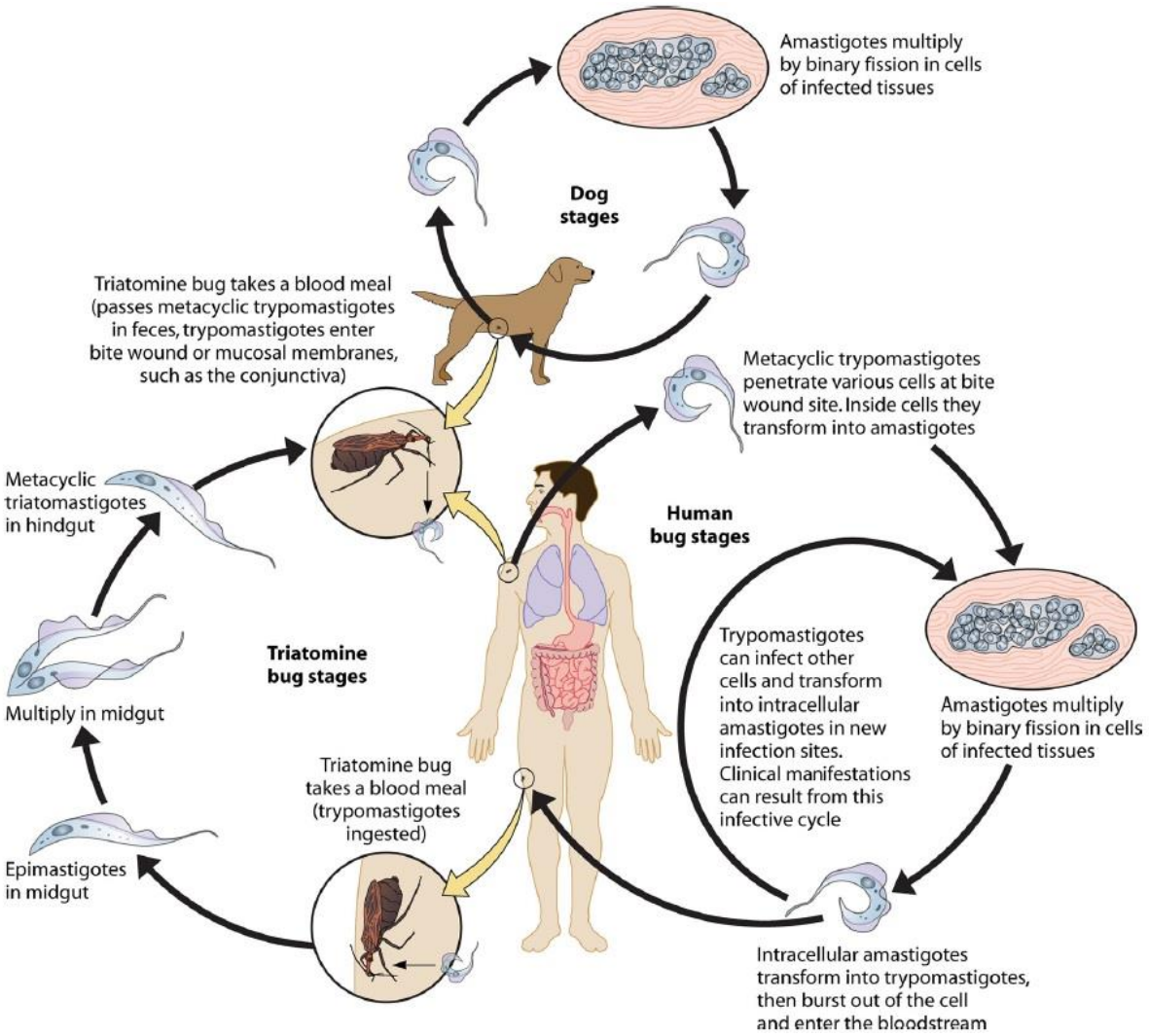

Figura 1 Ciclo de vida do *Trypanosoma cruzi* no inseto e no hospedeiro. Adaptado de Esch & Petersen. 2013.

1.3 Fases da Doença de Chagas

A doença possui duas fases clínicas: (1) fase aguda e (2) fase crônica. A primeira fase é normalmente assintomática com durabilidade de 4 a 8 semanas, sendo, fatal em apenas 2-8% dos casos. Esta fase é caracterizada por uma alta parasitemia sanguínea, muitas vezes associada à febre, dor de cabeça e náuseas, ou pode apresentar sinais característicos como o edema bipalpebral unilateral, conhecido como o sinal de *romaña*. A parasitemia é controlada por uma forte ativação do sistema imune, caracterizada por altos níveis de citocinas no plasma e ativação de linfócitos T e B (REEY, 2010; STANAWAY & ROTH, 2015; WHO, 2017).

Já na segunda fase da doença caracteriza-se pela baixa parasitemia e muitas vezes assintomática (HERNANDEZ & DUMONTEI, 2011), porém, anos após o contato inicial com o parasito, aproximadamente 30% dos pacientes desenvolvem sintomas cardíacos e/ou complicações no sistema digestivo (JUNQUEIRA *et al*., 2010), e aproximadamente 1/3 dos pacientes com danos no coração desenvolvem uma forma de cardiomiopatia dilatada, com disfunção ventricular e arritmia (CUNHA-NETO & CHEVILLARD, 2014). Em relação aos métodos diagnósticos, a fase aguda é identificada através da visualização microscópica das formas tripomastigotas sanguínea pela técnica de gota espessa ou esfregaço sanguíneo, enquanto, na fase crônica diagnóstico é realizado pela busca de anticorpos IgG contra o *T. cruzi* pela técnica de ELISA devido à baixa parasitemia sanguínea (BRASIL *et al*., 2010; WHO, 2002).

1.4 Tratamentos Contra Doença de Chagas

Os fármacos disponíveis para o tratamento da doença são escassos e atualmente os principais utilizados são nitrofurazone, nifurtimox e benznidazol, mas todos possuem limitações nas quais incluem: eficácia variável, cursos de tratamento longo e toxicidade. O benzonidazol tem efeito tripanocida e atua inibindo a síntese proteica de formas amastigotas e tripomastigostas (BERN et al., 2011). Apesar da sua eficácia durante a fase aguda, o benznidazol possui elevada toxicidade com vários efeitos adversos como reações de hipersensibilidade na pele, alterações sanguíneas e neuropatia periférica (OLIVEIRA *et al*., 2008).

O controle da dispersão da doença de Chagas também é feito através do uso de inseticidas, principal forma de combate aos vetores contaminados das áreas endêmicas. A busca por novos fármacos é um processo lento e possui poucos aspirantes, (RIBEIRO *et al*., 2009). Tendo em vista o crescimento do número de casos em áreas não endêmicas e de formas não vetoriais de transmissão da doença, além do tardio ou ausente diagnóstico e toxicidade da droga de escolha, é importante desenvolver novas estratégias de prevenção e terapia como é o caso das vacinas. (DUMONTELI & Herrera., 2017).

1.5 Resposta Imunológica contra o *Trypanossoma cruzi.*

Protagonista na defesa contra agentes infecciosos, a resposta imune possui papel fundamental na eliminação do patógeno. De modo geral, doenças causadas por parasitos possuem em comum a complexidade do ciclo biológico de seus patógenos, sendo, importante entender a complexidade dos mecanismos imunológicos envolvidos na resistência à infecção (GAZZINELLI & DENKERS, 2006). Vale destacar que o *T. cruzi* desenvolveu mecanismos de escapes do sistema imunológico, entretanto, o organismo do hospedeiro é parcialmente prejudicado garantindo assim sua sobrevivência. (ACEVEDO *et al*., 2018).

Uma vez dentro do hospedeiro mamífero, o *T. cruzi* infecta uma variedade de células. Este parasito interagem com moléculas da superfície celular, como proteínas com âncoras de glicosilfosfatidilinositol e, assim, se adere á célula.. (EPTING & ENGMAN., 2010). Após a ancoragem esses parasitos invadem as células através do recrutamento de vesículas lisossomais, formando o fagolissomo. Posteriormente, as formas tripomastigotas são liberadas no citoplasma e se diferenciam em amastigotas, que se replicam intensamente por divisão binária. Após a replicação, ocorre o rompimento da célula hospedeira e liberação das formas tripomastigotas na corrente sanguínea (CUNHA-NETO & CHEVILLARD, 2014).

A resposta inicial ao *T. cruzi* conta com a presença de macrófagos e neutrófilos, com participação de padrões de reconhecimento associados a patógenos (PAMPs), descritos como uma das primeiras linhas de defesa do sistema imunológico, essenciais na resposta contra vários micro-organismos (GAZZINELLI & DENKERS, 2006). A imunidade inata é ativada a partir do reconhecimento dos macrófagos residentes quando o parasito evade do fagolisossomo para o citoplasma e libera enzimas inibidoras a espécies reativas de oxigênio e nitrogênio (ERO e ERN) (CARDOSO *et al*., 2016). Além disso, ocorre a secreção de citocinas, como a IL-12, produzida pelos macrófagos e células dendríticas, além de, TNF-α e óxido nítrico (NO) induzindo a resposta inflamatória e produção de IFN-γ pelas células do tipo Th1 (KAYAMA & TAKEDA., 2010; GEIGER *et al*., 2016). Após o reconhecimento dos componentes celulares do *T. cruzi*, como DNA ou glicoproteínas que são capazes de ativar os receptores do tipo toll-like (TLR) presente nos fagócitos (como por exemplo nos macrófagos) e por sua vez respondem à presença de patógenos, detectando os

PAMPs que se localizam na superfície celular. A ativação dos TLRs presentes em macrófagos ou células dendríticas acarretam a produção de citocinas pró inflamatórias e quimiocinas que são considerados agentes importantes no controle inicial da infecção, pois, induzem o recrutamento de células fagocíticas nos tecidos infectados, como também, atuam na resposta imune adaptativa (GAZZINELLI, 2014). Por exemplo, a ativação do heterodímero TLR2 e TLR6 ocorre após o reconhecimento das mucinas do parasito, que por sua vez são reconhecidos pelo TLR4. (CAMPOS *et al.*, 2001; OLIVEIRA *et al.*, 2004).

Posteriormente, a atuação da reposta imune inata desencadeia uma ativação dos linfócitos B e T. A resposta das células B é de extrema importância nesse processo de proteção contra o protozoário, uma vez que estas células secretam anticorpos específicos contra o *T. cruzi,* permitindo a lise pelo sistema complemento. (KRATUZ, KISSINGER & KRETTLI., 2000). Esses anticorpos são essenciais uma vez que os animais são geneticamente deficientes para as células B, na ausência de uma resposta de anticorpos, camundongos infectados com *T. cruzi* exibem evidências de um controle inicial da infecção, mas, não conseguem conter a replicação do parasito e sucumbem à infecção. (KUMAR & TARLETON., 1998).

1.6 Importância das células T na infecção pelo *T. cruzi.*

Durante a replicação intracelular do parasito, ocorre a resposta das células T a partir do reconhecimento do complexo principal de histocopatibilidade MHC-peptídeo na superfície das células apresentadores de antígeno (APC) pelos receptores de células T (TCR). A partir dessa ativação teremos as células T naives gerando várias células T efetoras específicas. As células T se diferenciam a partir do aumento da expressão de CD69, CD25, CD40L e CTLA-4. (ACEVEDO *et al.*, 2018). Concomitantemente, as células T ativadas elevam a expressão de moléculas de adesão, ou seja, as CAM e receptores de quimiocinas que propiciam a migração e retenção em órgãos linfóides. As células T ativadas podem ser monofuncionais, ou seja, que produzem apenas uma citocina ou polifuncionais, que produzem diversas citocinas. Geralmente, a polifuncionalidade é essencial no âmbito da infecção e vacinação (LEWINSOHN, LEWIMSOHN & SCRIBA., 2017, THAKUR, PEDERSEN & JUNGERSEN., 2012).

Células T $CD4^+$ secretam citocinas e expressam moléculas que modulam a atividade de outras células, principalmente os macrófagos, células dendríticas e outros linfócitos. Os amplos perfis de células auxiliares (Th) são definidos de acordo com as citocinas e expressão de fatores de transcrição, ambos diretamente ligados à natureza do patógeno (SALLUSTO., 2016). Estudos demonstraram que em modelo murino a coordenação entre os perfis Th1 e Th2 são eficientes para proteção dos camundongos na infecção pelo *T. cruzi,* embora os mecanismos de reposta Th1 são predominantes para a eliminação do parasito principalmente pela produção de IFN-γ. (PETRAY *et al.*,1993; RODRIGUES *et al.*, 1999; KUMAR & TARLETON., 2001). Também já foi descrito o perfil Th17, demonstrando que essas células conferem uma forte proteção contra o *T. cruzi.* (CAI *et al.,* 2016).

Por sua vez, os linfócitos T CD8+ são primordiais no controle de patógenos intracelulares, como o *T. cruzi.* No citoplasma, o parasito libera antígenos que terão sua apresentação via MHC de classe I. Após o reconhecimento do antígeno via TCR-MHC-I ocorre a ativação das células T $CD8^+$ resultando na secreção de citocinas e produção de proteínas citotóxicas que eliminam a célula-alvo. (GARG, NUNES & TARLETON., 1997; WENINGER, MANJUNATH & VON ADRIAN., 2002).

Após a tentativa de neutralização da infecção pelo *T. cruzi*, uma pequena porção da população de células T específicas que sobreviveram instaura a memória imunológica. Essas células conseguem se manter mesmo com o antígeno ausente e são capazes de realizar a imunovigilância. As características mais importantes das células T $CD8^+$ de memória são a rápida resposta a reinfecções produzindo citocinas apresentando atividade citotóxica, por fim, realizar a imunidade protetora depois do contato com o patógeno (BADOVINAC & HARTY., 2006).

Linfócitos T $CD8^+$ de memória são diferenciados em 3 principais tipos: as células T efetoras (TE), as células efetoras de memórias (TEM) que estão localizadas nos tecidos periféricos e estão envolvidas na proteção imediata podendo produzir citocinas efetoras, porém, possuem baixa capacidade proliferativa. Em relação as células de memória central (TCM), essas estão localizadas em órgãos linfoides secundários que possuem capacidade proliferativa e tornam-se células efetoras mediante a estimulação secundária. (LANZAVECCHIA & SALLUSTO., 2005; MUELLER *et al.*, 2012). Elas se diferenciam de acordo com o nível de expressão de alguns marcadores de ativação e *homing,* além das diferenças nas

suas proliferações e funções efetoras. (ANGELOSANTO & WHERRY., 2010; AHMED & AKONDY., 2011).

Em camundongos, o fenótipo de cada subtipo celular está relacionado com o nível da expressão de moléculas de superfície, sendo, os marcadores utilizados TE ($CD44^{alto}$, $CD11a^{alto}$ $CD62L^{baixo}$, $CD127^{baixo}$ e $KLRG1^{alto}$); TCM ($CD44^{alto}$, $CD11a^{alto}$ $CD62L^{alto}$, $CD127^{alto}$ e $KLRG1^{alto}$); TEM ($CD44^{alto}$, $CD11a^{alto}$ $CD62L^{baixo}$, $CD127^{alto}$ e $KLRG1^{alto}$). (HIKONO *et al.* 2007; VASCONCELOS *et al.*, 2012; VASCONCELOS *et al.*, 2014).

Em camundongos infectados pelo *T. cruzi*, demonstraram que a fase inicial da memória é formada por células T $CD8^+$ com o perfil TEM semelhante a outras infecções com o mesmo caráter (WHERRY *et al.*, 2004; SHIN *et al.*, 2007). Durante a fase aguda tardia, devido à baixa carga antigênica ocorre a diferenciação da subpopulação de células TCM, e podemos observar um aumento da sua frequência paralelamente a cronificação da infecção (TARLETON., 2015).

A importância dos linfócitos T $CD8^+$ no controle da infecção pelo *T. cruzi* já foi demonstrada durante a infecção de animais deficientes para esta célula, ou pelo bloqueio da mesma utilizando anticorpos monoclonais. Ambos os animais deficientes ou tratados não sobreviveram a infecção em relação aos animais imunocompetentes (ROTTENBERG *et al*., 1993; TARLETON, 1990). As ações antiparasitárias são diversas, incluindo secreção de citocinas e citotoxicidade direta mediada por granzimas e perforina contra células infectadas (MARTIN & TARLETON, 2004; TZELEPIS *et al*., 2006). Trabalhos realizados pelo nosso grupo de pesquisa finalmente descreveram epítopos CD8 reconhecidos durante a infecção com parasitos de diferentes cepas de *T. cruzi* em camundongos de linhagens distintas (TZELEPIS *et al*., 2006; TZELEPIS *et al.,* 2008).

Os epítopos reconhecidos por linfócitos T $CD8^+$ de camundongos da linhagem C57BL/6 infectados com parasitos da cepa Y de *T. cruzi* são VNHRFTLV (da Proteína 2 da Superfície de amastigotas), TsKb-18 (ANYDFTLV, do antígeno TSA) e TsKb-20 (ANYKFTLV do antígeno TSA) (TZELEPIS *et al*., 2006; TZELEPIS *et al*., 2008). Esta descrição permitiu o avanço dos estudos envolvendo a cinética das células T $CD8^+$ citotóxicas, assim como, a de células produtoras de IFN-γ específicas durante a infecção experimental (TZELEPIS *et al*., 2006; TZELEPIS *et al*., 2008). Observou-se que a maturação e expansão dessas células específicas foram

dependentes de células T $CD4^+$ e da carga parasitária, além disso, o mecanismo mediador da atividade citotóxica das células T $CD8^+$ contra as células infectadas pelo parasito foi dependente de perforina (TZELEPIS *et al*., 2006; Martin *et al*., 2006).

Sabe-se que os linfócitos T $CD4^+$ desempenham papel essencial, com a habilidade de induzir memória de células T $CD8^+$ e aumentar a expansão clonal (JANSSESN *et al.,* 2003). Além disso, a recirculação dessas das células T $CD8^+$ é importante para a resistência contra a infecção pelo *T. cruzi,* (DOMINGUEZ, 2012) e por isso, iniciou-se estudos para descrever quais moléculas de quimiocinas e integrinas poderiam estar relacionadas no processo de migração celular, sendo um processo fundamental na infecção pelo *T. cruzi*, e se estariam afetando a função das células T $CD8^+$.

1.7 Papel dos receptores de quimiocinas e integrinas durante respostas do tipo Th1.

Quimiocinas são pequenas moléculas com aproximadamente 8-10 kDa, caracterizadas por possuírem resíduos de cisteínas conservados. Essas moléculas são divididas em quatro famílias, C, CC, CXC e CX3C. A organização dessas famílias é baseada de acordo com a porção animo terminal da cadeia polipeptídica, além disso, seus receptores são redundantes, sendo que um ligante pode ter afinidade por mais de um receptor e vice-versa (ZLOTNIK & YOUSHIE, 2000).

Essas moléculas são responsáveis pela migração leucocitária durante a homeostase e inflamação. O direcionamento celular necessário para iniciar as respostas imunes durante esses eventos, ocorre através da interação do receptor do tipo sete α-hélice acoplado a proteína G trimérica com seus ligantes cognatos. Essa interação atrai as APC para os sítios de inflamação permitindo a apresentação de antígenos aos linfócitos T, além disso, o movimento dos linfócitos T efetores também depende dessas moléculas (MACKAY, 2001; THELEN, 2001; KUFAREVA *et al*., 2015).

Além da migração celular, as quimiocinas estão envolvidas na ativação de linfócitos T atuando como moléculas co-estimuladoras, e também participam na diferenciação e proliferação dessas células. Essas funções desencadeadas pelos

receptores de quimiocinas decorrem após a proteína G ser ativada, assim que a subunidade Gα se liga ao ATP e dissocia-se do dímero Gβγ. Consequentemente, a subunidade Gα inibe adenilil ciclase e ativa tirosinas quinases como a proteína quinase não receptora (Src), que ativa MAP quinases e PI3 quinase, responsáveis pela transcrição gênica, diferenciação e proliferação. Ao ser formado o dímero Gβγ, ocorre a ativação de fosfolipases como por exemplo a PLCβ, em seguida ocorre a formação de dois fatores essências denominados como: inositosol trifosfato (IP3), e diacilglicerol (DAG), que ao se ligarem ao receptor IP3 localizado na membrana plasmática do retículo endoplasmático, promove a liberação de cálcio intracelular para o citoplasma e sequencialmente estimula a ativação de proteínas dependentes de cálcio como: quinase PCK e PI3γ quinase que são responsáveis pelo rearranjo do citoesqueleto e movimento celular. Ademais, os receptores de quimiocinas também são suscetíveis a fosforilação por JAK-STAT e quando ativados expõem domínios citoplasmáticos capazes de estimular esta via de sinalização (MURDOCH & FINN, 2000; SOLDEVILA & GARCA-ZEPADA, 2007; GUERREIRO *et al*., 2011).

As integrinas são heterodímeros constituídos por uma subunidade alfa (α) e outra beta (β), expressos na superfície dos linfócitos. O LFA-1 é constituído pelas cadeias β2 ou CD18 e α2 ou CD11a (STANLEY *et al*., 2012) e é necessário para a adesão de leucócitos, migração, formação das sinapses imunológicas e co-estimulação dos linfócitos T. O LFA-1 ativado se liga às moléculas de adesão intercelular (ICAMs) presentes na superfície das células endoteliais.

Em modelo de infecção por patógeno intracelular como *Toxoplasma gondii,* foi demonstrado que o parasito prejudica a capacidade dos monócitos em redistribuir as moléculas de LFA-1 e VLA-4 em resposta ao ICAM-1 e VCAM-1, afetando a capacidade migratória dessas células (HARKER *et al*., 2013). O papel do LFA-1 também tem sido estudado em modelos de rejeição de aloenxertos, sendo que o antagonismo desta molécula é muito eficaz na inibição da rejeição aguda e prolongamento da sobrevivência de aloenxertos em roedores (KWUN *et al*., 2015). Já estudos com infecção pelo *T. cruzi* apresentaram predomínio de linfócitos T $CD8^+$ no miocárdio em camundongos infectados com a cepa Colombiana de *T. cruzi* e a análise fenotípica dessas células mostraram que são $CD62L^{low}$, $LFA\text{-}1^{high}$ e $VLA\text{-}4^{high}$, sendo que seu predomínio no tecido cardíaco favorece a progressão da reação inflamatória, levando ao desenvolvimento de Cardiopatia Chagásica Crônica (DOS

SANTOS *et al*., 2001). Além da participação do LFA-1 na migração dos linfócitos T, essa molécula tem um importante papel como na co-estimulação dos linfócitos, promovendo a interação entre os linfócitos T e as APC durante a ativação, e, na citotoxicidade direta (BACHMANN *et al*., 1997; DUSTIN & BROMLEY, 2002; DUSTIN, 2009), esse contato entre as células T $CD8^+$ e as células APCs é fundamental para geração de células T $CD8^+$ específicas de memória (BADOVINAC *et al*., 2005).

Durante respostas do tipo Th1 que são desencadeadas por patógenos intracelulares, como o *T. cruzi*, as células T virgens diferenciam–se em células produtoras de citocinas como IFN-γ, IL-2 e TNF-α e essa diferenciação ocorre por meio da expressão da interleucina IL-12 e pelo fator de transcrição de T-bet As células T efetoras já diferenciadas expressam altos níveis do receptor de quimiocina CXCR3 e seus ligantes CXL10 (IP-10), CXCL11 e CXCL9 (MIG), assim como, do LFA-1 (TEIXEIRA, *et al*., 2002). A alta expressão de CXCR3 e produção de IFN-γ nessas células é devido ao fator T-bet, responsável pela transcrição desses genes.

O papel do receptor CXCR3 na migração dos linfócitos T efetores durante respostas do tipo Th1 foi apontado durante a infecção pelo protozoário *T. gondii* em modelo murino, sendo esse receptor altamente expresso nas células T $CD4^+$ responsável pela migração dos linfócitos T para o intestino, permitindo o controle da carga parasitária e do dano tecidual, e consequentemente a sobrevivência desses animais infectados (COHEN *et a.l*, 2013).

Já em modelo de infecção viral utilizando o citomegalovírus (LCMV), o receptor CXCR3 auxilia no controle da viremia, porém, não participa na migração das células efetoras para os sítios de infecção sendo sugerido que esse receptor participa na sinapse imunológica entre as células T CD8 efetoras e as células alvo infectadas (HICKMAN *et al*., 2015).

Somada a migração celular, os receptores de quimiocinas como CXCR3 e CX3CR1 influenciam a diferenciação dos linfócitos T. Na literatura, encontra-se que a molécula CXCR3 favorece a diferenciação de células T $CD8^+$ efetoras de memória, caracterizada pela expressão de $CD127^{high}$, KLGR-1^{low} IL-$17R^{high}$, evidenciando que essa possui um papel de co-estimulação dos linfócitos T (KURACHI *et al*., 2011). O receptor CX3CR1 é altamente expresso nas células precursoras de memória durante infecções por patógenos intracelulares e as diferenças no nível de

expressão desse receptor caracteriza subtipos de células efetoras precursoras de memória (GERLACH *et al*., 2016).

Diante do exposto, a hipótese deste estudo é que o bloqueio da integrina LFA-1 e dos receptores de quimiocina CXCR3 e CX3CR1 interfere na diferenciação e ativação das células T $CD8^+$ durante a infecção experimental pelo *T. cruzi.* Sendo assim, o objetivo desse estudo é avaliar o papel dos receptores de quimiocinas CXCR3, CX3CR1 e da integrina LFA-1 na diferenciação e ativação das de células T $CD8^+$ durante a infecção pelo *T. cruzi.*

2 OBJETIVOS

2.1 Objetivo geral

Avaliar o papel dos receptores de quimiocinas CXCR3, CX3CR1 e da integrina LFA-1 na diferenciação e ativação das de células T $CD8^+$ durante a infecção pelo *T. cruzi.*

2.2 Objetivos específicos

2.2.1 Avaliar a influência do tratamento com os anticorpos anti-LFA-1 e anti-CXCR3 na sobrevida de animais infectados e na carga parasitária.

2.2.2 Avaliar o efeito do tratamento com anticropo anti-LFA-1 na resposta de células T $CD8^+$ em camundongos infectados;

2.2.3 Analisar o impacto do tratamento com os anticorpos anti-LFA-1 e anti-CXCR3 na histopatologia do coração;

2.2.4 Avaliação da migração das células T CD8 e T CD4 após o tratamento com anti-LFA-1;

2.2.5 Avaliação da resposta imune das células T CD8 totais após o tratamento in vivo com o anticorpo anti-LFA-1 em camundongos da linhagem OT-I infectados com a cepa Y-OVA;

2.2.6 Análise da expressão génica das células T CD8, T CD4, *N.K* e citocinas no tecido cardiaco de camundongos C57BL/6 infectados e/ou trados *in vivo* com anti-LFA-1;

2.2.7 Análise da parasitemia e sobrevivência em camundongos $CX3CR1^{gfp/gfp}$ infectados com a cepa Y de *T. cruzi*;

2.2.8 Quantificação de IFN-γ em camundongos $CX3CR1^{gfp/gfp}$ infectados com a cepa Y de *T. cruzi*.

3 METODOLOGIA

3.1 Comitê de ética

Todos os procedimentos desse estudo foram submetidos e aprovados pelo Comitê de Ética no Uso de Animais da Universidade Federal de São Paulo (CEUA/UNIFESP) sob o número 9081250517 e respeitaram as normativas estabelecidas pelo Conselho Nacional de Controle de Experimentação Animal (CONCEA).

3.2 Delineamento experimental

Foram utilizados camundongos fêmeas com 8 semanas de vida, da linhagem C57BL/6 que são resistentes à infecção experimental pelo *T. cruzi*. Os grupos foram divididos de acordo com a **Tabela 1**. Também foram utilizados animais da linhagem OT-I, que possuem receptor das células T restritos a reconhecer o peptídeo SINFEKL da ovalbumina. Os grupos foram distribuídos na **Tabela 3**. Ambas linhagens foram proveinientes do CEDEME. Por fim utilizamos animais CX3CR1$^{gfp/gfp}$ (JUNG *et al*., 2000) para verificar se a ausência dessa molécula no âmbito da infecção pelo *T. cruzi*. Os grupos foram organizados na **Tabela 4**. Os delineamentos experimentais desses grupos estão na **Figura 2 A-C**. Os animais foram mantidos em gaiolas (4 a 5 animais por gaiola), com livre acesso à água e ração, ciclo claro/escuro de 12 horas (7h/19h) e temperatura controlada (22 ± 1°C), no Biotério de Experimentação do Departamento de Biociências – (BIOEX) da Universidade Federal de São Paulo (UNIFESP), *campus* Baixada Santista.

Tabela 1. Divisão de grupos experimentais tratados com anti-LFA-1 e anti-CXCR3.

Linhagem de camundongos	Grupos	Número de camundongos	Infecção 10^4 formas	Tratamento 250μg/cam.
C57BL/6	1	4	----	-------
C57BL/6	2	4	*T. cruzi*	IgG de rato
C57BL/6	3	4	*T. cruzi*	αLFA-1
C57BL/6	4	4	*T. cruzi*	αCXCR3

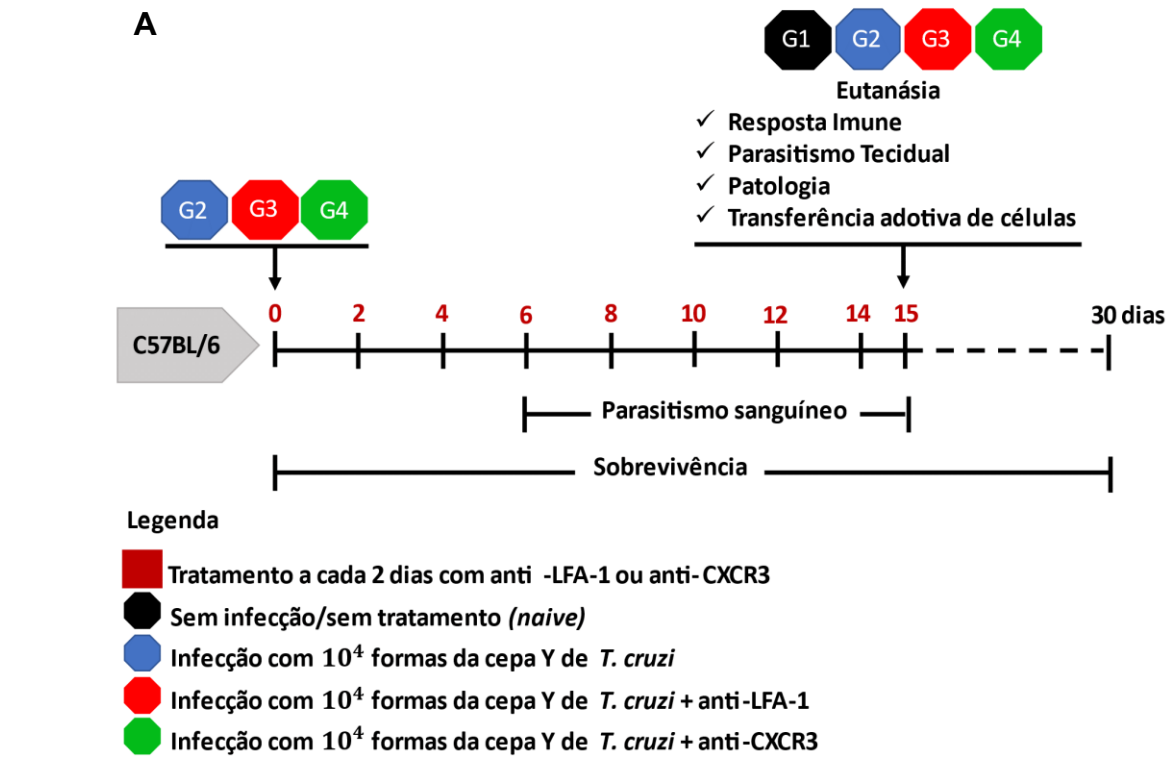
A
G1 G2 G3 G4
Eutanásia
✓ Resposta Imune
✓ Parasitismo Tecidual
✓ Patologia
✓ Transferência adotiva de células
G2 G3 G4
C57BL/6
0 2 4 6 8 10 12 14 15 30 dias
Parasitismo sanguíneo
Sobrevivência
Legenda
Tratamento a cada 2 dias com anti -LFA-1 ou anti- CXCR3
Sem infecção/sem tratamento (naive)
Infecção com 10^4 formas da cepa Y de T. cruzi
Infecção com 10^4 formas da cepa Y de T. cruzi + anti-LFA-1
Infecção com 10^4 formas da cepa Y de T. cruzi + anti-CXCR3

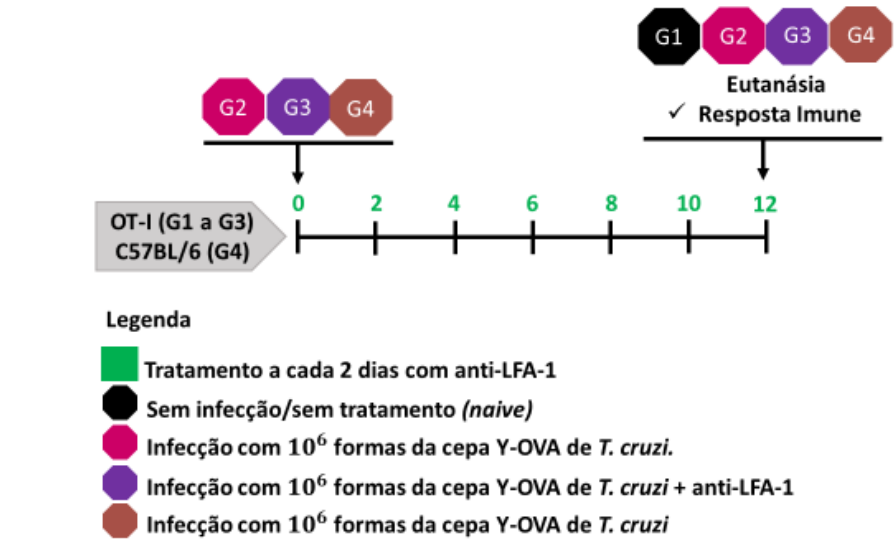
B
G1 G2 G3 G4
Eutanásia
✓ Resposta Imune
G2 G3 G4
OT-I (G1 a G3)
C57BL/6 (G4)
0 2 4 6 8 10 12
Legenda
Tratamento a cada 2 dias com anti-LFA-1
Sem infecção/sem tratamento (naive)
Infecção com 10^6 formas da cepa Y-OVA de T. cruzi.
Infecção com 10^6 formas da cepa Y-OVA de T. cruzi + anti-LFA-1
Infecção com 10^6 formas da cepa Y-OVA de T. cruzi

C

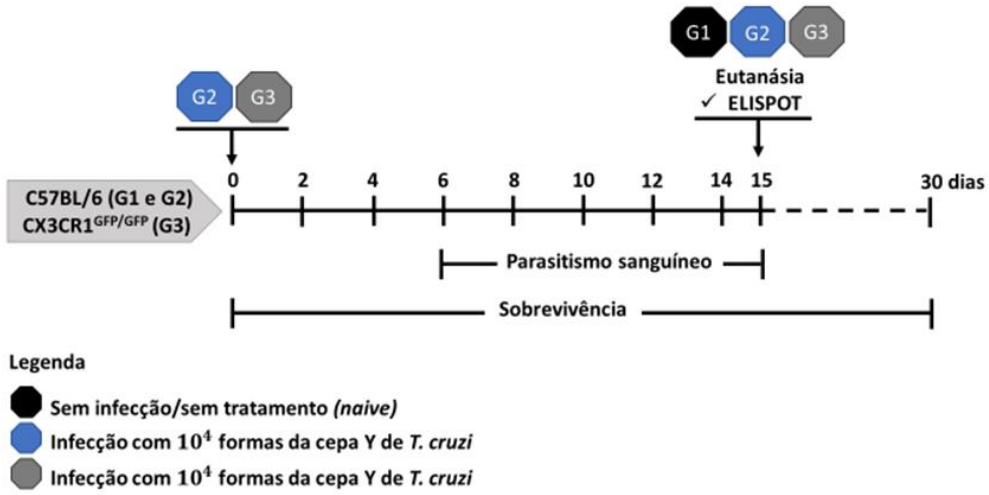

Figura 2. **Delineamentos experimentais. Protocolo de infecção e tratamento. (A)** Protocolo com camundongos C57BL/6. **(B)** Protocolo com camundongos OT-I. **(C)** Protocolo com camundongos CX3CR1$^{gfp/gfp}$

3.3 Avaliar a influência do tratamento com os anticorpos anti-LFA-1 e anti-CXCR3 na sobrevida de animais infectados e na carga parasitária.

Foram infectados com 10^4 formas tripomastigotas sanguíneas da cepa Y de *T. cruzi*, camundongos C57BL/6 a infecção foi administrada pela via subcutânea, especificamente na base da cauda. No momento da infecção os camundongos foram tratados a cada 48 horas com 250μg do anticorpo monoclonal anti-LFA-1(anti-CD11a, clone M17-4, BioXcell) e/ou o isotipo controle (IgG de rato, clone 2a3), administrado pela via intraperitoneal (Reisman *et al.*, 2011). A divisão de grupos está ilustrada acima conforme a tabela 1. No sexto dia após a infecção a parasitemia sanguínea foi acompanhada por meio da coleta de 5 μL de sangue da cauda dos animais, e a contagem dos parasitos foi feita em 40 campos de uma lamínula de 18 X 18mm observados em microscópio de luz. A parasitemia foi realizada até o 15°dia

de infecção, a contagem foi multiplicada por 8000 para se obter o valor por mL de sangue. A sobrevivência foi monitorada todos os dias, até o 30°dia de infecção.

Para avaliação, do parasitismo tecidual, o coração foi extraído dos diferentes grupos, para quantificação do DNA de *T. cruzi* por PCR em tempo real e descrito em detalhes abaixo.

O DNA genômico do coração, baço, fígado e tecido adiposo foi extraído da seguinte forma: Os órgãos foram retirados no 15°dia após infecção com 10^4 formas da cepa Y de *T. cruzi* e armazenados no freezer -80°C até o momento da extração. Para extração, os tecidos foram picotados com uma lâmina de bisturi estéril em pequenos pedaços, com auxílio de uma pinça estéril. Os pedaços foram macerados com o auxílio do nitrogênio líquido. Após a maceração, o tecido foi colocado em microtubos de 1,5mL acrescentando a eles 5 volumes de tampão de lise que consiste em 10mM Tris–HCl (pH 7.6), 0.1M NaCl, 10mM EDTA, 0.5% SDS, e 300µg/mL de proteinase K (SIGMA). Estes microtubos foram incubados em banho maria por 18 horas a temperatura de 56°C. A seguir foram acrescentados dois volumes de fenol-clorofórmio-álcool isoamílico (25:24:1) (SIGMA) e centrifugados por 20 minutos a 4.200 x g. O sobrenadante resultante da centrifugação foi transferido para um novo microtubo de 1,5mL, devidamente etiquetado e, acrescentou-se dois volumes de isopropanol gelado, seguido de incubação no freezer -80°C por 18 horas para o auxílio na precipitação de DNA. Após a incubação, os microtubos foram centrifugados por 30 minutos a 16.000 x g, o isopropanol foi descartado e o pellet de DNA foi lavado com 1mL de etanol 70% e imediatamente centrifugado por 20 minutos a 16.000 x g. O etanol foi descartado e o *pellet*, submetido a secagem a temperatura ambiente por 30 minutos. Após essa etapa o mesmo foi ressuspendido com 100 µL de água DEPC estéril. A quantificação de DNA foi realizada pelo NANODROP (Thermofisher).

Para a padronização da curva, coração, de camundongos sem infecção foram retirados e adicionou-se 10^4 formas de tripomastigotas da cepa Y de *T. cruzi* (Cummings *et al*., 2003). Os tecidos foram infectados e o DNA extraído conforme descrito acima. Uma vez ressuspenso, o DNA foi diluído para uma concentração de 25ng/µL de DNA de tecido. O padrão de diluição foi 10 vezes, variando de 100000 parasitos para o coração, músculo esquelético, fígado e tecido adiposo, equivalentes

a 50ng de DNA total. A curva padrão foi gerada a partir dessas diluições para a determinação da carga parasitária de tecidos infectados.

A reação de PCR em tempo real continha 2µL de DNA genômico do coração (50ng), 0,1µL dos primers iniciadores específicos para uma região satélite nuclear do genoma de *T. cruzi*, CZF1 5'- AST CGG CTG ATC GTT TTC GA-3',e CZR2 3'- AAT TCC TCC AAG CAG CGG ATA-5' (INVITROGEN™) que amplifica uma sequência de 166 pares de bases (Pirona *et al.* 2007), 0,5 µL TaqMan MGB Probe CZ3P-6FAMCAC ACA CTG GAC ACC AAMGBNFQ, 5,0 µL do TaqMan® Universal Master Mix II, com UNG, e água MilliQ para completar volume final de 10µL. Separadamente outra reação foi realizada, contendo 2µL de DNA genômico (50ng), 0,5µL dos primers juntamente com a sonda do controle endógeno normalizador (TaqMan Gene Ex Assays MTO Med VIC, INVITROGEN™), que amplifica um fragmento de 115 pares de bases do gene β-actina de *Mus musculus*, 5,0 µL do TaqMan® Universal Master Mix II, com UNG, e água MilliQ para completar um volume final de 10µL. As reações foram distribuídas em placas de 96 wells (MicroAmp®Fast Optical 96-Well, 0,1mL) as placas foram levadas ao termociclador StepOnePlus (applied biosystems®) e as condições de termociclagem foram as seguintes: 50°C por 2 minutos, 95°C por 10 minutos, e 40 ciclos de 95°C por 15 segundos e 60°C por 1 minutos. Cada placa continha em triplicata, controle negativo da reação usando água e como controle da extração, DNA de camundongo não infectado.

3.4 Avaliar o efeito do tratamento com anticropo anti-LFA-1 na resposta de células T CD8+ em camundongos infectados;

Camundongos da linhagem C57BL/6 foram infectados e tratados de acordo com o protocolo descrito no item 1 da metodologia. No 15°dia de infecção os animais foram eutanasiados para a avaliação da resposta imune, por meio das seguintes técnicas descritas abaixo em 3.4.1 a 3.4.3:

3.4.1 ELISPOT

Para o ensaio de ELISPOT, foram utilizadas placas de nitrocelulose de 96 poços (Multiscreen HA, Milipore) cobertas com 60µl/poço de PBS estéril contendo 10 µg/ml do anticorpo monoclonal anti-IFNγ de camundongo (R4- 6A2, Pharmingen). Após incubação durante a noite a temperatura ambiente, a solução contendo o anticorpo monoclonal foi removida por aspiração em ambiente estéril e as placas foram então lavadas por 3 vezes com RPMI. As placas foram bloqueadas pela incubação dos poços com 100µl do meio RPMI contendo 10% de soro fetal bovino por, pelo menos, 2 horas a 37ºC. As células respondedoras foram obtidas do baço de camundongos infectados com *T. cruzi.* Estas células foram lavadas 3 vezes em meio RPMI e então ressuspensas em meio RPMI completo na concentração de $1x10^6$ células viáveis/ml. O meio completo continha 1% de NEAA, L-glutamina, vitaminas e piruvato, $5X10^{-5}$M 2-ME, 10% de soro fetal bovino (HyClone) e 30 U/ml de interleucina-2 (IL-2) recombinante de camundongo (SIGMA). A placa foi incubada, na presença ou não do peptídeo VNHRFLTV, em condições estáticas por 24 horas a 37ºC em atmosfera contendo 5% de CO_2. Após a incubação, as células foram desprezadas. Para retirada de qualquer célula residual, as placas foram sequencialmente lavadas 3 vezes com PBS e 5 vezes com PBS-Tween 20. Cada poço recebeu 75 µl do anticorpo monoclonal anti-camundongo biotinilado XMG1.2 (Pharmingen) diluído em PBS-Tween 20 na concentração final de 2µg/ml. As placas foram incubadas durante a noite a 4ºC. Os anticorpos inespecíficos foram removidos lavando essas placas por 6 vezes com PBS-Tween 20. Posteriormente, foi adicionado estreptavidina-peroxidase (BD) na proporção de 1:500 em PBS-Tween 20 em volume final de 100µl/poço.

As placas foram incubadas entre 1 a 3 horas a temperatura ambiente e então lavadas de 3 a 5 vezes com PBS-Tween 20 e mais 3 vezes com PBS. As placas foram reveladas adicionando- se 100 µl/poço do substrato da peroxidase (50mM Tris-HCl, pH 7.5, contendo 1mg/ml de DAB e 1µl/ml de 30% de peróxido de hidrogênio, ambos da SIGMA). Após a incubação de 15 minutos em temperatura ambiente, a reação foi interrompida descartando o substrato e lavando-se as placas com água corrente. As placas foram então secas a temperatura ambiente e o número de células produtoras de IFN-γ foram contadas com a ajuda de um estereoscópio (Nikon SMZ745T With Nikon Ni-150).

3.4.2 Marcação intracelular

Dois milhões de células do baço foram cultivadas por no máximo 12 horas, a 37ºC, 5% CO2, na presença ou ausência de 10μg do peptídeo VNHRFTLV (pA8), do anticorpo CD107a e brefeudina (10μg/mL). Após essa incubação, as células foram transferidas para tubos eppendorff e lavadas uma vez com tampão de lavagem MAC's (PBS 1x + 2mM EDTA + 0.5% BSA). As células foram ressuspendidas em 50μl de tampão de lavagem, adicionado o anticorpo de superfície anti-CD8 e incubado por 30 minutos, a 4ºC, no escuro. Foi lavado as células duas vezes com tampão de lavagem. Após a lavagem foi feita uma centrifugação a 300 rcf, por 5 minutos a 15ºC, adicionado 100μl de paraformaldeído 4% e incubado por 15 minutos, no escuro, a temperatura ambiente. Em seguida, foi adicionado 100μl de permeabilizante ao paraformaldeído. As células foram centrifugadas novamente a 300 rcf, por 5 minutos a 15ºC, em seguida foram ressuspensas em 100μl com o tampão de permeabilização e incubado por 10 minutos, no escuro, a temperatura ambiente. Foi adicionado 100μl de tampão de lavagem em seguida as células foram centrifugadas a 300 rcf, por 5 minutos a 15ºC. As células foram ressuspensas em 50μl de tampão de lavagem e os anticorpos anti-IFN-γ (clone XMG1,2, BD) e anti-TNF-α (clone MPC-XT22, BD) foi adicionado. Incubou-se por 30 minutos, a 4ºC, no escuro. Foi lavado as células duas vezes com tampão MAC's e ressuspensas em PBS com 1% de paraformaldeído. A leitura das amostras foi feita pela aquisição de 700.000 eventos no Citômetro de Fluxo Canto II.

3.4.3 Citotoxicidade

As suspensões de células foram isoladas do baço de camundongos da linhagem C57BL/6. Os eritrócitos foram lisados usando tampão de lise (0.15 M NH_4Cl, 1mM $KHCO_3$, 0.1mM Na+ EDTA, pH 7.2-7.3). Após duas lavagens com RPMI, as células foram ressuspensas em meio R10% - RPMI 1640 com 10% de soro fetal bovino. A viabilidade celular foi avaliada utilizando o corante Azul de Tripan (0.2%) para a

diferenciação de células vivas e mortas. A concentração celular foi obtida em câmara de Neubauer. Metade dos esplenócitos foram corados com 1μM ($CFSE^{low}$) e a outra metade com 10μM ($CFSE^{high}$) de CFSE (Molecular Probes) em PBS pré-aquecido por 15 minutos a 37ºC. Após centrifugação, as células foram ressuspensas em R10% pré-aquecido. As células alvo $CFSE^{high}$ foram pulsadas com 2,5μM do peptídeo (pA8) em meio R10% por 40 minutos a 37ºC (R10% pré-aquecido), lavadas extensivamente, ressuspensas em R10% e contadas novamente. Ambas as populações de CFSE foram misturadas na concentração de 1:1, centrifugadas, ressuspensas em RPMI e injetadas intravenosamente (via retro-orbital) em camundongos infectados, tratados ou naives numa concentração de 1-2 $x10^7$ células/camundongo. Aproximadamente 20 horas, após a injeção dessas populações supracitadas, o baço dos camundongos foram retirados, e as suspensões de células foram fixadas em PBS contendo 1% de paraformaldeído por 5 minutos a temperatura ambiente. As células foram lavadas uma vez em PBS e sequencialmente ressuspendidas em tampão de FACs. As populações de linfócitos $CFSE^{low}$ e $CFSE^{high}$ foram detectadas no baço via citometria de fluxo, usando o FACS Celesta e analisadas com o software FlowJo. A porcentagem de lise específica para o peptídeo foi determinada pela fórmula.

$$\% \text{ de lise} = 1 - \left(\frac{\%CFSE^{high} \text{ infectado} / \%CFSE^{low} \text{ infectado}}{(\%CFSE^{high} \text{ normal} / \%CFSE^{low} \text{ normal})} \times 100\right).$$

3.4.4 Imunofenotipagem

As células do baço dos grupos descritos na tabela 1 foram utilizadas para marcação de moléculas de superfície relacionadas com ativação e diferenciação das células T CD8+. Para tal, dois milhões de células de foram utilizadas para realização da imunofenotipagem. Essas células foram marcadas por 30 minutos, a 4°C em tampão de amostra (0,5% de BSA, 2mM de EDTA) com os seguintes anticorpos: anti-CD3 BV510 (clone 145-2C11, BD), anti-CD8 APCR700 (clone 53-67, BD) ou PE (clone 53-67, eBioscience), anti-CD11a FITC (clone 2D7, BD), anti-CD44 FITC

(clone IM7, BD), anti-CD62L APC (clone MEL-14, BD), anti-CX3CR1 (clone SA011F11, Biolegend), anti-CD183 PERCP/Cy5.5 (CXCR3, clone CXCR3-173, BioLegend), anti-CD4 PECF594 (clone GK15, Biolegend) anti-KLRG1 BV786 (clone 2F1, BD), anti-CD95 FITC (clone JO2, BD), anti-CD127 PE (clone SB/199, BD). Para as células T CD8+ específicas o foi utilizado o pentâmero $H2k^{b}$– VNHRFTLV biotinilado (ProImmune INC). A leitura das amostras foi feita pela aquisição de 700.000 eventos no Citômetro de Fluxo FACS Celesta.

3.5 Analisar o impacto do tratamento com os anticorpos anti-LFA-1 e anti-CXCR3 na histopatologia do coração.

Os corações dos animais descritos na tabela 1 foram retirados e fixados em formol tamponado a 4%. Os cortes foram analisados por microscopia de luz após a inclusão em parafina e coloração com hematoxilina–eosina padrão. A quantificação do número de ninhos de amastigotas no coração foi feita a partir 50 campos/lâmina. Os cortes dos tecidos selecionados foram fotografados com uma câmera Nikon FE2 acoplada a um microscópio Zeis.

3.6 Avaliação da migração de células T $CD8^{+}$ e T CD4 de camundongos infectado e/ou tratados com anti-LFA-1.

Para avaliar papel da molécula LFA-1 na migração das células T $CD8^{+}$ e T CD4, animais da linhagem C57BL/6 foram infectados e tratados conforme o item 3.3 da metodologia e os grupos experimentais estão descritos na tabela 2. As células T $CD8^{+}$ e T CD4 dos animais da linhagem C57BL/6 infectados e/ou tratados foram isoladas através da purificação por coluna magnética utilizando as beads do Kit $CD8a^{+}$ T Cell Isolation (Miltenyi Biotec) e Kit CD4 T Cell Isolation (Miltenyi Biotec), o protocolo do fabricante foi restritamente obedecido e somente as células com 96% de pureza foram utilizadas no experimento. Após as células T $CD8^{+}$ e T CD4 isoladas, $5x10^{6}$ células T $CD8^{+}$ foram transferidas adotivamente, pela via retro orbital para os animais da linhagem B6.129S2-Cd8atm1Mak/J que são geneticamente deficientes para a célula T $CD8^{+}$. Já as células T CD4 foram transferidas

adotivamente, pela via retro orbital para os animais da linhagem B6.129S2-Cd4tm1Mak/J que são geneticamente deficientes para a célula T CD4. Esses animais estavam no 14°dia de infecção no momento da transferência. Após 5 dias de transferência o coração desses animais deficientes para células TCD8 ou T CD4 foram retirados e realizado a expressão gênica (Adaptado de SILVERIO *et al.,* 2012). A metodologia da extração e quantificação está descrita abaixo no item 3.7.

Tabela 2. Estudo da importância da molécula LFA- 1 na migração das células T CD8 e T CD4.

Linhagem de camundongo	**Grupos**	**Número de camundongos**	**Infecção 10^4 formas**	**Transferência adotiva**	**Retirada coração 5º dia**
B6.129S2-Cd8atm1Mak/J	1	2	*T. cruzi*	Salina (PBS)	
B6.129S2-Cd8atm1Mak/J	2	4	*T. cruzi*	T $CD8^+$ (C57BL/6 + *T. cruzi*)	
B6.129S2-Cd8atm1Mak/J	3	4	*T. cruzi*	T $CD8^+$ (C57BL/6 + *T. cruzi* + αLFA-1)	
B6.129S2-Cd4tm1Mak/J	1	2	*T. cruzi*	Salina (PBS)	
B6.129S2-Cd4tm1Mak/J	2	4	*T. cruzi*	T $CD8^+$ (C57BL/6 + *T. cruzi*)	
B6.129S2-Cd4tm1Mak/J	3	4	*T. cruzi*	T $CD8^+$ (C57BL/6 + *T. cruzi* + αLFA-1)	

3.7 Análise da expressão génica das células T CD8, T CD4, N.K e citocinas no tecido cardíaco de camundongos C57BL/6 infectados e/ou trados *in vivo* com anti-LFA-1.

Para a quantificação das quimiocinas e células T CD8, T CD4 e N.K os camundongos da linhagem C57BL/6 foram infectados com 10^4 formas de tripomastigotas da cepa Y de *T. cruzi* e/ou tratados a cada 48 horas com anticorpo monoclonal anti-LFA-1, após 15 dias de infecção os animais foram eutanasiados, retirado o coração desses animais e lavados com PBS1X até retirar totalmente o sangue da cavidade interna do coração. O RNA do tecido foi extraído utilizando o kit Pure link RNA mini kit (life Technologies) o protocolo foi seguido rigorosamente e o DNA complementar (cDNA) foi preparado utilizando o kit high capacity cDNA reverse transcription (Applied Biosystems). A PCR foi realizada com SYBR Green Master Mix (Applied Biosystems) e as sequencias utilizadas para mensurar a expressão das quimiocinas e as células foram: CD8, 5'-GACGAAGCTGACTGTGGTTGA-3' CD8, 5'-GCAGGCTGAGGGTGGTAAG-3'; CD4, 5'-TCCTAGCTGTCACTCAAGGGA-3' CD4, 5'-TCAGAGAACTTCCAGGTGAAGA-3'; N.K, 5'-GGACTAAGGTTCACATTGCCA-3' N.K, 5'-TCCTAAGATGGAGGCACAGC-3'; TNF, 5'-AGGGTCTGGGCCATAGAACT-3' TNF, 5'- CCACCACGCTCTTCTGTCTAC-3' ; IFN-γ, 5′-AACGCTACACACTGCATCTTGG-3′ IFN-γ, 5′-GCCGTGGCAGTAACAGCC-3′; Granzima B, 5'-TGTCTCTGGCCTCCAGGACAA-3', Granzima B, 5'-CTCAGGCTGCTGATCCTTGATCGA-3,' Perforina, 5'-GTACAACTTTAATAGCGACACAGTA-3' Perforina, 5'-AGTCAAGGTGGAGTGGAGGT-3', as amostras foram normalizadas usando o gene GAPDH com os seguintes primers 5′-GTGGTGAAGCAGGCATCTGA-3′ e 5′-GGGAGTCACTGTTGAAGTCGC-3′. Também realizamos as mesmas mensurações citadas a cima no tecido cardíaco dos animais T CD8 K.O e T CD4 K.O que tiveram a transferência adotiva das células como citado no item 3.6 da metodologia.

3.8 Avaliação da resposta imune das células T CD8+ totais após o tratamento in vivo com o anticorpo anti-LFA-1 em camundongos OT-I infectados com *T. cruzi* cepa Y-OVA.

Camundongos da linhagem OT-I foram infectados e tratados a cada 48 horas de acordo com o protocolo descrito na Tabela 3, no 12º dia após a infecção foi realizada a eutanásia e analisado a resposta imune pela técnica de Marcação Intracelular e ELISPOT descritos nos itens 3.4.1 e 3.4.2

Tabela 3. Estudo da resposta imune em camundongos da linhagem OT-I

Linhagem de camundongos	Grupos	Número de camundongos	Infecção 10^6 formas cepa Y-OVA	Tratamento 250μg/cam.	Resposta imune 12º dia
OT-I	1	4	----	-------	
OT-I	2	4	*T. cruzi* Y-OVA	IgG de rato	
OT-I	3	4	*T. cruzi* Y-OVA	Anti-LFA-1	
C57BL/6	4	4	*T. cruzi* Y-OVA	----------	

3.9 Análise da parasitemia e sobrevivência em camundongos CX3CR1$^{gfp/gfp}$ infectados com a cepa Y de *T. cruzi*.

Camundongos da linhagem C57BL/6 e CX3CR1$^{gfp/gfp}$ foram infectados com 10^4 formas tripomastigotas sanguíneas da cepa Y de *T. cruzi*, a infecção foi administrada pela via subcutânea, especificamente na base da cauda. A divisão de grupos está ilustrada abaixo conforme a tabela 4. No sexto dia após a infecção a parasitemia sanguínea foi acompanhada por meio da coleta de 5 μL de sangue da cauda dos animais, e a contagem dos parasitos foi feita pela observação em microscópio de luz das formas tripomastigotas sanguíneas (40/campos). A parasitemia foi realizada até o 15°dia de infecção e posteriormente a sobrevivência foi monitorada todos os dias, até o 30°dia de infecção.

Tabela 4. Divisão de grupos experimentais CX3CR1$^{gfp/gfp}$.

Linhagem de camundongos	Grupos	Número de camundongos	Infecção 10^4 formas cepa Y
C57BL/6	1	4	*T. cruzi*
CX3CR1$^{gfp/gfp}$	2	4	*T. cruzi*

3.10 Quantificação de IFN-γ em camundongos CX3CR1$^{gfp/gfp}$ infectados com a cepa Y de *T. cruzi*.

Para quantificar a secreção de IFN-γ, foi realizado a técnica de ELISPOT conforme a metodologia está descrita no item 3.4.1 e com a divisão de grupos descrita na tabela 4.

3.11 Análise Estatística.

Os resultados correspondente ao número de parasitos/mL correspondentes ao pico de parasitemia, o número de células produtoras de IFN-γ(ELISPOT), a polifuncionalidade de células T CD8 + e citotoxicidade, foram comparados por análise de variância unidirecional (ANOVA); posteriormente, foi utilizado o teste HSD de Tukey. Os resultados correspondentes a PCR em tempo real, ninhos de amastigota, expressão gênica, foram comparados por teste t de Student. Os resultados encontram-se expressos em média +/- DP. Valores de $p<0,05$ foram considerados significativos.

4 RESULTADOS

4.1 Avaliar a influência do tratamento com os anticorpos anti-LFA-1 e anti-CXCR3 na sobrevida de animais infectados e na carga parasitária.

Para analisar se o bloqueio do receptor de quimiocina CXCR3 ou da integrina LFA-1 tornam os camundongos da linhagem C57BL6 suscetíveis à infecção pelo *T. cruzi*, os mesmos foram infectados e tratados a cada 48 horas com os anticorpos monoclonais anti-CXCR3 ou anti-LFA-1. A parasitemia foi acompanhada do 6º dia até o 15º dia após a infecção e em geral houve um aumento do parasitismo nos grupos tratados com anti-LFA-1 ou anti-CXCR3, e esse aumento foi estatisticamente significativo (p=0.0394). Em relação ao grupo controle apenas infectado e tratado com o IgG (**Figura 3A**). Já em relação à sobrevivência (**Figura 3B**) todos os camundongos do grupo tratado com anti-LFA-1 sucumbiram após o 15° dia de infecção, enquanto o grupo tratado com anti-CXCR3 todos sucumbiram após o 23°dia de infecção, e os camundongo do grupo controle infectado tiveram 100% de sobrevivência após a infecção. Esses resultados demonstram que tanto a integrina LFA-1 quanto o receptor CXCR3 são importantes para o controle da infecção pelo *T. cruzi*, sendo que o bloqueio dessas moléculas torna os camundongos antes resistentes, suscetíveis à infecção. Com relação ao parasitismo tecidual no 15º dia após infecção, os órgãos foram coletados e submetidos à extração de DNA, conforme descrito no item 3.3 da metodologia. Foi observado aumento no número de parasitos em log/50ng em todos os tecidos analisados, coração, braço, fígado e tecido adiposo, tanto no grupo tratado com o anticorpo monoclonal anti-LFA-1 (**Figura 4A-D**), quanto no grupo tratado com anticorpo monoclonal anti-CXCR3 (**Figura 5A-D**) ambos em relação ao grupo apenas infectado com aumento estatisticamente significativo, p=0.0126 e p=0.0475 respectivamente. Os dados da quantificação são complementares ao parasitismo sanguíneo, demonstrando a importância dessas moléculas para o controle do parasitismo.

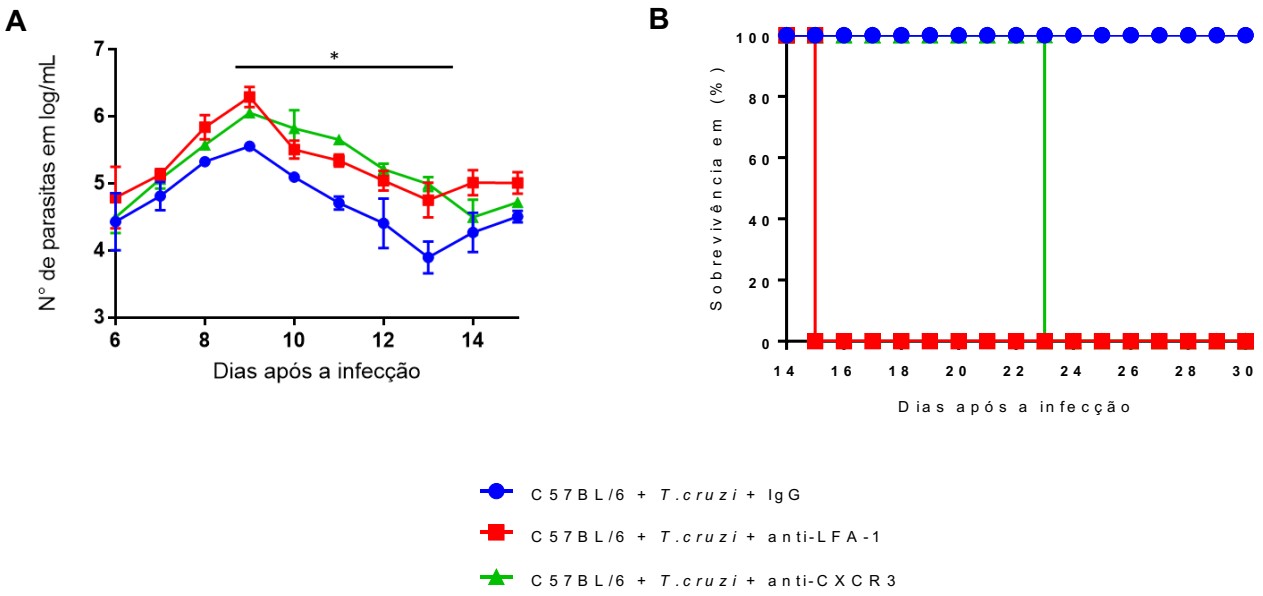

Figura 3. Avaliação da parasitemia e sobrevivência em camundongos da linhagem C57BL/6infectados com *T. cruzi* da cepa Y e tratados com anti-CXCR3, e anti-LFA-1. O gráfico (**A**) representa a média e o desvio padrão da parasitemia, monitorada no 6º dia após infecção, até o 15º dia. O gráfico (**B**) representa a curva de sobrevivência e os camundongos tratados com anti-LFA-1 e anti-CXCR3 tornaram-se suscetíveis à infecção pelo *T. cruzi*. p= 0,0394 Análise One way ANOVA.

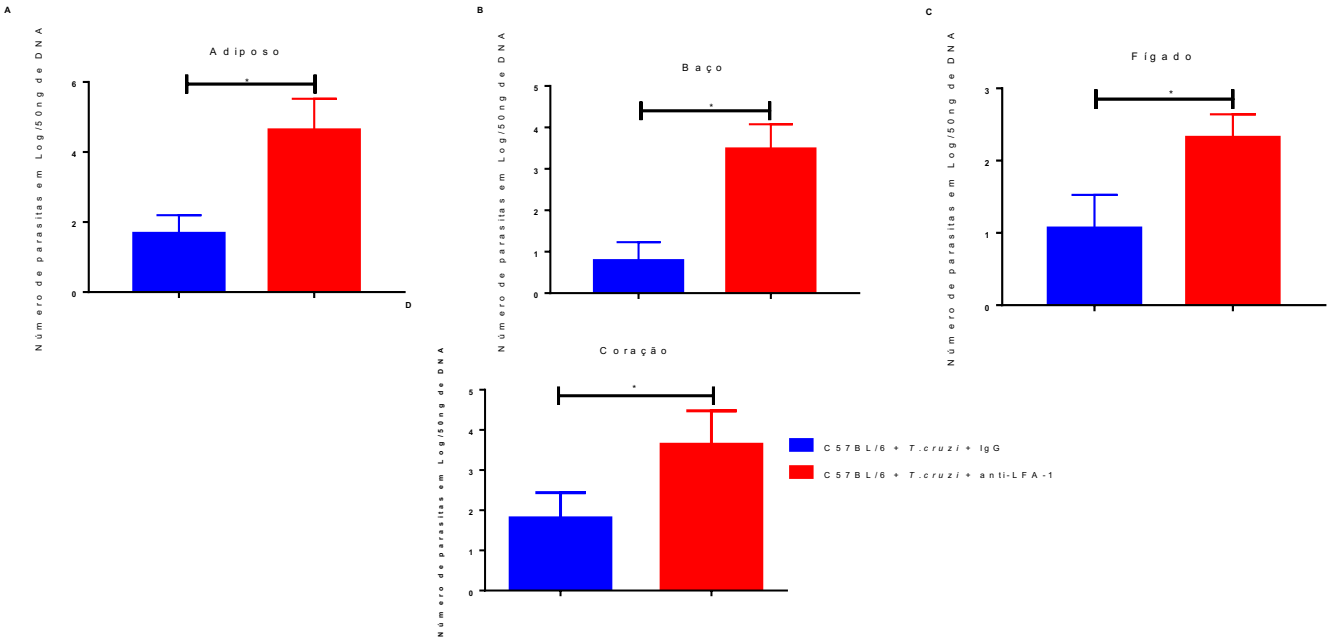

Figura 4. Quantificação do parasitismo no coração, baço, tecido adiposo e fígado de camundongos da linhagem C57BL/6 infectados e tratados com anti-LFA-1. A quantidade de parasitos aumenta após o tratamento com

anticorpo anti-LFA-1 (**Figura 4 A-D**), em comparação ao grupo apenas infectado (grupo controle). O aumento do parasitismo após o tratamento com o anticorpo citado corrobora com o aumento no parasitismo sanguíneo. São apresentados os valores em log e barras que indicam a média ± o desvio padrão de cada grupo citados na legenda. Os asteriscos indicam diferença estatística entre o grupo infectado, e o grupo infectado e tratado com anti-LFA-1. Gráfico A *p=0.0012 Gráfico B *p=0.0004 Gráfico C *p=0.0042 Gráfico D p*=0.0126. Análise, Teste T de Student.

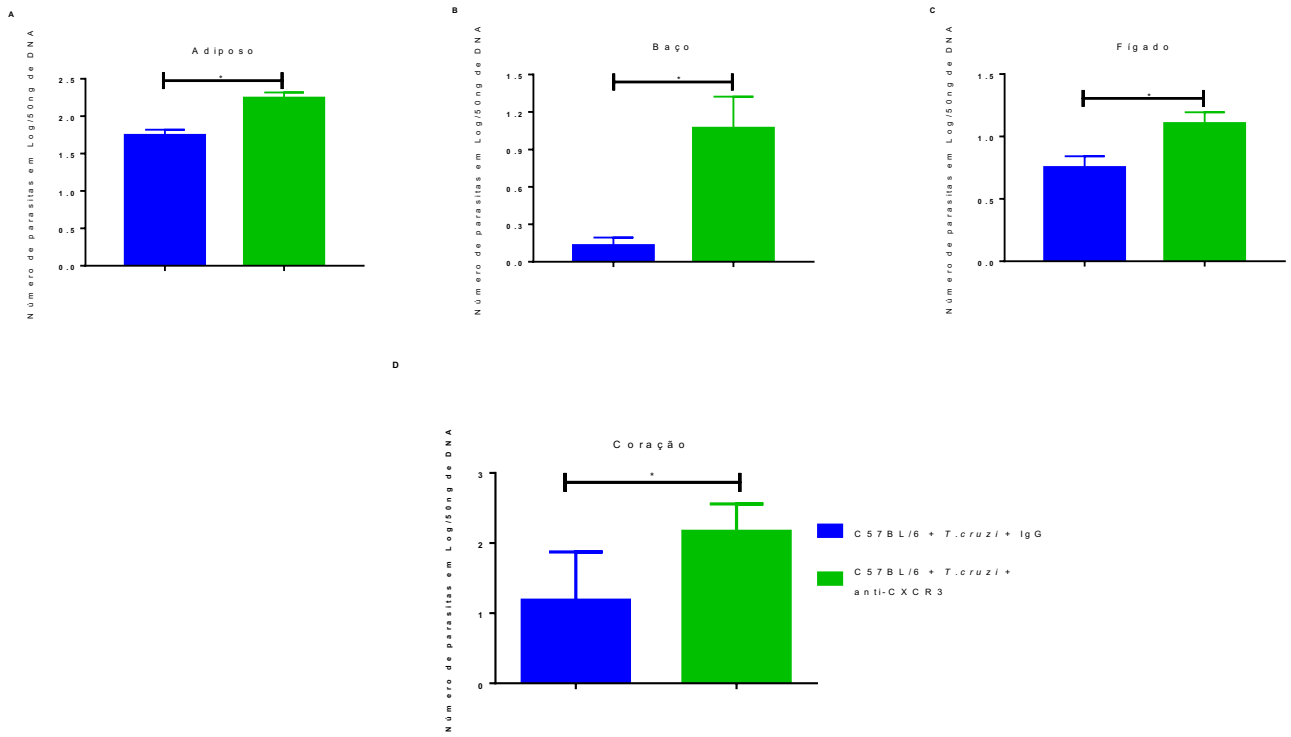

Figura 5. Quantificação do parasitismo no coração, baço, tecido adiposo e fígado de camundongos da linhagem C57BL/6 infectados e tratados com anti-CXCR3. A quantidade de parasitos aumenta após o tratamento com anti-CXCR3 (**Figura 5 A-D**), em comparação ao grupo apenas infectado (grupo controle). O aumento do parasitismo após o tratamento com o anticorpo citado corrobora com o aumento no parasitismo sanguíneo. São apresentados os valores em log e barras que indicam a média ± o desvio padrão de cada grupo citados na legenda. Os asteriscos indicam diferença estatística entre o grupo infectado, e o grupo infectado e tratado com o anticorpo anti-CXCR3. Gráfico A *p<0.0001 Gráfico B *p=0.0004 Gráfico C *p=0.0014 Gráfico D p=0.0475. Análise, Teste T de Student.

4.2 Analisar o impacto do tratamento com os anticorpos anti-LFA-1 e anti-CXCR3 na histopatologia do coração

Para analisar a quantidade de ninhos de amastigota no tecido cardíaco, camundongos da linhagem C57BL/6 foram infectados e tratados a cada 48 horas com os anticorpos monoclonais anti-CXCR3 e anti-LFA-1, no 15º dia esses animais foram eutanasiados e retirado o coração para coloração com hematoxilina e eosina (HE). A quantidade do número de ninhos de amastigota foi gerada após a contagem de 50 campos e observou-se que ocorre um aumento tanto no grupo infectado e tratado com anti-LFA-1 (**Figura 6A-B**) como no grupo infectado e tratado com anti-CXCR3 (**Figura 7 A-B**) em relação ao grupo apenas infectado e esse aumento foi estatisticamente significativo, além disso, de uma maneira geral houve aumento do infiltrado inflamatório nos grupos tratados com anti-LFA-1 ou anti-CXCR3 em relação ao grupo apenas infectado, esses resultados corroboram com o aumento no nível do parasitismo sanguíneo e tecidual, ocorrendo também um aumento no número de amastigota.

A

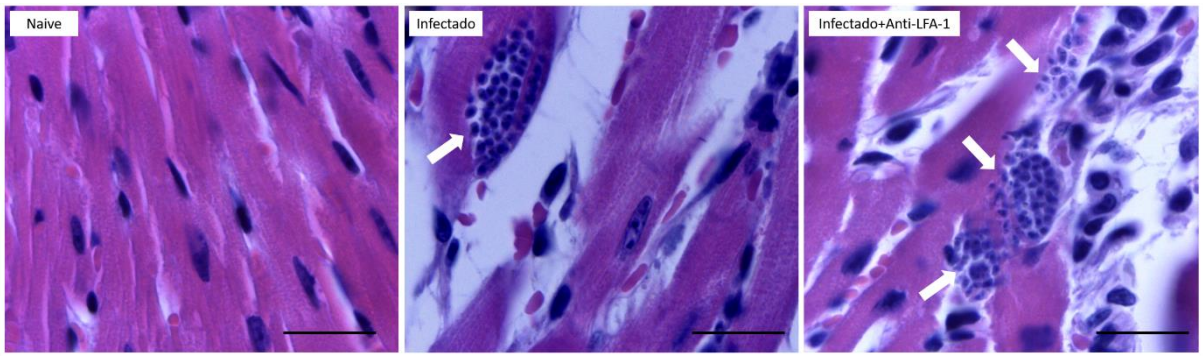

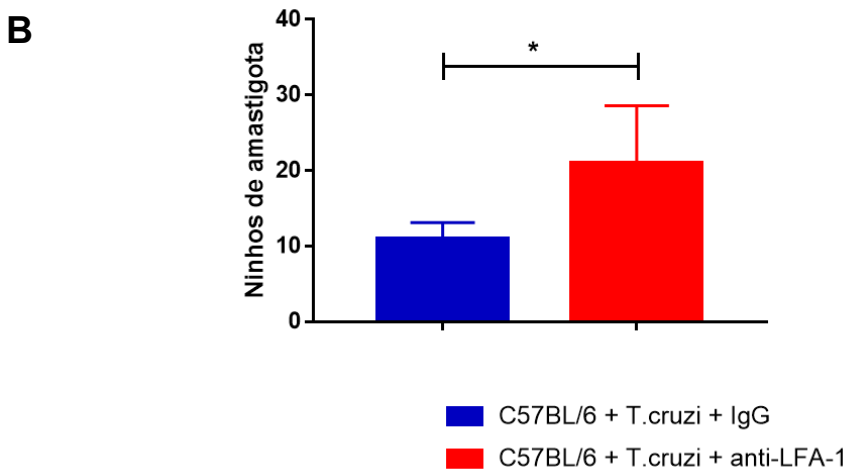

Figura 6. Ninhos de amastigota após o tratamento com o anticorpo anti-LFA-1. Na figura **A** temos fotomicrografias do coração de camundongos C57BL/6 representando os grupos Naive, Infectado e Infectado+Anti-LFA-1. O grupo Naive não apresentou ninhos de amastigotas. Já nos grupos Infectado e Infectado+Anti-LFA-1 foram encontrados ninhos (setas). Coloração realizada Hematoxilina e eosina. Barra de escala=10µm. Na figura **B** tivemos a contagem do numero de ninhos de amastigota e após o tratamento com o anti-LFA-1 ocorre um aumento em relação ao grupo infectado e esse aumento foi estatisticamente significativo *p=0,049. Análise, Teste T de Student.

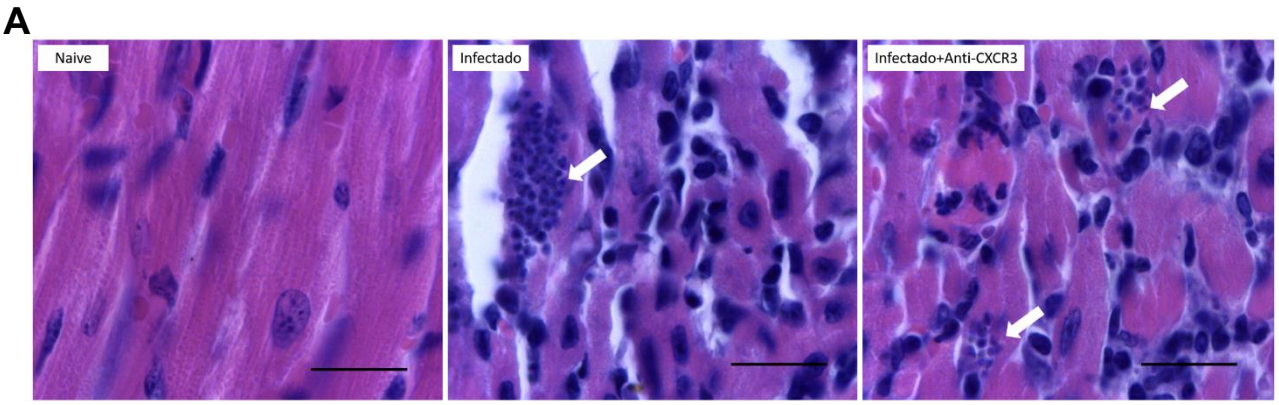

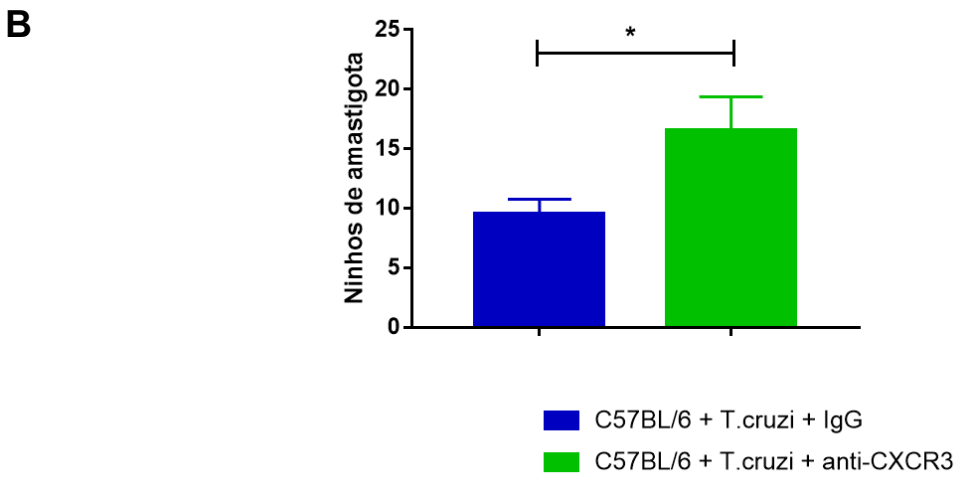

Figura 7. **Ninhos de amastigota após o tratamento com o anticorpo anti-CXCR3.** Na figura **A** temos fotomicrografias do coração de camundongos C57BL/6 representando os grupos Naive, Infectado e Infectado+Anti-CXCR3. O grupo Naive não apresentou ninhos de amastigotas. Já nos grupos Infectado e Infectado+Anti-CXCR3 foram encontrados ninhos (setas). Coloração realizada Hematoxilina e eosina. Barra de escala=10µm. Na figura **B** tivemos a contagem do numero de ninhos de amastigota e após o tratamento com o CXCR3 ocorre um aumento em relação ao grupo infectado e esse aumento foi estatisticamente significativo *p=0,004. Análise, Teste T de Student.

4.3 Avaliação da resposta imune das células T CD8$^+$ totais após o tratamento *in vivo* com o anticorpo anti-LFA-1 em camundongos infectados.

As células T CD8$^+$ exercem um forte papel antiparasitário que é mediado largamente por IFN-γ e outros mediadores que também participam na eliminação do parasito. Analisamos a produção de mediadores importantes como IFN-γ e TNF-α, assim como a degranulação celular, além da citotoxicidade *in vivo* das células T CD8$^+$ do baço de camundongos da linhagem C57BL/6 que receberam o tratamento com o anticorpo monoclonal anti-LFA-1. A divisão dos grupos experimentais está descrito na **Tabela 5.** As técnicas de marcação intracelular e ELISPOT foram utilizadas para a detecção de citocinas. Os dot-plots da **Figura 8 (painéis A-C)** representam células T CD8+ específicas do baço dos diferentes grupos de camundongos, e como é observado houve diminuição na degranulação, produção de IFN-γ e TNF-α entre o grupo que recebeu o tratamento com o anticorpo monoclonal anti-LFA-1 e o grupo apenas infectado. Com relação à polifuncionalidade, o grupo tratado com anti-LFA-1 teve uma diminuição da polifuncionalidade e amplitude da resposta imune (**Figuras 8D e 9**). O ensaio de ELISPOT confirmou que o tratamento com o anticorpo monoclonal anti-LFA-1, diminuiu a secreção de IFN-γ pelas células T CD8+ específicas (**Figura 10**) onde

ambos são estatisticamente significativos. Com relação a citotoxicidade, como podemos observar, o tratamento com anti-LFA-1, acarreta na diminuição da citotoxicidade em relação ao grupo infectado (**Figura 11 A e B**), sendo que, a porcentagem de citotoxicidade no grupo tratado com anti-LFA-1 é de 61% enquanto que a porcentagem de citotoxicidade nos animais infectados é de 94%, sendo essa diferença estatisticamente significativa.

Tabela 5 – Divisão dos grupos: 1 sem infecção e sem tratamento (naive), 2 apenas infectado e tratado com IgG e 3 infectado e tratado com anticorpo monoclonal anti-LFA-1

Grupos	n°	Tratamento com anticorpo a cada 48H	Desafio
1	4	Sem tratamento	Sem infecção
2	4	IgG - Rato	*T. cruzi*
3	4	Anti-LFA-1	*T. cruzi*

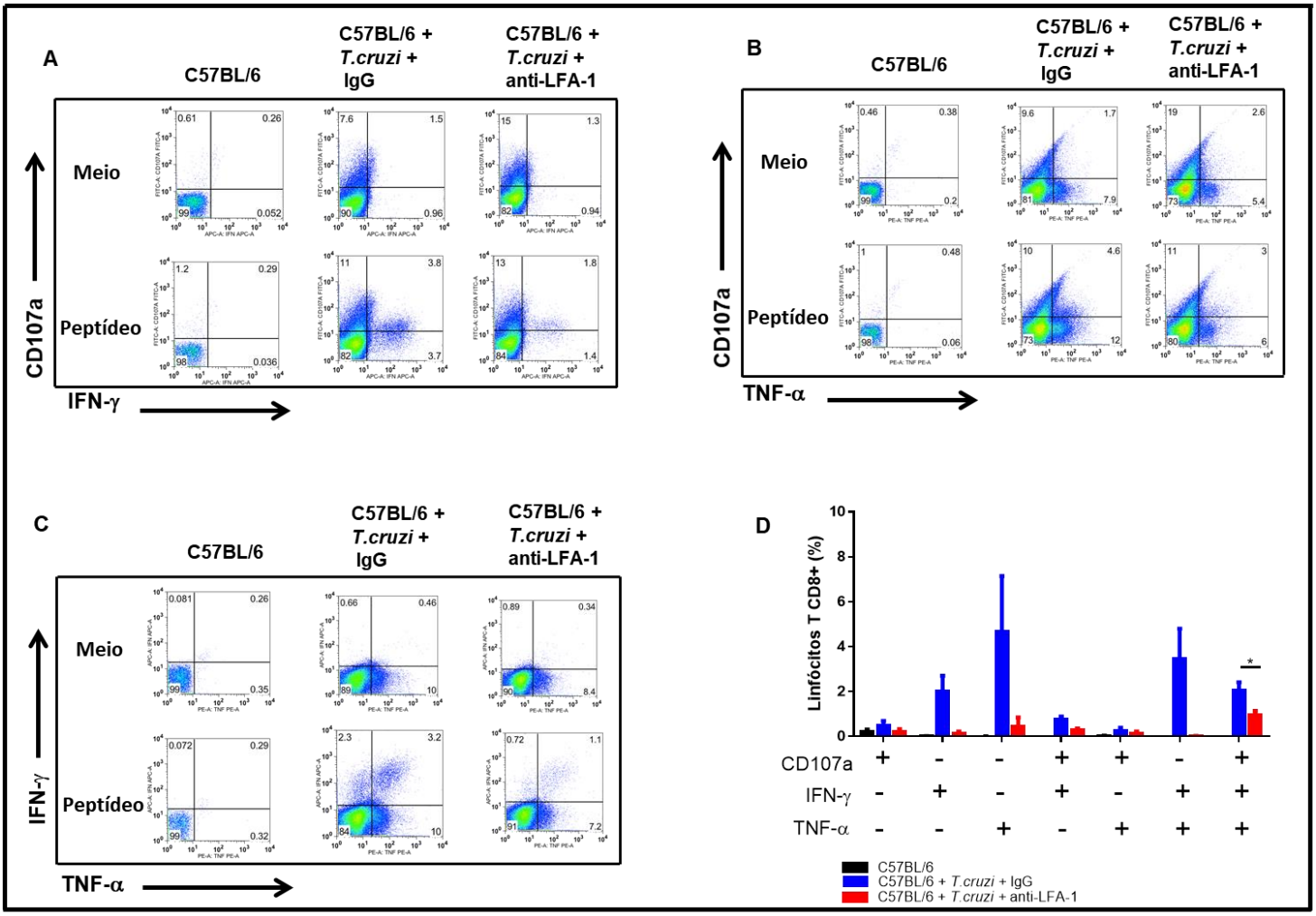

Figura 8. Análise do perfil funcional dos linfócitos T CD8+ específicos do baço, de camundongos C57BL/6 após infecção e tratamento com anticorpo anti-LFA-1. Camundongos C57BL/6 foram infectados e tratados com anti-LFA-1, os baços desses camundongos foram coletados e as células cultivadas com anti-CD107a e anti-CD28, na presença do peptídeo VNHRFTLV. Os dot-plots ilustram a frequência das combinações de degranulação, IFN-γ e TNF-α no baço (**Painéis A, B, C**). Na figura **D**, a análise de Boolean demonstra que o tratamento com o anticorpo anti-LFA-1 interferiu na polifuncionalidade das células T CD8+ específicas, do baço. Resultados são representativos de dois experimentos independentes. *p<0.01. Análise One Way ANOVA.

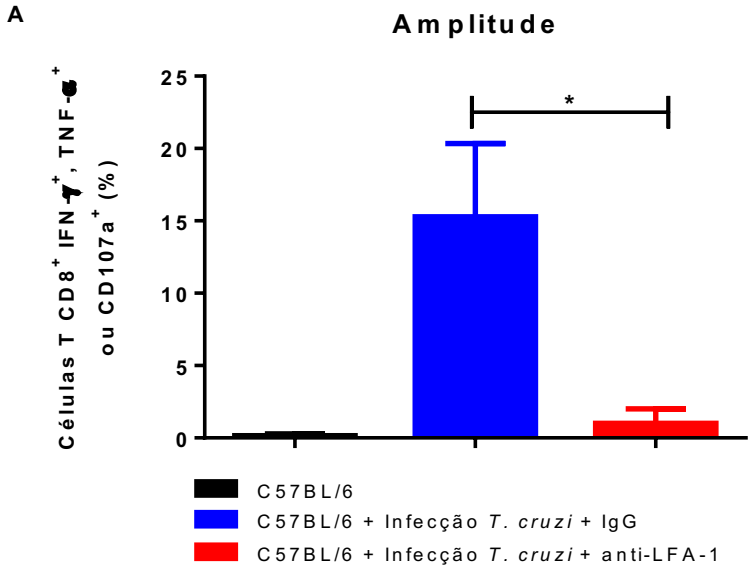

Figura 9. Amplitude da resposta imune dos linfócitos T CD8⁺ específicos do baço dos camundongos C57BL/6, infectados e tratados com o anticorpo monoclonal anti-LFA-1. Os resultados das frequências de linfócitos T CD8+ que secretam pelo menos uma das citocinas IFN-γ e TNF-α ou que degranulam são apresentados no gráfico A. O gráfico A representa o baço, e houve diferença na amplitude da resposta entre o grupo infectado e o grupo infectado e tratado com anticorpo anti-LFA-1. Resultados são representativos de dois experimentos independentes *p<0.05. Análise One Way ANOVA.

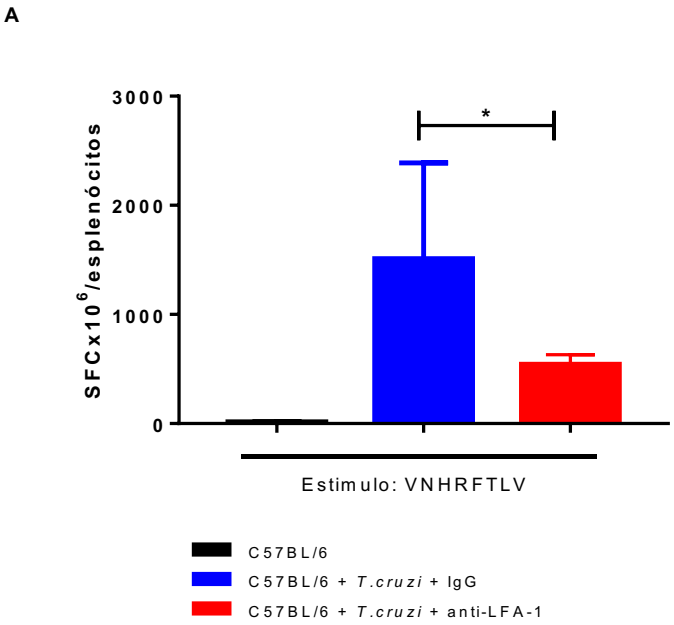

Figura 10. Quantificação do número de linfócitos T CD8$^+$ específicos secretores de IFN-γ no baço de camundongos C57BL/6 infectados e tratados com anticorpo monoclonal anti-LFA-1. Camundongos C57BL/6 foram infectados e tratados com anticorpo anti-LFA-1. As células do baço desses camundongos foram coletadas e o número de células produtoras de IFN-γ foram estimadas pela técnica de ELISPOT. A Indica o número de células produtoras de IFN-γ no baço, dos diferentes grupos e houve diferença na secreção de IFN-γ entre os grupos infectado e infectado e tratado com anti-LFA-1. Resultados são representativos de dois experimentos independentes. SFC: células formadoras de *spots* *p<0.02. Análise, One Way ANOVA.

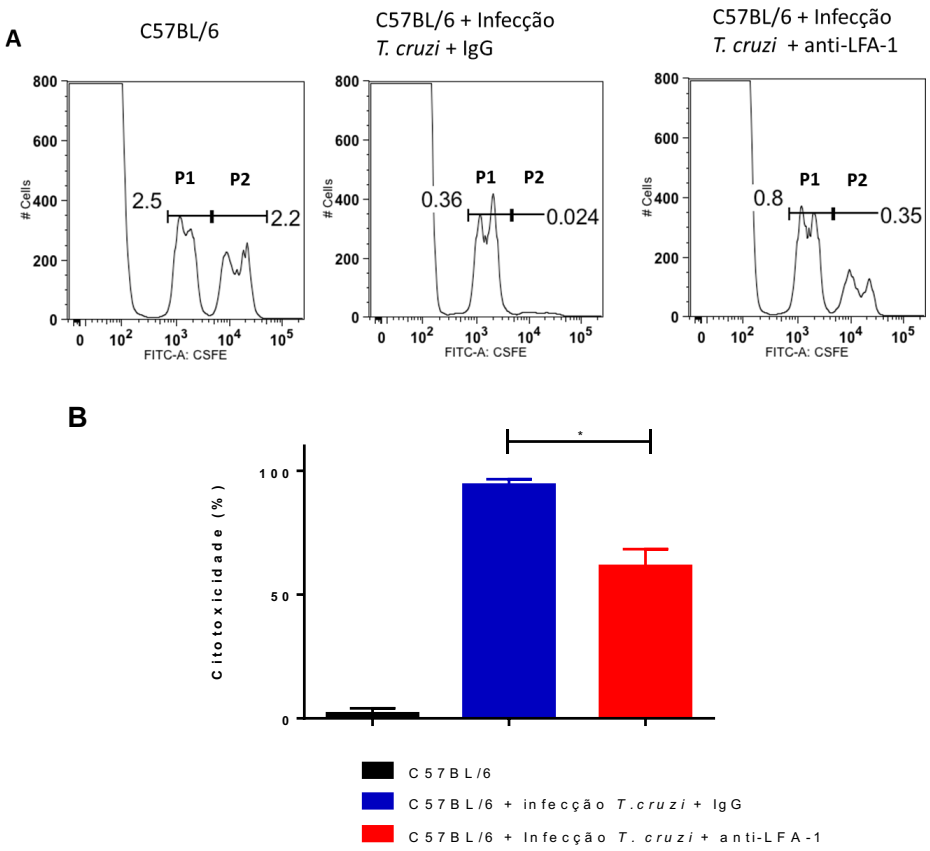

Figura 11. **O tratamento com o anticorpo anti-LFA-1 diminui a citotoxicidade *in vivo* das células T CD8^{+} específicas.** Esplenócitos de camundongos naive foram usados para a marcação de CFSE^{low} (1mM) e CFSE^{high} (10mM). A população de CFSE^{high} foi pulsada com o peptídeo VNHRFTLV. (**A**) Os histogramas representam os eventos de CFSE^{low} (P1) e CFSE^{high} (P2) de cada grupo. (**B**) Porcentagem de citotoxicidade das células T CD8+ específicas com média e desvio padrão de cada grupo. Resultados provenientes de dois experimentos independentes Análise One-Way ANOVA. *p<0,0001.

4.4 Imunofenotipagem das células T CD8+ totais, e avaliação, da integrina LFA-1 na diferenciação das células T CD8+ efetoras, após infecção com *T. cruzi* e o tratamento *in vivo* com anticorpo anti-LFA-1.

Ao verificar que as células T CD8+ possuem um comprometimento na sua polifuncionalidade e função efetora, após o bloqueio do LFA-1, verificamos se após o tratamento o fenótipo dessas células poderia estar afetados, como podemos observar, após o bloqueio do LFA-1 observamos uma diminuição na frequência do número de células específicas marcadas com o pentâmero H2K^{b}-VNHRFTLV, assim como o número absoluto de células T CD8 específicas, sendo essa redução estatisticamente significativa **(Figura 12 A e B)**. Em relação ao fenótipo, as células de camundongos infectados por se tratar de 15 dias após a infecção demonstram um perfil de células T efetoras (TE), caracterizado pela expressão de (CD44^{alto}, CD11a^{alto} CD62L^{baixo}, CD127^{baixo} e KLRG1^{alto}). Quando observamos esses marcadores no grupo infectado e tratado com o anti-FA-1, a média de intensidade de fluorescência (MIF) se assemelha aos de camundongos naive, representado pela linha vermelha, **(Figura 12 C)** demonstrando que o bloqueio do LFA-1 além de comprometer a polifuncionalidade e função efetora, interfere na diferenciação de células T CD8 após a infecção com o *T .cruzi*.

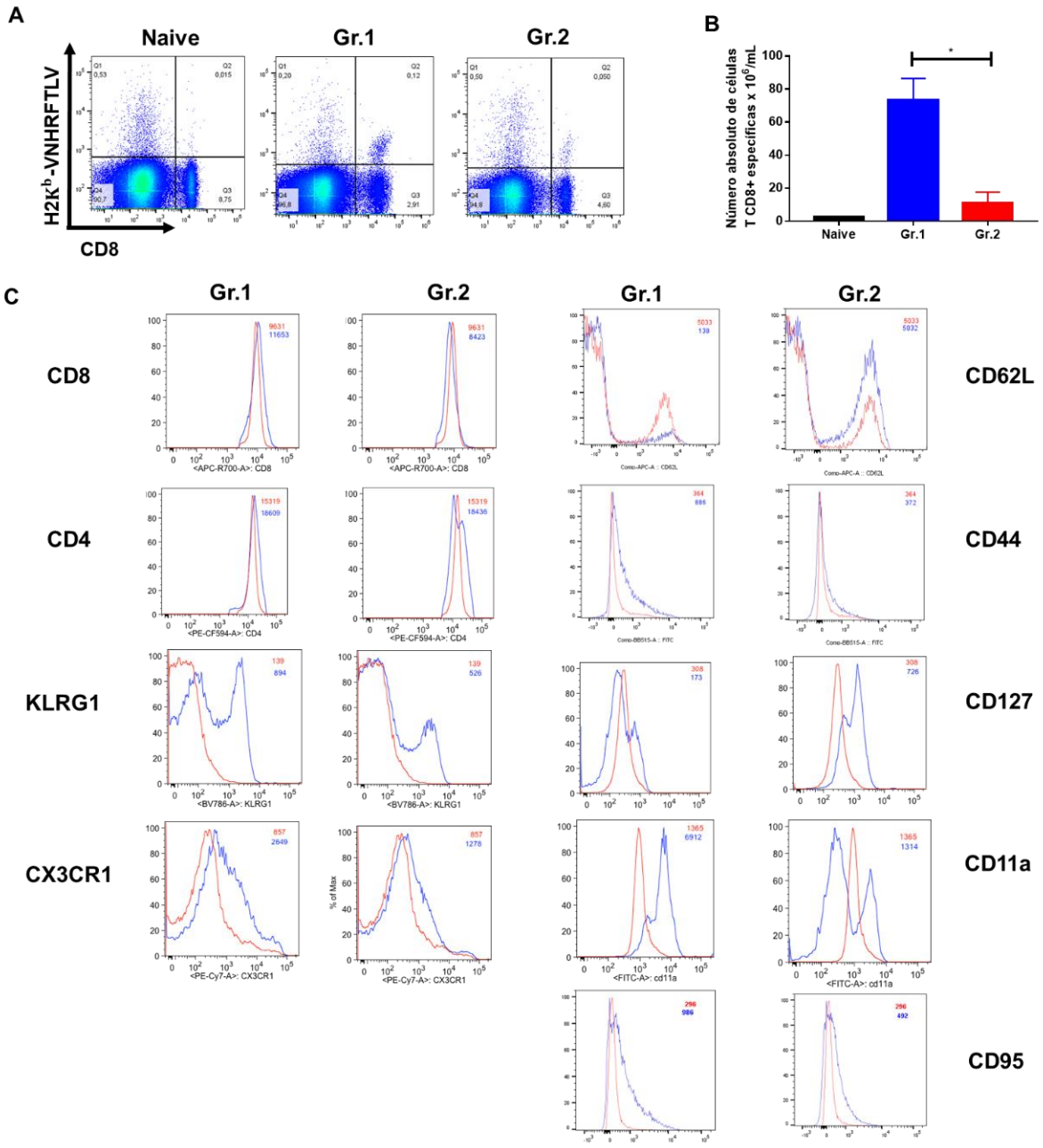

Gr.1 C57BL/6 + *T.cruzi* + IgG

Gr.2 C57BL/6 + *T.cruzi* + anti-LFA-1

Figura 12. Imunofenotipagem de linfócitos T CD8$^+$ de camundongos infectados e tratados com anticorpo anti-LFA-1. Camundongos C57BL/6 foram infectados e tratados com anti-LFA-1, os baços desses camundongos foram coletados e marcados com anti-CD8, pentâmero H2Kb-VNHRFTLV e os marcadores mencionados na figura. (**A**) temos os *dot plots* representativos de cada grupo os números representam a frequência de células específicas no baço. (**B**) o número total de linfócitos T CD8 foi estimado. (**C**) os histogramas são representados pela MIF de cada marcador analisado, em vermelho representa os animais naive e em azul os grupos 1 e 2. * p=0,012 Análise de One Way ANOVA. Resultado proveniente de dois experimentos independentes.

4.5 Avaliação da resposta imune das células T CD8+ totais após o tratamento *in vivo* com o anticorpo anti-LFA-1 em camundongos OT-I infectados com *T. cruzi* cepa Y-OVA.

Nos resultados descritos acima, foi demonstrado que no modelo de infecção de camundongos C57BL/6 ocorre uma diminuição em marcadores de degranulação como o CD107a e citocinas IFN-γ e TNF-α importantes na resposta imune frente ao parasito após tratamento com o anticorpo monoclonal anti-LFA-1. Com o objetivo de verificar se esse fenômeno aconteceria em outro modelo de infecção, analisamos a produção desses marcadores nas células T CD8+ específicas do baço de camundongos da linhagem OT-I, que são restritos apenas ao peptídeo OVA albumina, e infectamos os animais com a cepa y de *T. cruzi* expressando OVA. Esses animais também receberam o tratamento com o anticorpo monoclonal anti-LFA-1. A divisão dos grupos experimentais está descrita na **Tabela 3**. As técnicas de marcação intracelular e ELISPOT foram utilizadas para a detecção das citocinas mencionadas acima. Os *dot- plots* da **Figura 13 (painéis A-C)** representam células T CD8+ específicas secretoras de IFNγ, TNFα e que degranulam do baço dos diferentes grupos de camundongos, e como é observado houve diminuição na degranulação, produção de IFN-γ e TNF-α entre o grupo que recebeu o tratamento com o anticorpo monoclonal anti-LFA-1 e o grupo apenas infectado. Com relação à polifuncionalidade o grupo tratado com anti-LFA-1 teve uma diminuição da

polifuncionalidade e amplitude da resposta imune **(Figuras 13D e 14)**. O ensaio de ELISPOT confirmou que o tratamento com o anticorpo monoclonal anti- LFA-1, diminuiu a secreção de IFN-γ pelas células T CD8+ específicas **(Figura 15)** no modelo de infecção e tratamento com anti-LFA-1 em camundongos da linhagem OT-I, o que confirma todos os achados com relação a funcionalidade celular encontrados na linhagem C57BL/6.

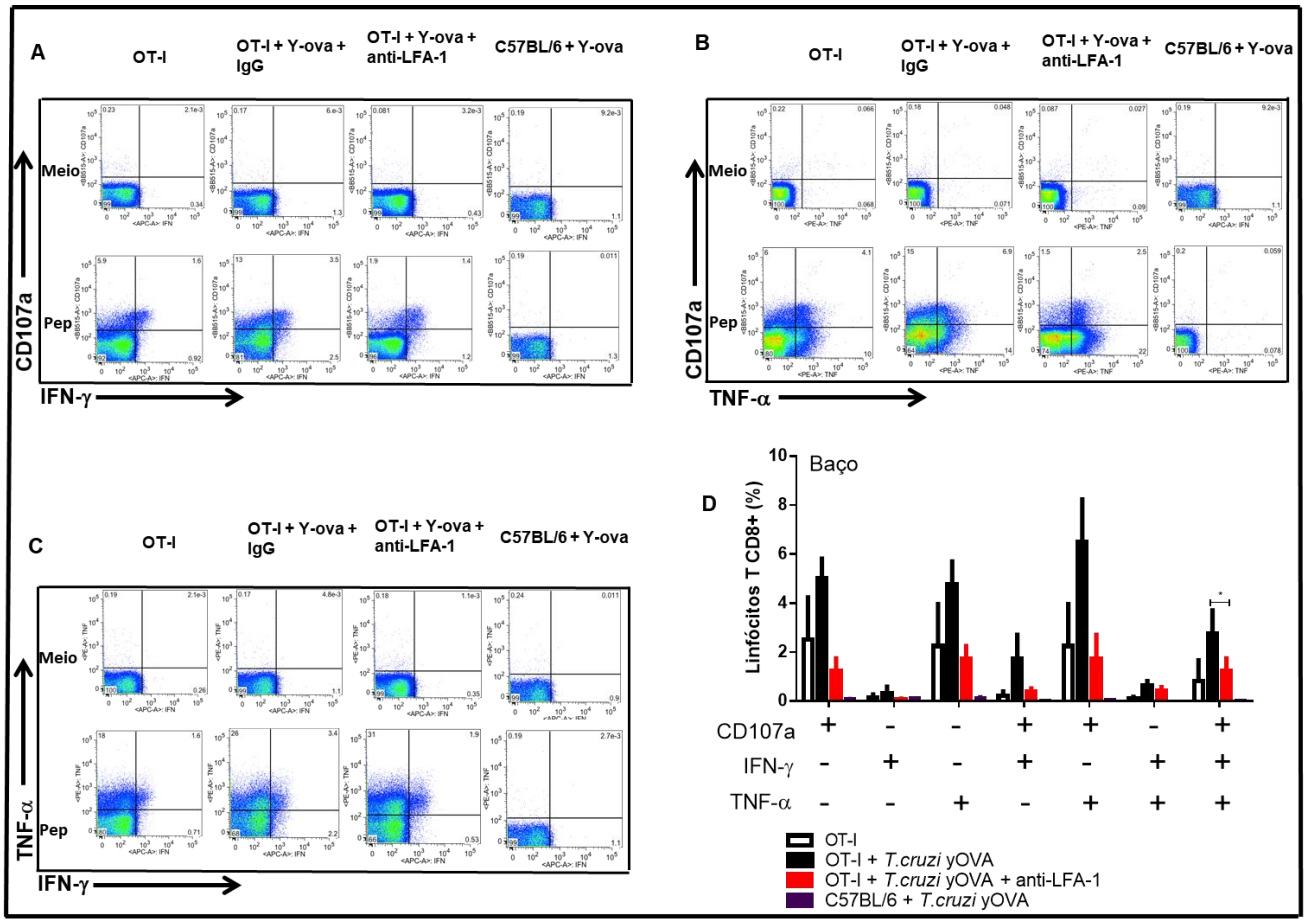

Figura 13. Análise do perfil funcional dos linfócitos T CD8⁺ específicos do baço, de camundongos OT-I após infecção e tratamento com anticorpo anti-LFA-1. Camundongos OT-I foram infectados e tratados com anti-LFA-1, os baços desses camundongos foram coletados e as células cultivadas com anti-CD107a e anti-CD28, na presença do peptídeo SIINFEKL Após 12 horas, as células foram marcadas com anti-CD8, fixadas, permeabilizadas e então incubadas com anti-IFN-γ, anti-TNF-α. As amostras foram lidas no FACS Canto II e analisadas no software Flojow (versão 9.4). Os dot-plots ilustram a frequência das combinações de degranulação, IFN-γ e TNF-α no baço (Painéis A, B, C). Na figura D, a análise de Boolean demonstra que o tratamento com o anticorpo anti-LFA-1 diminuiu a polifuncionalidade das células T CD8+ específicas, do baço. *p<0.05. Análise One Way ANOVA. Resultado proveniente de dois experimentos independentes.

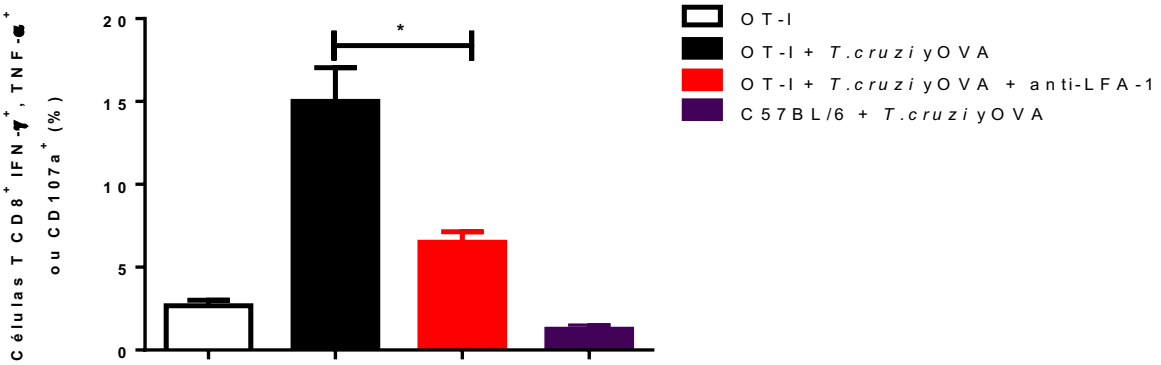

Figura 14. Amplitude da resposta imune dos linfócitos T CD8⁺ específicos do baço dos camundongos OT-I, infectados e tratados com o anticorpo monoclonal anti-LFA-1. Os resultados expressão as frequências de linfócitos T CD8+ que secretam pelo menos uma das citocinas IFN-γ e TNF- α ou que degranulam são apresentados no gráfico acima. O gráfico representa o baço, e houve diferença na amplitude da resposta entre o grupo infectado e o grupo infectado e tratado com anticorpo anti-LFA-1. *p<0.001. Análise One Way ANOVA. Resultados provenientes de dois experimentos independentes.

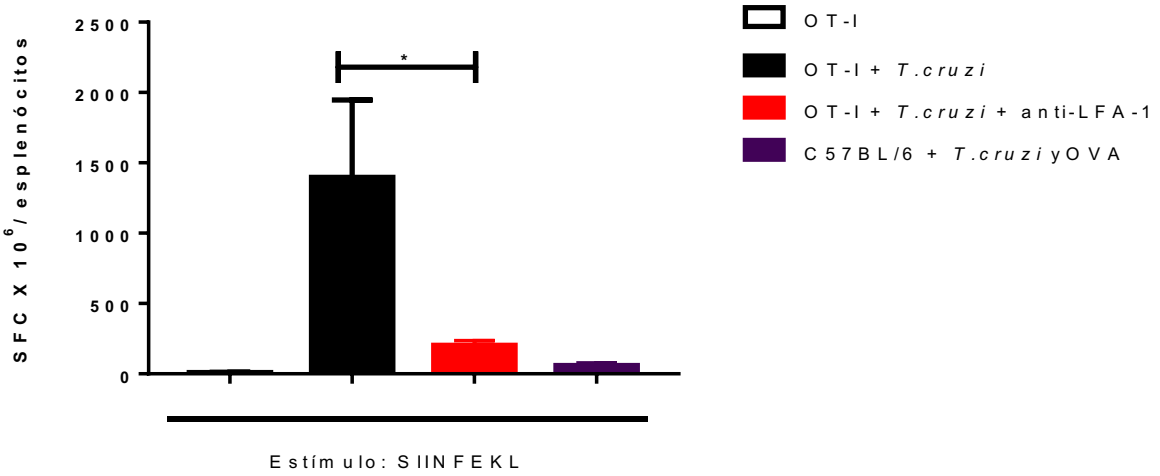

Figura 15. Quantificação do número de linfócitos T CD8⁺ específicos secretores de IFN-γ no baço de camundongos OT-I infectados e tratados com anticorpo monoclonal anti-LFA-1. Camundongos OT-I foram infectados e tratados com anticorpo anti-LFA-1. Foram coletados os

esplenócitos e estimou-se o número de células produtoras de IFN-γ após o estímulo do peptídeo SIINFEKL, por ELISPOT. O gráfico indica o número de células produtoras de IFN-γ no baço, dos diferentes grupos e houve diferença na secreção de IFN-γ entre os grupos infectado e infectado e tratado com anti-LFA-1. SFC: células formadoras de spots *p=0.0088. Análise, One Way ANOVA. Resultados provenientes de dois experimentos independentes.

4.6 Análise da expressão génica das células T CD8, T CD4, N.K e citocinas no tecido cardíaco de camundongos C57BL/6 infectados e/ou trados *in vivo* com anti-LFA-1.

Camundongos da linhagem C57BL/6 foram infectados e tratados conforme tabela 3 no 15º dia após a infecção o coração dos animais foi retirado, o RNA extraído e transformado em cDNA, para avaliar se ocorre uma diminuição da expressão das células T CD8, T CD4 células NK e das quimiocinas citotóxicas granzima B e perforina, além da expressão de *T. cruzi* (**Figura 16 A-G**) após o bloqueio da integrina LFA-1. Nossos resultados demonstram a diminuição da expressão de todas as moléculas analisadas coração no grupo tratado com anti-LFA-1 em relação ao grupo apenas infectado, concomitantemente demonstram diminuição na expressão genica de perforina e granzima B no grupo tratado com anti-LFA-1 em relação ao grupo infectado, sendo ambas diminuições estaticamente significativa, em relação a quantidade de parasito os resultados encontrados corroboram com os achados encontrados na quantificação do parasitismo tecidual demonstrando o aumento do parasito no grupo tratado com LFA-1.

A

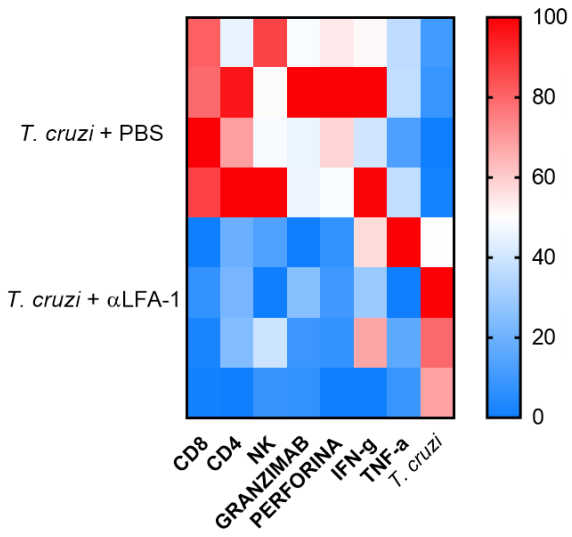

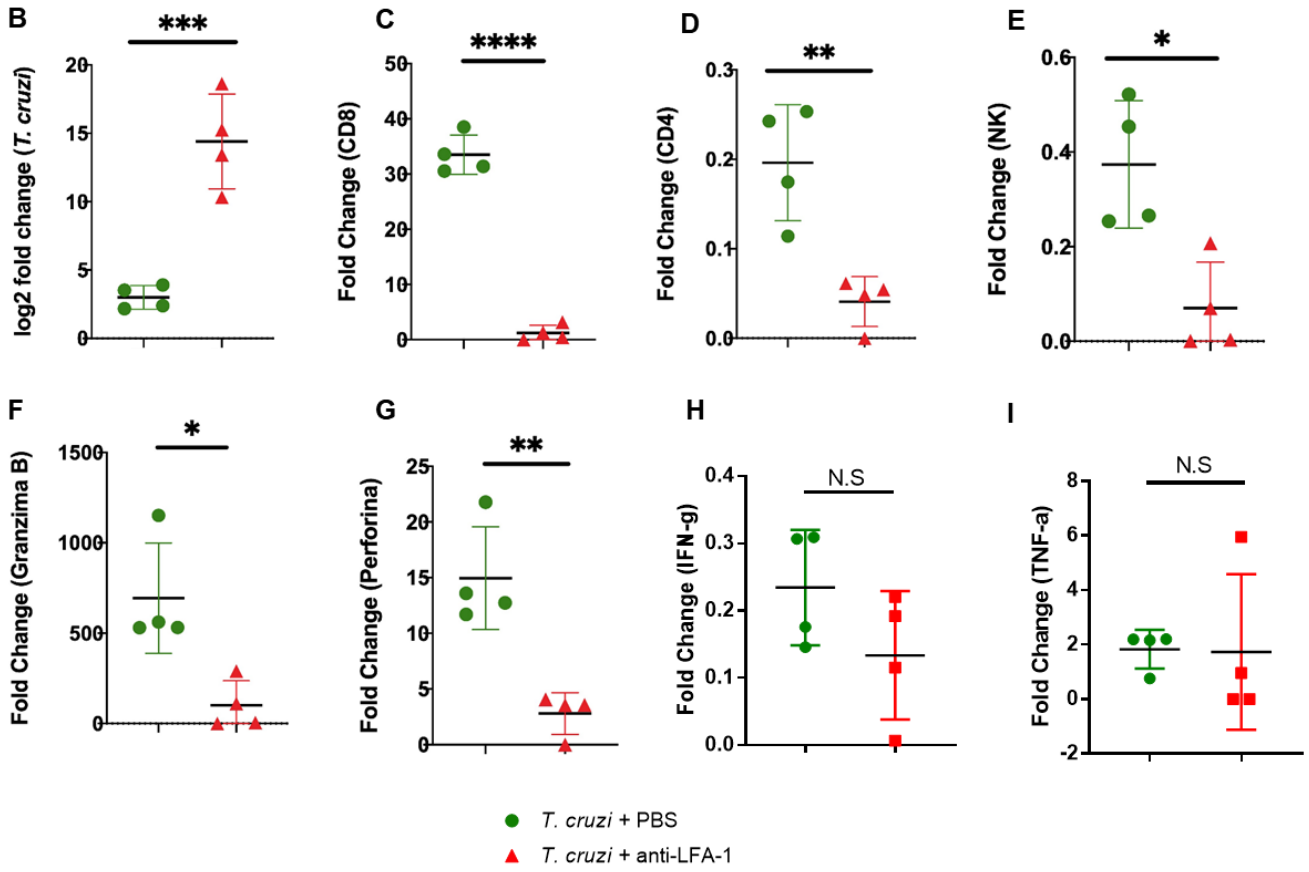

Figura 16. Expressão gênica das células T CD8, T CD4, NK, granzima B, perforina e T. cruzi no coração de camundongos C57BL/6 infectados e tratados com anticorpo monoclonal anti-LFA-1. Camundongos C57BL/6 foram infectados e tratados com anticorpo anti-LFA-1. O cDNA foi extraído das células cardíacas e quantificados a expressão das moléculas acima após a normalização com GAPDH. O gráfico (**A**) indica o quanto essas moléculas estão aumentadas a expressão delas em relação ao seu nível basal. (**B**) inidica aumento de T. cruzi no grupo tratado com LFA-1. (**C**) indica diminuição na expressão de células T CD8. (**D**) inidica diminuição na expressão de células T CD4. (**E**) inidica diminuição na expressão de células NK. (**F**) indica diminuição na expressão de granzima B. (**G**) inidica diminuição na expressão de perforina. (**H**) expressão de IFN-γ (**I**) expressão de TNF-a Ambas diminuições foram no grupo infectado e tratado com anti-LFA-1 em relação ao grupo apenas infectado *p=0.0106; **p=0.0028; ***p=0.0007 *****p<0.0001 n.s= não estatístico. Analise teste T. Resultados provenientes de um experimento independente.

4.7 Análise da expressão gênica das células T CD8, T CD4, NK, granzima B e perforinas nas células cardíacas de camundongos CD4 e CD8 K.O, após a transferência de células T CD8 provenientes de camundongos C57BL/6 infectados e/ou tratados *in vivo* com anti-LFA-1.

Camundongos da linhagem C57BL/6, B6.129S2- Cd8atm1Mak/J (CD8 K.O) e B6.129S2-Cd4tm1Mak/J (CD4 K.O) foram infectados e tratados conforme tabela 2. No 10º dia após a infecção o baço dos animais C57BL/6 foi retirado e as células T CD8 foram isoladas e transferidas para os camundognos CD8 K.O, já as células T CD4 foram isoladas e transferidas para os camundongos CD4 K.O. Após 7 dias de transferência os animais foram eutanasiados e retirados os corações, quatro animais o coração foi embebido no tissue-tek para posterior cortes no criostato e marcação de DAPI, T CD8 e T CD4, os outros quatro o RNA foi extraído e transformado em cDNA para avaliação do bloqueio da integrina LFA-1 na migração linfocitária. Nossos resultados demonstram a diminuição da expressão das moléculas analisadas no coração do grupo tratado com anti-LFA-1 em relação ao grupo apenas infectado, além da diminuição na expressão gênica de perforina e granzima B no grupo tratado com anti-LFA-1 em relação ao grupo infectado, após a transferência adotiva das células T CD8 e T CD4, sendo ambas diminuições estaticamente significativa (**Figura 17 A-F e 18 A-F**)

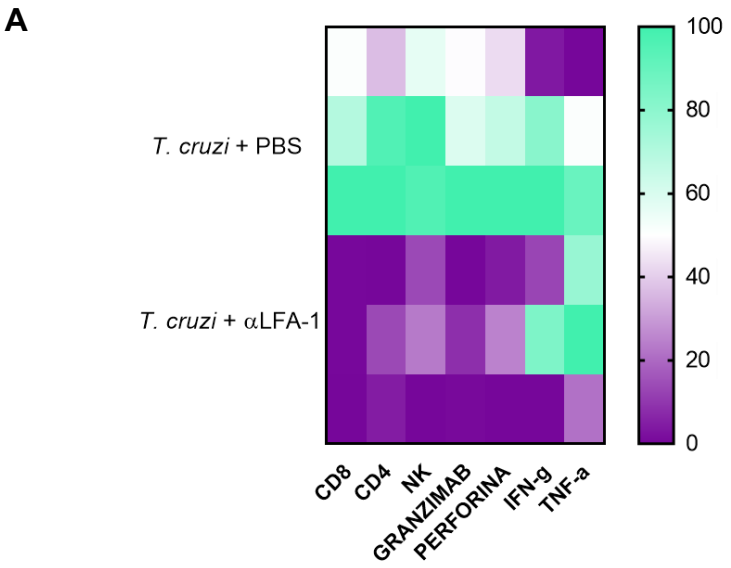

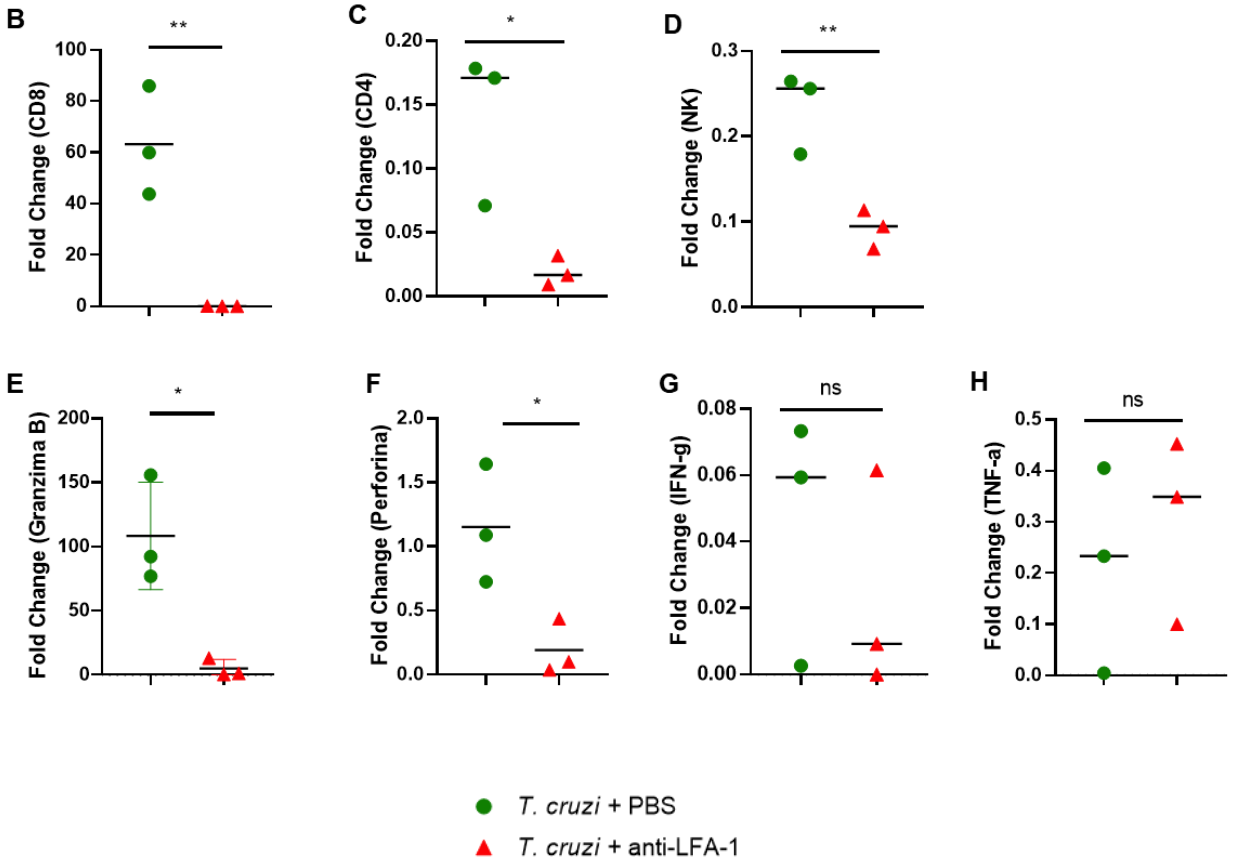

Figura 17. Expressão gênica das células T CD8, T CD4, NK, granzima B, perforina no coração de camundongos CD8 K.O após a transferência de células T CD8 proveninetes de camundongos C57BL/6 infectados e tratados com anticorpo monoclonal anti-LFA-1. Células T CD8 foram isoladas de camundongos C57BL/6 previamente infectados e tratados com anticorpo anti-LFA-1 e transferidas para os camundognos CD8 K.O. O cDNA foi extraído das células cardíacas e quantificados a expressão das moléculas acima após a normalização com GAPDH. O gráfico **A** indica o quanto essas moléculas estão aumentadas a expressão delas em relação ao seu nível basal. **B** indica diminuição na expressão de células T CD8. **C** inidica diminuição na expressão de células T CD4. **D** inidica diminuição na expressão de células NK. **E** indica diminuição na expressão de granzima B. **F** inidica diminuição na expressão de perforina. **G** expressão de IFN-γ **H** expressão de TNF-a. Ambas diminuições foram no grupo infectado e tratado com anti-LFA-1 em relação ao grupo apenas infectado *p< 0.0135 **p< 0.0094; Analise teste T. Resultados provenientes de um experimento independente.

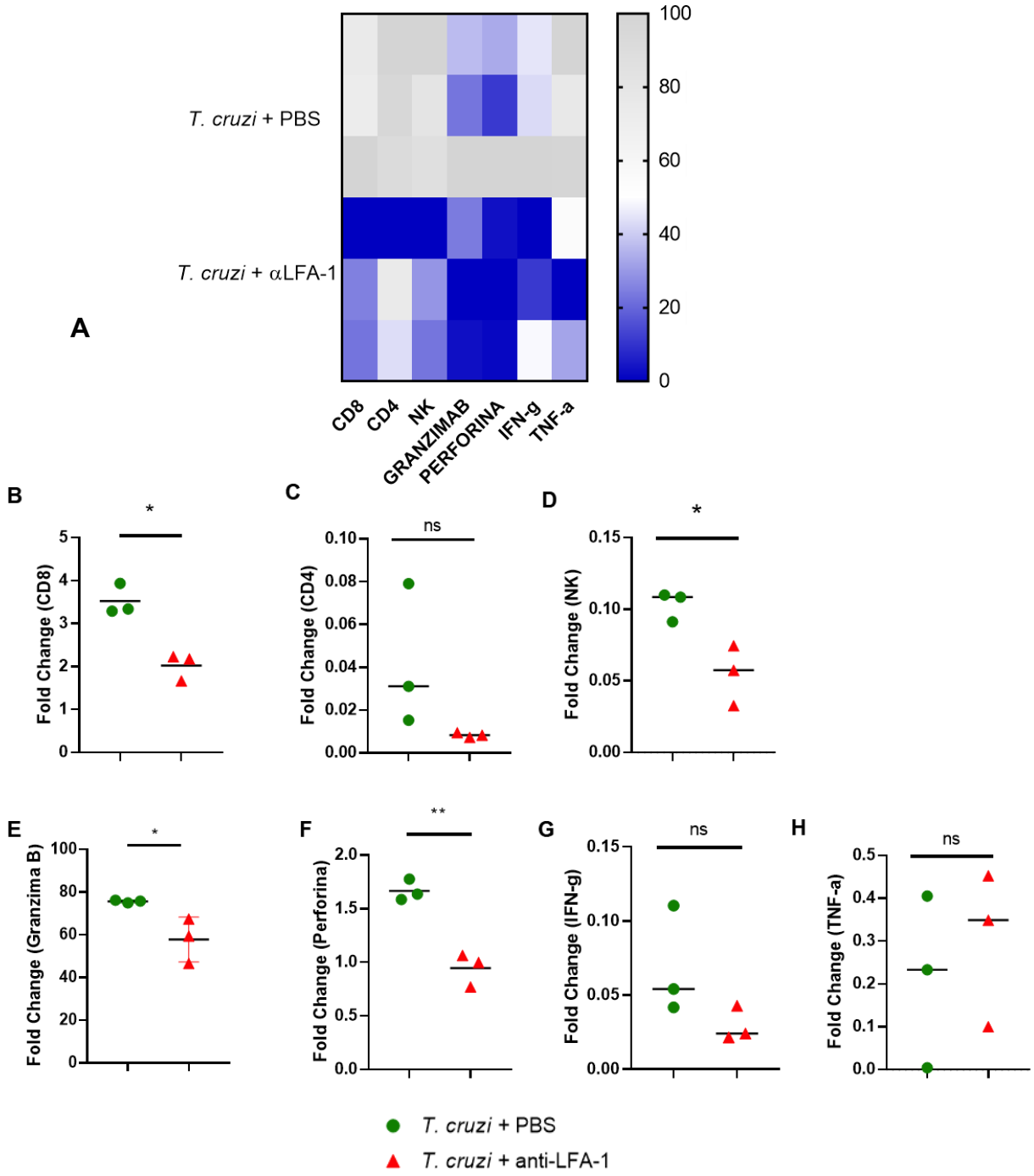

Figura 18. Expressão gênica das células T CD8, T CD4, NK, granzima B, perforina no coração de camundongos CD4 K.O após a transferência de células T CD4 proveninetes de camundongos C57BL/6 infectados e tratados com anticorpo monoclonal anti-LFA-1. Células T CD4 foram isoladas de camundongos C57BL/6 previamente infectados e tratados com anticorpo anti-LFA-1 e transferidas para os camundognos CD4 K.O. O cDNA foi extraído das células cardíacas e quantificados a expressão das moléculas acima após a normalização com GAPDH. O gráfico **A** indica o quanto essas moléculas estão aumentadas a expressão delas em relação ao seu nível basal. **B** indica diminuição na expressão de células T CD8. **C** inidica diminuição na expressão de células T CD4. **D** inidica diminuição na expressão de células NK. **E** indica diminuição na expressão de granzima B. **F** inidica diminuição na expressão de perforina. **G** expressão de IFN-γ **H** expressão de TNF-α. Ambas diminuições foram no grupo infectado e tratado com anti-LFA-1 em relação ao grupo infectado. *p<0,0497, ** p<0,0024. Analise de teste T. Resultado proveniente de um experimento independente

4.8 Análise da parasitemia sanguínea e sobrevivência em camundongos CX3CR1$^{gfp/gfp}$ infectados com a cepa Y de *T. cruzi.*

Outra molécula analisada foi o CX3CR1, Para analisar se a aussencia do receptor de quimiocina CX3CR1 interfere na proteção contra o parasito intracelular *T. cruzi*, os camundongos CX3CR1gfp/gfp foram produzidos e genotipados, após 8 semanas os animais foram infectados com 10^4 formas de cepa Y de *T. cruzi*. A parasitemia sanguínea foi acompanhada do 6º dia até o 15º dia após a infecção e em geral houve um discreto aumento do parasitismo, porém esse aumento não foi estatisticamente significativo (p=0.0601659). Em relação ao grupo controle camundongo C57BL/6 infectado. **(Figura 19 A**). Já em relação à sobrevivência (**Figura 19 B)** todos os camundongos de ambos os grupos sobreviveram a infecção. Esses resultados nos levaram a investigar se as células T CD8 estariam deficientes em alguma produção de citocina, como por exemplo o IFN-γ que é de suma importância nas respostas do tipo Th1.

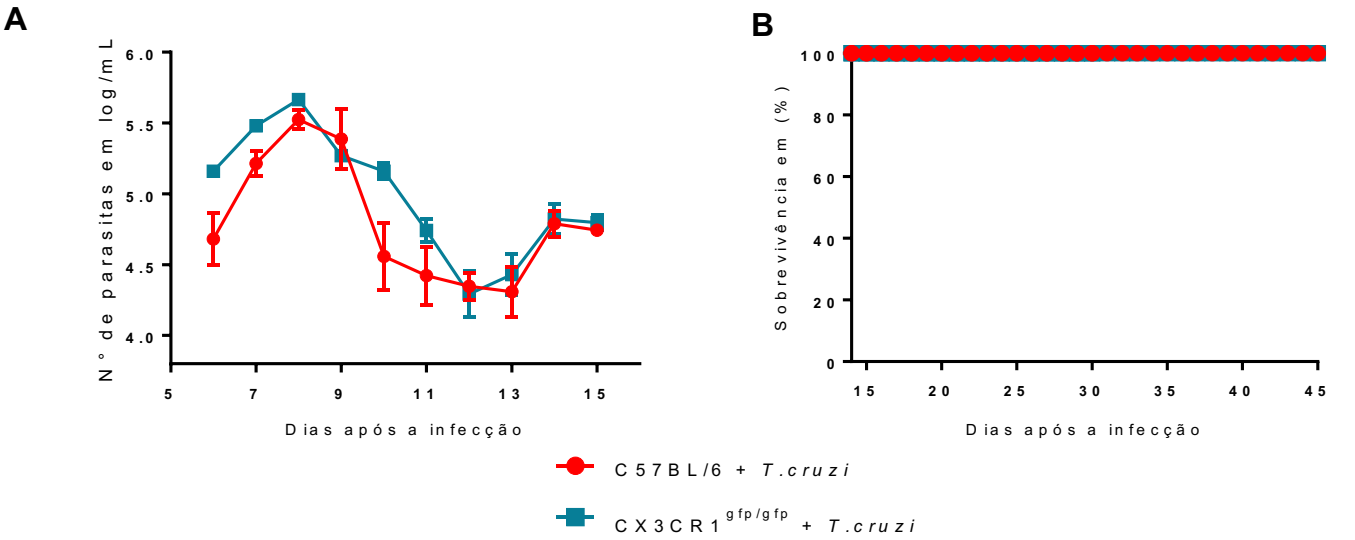

Figura 19. Análise da parasitemia sanguínea e sobrevivência em camundongos CX3CR1$^{gfp/gfp}$ infectados com a cepa Y de *T. cruzi*. Camundongos CX3CR1$^{gfp/gfp}$ foram infectados e observado a parasitemia sanguínea e sobrevivência. Na figura (**A**) temos a sobrevivência e a diferença entre os grupos não foi estatisticamente significativa (p=0.0601659), Na figura (**B**) temos a sobrevivência e todos os animais sobreviveram a infecção experimental pelo *T. cruzi*. Os resultados são provenientes de dois experimentos.

O ensaio de ELISPOT foi utilizado para verificar se a ausência da molécula CX3CR1 estaria comprometendo a secreção de IFN-γ, como podemos observar na **(Figura 20)**, a ausência dessa molécula ocorre uma pequena diminuição na produção de IFN-γ, porém não é estatisticamente significante demonstrando que a falta do CX3CR1 não compromete a secreção de IFN-γ no modelo de infecção com *T. cruzi*.

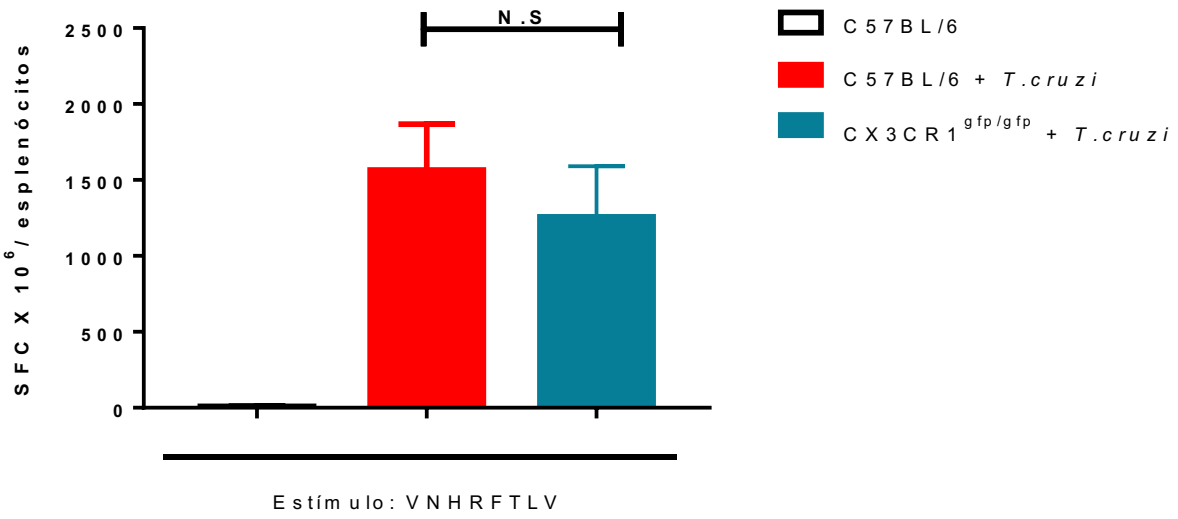

Figura 20. Avaliação da secreção de IFN-γ em camundongos CX3CR1$^{gfp/gfp}$ infectados com a cepa Y de *T. cruzi*. Camundongos CX3CR1$^{gfp/gfp}$ foram infectados com cepa y de *T. cruzi*. As células do baço desses camundongos foram coletadas e o número de células produtoras de IFN-γ foram estimadas pela técnica de ELISPOT após o estímulo do peptídeo VNHRFTLV. O gráfico indica o número de células produtoras de IFN-γ no baço, dos diferentes grupos e não houve diferença entre os grupos. SFC: células formadoras de spots N.S = não estatístico p=0.3072. Análise, One Way ANOVA. Resultados provenientes de dois experimentos independentes.

5. DISCUSSÃO

No presente trabalho, a integrina LFA-1 e os receptores de quimiocina CXCR3 e CX3CR1 foram objetos de estudo para analisar a importância da ativação de células T CD8+ específicas geradas pela infecção por *T. cruzi*. As integrinas, quimiocinas e os seus receptores apresentam relevante papel na ativação, co-estimulação, diferenciação e no recrutamento de células para sítios de injúria (LUSTER, *et al*., 2005; WALLING & KIM, 2018), bem como na resistência à infecção (MACHADO, *et al*., 2000; TEIXEIRA, *et al*., 2002). Em vista disso, infectamos os camundongos da linhagem C57BL/6 e tratamos com anti-LFA-1 ou anti-CXCR3 (**Figura 3**). O tratamento com essas moléculas torna os camundongos antes resistentes em suscetíveis à infecção, ilustrando a importância dessas moléculas na resposta imune.

Sabe-se que o bloqueio do LFA-1 e CXCR3 levam a um aumento na parasitemia sanguínea e consequentemente o óbito dos camundongos, sendo assim, o próximo passo foi investigar se tal bloqueio estaria relacionado também com o comprometimento de outros órgãos como o coração, baço, fígado e tecido adiposo. Em relação a isso, nossos resultados apontaram que no grupo dos animais tratados com anti-LFA-1 ou anti-CXCR3, houve uma diminuição no controle da infecção, demonstrado por meio do aumento do DNA do parasito nos tecidos supracitados (**Figura 4 A-D e 5 A-D**). Já em relação ao tecido cardíaco em particular, observou-se um aumento no número de ninhos de amastigota nos grupos dos animais tratados com os anticorpos em comparação ao grupo infectado (**Figura 6 e 7**). Tais resultados sugerem que essas moléculas estão envolvidas não somente na ativação como na migração das células T $CD8^+$ para o local de infecção.

O receptor de quimiocina CXCR3 e a integrina LFA-1 também foi avaliado quanto ao seu papel na imunidade em outros protozoários patogênicos, incluindo *Leishmania* e *Plasmodium*, e a função dessas moléculas diferem dependendo do parasito, a via de infecção e o local examinado (COHEN, *et al*., 2013; KNIGHT, *et al*., 2014; MCNAMARA, *et al*., 2017). Por exemplo, camundongos deficientes para

CXCR3-/- exibem deficiência na produção de IFN-γ e aumento do desenvolvimento da lesão durante a infecção cutânea *Leishmania major*, embora os camundongos *knockout* não são mais suscetíveis à infecção hepática por *Leishmania donovani* (ROSAS, *et al*., 2005; BARBI, *et al*., 2007).

No modelo de *T. cruzi* a molécula CXCR3 demonstrou-se fundamental para o controle da carga parasitária, além da produção de células T CD8 específicas, ativação e polifuncionalidade dessas células (PONTES FERREIRA *et al.*, 2020). Em outro modelo experimental, o receptor CXCR3 e os seus ligantes promovem a inflamação cerebral e mortalidade durante infecção experimental por malária, demonstrando ser importante durante as resposts imunológicas em outros modelos. (CAMPANELLA, *et al*., 2008; NIE, *et al.,* 2009). Com relação ao LFA-1, no modelo de camundongos A/Sn que foram imunizados, infectados com *T. cruzi* e tratados com anti-LFA-1 foram encontrados resultados similares em relação ao parasitismo sanguíneo e tecidual (FERREIRA *et al*., 2017)

Para explicar o porquê esses animais não conseguem controlar a carga parasitária após o bloqueio da integrina LFA-1 , foi analisado se a função efetora da célula T CD8+ estava comprometida, sabe-se que para a resposta imune ser efetiva contra parasitos intracelulares é necessária à produção de inúmeras quimiocinas e citocinas, dentre as citocinas o IFN-γ tem um papel importante após a infecção pelo *T. cruzi* (ALENCAR, *et al*., 2009), por essa razão foi feito o ensaio *intracellular staining* (ICS) e nossos resultados demonstram que após a infecção e tratamento com o anti-LFA-1 ocorre redução na frequência das células T $CD8^+$ com o perfil polifuncional (**Figura 8 e 9**), também foi feito o ensaio de ELISPOT (**Figura 10**) que corrobora com os achados do ICS demonstrando a diminuição na secreção de IFN-γ.

Esses resultados sugerem que o LFA-1 tem um papel fundamental na interação célula a célula, tendo em vista que as integrinas possuem um importante papel nas interações célula-célula e célula-matriz extracelular,essas interações são responsáveis pela transdução de sinal intracelular que culmina na migração (HOGG, *et al*., 2003) e na formação da sinapse imunológica (DUSTIN., 2009). De acordo com REISMAN e colaboradores (2011), animais da linhagem C57BL/6 que receberam enxertos de pele de camundongos BALB/c e tratados com anti-LFA-1 apresentam uma diminuição no número de células produtoras de TNF e IFN-γ quando comparados ao grupo sem tratamento.

Em modelo de infecção camundongos da linhagem C57BL/6 que foram infectados com o vírus da coriomeningite linfocítica (LCMV) e após as células T CD8 efetoras terem sido reestimuladas *ex vitro* por diversos peptídeos, tiveram redução na sua secreção de TNF-α e/ou IFN-γ no grupo tratado com anti-LFA-1 em relação ao grupo controle (PERRO *et al*., 2020). De modo a comparar os resultados encontrados nos animais C57BL/6, utilizamos um modelo animal que não responderia ao antígeno do *T. cruzi* e sim o da OVA, a fim de verificar se o tratamento com anti-LFA-1 estaria comprometendo as células T CD8 em outro modelo experimental. Os animais transgênicos OT-I, pousem um receptor nas células T CD8, com alta especificidade para os peptídeos OVA (MIYAGAWA *et al*., 2010). Estes foram infectados com a cepa Y-OVA e receberam o tratamento anti-LFA-1, os resultados obtidos (**Figuras 13, 14 e 15**) corroboram com os achados no modelo de C57BL/6 em relação a polifuncionalidade da célula e secreção de IFN-γ, demonstrando assim, de fato que o LFA-1 exerce um papel fundamental na função efetora, polifuncionalidade e secreção de citocinas nas células T CD8.

Com base nos resultados anteriores, verificamos que, a citotoxicidade, uma das principais funções da célula T CD8, estava comprometida após o bloqueio do LFA-1, e como demonstrado na (**Figura 11**) a redução da função celular fora estimada em 40%, quando comparado ao grupo apenas infectado. Resultados similares foram encontrados em células T CD8 de humanos na presença do anticorpo anti-LFA-1 (ANIKEEVA, *et al.*, 2005).

Recentemente nosso grupo de estudo demonstrou em outro modelo experimental que consiste na imunização, infecção e tratamento com anti-LFA-1 a ocorrência do comprometimento da citotoxicidade exercida pelas células T CD8 (FERREIRA, *et al.,* 2017). Essa redução deve-se ao fato do LFA-1 atuar como um mediador de contato entre as membranas das células-alvo e das células T (PETIT *et al.,* 2016).

Nosso grupo conduziu, anteriormente, um estudo de fenótipo celular com base na expressão de moléculas de superfície de células T efetoras, como $CD44^{alto}$, $CD11a^{alto}$ $CD62L^{baixo}$, $CD127^{baixo}$ e $KLRG1^{alto}$ (Vasconcelos *et al*., 2012). De acordo com estes resultados obtidos, o presente trabalho avaliou se LFA-1 alteraria o fenótipo das células T CD8, uma vez esta integrina atua na co-estimulação durante a ativação das células T CD8 (BACHMANN *et al*., 1997) Assim, analisamos a

expressão dos mesmos marcadores de superfície anteriormente descritos, frente ao tratamento com ant-LFA-1.

Com base nos resultados encontrados na (**Figura 12**) notou-se que o bloqueio do LFA-1 reduz a indução de células T CD8+ específicas, além de prejudicar o perfil das células, se assemelhando a MIF dos animais do grupo naive. Corroborando com os resultados obtidos anteriormente (Vasconcelos *et al*., 2012), observamos uma supra regulação para o CD95 (receptor de apoptose FAS) da molécula CD 95 em linfócitos T CD8 no grupo de animais infectados. Acreditamos que a diminuição da expressão de CD95 nos animais infectados/tratados com anti-LFA-1, esteja relacionado com a diminuição da expressão dos marcadores de células T efetoras anteriormente citados. Tal redução de densidade em superfície celular da molécula CD95, sugerindo que o tratamento com anti-LFA-1 induz uma menor ativação celular, consequentemente uma menor morte das mesmas.

No contexto da migração celular, a interação entre a integrina LFA-1 e seu ligante ICAM-1, tem um papel determinante na regulação da direção da migração das células T no vaso sanguíneo (WALLING e KIM., 2018), analisamos então se o nosso tratamento com o LFA-1 estaria interferindo na migração das células para o tecido cardíaco. Os resultados obtidos na (**Figura 16**) demonstraram o comprometimento na migração celular das células T CD8, T CD4 e NK para o coração, além disso ocorre a diminuição na expressão da proteína citotóxica perforina e da enzima granzimas no grupo tratado com relação ao grupo infectado apenas. Esse fenômeno pode explicar o motivo da maior expressão gênica do *T. cruzi* após o bloqueio do LFA-1. Com relação expecificamente a perforina, em outro modelo experimental, envolvendo o vírus ebola, apresentam um importante papel as células T CD8 infectadas com o vírus, que demonstraram-se dependentes de perforina para o desenvolvimento de proteção imunológica mais eficaz. (GUPTA *et a*l., 2005)

A partir dos resultados mencionados previamente, buscamos avaliar se apóa a transferência adotiva das células T CD8 e T CD4 estariam ainda comprometidas a migração celular para o tecido alvo, após o tratamento com anti-LFA-1, como observado nas (**Figura 17 e 18**) pudemos observar, de uma maneira geral há um comprometimento na migração dessas células para o tecido cardíaco além da redução da expressão de perforina e granzimas no grupo que recebeu o tratamento.

De acordo com DOTIWALA *et al.* (2016) pacientes infectados pelo *T. cruzi* possuem células NK citotóxicas e linfócitos T citotóxicos que expressam granzimas e perforina, demonstrando a importância desses mediadores para resposta imune. Sabe-se que macrófagos expressam amplamente TNF-α em processos inflamatórios e na resposta imune contra T. cruzi (LAFUSE *et al*., 2020; CRONEMBERGER-ANDRADE *et al*., 2020) entretanto, de modo interessante, não observamos diferença entre a expressão de TNF-α e IFN-γ. Com relação ao IFN-γ apesar de ocorrer uma diminuição na expressão gênica das células T CD8, T CD4 e NK no grupo tratado com anti-LFA-1, essas células podem estar produzindo IFN-γ o que leva a expressão desse gene.

Quanto ao receptor de quimiocina CX3CR1, sua expressão está relacionada com o grau de diferenciação das células T CD8+ efetoras, além de um marcador nas subpopulações das células T CD8+ em infecções com o vírus LCMV (GERLACH *et al*., 2016; SANDU *et al*., 2020). Avaliamos se a ausência do receptor CX3CR1$^{gfp/gfp}$ estaria atuando sobre o parasitismo sanguíneo, e portanto, na sobrevivência dos animais infectados com *T. cruzi*. Como observado na (**Figura 19**) embora a carga parasitária dos animais knockouts ser superior aos animais do grupo controle no 10º dia após a infecção, mas não difere, ainda assim, a ausência do receptor não foi elemento preponderante na sobrevivência dos animais.

Esses achados nos levaram a investigar se a ausência do receptor poderia impactar na produção da citocina IFN-γ. Na (**Figura 20**) observamos que a produção dessa de IFN-γ é bem similar entre os grupos. Tendo em vista o nível de expressão do receptor CX3CR1 está relacionado com o recrutamento dos linfócitos T efetores com atividade citotóxica (NISHIMURA *et al*., 2002). Apesar dos resultados obtidos neste trabalho, demonstrarem que o CX3CR1 não parecer tão relevante para a resposta contra o *T. cruzi* da cepa Y, estudos futuros avaliarão se a ausência do receptor CX3CR1 altera a função efetora e citotoxicidade e fenótipo das células T CD8$^+$.

Em conjunto, nossos resultados demonstram que o receptor de quimiocina CXCR3 é importante para o controle da infecção pelo *T. cruzi* e sobrevivência dos animais, além disso, a integrina LFA-1 tem um papel crucial na migração, diferenciação, citotoxicidade e função efetora das células T CD8$^+$ específicas no

âmbito da infecção pelo *T. cruzi.* Apesar do receptor de quimiocina CX3CR1 não demonstrar inicialmente um papel crítico na imunidade protetora é necessário pesquisar seu papel na diferenciação das células T CD8 contra o patógeno intracelular *T. cruzi.*

6. CONCLUSÃO

O bloqueio da integrina LFA-1 e do receptor de quimiocina CXCR3 tornam os camundongos antes resistentes à infecção pelo *T. cruzi*, suscetíveis a ela. No caso do bloqueio do LFA-1 a função efetora e a citotoxicidade das células T $CD8^+$ estão diminuídas, além disso o LFA-1 demonstrou um papel fundamental para migração celular para os locais da infecção. Já em relação ao fenótipo das células T CD8 após o bloqueio da molécula ocorre o comprometimento da diferenciação das células T, demonstrando que essas moléculas são críticas para a resposta imune protetora, demonstrando que o LFA-1 pode ser um forte candidato para o design de vacinas direcionais, aumentando a eficácia de vacinações genéticas contra a infecção experimental pelo *T. cruzi.* Finalmente, em relação á molécula CX3CR1, podemos observar que sua ausência não é determinante para o comprometimento da imunidade, entretanto ainda é necessário aprofundar os estudos para um melhor entendimento da sua função nas células de memória.

7. REFERÊNCIAS

Acevedo, G. R., Girard, M. C., Gómez, K. A. The Unsolved Jigsaw Puzzle of the Immune Response in Chagas Disease. Front Immunol. 2018. 9:1929.

Ahmed, R., Akondy, R. S. Insights into human CD8(+) T-cell memory using the yellow fever and smallpox vaccines. Immunol Cell Biol. 2011. Mar; 89(3):340-5.

Alencar, B. C., Persechini, P. M., Haolla, F. A., de Oliveira, G., Silverio, J. C., Lannes-Vieira, J., Machado, A. V., Gazzinelli, R. T., Bruna-Romero, O., Rodrigues ,M. M. Perforin and gamma interferon expression are required for CD4+ and CD8+T-cell-dependent protective immunity against a human parasite, Trypanosoma cruzi,elicited by heterologous plasmid DNA prime-recombinant adenovirus 5 boostvaccination. Infect Immun. 2009. Oct;77(10):4383-95.

Angelosanto, J. M., Wherry, E. J. Transcription factor regulation of CD8+ T-cell memory and exhaustion. Immunol Rev. 2010. Jul; 236:167-75.

Anikeeva, N., Somersalo, K., Sims, T. N., Thomas, V. K., Dustin, M. L., Sykulev, Y. Distinct role of lymphocyte function-associated antigen-1 in mediating effective cytolytic activity by cytotoxic T lymphocytes. Proc Natl Acad Sci U S A. 2005. May 3;102(18):6437-42.

Bachmann, M. F., McKall-Faienza, K., Schmits, R., Bouchard, D., Beach, J., Speiser, D. E., Mark T. W., and Ohashi, P. S. Distinct Roles for LFA-1 and CD28 during Activation of Naive T Cells: Adhesion versus Costimulation. Immunity. 1997. 7: 549–557.

Badovinac, V. P., Harty, J. T. Programming, demarcating, and manipulating CD8+ T-cell memory. Immunol Rev. 2006. Jun; 211:67-80.

Badovinac, V. P., Messingham, K. A. N., Jabbari, A., Haring, J. S., and Harty, J. T. Accelerated CD8+ T-cell memory and prime-boost response after dendritic-cell vaccination. Nature Medicine. 2005. 11: 748-756.

Barbi, J., Oghumu, S., Rosas, L. E., Carlson, T., Lu, B., Gerard, C., Lezama-Davila, C. M., Satoskar, A. R. Lack of CXCR3 delays the development of hepatic inflammation but does not impair resistance to Leishmania donovani. J Infect Dis. 2007. Jun 1;195(11):1713-7.

Bern, C., Kjos, S., Yabsley, M. J., Montgomery, S. P. Trypanosoma cruzi and Chagas'Disease in the United States. Clinical microbiology reviews. 2011. 24(4): 655–681a.

Brasil, P. E., De Castro, L., Hasslocher-Moreno, A. M., Sangenis, L. H., Braga, J. U. ELISA versus PCR for diagnosis of chronic Chagas disease: systematic review and meta-analysis. BMC Infect Dis. 2010. Nov 25;10:337.

Cai, C. W., Blasé, J. R., Zhang, X., Eickhoff, C. S., Hoft, D. F. Th17 Cells Are More Protective Than Th1 Cells Against the Intracellular Parasite Trypanosoma cruzi. PLoS Pathog. 2016. Oct 3;12(10):e1005902.

Campanella, G. S., Tager, A. M., El Khoury, J. K., Thomas, S. Y., Abrazinski, T. A., Manice, L. A., Colvin, R. A., Luster, A. D. Chemokine receptor CXCR3 and its ligands CXCL9 and CXCL10 are required for the development of murine cerebral malaria. Proc Natl Acad Sci U S A. 2008. Mar 25;105(12):4814-9.

Campos, M. A., Almeida, I. C., Takeuchi, O., Akira, S., Valente, E. P., Procópio, D. O., Travassos, L. R., Smith, J. A., Golenbock, D. T., Gazzinelli, R. T. Activation of Toll-like receptor-2 by glycosylphosphatidylinositol anchors from a protozoan parasite. J Immunol. 2001. Jul 1;167(1):416-23.

Cardoso, M. S., Reis-Cunha, J. L., Bartholomeu, D. C. Evasion of the Immune Response by Trypanosoma cruzi during Acute Infection. Front Immunol. 2016. 6:659.

Centers of Diseas Control and Prevention. 2019. https://www.cdc.gov/parasites/chagas/

Cohen, S. B., Maurer, K. J., Egan, C. E., Oghumu, S., Satoskar, A. R., and Denkers, E. Y. CXCR3-Dependent CD4+ T Cells Are Required to Activate Inflammatory Monocytes for Defense against Intestinal Infection. PLoS Pathog, 9. 2013.

Coura, J. R. Dinâmica das doenças infecciosas e parasitárias. Rio de Janeiro: Guanabara Koogan, 2013. 2. Ed.

Cronemberger-Andrade, A., Xander, P., Soares, R. P., Pessoa, N. L., Campos, M. A., Ellis, C. C., Grajeda, B., Ofir-Birin, Y., Almeida, I. C., Regev-Rudzki, N., Torrecilhas, A. C. Trypanosoma cruzi-Infected Human Macrophages Shed Proinflammatory Extracellular Vesicles That Enhance Host-Cell Invasion via Toll-Like Receptor 2. Front Cell Infect Microbiol. 2020. Mar 20;10:99.

Cummings KL, Tarleton RL. Rapid quantitation of Trypanosoma cruzi in host tissue by real-time PCR. Mol Biochem Parasitol. 2003.

Cunha-Neto, E., and Chevillard, C. Chagas Disease Cardiomyopathy: Immunopathology and Genetics. Hindawi. 2014. 2014: 1-11.

Dos Santos, P. V., Roffê, E., Santiago, H. C., Torres, R. A., Marino, A. P., Paiva, C. N., Silva, A. A., Gazzinelli, R.T., and Lannes-Vieira, J. Prevalence of CD8(+)alpha beta T cells in Trypanosoma cruzi-elicited myocarditis is associated with acquisition of CD62LLow LFA-1HighVLA-4High activation phenotype and

expression of IFN-gamma-inducible adhesion and chemoattractant molecules 1. Microbes Infect . 2001. 3: 971-84.

Dotiwala, F., Mulik, S., Polidoro, R. B., Ansara, J. A., Burleigh, B. A., Walch, M., Gazzinelli, R. T., Lieberman, J. Killer lymphocytes use granulysin, perforin and granzymes to kill intracellular parasites. Nat Med. 2016. Feb;22(2):210-6.

Dumonteil, E., Herrera, C. Ten years of Chagas disease research: Looking back to achievements, looking ahead to challenges. PLoS Negl Trop Dis. 2017. Apr 20;11(4):e0005422.

Dustin, M. L. The cellular context of T cell signaling. Immunity. 2009. Apr. 17;30(4):482-92.

Dustin, M. L., and Bromley, S. K. Stimulation of naive T-cell adhesion and immunological synapse formation by chemokine-dependent and -independent mechanisms. Immunology. 2002. 106: 289 – 298.

Epting, C. L., Coates, B. M., Engman, D. M. Molecular mechanisms of host cell invasion by Trypanosoma cruzi. Exp Parasitol. 2010. Nov;126(3):283-91.

Esch, K. J., Petersen, C. A. Transmission and epidemiology of zoonotic protozoal diseases of companion animals. Clin Microbiol Rev. 2013. Jan;26(1):58-85.

Ferreira, C. P., Cariste, L. M., Santos Virgílio, F. D., Moraschi, B. F., Monteiro, C. B., Vieira Machado, A. M., Gazzinelli, R. T., Bruna-Romero, O., Menin Ruiz, P. L., Ribeiro, D. A., Lannes-Vieira, J., Lopes, M. F., Rodrigues, M. M., de Vasconcelos, J. R. C. LFA-1 Mediates Cytotoxicity and Tissue Migration of Specific CD8(+) T Cells after Heterologous Prime-Boost Vaccination against Trypanosoma cruzi Infection. Front Immunol. 2017. Oct 13;8:1291.

Ferreira, R. T. B., Branquinho, M. R., Leite, P. C. Transmissão oral da doença de Chagas pelo consumo de açaí: um desafio para a Vigilância Sanitária. Vigilância Sanitária em Debate, Rio de Janeiro. 2014. 2: 4. 4-11.

Ferreira, R. T. B., Branquinho, M. R., Leite, P. C. Transmissão oral da doença de Chagas pelo consumo de açaí: um desafio para a Vigilância Sanitária. Vigilância Sanitária em Debate, Rio de Janeiro. 2014. 2: 4. 4-11.

Garg, N., Nunes, M. P., Tarleton, R. L. Delivery by Trypanosoma cruzi of proteins into the MHC class I antigen processing and presentation pathway. J Immunol. 1997. Apr 1;158(7):3293-302.

Gazzinelli, R. T. & Denkers, E. Y. Gazzinelli, R.T. & Denkers, E.Y. Protozoan encounters with Toll-like receptor signalling pathways: implications for host parasitism. Nat. Rev. Immunol. 6, 895-906. Nature reviews. Immunology. 2007. 6. 895-906. 10.1038/nri1978.

Gazzinelli, R.T, Campos, M. A., Ropert, C.. Role of the Toll/interleukin-1 receptor signaling pathway in host resistance and pathogenesis during infection with protozoan parasites. Immunological Reviews , 2004. v. 201, p. 9-25.

Geiger, A., Bossard, G., Sereno, D., Pissarra, J., Lemesre, J., Vincendeau, P., and Holzmuller, P. Escaping Deleterious Immune Response in Their Hosts: Lessons from Trypanosomatids. Front. Immunol. 2016. 7: 212.

Gerlach, C., Moseman, E. A., Loughhead, S. M., Alvarez, D., Zwijnenburg, A. J., Waanders, L., Garg, R., de la Torre, J. C., von Andrian, U. H. The Chemokine Receptor CX3CR1 Defines Three Antigen-Experienced CD8 T Cell Subsets with Distinct Roles in Immune Surveillance and Homeostasis. Immunity. 2016. Dec 20;45(6):1270-1284.

Guerreiro, R., Santos-Costa, Q., and Azevedo-Pereira, J. M. AS Quimiocinas e os seus receptores Características e Funções Fisiológicas. Acta Med Port. 2011. 24: 967 – 976.

Gupta, M., Greer, P., Mahanty, S., Shieh, W. J., Zaki, S. R., Ahmed, R., Rollin, P. E. CD8-mediated protection against Ebola virus infection is perforin dependent. J Immunol. 2005. Apr 1;174(7):4198-202.

Harker, K. S., Ueno, N., Wang, T., Bonhomme, C., Liu, W., and Lodoen, M. B. Toxoplasma gondii modulates the dynamics of human monocyte adhesion to vascular endothelium under fluidic shear stress. J Leukoc Biol, 2013. 93: 789-800.

Hernandez, I. Q. and Dumontei, E. Advances and challenges toward a vaccine against Chagas disease. Human Vaccines. 2011. 7: 1184-1191.

Hickman, H. D., Reynoso, G. V., Ngudiankama, B. F., Cush, S. S., Gibbs, J., Bennink, J. R., and Yewdell, J. W. CXCR3 Chemokine Receptor Enables Local CD8+ T Cell Migration for the Destruction of Virus-Infected Cells. Immunity, 2015. 42: 1–14.

Hikono, H., Kohlmeier, J. E., Takamura, S., Wittmer, S. T., Roberts, A. D., Woodland, D. L. Activation phenotype, rather than central- or effector-memory phenotype, predicts the recall efficacy of memory CD8+ T cells. J Exp Med. 2007. Jul 9;204(7):1625-36.

Hogg, N., Laschinger, M., Giles, K., McDowall, A. T-cell integrins: more than juststicking points. J Cell Sci. 2003. Dec 1;116(Pt 23):4695-705.

Janssen, E. M.; Lemmens, E. E.; Wolfe, T.; Christen, U.; Von Herrath, M. G.; Schoenberger, S. P. CD4+ T cells are required for secondary expansion and memory in CD8+ T lymphocytes. Nature, 2003. v. 421, n. 6925, p. 852–856.

Jung, S., Aliberti, J., Graemmel, P., Sunshine, M. J., Kreutzberg, G. W., Sher, A., Littman, D. R. Analysis of fractalkine receptor CX(3)CR1 function by targeted deletion and green fluorescent protein reporter gene insertion. Mol Cell Biol. 2000. Jun;20(11):4106-14.

Junqueira, C., Caetano, B., Bartholomeu, D. C., Melo, M. B., Ropert, C., Rodrigues, M. M., Gazzinelli, R. T. "The endless race between Trypanosoma cruzi and host immunity: Lessons for and beyond Chagas disease," Molecular Medicine, 2010. 12: 29.

Kayama, H., Takeda, K. The innate immune response to Trypanosoma cruzi infection. Microbes Infect. 2010. Jul;12(7):511-7.

Knight, J. M., Lee, S. H., Roberts, L., Smith, C. W., Weiss, S. T., Kheradmand, F., Corry, D. B. CD11a polymorphisms regulate TH2 cell homing and TH2-related disease. J Allergy Clin Immunol. 2014. Jan;133(1):189-97.e1-8.

Kufareva, I., Salanga, C. L., and Handel, T. M. Chemokine and chemokine receptor structure and interactions: implications for therapeutic strategies. Immunol Cell Biol. 2015. 93: 372-383.

Kumar, S., Tarleton, R. L. Antigen-specific Th1 but not Th2 cells provide protection from lethal Trypanosoma cruzi infection in mice. J Immunol. 2001. Apr 1;166(7):4596-603.

Kurachi, M., Kurachi, J., Fumiko, S., Tatsuya, T., Jun, A., Satoshi, Ueha., Michio, T., Kei, S., Shiki, T., Kazuhiro, K., and Kouji, M. Chemokine receptor CXCR3 facilitates CD8+ T cell differentiation into short-lived effector cells leading to memory degeneration. Rev. Immunol. 2011. 208:1605–1620

Kwun, J., Farris, A. B., Song, H., Mahle, W. T., Burlingham, W. J., and Knechtle, S. J. Impact of Leukocyte Function-Associated Antigen-1 Blockade on Endogenous

Allospecific T Cells to Multiple Minor Histocompatibility Antigen Mismatched Cardiac Allograft. Transplantation. 2015. 99: 12.

Lafuse, W. P., Wozniak, D. J., Rajaram, M. V. S. Role of Cardiac Macrophages on Cardiac Inflammation, Fibrosis and Tissue Repair. Cells. 2020. 10(1):51.

Lanzavecchia, A., Sallusto, F. Understanding the generation and function of memory T cell subsets. Curr Opin Immunol. 2005. Jun;17(3):326-32.

Lewinsohn, D. A., Lewinsohn, D. M., Scriba, T. J. Polyfunctional CD4+ T Cells As Targets for Tuberculosis Vaccination. Front Immunol. 2017. Oct 5;8:1262.

Luster, A. D., Alon, R., von Andrian, U. H. Immune cell migration in inflammation: present and future therapeutic targets. Nat Immunol. 2005. Dec;6(12):1182-90.

Machado, F. S., Martins, G. A., Aliberti, J. C., Mestriner, F. L., Cunha, F. Q., Silva, J. S. Trypanosoma cruzi-infected cardiomyocytes produce chemokines and cytokines that trigger potent nitric oxide-dependent trypanocidal activity. Circulation. 2000. Dec 12;102(24):3003-8.

Mackay, C. R. Chemokines:immunology's high. Nature Immunology. 2001. 2: 95 – 101.

Martin, D. and R. Tarleton. Generation, specificity, and function of CD8+ T cells in Trypanosoma cruzi infection. Immunol. 2004. Rev. 201:304-317.

Martin, D. L., D. B. Weatherly, S. A. Laucella, M. A. Cabinian, M. T. Crim, S. Sullivan, M. Heiges, S. H. Craven, C. S. Rosenberg, M. H. Collins, A. Sette, M. Postan, and R. L. Tarleton. CD8+ T-Cell responses to Trypanosoma cruzi are highly focused on strain-variant trans- sialidase epitopes. 2006. PLoS. Pathog. 2:e77.

McNamara, H. A., Cai, Y., Wagle, M. V., Sontani, Y., Roots CM, Miosge LA, O'Connor JH,Sutton HJ, Ganusov VV, Heath WR, Bertolino P, Goodnow CG, Parish IA, Enders A,Cockburn IA. Up-regulation of LFA-1 allows liver-resident memory T cells topatrol and remain in the hepatic sinusoids. Sci Immunol. 2017. Mar;2(9).

Melo, F. R. M., Alencar, C. H., Ramos, A. N. Jr., Heukelbach, J. Epidemiology of mortality related to Chagas' Disease in Brazil, 1999-2007. Plos Negl Trop Dis 2012

Mendonça, R. M., Rocha, A. M., Andrade, M. S., Silva, A. B. S. Doença de chagas: serviço de referência e epidemiologia. Rev Bras Promoção Saúde. 2020. 33:9364.

Miyagawa, F., Gutermuth, J., Zhang, H., Katz, S. I. The use of mouse models to better understand mechanisms of autoimmunity and tolerance. J Autoimmun. 2010. Nov;35(3):192-8.

Mueller, S. N., Gebhardt, T., Carbone, F. R., Heath, W. R. Memory T cell subsets, migration patterns, and tissue residence. Annu Rev Immunol. 2013. 31:137-61.

Murdoch, C., and Finn, A. Chemokine receptors and their role in inflammation and infectious diseases. Blood. 2000. 95: 3032 – 3043.

Nie, C. Q., Bernard, N. J., Norman, M. U., Amante, F. H., Lundie, R. J., Crabb, B. S., Heath, W. R., Engwerda, C. R., Hickey, M. J., Schofield, L., Hansen, D. S. IP-10-mediated T cell homingpromotes cerebral inflammation over splenic immunity to malaria infection. PLoS Pathog. 2009. Apr;5(4):e1000369.

Nishimura, M., Umehara, H., Nakayama, T., Yoneda, O., Hieshima, K., Kakizaki, M., Dohmae, N., Yoshie, O., Imai, T. Dual functions of fractalkine/CX3C ligand 1

in trafficking of perforin+/granzyme B+ cytotoxic effector lymphocytes that are defined by CX3CR1 expression. J Immunol. 2002. Jun 15;168(12):6173-80.

Oliveira, A. C., Peixoto, J. R., de Arruda, L. B., Campos, M. A., Gazzinelli, R. T, Golenbock, D. T, Akira, S., Previato, J. O., Mendonça-Previato, L., Nobrega, A., Bellio, M. Expression of functional TLR4 confers proinflammatory responsiveness to Trypanosoma cruzi glycoinositolphospholipids and higher resistance to infection with T. cruzi. J Immunol. 2004. Nov 1;173(9):5688-96.

Oliveira, M. Nagao-Dias, A. T.,Pontes, V. M. O., Júnior, A. S. S., Coelho, H. L. L and Coelho, I. C. B. Tratamento etiológico da doença de chagas no Brasil. Revista de patologia tropical. 2008. 37: 209-228.

Perro, M., Iannacone, M., von Andrian, U. H., Peixoto, A. Role of LFA-1 integrin in the control of a lymphocytic choriomeningitis virus (LCMV) infection. Virulence. 2020. Dec;11(1):1640-1655.

Petray, P. B., Rottenberg, M. E., Bertot, G., Corral, R. S., Diaz, A., Orn, A., Grinstein, S. Effect of anti-gamma-interferon and anti-interleukin-4 administration on the resistance of mice against infection with reticulotropic and myotropic strains of Trypanosoma cruzi. Immunol Lett. 1993. Jan;35(1):77-80.

Pontes Ferreira, C., Moro Cariste, L., Henrique Noronha, I., Fernandes Durso, D., Lannes-Vieira, J., Ramalho Bortoluci, K., Araki Ribeiro, D., Golenbock, D., Gazzinelli, R. T., Vasconcelos, J. R. C. CXCR3 chemokine receptor contributes to specific CD8+ T cell activation by pDC during infection with intracellular pathogens. PLoS Negl Trop Dis. 2020. Jun 23;14(6):e0008414.

Reey, L. Base de parasiotologia médica 3ª edição Guanaraba Koogan. 2010.

Reisman, N. M., Floyd, T. L., Wagener, M. E., Kirk, A. D., Larsen, C. P., Ford, M. L. LFA-1 blockade induces effector and regulatory T-cell enrichment in lymph

nodes and synergizes with CTLA-4Ig to inhibit effector function. Blood. 2011. Nov 24;118(22):5851-61.

Ribeiro, I., Sevcsik, A. M., Alves, F., Diap, G., Don, R., Harhay, M. O., Chang, S., Pecoul, B. New, improved treatments for Chagas disease: from the R&D pipeline to the patients. PLoS Negl Trop Dis. 2009, Jul 7;3(7):e484.

Rodrigues, M. M., Alencar, B. C., and Tzelepis, F. Immunodominance: a new hypothesis to explain parasite escape and host/parasite equilibrium leading to the chronic phase of Chagas' disease?. Braz. J. Med. Biol. 2009. Res. 42: 220-223.

Rodrigues, M. M., Ribeirão, M., Pereira-Chioccola, V., Renia, L., Costa, F. Predominance of CD4 Th1 and CD8 Tc1 cells revealed by characterization of the cellular immune response generated by immunization with a DNA vaccine containing a Trypanosoma cruzi gene. Infect Immun. 1999. Aug;67(8):3855-63.

Rosas, L. E., Barbi, J., Lu, B., Fujiwara, Y., Gerard, C., Sanders, V. M., Satoskar, A. R. CXCR3-/- mice mount an efficient Th1 response but fail to control Leishmaniamajor infection. Eur J Immunol. 2005. Feb;35(2):515-23.

Rottenberg, M. E., M. Bakhiet, T. Olsson, K. Kristensson, T. Mak, H. Wigzell, and A. Orn. Differential susceptibilities of mice genomically deleted of CD4 and CD8 to infections with Trypanosoma cruzi or Trypanosoma brucei. Infect. Immun. 1993. 61:5129-5133.

Sallusto, F. Heterogeneity of Human CD4(+) T Cells Against Microbes. Annu Rev Immunol. 2016, May 20;34:317-34.

Sandu, I., Cerletti, D., Oetiker, N., Borsa, M., Wagen, F., Spadafora, I., Welten, S. P. M., Stolz, U., Oxenius, A., Claassen, M. Landscape of Exhausted Virus-

Specific CD8 T Cells in Chronic LCMV Infection. Cell Rep. 2020. Aug 25;32(8):108078

Secretaria de Saúde do Estado (PE), Secretaria Executiva de Vigilância em Saúde. Programa Sanar: Cadernos de Monitoramento. Doença de Chagas Recife: Secretaria Estadual de Saúde. 2014, vol 4

Shin, H., Blackburn, S. D., Blattman, J. N., Wherry, E. J. Viral antigen and extensive division maintain virus-specific CD8 T cells during chronic infection. J Exp Med. 2007. Apr 16;204(4):941-9.

Silverio, J. C., Pereira, I. R., Cipitelli, Mda. C., Vinagre, N. F., Rodrigues, M. M., Gazzinelli, R. T., Lannes-Vieira, J. CD8+ T-cells expressing interferon gamma or perforin play antagonistic roles in heart injury in experimental Trypanosoma cruzi-elicited cardiomyopathy. PLoS Pathog. 2012. 8(4):e1002645.

Soldevila, G., and Garca-Zepeda, E. A. The role of the Jak-Stat pathway in chemokine-mediated signaling in T lymphocytes. Signal Transduction. 2007. 7: 427 – 438.

Stanaway J. D., Roth G. The burden of Chagas disease: estimates and challenges. Glob heart, 2015. 10(3):139-44. Review.

Stanley, P., Tooze, S., Hogg, N. A role for Rap2 in recycling the extended conformationof LFA-1 during T cell migration. Biology Open. 2012. 1: 1161–1168.

Tarleton, R. L. CD8+ T cells in Trypanosoma cruzi infection. Semin Immunopathol. 2015. May;37(3):233-8.

Tarleton, R. L. Depletion of CD8+ T cells increases susceptibility and reverses vaccine-induced immunity in mice infected with Trypanosoma cruzi. J. Immunol. 1990. 144:717-724.

Teixeira, M. M., Gazzinelli, R. T., and Silva, J. S. Chemokines, inflammation and Trypanosoma cruzi infection. Cell Press. 2002. 18: 262 – 265.

Thakur, A., Pedersen, L. E., Jungersen, G. Immune markers and correlates of protection for vaccine induced immune responses. Vaccine. 2012. Jul 13;30(33):4907-20.

Thelen, M. Dancing to the tune of chemokines. Nature Immunology. 2001. 2: 129 – 134.

Tzelepis, F., B. C. de Alencar, M. L. Penido, C. Claser, A. V. Machado, O. Bruna-Romero, R. T. Gazzinelli, and M. M. Rodrigues.. Infection with Trypanosoma cruzi restricts the repertoire of parasite-specific CD8+ T cells leading to immunodominance. J. Immunol. 2008. 180:1737-1748.

Tzelepis, F., B. C. de Alencar, M. L. Penido, R. T. Gazzinelli, P. M. Persechini, and M. M. Rodrigues. Distinct kinetics of effector CD8+ cytotoxic T cells after infection with Trypanosoma cruzi in naive or vaccinated mice. Infect. Immun. 2006. 74:2477-2481.

Uppaluri, R., Sheehan, K. C., Wang, L., Bui, J. D., Brotman, J. J., Lu, B., Gerard, C., Hancock, W. W., Schreiber, R. D. Prolongation of cardiac and islet allograft survival by a blocking hamster anti-mouse CXCR3 monoclonal antibody. Transplantation. 2008. Jul 15;86(1):137-47.

Vasconcelos, J. R., Bruña-Romero, O., Araújo, A. F., Dominguez, M. R., Ersching, J., de Alencar, B. C., Machado, A. V., Gazzinelli, R. T., Bortoluci, K. R., Amarante-Mendes, G. P., Lopes, M. F., Rodrigues, M. M. Pathogen-induced proapoptotic phenotype and high CD95 (Fas) expression accompany a suboptimal CD8+ T-cell response: reversal by adenoviral vaccine. PLoS Pathog. 2012. 8(5):e1002699.

Vasconcelos, J. R., Dominguez, M. R., Araújo, A. F., Ersching, J., Tararam, C. A., Bruna-Romero, O., Rodrigues, M. M. Relevance of long-lived CD8(+) T effector memory cells for protective immunity elicited by heterologous prime-boost vaccination. Front Immunol. 2012. Dec 4;3:358.

Vasconcelos, J. R., Dominguez, M. R., Neves, R. L., Ersching, J., Araújo, A., Santos, L. I., Virgilio, F. S., Machado, A. V., Bruna-Romero, O., Gazzinelli, R. T., Rodrigues, M. M. Adenovirus vector-induced $CD8^+$ T effector memory cell differentiation and recirculation, but not proliferation, are important for protective immunity against experimental Trypanosoma cruzi Infection. Hum Gene Ther. 2014. Apr;25(4):350-63.

Victora, C. G., Wagstaff, A., Schellenberg, J. A., Gwatkin, D., Claeson, M., Habicht, J. P. Applying an equity lens to child health and mortality: more of the same is not enough. Lancet 2003

Virgilio, F. S., Pontes, C., Dominguez, M. R., Ersching, J., Rodrigues, M. M., Vasconcelos, J. R. CD8+ T Cell-Mediated Immunity during Trypanosoma cruzi Infection: A Path for Vaccine Development?. Hindawi. 2014. 2014: 1-12.

Walling, B. L., Kim, M. LFA-1 in T Cell Migration and Differentiation. Front Immunol. 2018. May 3; 9:952.

Weninger, W., Manjunath, N., von Andrian, U. H. Migration and differentiation of CD8+ T cells. Immunol Rev. 2002. Aug 186:221-33

Wherry, E. J., Barber, D. L., Kaech, S. M., Blattman, J. N., Ahmed, R. Antigen-independent memory CD8 T cells do not develop during chronic viral infection. Proc Natl Acad Sci U S A. 2004. Nov 9;101(45):16004-9.

WHO Expert Committee on the Control of Chagas Disease (2000: Brasilia, Brazil) & World Health Organization. (2002). Control of Chagas disease: second

report of the WHO expert committee. World Health Organization. https://apps.who.int/iris/handle/10665/42443

World Health Organization. 2017. http://www.who.int/en.

Zlotnik, A., and Youshie, O. 2000. Chemokines: A New Classification Review System and Their Role in Immunity. Braz. Cell Press. 12: 121-127.

ANEXOS

Estratégias de análise de citometria de fluxo.

Estratégia de *gates* para selecionar células T CD8⁺

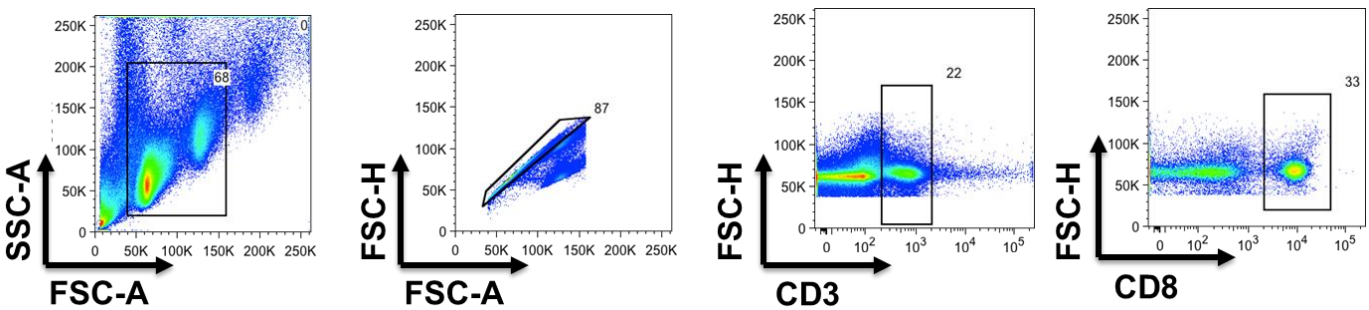

Estratégia de *gates* para selecionar células T CD8⁺ pentâmero⁺

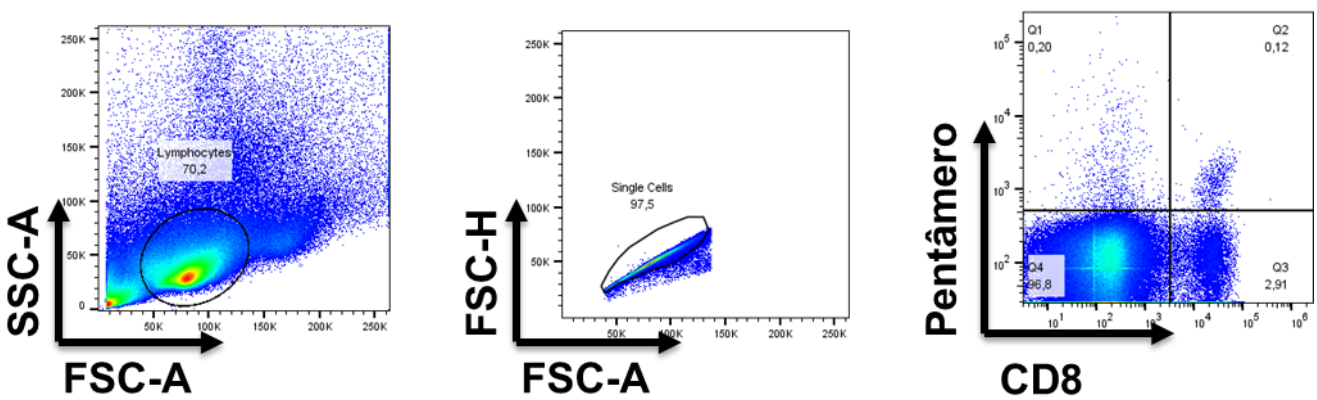

UNIFESP
UNIVERSIDADE FEDERAL DE SÃO PAULO
1933

Comissão de Ética no Uso de Animais

CERTIFICADO

Certificamos que a proposta intitulada "Papel dos receptores de quimiocinas CX3CR1 e da integrina LFA-1 na diferenciação e ativação de linfócitos T CD8+ durante a infecção pelo Trypanosoma cruzi.", protocolada sob o CEUA nº 9081250517 (ID 005905), sob a responsabilidade de **Leonardo Moro Cariste** *e equipe; José Ronnie Carvalho de Vasconcelos* - que envolve a produção, manutenção e/ou utilização de animais pertencentes ao filo Chordata, subfilo Vertebrata (exceto o homem), para fins de pesquisa científica ou ensino - está de acordo com os preceitos da Lei 11.794 de 8 de outubro de 2008, com o Decreto 6.899 de 15 de julho de 2009, bem como com as normas editadas pelo Conselho Nacional de Controle da Experimentação Animal (CONCEA), e foi **aprovada** pela Comissão de Ética no Uso de Animais da Universidade Federal de São Paulo (CEUA/UNIFESP) na reunião de 17/07/2017.

We certify that the proposal "Role of, CX3CR1 chemokine receptors and the LFA-1 integrin in differentiation and activation of CD8+ T lymphocytes during Trypanosoma cruzi infection.", utilizing 202 Isogenics mice (202 females), 24 Knockout mice (24 females), protocol number CEUA 9081250517 (ID 005905), under the responsibility of **Leonardo Moro Cariste** *and team; José Ronnie Carvalho de Vasconcelos* - which involves the production, maintenance and/or use of animals belonging to the phylum Chordata, subphylum Vertebrata (except human beings), for scientific research purposes or teaching - is in accordance with Law 11.794 of October 8, 2008, Decree 6899 of July 15, 2009, as well as with the rules issued by the National Council for Control of Animal Experimentation (CONCEA), and was **approved** by the Ethic Committee on Animal Use of the Federal University of Sao Paulo (CEUA/UNIFESP) in the meeting of 07/17/2017.

Finalidade da Proposta: Pesquisa (Acadêmica)

Vigência da Proposta: de 08/2017 a 06/2019 Área: Bioprocessos E Bioprodutos

Origem:	CEDEME - Centro de Desenvolvimento de Modelos Experimentais para Medicina e Biologia						
Espécie:	Camundongos isogênicos	sexo:	Fêmeas	idade:	8 a 9 semanas	N:	202
Linhagem:	C57BL/6			Peso:	24 a 26 g		
Origem:	CEDEME - Centro de Desenvolvimento de Modelos Experimentais para Medicina e Biologia						
Espécie:	Camundongos Knockout	sexo:	Fêmeas	idade:	8 a 9 semanas	N:	24
Linhagem:	B6.129S2-Cd8atm1Mak/J			Peso:	24 a 26 g		

Local do experimento: Unifesp- Campus baixada Santista

São Paulo, 25 de abril de 2022

Profa. Dra. Daniela Santoro Rosa
Coordenadora da Comissão de Ética no Uso de Animais
Universidade Federal de São Paulo

Profa. Dra. Kátia De Angelis Lobo d'Avila
Vice-Coordenadora da Comissão de Ética no Uso de Animais
Universidade Federal de São Paulo

Rua Botucatu, 740 - 2º andar - Vila Clementino - CEP 04023-061 - São Paulo/SP - tel: +55 (11) 5576-4848 VOIP 1239
Horário de atendimento: 2ª a 6ª, das 8h às 12h e das 14h às 17h : e-mail: ceuasecretaria@gmail.com
CEUA N 9081250517

UNIFESP
UNIVERSIDADE FEDERAL DE SÃO PAULO
1933

Comissão de Ética no Uso de Animais

São Paulo, 27 de novembro de 2017
CEUA N 9081250517

IImo(a). Sr(a).
Responsável: Leonardo Moro Cariste
Área: Bioprocessos E Bioprodutos

Título da proposta: "Papel dos receptores de quimiocinas CX3CR1 e da integrina LFA-1 na diferenciação e ativação de linfócitos T CD8+ durante a infecção pelo Trypanosoma cruzi.".

Parecer Consubstanciado da Comissão de Ética no Uso de Animais UNIFESP (ID 002013)

A Comissão de Ética no Uso de Animais da Universidade Federal de São Paulo, no cumprimento das suas atribuições, analisou e **APROVOU** a Emenda (versão de 31/outubro/2017) da proposta acima referenciada.

Resumo apresentado pelo pesquisador: "Os linfócitos T CD8+ exercem um importante papel no controle de infeções por patógenos intracelulares como Trypanosoma cruzi, agente causador da doença de Chagas. Esses linfócitos controlam a infecção por meio da liberação de IFN-? e pela eliminação das células alvo infectadas pela citotoxicidade direta. Para exercerem essas funções, os linfócitos precisam migrar para os tecidos infectados, estabelecer um contato estável com as células apresentadoras de antígenos e serem ativados por meio da interação do TCR com o complexo MHC-peptídeo e moléculas co-estimulatórias. Além disso, atualmente tem sido reportado o papel dessas moléculas na ativação e diferenciação dos linfócitos T CD8+ durante infecções virais e bacterianas. No entanto, não está claro o papel dessas moléculas durante a infecção pelo T. cruzi. Interessantemente, as moléculas de quimiocinas CX3CR1 e CXCR3 são altamente expressas na superfície dos linfócitos T CD8+ durante a infecção por patógenos intracelulares, como T. cruzi, e são importantes na ativação e diferenciação dessas células. Estudos indicam que as quimiocinas e as integrinas são importantes para facilitar o encontro desses linfócitos com as células apresentadoras de antígenos no linfonodo, e consequentemente, na ativação e posterior diferenciação dos linfócitos. A integrina LFA-1 também possui papel na ativação e diferenciação dos linfócitos, uma vez que é extremamente importante no estabelecimento do contato dos linfócitos com as células apresentadoras de antígenos. Com isso, o objetivo desse projeto é avaliar o papel das quimiocinas CXCR3 e CX3CR1 e da integrina LFA-1 na diferenciação de células efetoras de memória e ativação dos linfócitos T CD8+ durante a infecção pelo T. cruzi. O conhecimento dos mecanismos envolvidos com a indução de células efetoras que darão origem as células de memória é de extrema importância para a geração de estratégias vacinais.".

Comentário da CEUA: "APROVADO - Sr. Pesquisador, emenda aprovada. ANIMAIS: 44 Camundongos isogênicos C57BL/6, fêmeas, 24 e 26 g, 8 e 9 semanas Procedência: CEDEME Manutenção: Biotério de Experimentação do Departamento de Biociências 24 Camundongos Knockout CX3CR1 gfp/gfp, fêmeas, 24 e 26 g, 8 e 9 semanas Procedência: Biotério da Faculdade de Medicina de Ribeirão Preto Manutenção: Biotério de Experimentação Departamento de Biociências".

Profa. Dra. Daniela Santoro Rosa
Coordenadora da Comissão de Ética no Uso de Animais
Universidade Federal de São Paulo

Profa. Dra. Kátia De Angelis Lobo d'Avila
Vice-Coordenadora da Comissão de Ética no Uso de Animais
Universidade Federal de São Paulo

UNIFESP
UNIVERSIDADE FEDERAL DE SÃO PAULO
1933

Comissão de Ética no Uso de Animais

São Paulo, 28 de novembro de 2019
CEUA N 9081250517

Ilmo(a). Sr(a).
Responsável: Leonardo Moro Cariste
Área: Bioprocessos E Bioprodutos

Título da proposta: "Papel dos receptores de quimiocinas CX3CR1 e da integrina LFA-1 na diferenciação e ativação de linfócitos T CD8+ durante a infecção pelo Trypanosoma cruzi.".

Parecer Consubstanciado da Comissão de Ética no Uso de Animais UNIFESP (ID 004728)

A Comissão de Ética no Uso de Animais da Universidade Federal de São Paulo, no cumprimento das suas atribuições, analisou e **APROVOU** a Emenda (versão de 26/novembro/2019) da proposta acima referenciada.

Resumo apresentado pelo pesquisador: "Camundongos da linhagem OT-I que o MHC de classe I é restrito a reconhecer apenas os peptídeos da OVA albumina, serão utilizados para demonstrar o papel do receptor de quimiocinas CXCR3 e da integrina LFA1,tivermos resultados preliminares em camundongos C57BL/6 demonstrando a importância dessas moléculas, afim de demonstrar o papel das mesmas em relação as células T CD8+ os camundongos OT-I serão infectados com 10^6 formas de T.Cruzi Y-OVA e tratados a cada 48 horas com as moléculas LFA-1 e CXCR3, a parasitemia sanguínea será acompanhanda do 4º dia até o 11º dia após a infecção, no 12ºdia após a infecção será realizada a técnica de Marcação Intracelular e ELISPOT, as metodologias se encontram detalhadas no anexo1 no item 7 que está grifado.".

Comentário da CEUA: "Prezado Pesquisador, frente as justificativas enviadas a emenda está aprovada. Animais a serem adicionados: 32 camundongos isogênicos, OT-1 - C57bl/6-tg(tcratcrb)/j, machos, 20 e 25g, 7 e 8 semanas. 16 camundongos isogênicos, OT-1 - C57bl/6-tg(tcratcrb)/j, fêmeas, 20 e 25g, 7 e 8 semanas.".

Profa. Dra. Daniela Santoro Rosa
Coordenadora da Comissão de Ética no Uso de Animais
Universidade Federal de São Paulo

Profa. Dra. Kátia De Angelis Lobo d'Avila
Vice-Coordenadora da Comissão de Ética no Uso de Animais
Universidade Federal de São Paulo

UNIFESP
UNIVERSIDADE FEDERAL DE SÃO PAULO
1933

Comissão de Ética no Uso de Animais

São Paulo, 30 de setembro de 2021
CEUA N 9081250517

IImo(a). Sr(a).
Responsável: Leonardo Moro Cariste
Área: Bioprocessos E Bioprodutos

Título da proposta: "Papel dos receptores de quimiocinas CX3CR1 e da integrina LFA-1 na diferenciação e ativação de linfócitos T CD8+ durante a infecção pelo Trypanosoma cruzi.".

Parecer Consubstanciado da Comissão de Ética no Uso de Animais UNIFESP (ID 007986)

A Comissão de Ética no Uso de Animais da Universidade Federal de São Paulo, no cumprimento das suas atribuições, analisou e **APROVOU** a Emenda (versão de 20/setembro/2021) da proposta acima referenciada.

Resumo apresentado pelo pesquisador: "Após resultados promissores com os animais infectados e tratados com anti-LFA-1, observamos uma diminuição nas células T CD4 na migração para o tecido cardíaco, tendo em vista esses resultados gostaríamos de realizar a transferência adotiva das células T CD4 após infecção e/ou tratamento com anti-LFA-1 para animais T CD4 K.O, esses dado seria interessante para a publicação do artigo.".

Comentário da CEUA: "APROVADO Prezado Pesquisador, frente a justificativa enviada a emenda esta aprovada. Animais a serem adicionados: 20 Camundongos transgênicos CD4 - b6.129s2-, Fêmeas, de 15 a 18 g, de 7 a 8 semanas Procedência: CEDEME Manutenção: Biotério de Experimentação Animal Campus Baixada Santista".

Profa. Dra. Daniela Santoro Rosa
Coordenadora da Comissão de Ética no Uso de Animais
Universidade Federal de São Paulo

Profa. Dra. Kátia De Angelis Lobo d'Avila
Vice-Coordenadora da Comissão de Ética no Uso de Animais
Universidade Federal de São Paulo

frontiers in Immunology

ORIGINAL RESEARCH
published: 13 October 2017
doi: 10.3389/fimmu.2017.01291

LFA-1 Mediates Cytotoxicity and Tissue Migration of Specific CD8+ T Cells after Heterologous Prime-Boost Vaccination against *Trypanosoma cruzi* Infection

*Camila Pontes Ferreira[1,2†], Leonardo Moro Cariste[1,3†], Fernando Dos Santos Virgílio[1,2], Barbara Ferri Moraschi[1,2], Caroline Brandão Monteiro[3], Alexandre M. Vieira Machado[4], Ricardo Tostes Gazzinelli[4,5], Oscar Bruna-Romero[6], Pedro Luiz Menin Ruiz[3], Daniel Araki Ribeiro[3], Joseli Lannes-Vieira[7], Marcela de Freitas Lopes[8], Mauricio Martins Rodrigues[1,2‡] and José Ronnie Carvalho de Vasconcelos[1,2,3]**

[1] Molecular Immunology Laboratory, Center of Molecular and Cellular Therapy, São Paulo, Brazil, [2] Department of Microbiology, Immunology and Parasitology, Federal University of São Paulo (UNIFESP), São Paulo, Brazil, [3] Department of Biosciences, Federal University of São Paulo, São Paulo, Brazil, [4] René Rachou Research Center, Fiocruz, Minas Gerais, Brazil, [5] Division of Infectious Disease and Immunology, Department of Medicine, University of Massachusetts Medical School, Worcester, MA, United States, [6] Department of Microbiology, Immunology and Parasitology, Federal University of Santa Catarina, Florianópolis, Brazil, [7] Biology Interactions Laboratory, Oswaldo Cruz Institute, Fiocruz, Rio de Janeiro, Brazil, [8] Institute of Biophysics Carlos Chagas Filho, Federal University of Rio de Janeiro, Rio de Janeiro, Brazil

Integrins mediate the lymphocyte migration into an infected tissue, and these cells are essential for controlling the multiplication of many intracellular parasites such as *Trypanosoma cruzi*, the causative agent of Chagas disease. Here, we explore LFA-1 and VLA-4 roles in the migration of specific CD8+ T cells generated by heterologous prime-boost immunization during experimental infection with *T. cruzi*. To this end, vaccinated mice were treated with monoclonal anti-LFA-1 and/or anti-VLA-4 to block these molecules. After anti-LFA-1, but not anti-VLA-4 treatment, all vaccinated mice displayed increased blood and tissue parasitemia, and quickly succumbed to infection. In addition, there was an accumulation of specific CD8+ T cells in the spleen and lymph nodes and a decrease in the number of those cells, especially in the heart, suggesting that LFA-1 is important for the output of specific CD8+ T cells from secondary lymphoid organs into infected organs such as the heart. The treatment did not alter CD8+ T cell effector functions such as the production of pro-inflammatory cytokines and granzyme B, and maintained the proliferative capacity after treatment. However, the specific CD8+ T cell direct cytotoxicity was impaired after LFA-1 blockade. Also, these cells expressed higher levels of Fas/CD95 on the surface, suggesting that they are susceptible to programmed cell death by the extrinsic pathway. We conclude that LFA-1 plays an important role in the migration of specific CD8+ T cells and in the direct cytotoxicity of these cells.

Keywords: vaccination, *Trypanosoma cruzi*, migration, integrins, specific CD8+ T cells

OPEN ACCESS

Edited by:
Jeffrey K. Actor, UTHealth Science Center, United States

Reviewed by:
Sampa Santra, Harvard Medical School, United States
Darren Woodside, Texas Heart Institute, United States

***Correspondence:**
José Ronnie Carvalho de Vasconcelos
jrcvasconcelos@gmail.com.br

†These authors have contributed equally to this work.

‡In memoriam.

Specialty section:
This article was submitted to Vaccines and Molecular Therapeutics, a section of the journal Frontiers in Immunology

Received: *30 May 2017*
Accepted: *26 September 2017*
Published: *13 October 2017*

Citation:
Ferreira CP, Cariste LM, Santos Virgílio FD, Moraschi BF, Monteiro CB, Vieira Machado AM, Gazzinelli RT, Bruna-Romero O, Menin Ruiz PL, Ribeiro DA, Lannes-Vieira J, Lopes MF, Rodrigues MM and Vasconcelos JRC (2017) LFA-1 Mediates Cytotoxicity and Tissue Migration of Specific CD8+ T Cells after Heterologous Prime-Boost Vaccination against Trypanosoma cruzi Infection. Front. Immunol. 8:1291. doi: 10.3389/fimmu.2017.01291

INTRODUCTION

Chagas disease, caused by the intracellular parasite *Trypanosoma cruzi*, is a major public health problem, with about seven million people infected worldwide (1). $CD8^+$ T cells are crucial for controlling the multiplication of intracellular pathogens such as *T. cruzi*. These cells control the infection by secreting cytokines such as IFN-γ and TNF-α, or by direct cytotoxicity against infected target cells (2). The heterologous prime-boost vaccination strategy has shown significant results in the induction of specific $CD8^+$ T cells and the generation of an optimal protective immune response. Among several possible combinations of vectors for this type of immunization, we used a plasmid vector for priming and an adenovirus-Ad5 vector (replication-defective human Ad type 5) for boosting, both containing an insertion of the ASP-2 gene (*T. cruzi*'s amastigote surface protein 2 gene). This type of immunization was capable of protecting A/Sn mice that are highly susceptible to experimental infection with *T. cruzi* (3, 4).

The results obtained in preclinical experimental models with heterologous prime-boost immunization have boosted recent clinical trials (5–10). In 2013, the first results of a Phase II clinical trial were published. In that study, a number of volunteers, who were vaccinated with plasmid DNA followed by immunization with Ad5, both encoding the genes of the apical membrane antigen 1 and the immunodominant surface protein of the *Plasmodium falciparum* circumsporozoite protein, developed immunity to malaria (11).

To the $CD8^+$ T cells exert their effector function, these cells must migrate to non-lymphoid peripheral tissues where the infection occurs. Our group recently demonstrated that the protection generated by heterologous prime-boost immunization regimen depends on the recirculation of specific $CD8^+$ T cells, since immunized and protected A/Sn mice became susceptible to the experimental challenge with *T. cruzi* after FTY720 drug treatment (12). This immunosuppressive drug reduces lymphocyte recirculation by altering T cell signaling *via* sphingosine-1-phosphate receptor-1 (S1Pr1). This leads in sustained inhibition of S1Pr1 signaling, trapping T cells within the secondary lymphoid with no impairment of T cell activation (12, 13). Based on this knowledge, we hypothesized that other molecules, such as integrins, could be involved in the $CD8^+$ T cell migration. The integrins are heterodimers that composed of an alpha and beta chain; LFA-1 is composed of αLβ2 (CD11a/CD18) chains, and VLA-4, of α4β1 (CD49d/CD29) chains. These molecules play an important role in the formation of immunological synapses and signal transduction, which result, for example, in cell migration, activation, and/or proliferation (14, 15). During transendothelial migration, chemokine-triggered activation of both LFA-1 and VLA-4 leads them to change their conformations and strongly bind to intercellular adhesion molecules (ICAMs and VCAMs, respectively) on endothelial cells and, thus, migrate into the tissues (16). In β2 integrin-deficient mice, LFA-1 shows a significant reduction in the *in vitro* lymphocyte migration, strengthening the role of this molecule in leukocyte migration (17). The LFA-1 role in lymphocyte migration has also been demonstrated in the experimental autoimmune encephalomyelitis, in which regulatory $CD4^+$ T cells can migrate to the CNS *via* LFA-1 (18). Its role has also been demonstrated in allografts, and the antagonism of this molecule is a very effective inhibitor of acute rejection, thus prolonging allograft survival in rodents (19). VLA-4 has also been studied in liver allograft rejections, where it seems responsible for the migration of effector $CD8^+$ T cells and transplant rejection along with LFA-1 (20, 21). During infection by intracellular parasites such as *T. cruzi*, specifically by the Colombian strain, there is a predominance of effector $CD8^+$ T lymphocytes (CTLs) with high expression of LFA-1 and VLA-4 in the myocardium of infected mice (22). In addition, the high expression of LFA-1 on the surface of Pfn^+CD8^+ T cells during the acute and chronic phases has been demonstrated (23). However, the dominance of these cells in cardiac tissue favors the progression of the inflammatory reaction, culminating in Chronic Chagas heart disease (24).

Herein, we tested whether LFA-1 and VLA-4 integrins were key mediators for T cell-mediated protective immunity against *T. cruzi* infection. For that purpose, mice were vaccinated with heterologous prime-boost vaccine (recombinant plasmid DNA/AdHu5), challenged and treated with blocking antibodies to LFA-1 and/or VLA-4. Our results demonstrate that LFA-1, but not VLA-4, is essential for protective immune response of highly susceptible mice against *T. cruzi* infection. Also, the study demonstrated that LFA-1 mediates $CD8^+$ T cells migration into infected tissues, such as the heart, and plays an important role in $CD8^+$ T cells cytotoxicity for parasite clearance.

MATERIALS AND METHODS

Ethics Statement

This study was carried out in strict accordance with the recommendations in the Guide for the Care and Use of Laboratory mice of the Brazilian National Council of Animal Experimentation (http://www.mctic.gov.br/mctic/opencms/textogeral/concea.html). The protocol was approved by the Ethical Committee for Animal Experimentation at the Federal University of Sao Paulo (Id # CEP 7559051115).

Mice and Parasites

Female 5- to 8-week-old A/Sn or C57BL/6 mice were purchased from the Federal University of São Paulo. ICAM-1-deficient mice were kindly supplied by Dr. João Santana, Ribeirão Preto School of Medicine-FMPR. Parasites of the Y strain of *T. cruzi* were used in this study (2, 3). Blood trypomastigotes of the Y strain of *T. cruzi* were maintained by weekly passages in A/Sn mice at the Xenodiagnosis Laboratory of Dante Pazzenese Cardiology Institute. Bloodstream trypomastigotes were obtained from mice infected 7–28 days earlier with parasites of the Y strain. For *in vivo* experiments, each mouse was inoculated with 150 trypomastigotes (A/Sn) or 10^4 trypomastigotes (C57BL/6) diluted in 0.2 mL phosphate-buffered saline (PBS) and administrated subcutaneously (s.c.) in the base of the tail. Parasitemia was determined by collecting 5 μL of blood, and parasites were counted on the light microscope (25).

Immunization Protocol

In this study, we used the heterologous prime-boost immunization protocol with plasmid pIgSPCl.9 and the human replication-defective adenovirus type 5 containing the ASP-2 gene, as described previously (3, 26). Briefly, this immunization consists of a dose of plasmid DNA as a prime (pcDNA3 control or pIgSPClone9). The mice were intramuscularly inoculated (i.m.) with 50 μg of plasmid DNA into each *tibialis anterioris* muscle. Three weeks after the first immunization, mice were boosted with 2×10^8 plaque-forming units of the adenoviral vectors Adβ-gal or AdASP-2. Both injections were performed *via* intramuscular route (tibialis anterior muscle).

Peptide

TEWETGQI peptide was synthesized by GenScript and obtained at purity higher than 95%. The TEWETGQI epitope expressed on ASP-2 surface is target of $CD8^+$ T cells and was identified previously (27). It was used for specific $CD8^+$ T cell stimulation *in vitro* and *ex vivo*. The $H2K^K$-TEWETGQI multimer, labeled with fluorophore APC, was purchased from Immudex (Copenhagen, Denmark) and used for specific $CD8^+$ T cell detection in tissues.

Treatment with Monoclonal Antibodies

Anti-LFA-1 (anti-CD11a, clone M17-4) and anti-VLA-4 (anti-CD49d, clone PS/2) monoclonal antibodies were purchased from BioXcell; in addition, we used Rat IgG2a (clone 2A3) isotype control. The *in vivo* treatment was performed with 10 i.p. injections of 250 μg of mAb/mouse (every 48 h after infection, until day 20 after infection). The concentration of LFA-1 used for *in vivo* treatment was the same used by Reisman et al. (28). To evaluate the efficiency of LFA-1 integrin blockade, C57BL/6 mice were infected with 10^4 trypomastigote forms of Y strain, and 12 days post infection, the splenocytes were harvested and incubated *in vitro* for 24 h at 30°C with monoclonal 250 μg/mL of 2A3 isotype control or anti-LFA-1 in complete medium [1% NEAA, 1% L-glutamine, 1% vitamins and 1% pyruvate, 0.1% 2-ME, 10% fetal bovine serum (FBS) (HyClone)]. After incubation, splenocytes were washed and labeled with anti-CD8 PerCP (clone 53-6.7, BD) and anti-CD11a FITC (clone 2D7, BD), fixed with 1% paraformaldehyde and analyzed by flow cytometry. Concomitantly, we also evaluated the blockade of the LFA-1 molecule stimulating splenocytes *in vitro* with 1 μg/mL anti-CD3 (clone 145-2C11, eBioscience) in complete medium for 72 h at 37°C and 5% CO_2. On the second day of incubation, 250 μg of 2A3 isotype control or anti-LFA-1 monoclonal antibodies were added to the culture. On the third day of culture, cells were harvested and labeled with anti-CD8 PerCP and anti-CD11a FITC for flow cytometric analysis. LFA-1 expression was performed on gated $CD8^+$ T cells, according to Figures S1A,B in Supplementary Material, treatment with monoclonal anti-LFA-1 blocked most LFA-1 molecule expressed on activated $CD8^+$ T cells and after anti-LFA-1 FITC staining there was a lower CD11a MFI on the surface of these cells, indicating that there is competition between anti-LFA-1 monoclonal antibodies used for *in vivo* blocking (clone M17-4) and anti-CD11a FITC (clone 2D7, BD) used for flow cytometry labeling.

Real-time PCR

Hearts, livers, and spleens from the *T. cruzi*-infected, immunized, and/or treated mice with anti-LFA-1 A/Sn were used for extracting DNA. The extraction protocol, the specific primers for a satellite DNA region of the parasite, and the RT-PCR reaction using the TaqMan Universal Master Mix II with UNG were adapted from Piron and colleagues (29). For the race plates, we used StepOnePlus (Applied Biosystems®), and distilled water for negative control reaction.

Enzyme-Linked Immunospot (ELISPOT) Assay

Sterile PBS containing 10 μg/mL of anti-mouse IFN-γ monoclonal antibody (clone R4-6A2, Pharmingen) was added onto nitrocellulose 96-well flat-bottom plates; after 24 h, the plates were washed with RPMI and blocked with RPMI containing 10% FBS for 2 h. Following, 1×10^6 responder cells from spleen, liver, or lymph node were incubated with 3×10^5 antigen-presenting cells in complete medium [1% NEAA, 1% L-glutamine, 1% vitamins and 1% pyruvate, 0.1% 2-ME, 10% FBS (HyClone), and 20 U/mL mouse recombinant IL-2 (SIGMA)]. The plate was incubated in the presence or absence of 10 μM of peptide TEWETGQI. After 24 h, the plates were washed three times with PBS, and five times with PBS–Tween 20 (0.05% Tween). Each well received biotinylated anti-mouse monoclonal antibody (clone XMG1.2, Pharmingen) diluted in PBS-0.05% Tween 20 at a final concentration of 2 μg/mL. The plates were incubated with streptavidin-peroxidase (BD) and developed by adding peroxidase substrate (50 mM Tris–HCl, pH 7.5, containing 1 mg/mL DAB and 1 μL/mL 30% hydrogen peroxide, both from SIGMA). The number of IFN-γ-producing cells was determined using a stereoscope.

Intracellular Cytokine Staining

Two million cells from the spleen, lymph node, or liver were treated with ACK buffer (NH_4Cl, 0.15 M; $KHCO_3$, 10 mM; Na_2-EDTA 0.1 mM; pH = 7.4). ICS was performed after *in vitro* culture of splenocytes in presence or absence of 10 μM of peptide TEWETGQI as described previously (25). Cells were washed three times in plain RPMI and resuspended in cell culture medium consisting of RPMI 1640 medium supplemented with 10 mM HEPES, 0.2% sodium bicarbonate, 59 mg/L of penicillin, 133 mg/L of streptomycin, 10% HyClone FBS, 2 mM L-glutamine, 1 mM sodium pyruvate, 55 μM 2-mercaptoethanol. The viability of the cells was evaluated using 0.2% trypan blue exclusion dye to discriminate between live and dead cells. Cell concentration was adjusted to 2×10^6 cells/mL in cell culture medium containing CD107a FITC antibody (clone 1D4B, BD), anti-CD28 (clone 37.51, BD), BD Golgi-Plug (1 μL/mL), and monensin (5 μg/mL) and incubated no longer than 12 h in V-bottom 96-well plates (Corning) in a final volume of 200 μL in duplicate, at 37°C in a humid environment containing 5% CO_2. After 12 h incubation, cells were stained for surface markers with anti-CD8 PERCP antibody (clone 53-6.7, BD) on ice for 30 min. To detect IFN-γ, TNF or granzyme B by intracellular staining, cells were then washed twice in buffer containing PBS, 0.5% bovine serum

albumin (BSA), and 2 mM EDTA, fixed and permeabilized with BD perm/wash buffer. After being washed twice with BD perm/wash buffer, cells were stained for intracellular markers using APC-labeled anti-IFN-γ (clone XMG1.2, BD), PE-labeled anti-TNF-α (clone MP6-XT22, BD), and anti-granzyme B PE (clone GB11, INVITROGEN) for 20 min on ice. Finally, cells were washed twice with BD perm/wash buffer and fixed in 1% PBS–paraformaldehyde. At least 700,000 cells were acquired on a BD FACS Canto II flow cytometer and then analyzed with FlowJo. Figures S3A,B in Supplementary Material shows the representative ICS gate strategies.

Purification of Liver and Heart Lymphocytes

The perfused liver was lysed with collagenase buffer composed of 0.2 mg/mL collagenase IV (SIGMA), 0.02 mg/mL DNase (SIGMA), and 5% FBS. The leukocytes were separated on a 35% Percoll gradient (GE Healthcare), followed by centrifugation at 600 × *g* for 20 min and at 4°C. The pellet was suspended in RPMI 1640 (SIGMA) with 10% FBS (30). For the purification of the lymphocytes of the heart, we followed the protocol of Gutierrez et al. (31). Briefly, hearts collected from five mice at day 20 d.p.i. were minced, pooled, and incubated for 1 h at 37°C with RPMI 1640, supplemented with $NaHCO_3$, penicillin–streptomycin gentamicin, and 0.05 g/mL of liberase blendzyme CI (Roche, Basel, Switzerland). The organs were processed in a Medimachine (BD Biosciences) in PBS containing 0.01% BSA. After tissue digestion and washes, cell viability was assessed by trypan blue exclusion, counted in a hemocytometer.

Flow Cytometry Analysis

Splenocytes were treated with ACK buffer for red cell lysis and washed with RPMI with 10% FBS. The spleen, heart, lymph node, and liver cells were stained with $H2K^k$-TEWETGQI multimer for 10 min at RT. The cell surface was stained for 30 min at 4°C. The following antibodies were used for surface staining: anti-CD3 APCcy7 (clone 145-2C11, BD), anti-CD8 PERCP or anti-CD8 PACIFIC BLUE (clone 53-6.7, BD), anti-CD11a FITC (clone 2D7, BD), anti-CD11c APCcy7 (clone HL3, BD), anti-CD44 FITC (clone IM7, BD), anti-CD62L PE (clone MEL-14, BD), anti-CXCR3 PERCP/Cy5.5 (clone 173, BioLegend), anti-CD27 FITC (clone LG3A10, BD), anti-CD4 PEcy7 (clone RM4-5, BD), anti-KLRG1 FITC (clone 2F1, eBioscience), anti-CD49d PEcy7 (clone R1-2, BD), anti-CD69 PERCP (clone H1.2F3, BD), anti-CD43 PEcy7 (1B11, BioLegend), anti-CD95 PEcy7 (clone JO2, BD), anti-CD25 FITC (clone LG3A10, BD), anti-CD127 PE (clone SB/199, BD), anti-CD122 FITC (clone TM-β1, BD), anti-CD38 PE (clone 90, BD), anti-β7 PERCP (clone FIB27, BioLegend), anti-CD31 FITC (clone MEC 13.3, BD), anti-CD272 PE (clone 8F4, eBioscience), anti-PD-1 FITC (clone J43, eBioscience), anti-CTLA-4 PE (clone UC10-4B9, eBioscience), and anti-CCR7 PE (clone 4B12, BD). At least 500,000 cells were acquired on a BD FACS Canto II flow cytometer and analyzed with FlowJo 8.7.

In Vivo Proliferation Assay

A/Sn were immunized with ASP-2 using the heterologous "prime-boost" vaccination regimen and infected with 150 trypomastigotes forms of *T. cruzi*. At the moment of infection, mice were treated with monoclonal antibodies (LFA-1 or 2A3 isotype control) and 2 mg of BrdU (5-bromo-2′-deoxyuridine, SIGMA) by route i.p., at every 48 h, until the 20th day after challenge. Then, 2×10^6 splenocytes were treated with ACK buffer for red cell lysis, washed with RPMI plus 10% FBS, and stained with $H2K^k$-TEWETGQI multimer and anti-CD8 antibody. The specific $CD8^+$ T cells were stained according BrdU-FITC Kit protocol (BD Pharmingen) for analysis of BrdU incorporation. A minimum of 700,000 cells were acquired on a BD FACS Canto II flow cytometer and analyzed with FlowJo 8.7.

In Vivo Cytotoxicity Assay

For the *in vivo* cytotoxicity assays, splenocytes collected from naive A/Sn mice were treated with ACK buffer to lyse the red blood cells, as described by Silverio et al. (23). The cells were divided into two populations and were labeled with the fluorogenic dye carboxyfluorescein diacetate succinimidyl diester (CFSE; Molecular Probes, Eugene, OR, USA) at a final concentration of 10 μM ($CFSE^{high}$) or 1 μM ($CFSE^{low}$). $CFSE^{high}$ cells were coated with 2.5 μM of the TEWETGQI ASP-2 peptide for 40 min at 37°C. $CFSE^{low}$ cells remained uncoated. Subsequently, $CFSE^{high}$ cells were washed and mixed with equal numbers of $CFSE^{low}$ cells before intravenous injection (2×10^7 cells per mouse) into *T. cruzi*-infected, immunized and/or treated mice with anti-LFA-1 A/Sn recipients that were sedated with diazepam (20 mg/kg). Spleen cells from the recipient mice were collected at 20 h after adoptive cell transfer and fixed with 1.0% paraformaldehyde. At least 100,000 cells were acquired on a BD FACS Canto II flow cytometer and analyzed with FlowJo 8.7. The percentage of specific lysis was determined using the following formula:

$$\%\ \text{lysis} = 1 - \frac{\left(\%CFSE^{high}\ \text{infected}/\%CFSE^{low}\ \text{infected}\right)}{\left(\%CFSE^{high}\ \text{naive}/\%CFSE^{low}\ \text{naive}\right)\times 100}.$$

Histology and Immunohistochemistry

The mice's heart, spleen, and liver were fixed in 10% formalin, and then dehydrated, embedded in paraffin blocks, and sectioned on a microtome. Staining was obtained with hematoxylin and eosin, and the number of amastigotes nests was quantified using a light microscope with 40× objective lens. Overall, 50 fields/group were counted. For immunohistochemistry the hearts of the animals were removed and frozen in Tissue-Tek O.C.T. (Sakura Finetek), and the 7 μm thickness cuts were made in the cryostat (Leica) and then fixed in ice-cold acetone for 15 min. The samples were stained with 20 μg of the biotinylated anti-CD8 antibody (clone 53-6.7, RD systems) for 12 h in the wet chamber, and after incubation was labeled with streptavidin Alexa Fluor® 488 (Thermo Fischer) at the concentration of 0.5 mg/mL, diluted 1:100 for 1 h and room temperature. The DAPI (4′,6-diamidino-2-phenylindole, SIGMA) dye was used for labeling the 5 mg/mL cell nucleus, diluted 1:1,000 for 15 min at room temperature. The images were acquired in the Confocal Leica TCS SP8 CARS microscope of the Institute of Pharmacology and Molecular Biology (INFAR)

of the Paulista School of Medicine of the Federal University of São Paulo. The images were obtained using the 63× objective and processed by the ImageJ program.

Statistical Analysis

The number of parasites/mL corresponding to the peak of parasitemia, the number of IFN-γ-producing cells (ELISPOT), and the absolute number of $CD8^+$ T cells were compared by analysis of unidirectional variance (ANOVA); subsequently, the Tukey's HSD test was used. To compare the survival of mice after challenge with *T. cruzi,* we used the Log-rank test. The receptor expression was compared using MFI (mean fluorescence intensity), and the *naive* group MFI was taken as the baseline. MFI was determined by the FlowJo software. Differences were considered significant when P value was <0.05.

RESULTS

LFA-1 Is Essential for Survival of A/Sn Mice during the Experimental Challenge with *T. cruzi*

Previously, we demonstrated that treatment with FTY720, which retains $CD8^+$ T cells in the lymph nodes *via* blockade of receptor S1Pr1, culminates in death of immunized mice. As LFA-1 and VLA-4 integrins were expressed on those specific $CD8^+$ T cells we investigated the role of these molecules following immunization and *T. cruzi* infection. To this end, immunized and infected mice were treated with 250 μg of monoclonal antibodies anti-LFA-1 and/or anti-VLA-4 every 48 h to block those molecules. Initially, we analyzed blood parasitemia and, as shown in **Figure 1A**, mice treated with anti-LFA-1 (green) antibody had increased blood parasitemia when compared with the group only immunized and treated with the control isotype (red), whereas mice treated with anti-VLA-4 (yellow) had a parasite burden similar to the immunized (red). To examine whether these two integrins exhibit synergism, one group was treated with both antibodies simultaneously (**Figure 1A**, blue group). Simultaneous treatment resulted in increased blood parasitemia, but this increase was not significant when compared with the group treated with anti-LFA-1 only, indicating that LFA-1, but not VLA-4, is important to control blood parasites. With respect to survival (**Figure 1B**), all mice treated with anti-LFA-1 died after 26 days, whereas all anti-VLA-4-treated mice and isotype control treated mice survived. Therefore, no statistical differences were observed in the survival rate between the mice treated with anti-LFA-1 (green) and the mice treated with both antibodies (blue), but there were differences in survival rate between the mice treated with anti-LFA-1 and mice treated with isotype control. Therefore, during LFA-1 blockade, mice displayed increased blood parasitemia and succumbed after challenge with *T. cruzi*, while VLA-4 blockade does not interfere with parasitemia and survival of treated mice.

To confirm the role of LFA-1 during *T. cruzi* infection, C57BL/6 mice naturally resistant to *T. cruzi* infection were infected and treated. C57BL/6 mice treatment with anti-LFA-1 was able to control blood parasitemia until 12th day after infection, but after that, the blood parasitemia increased and all mice treated with anti-LFA-1 rapidly succumbed to infection (**Figures 1C,D**) when compare the mice treated with the isotype control.

Since LFA-1 blockade increased mouse susceptibility to infection by *T. cruzi*, we investigated the importance of the ICAM-1 integrin, a major ligand of LFA-1. To this end, genetically ICAM-1-deficient mouse was used. These mice were immunized and infected for parasitemia and survival analysis. Both C57BL/6 and ICAM-1 knockout mice displayed similar parasitemia, and the two groups immunized with the ASP-2 gene showed a decreased parasitemia when compared with the vector control immunized groups (**Figure 1E**). In addition, all mice survived the experimental challenge with *T. cruzi* (**Figure 1F**). **Figure 1G** shows the expression of CD54 (ICAM-1) on spleen of $CD8^+$ T cells of WT and deficient mice, and, as expected, the latter ones have lower expression of CD54 compared with WT mice. Altogether, these results indicate that the absence of ICAM-1 does not increase susceptibility to *T. cruzi* infection and suggest that, even though ICAM-1 is a major ligand of LFA-1, there is another ligand (i.e., ICAM-2) that binds to LFA-1 allowing it to exert its functions.

LFA-1 Blockade Increases Tissue Parasite of Immunized and Infected A/Sn Mice

Since anti-VLA-4 treatment did not interfere in the mice parasitemia and/or survival, all following experiments were performed by blocking LFA-1 integrin only. As the LFA-1 blockade leads to increased blood parasitemia and rapid death of the mice, we investigated whether the parasitic increase also occurs in the tissues of infected, immunized, and/or anti-LFA-1-treated A/Sn mice. The heart, liver, and spleen of these mice were extracted after the 20th day of infection for quantification of the parasite's DNA by real-time PCR; in addition, the number of amastigote nests in the heart was quantified using hematoxylin–eosin staining. There was a statistical increase in the number of amastigote nests in the hearts of the LFA-1-treated mice compared with the immunized and infected group, and the largest amount of nests was found in the hearts of mice solely infected (**Figures 2A,B**). In addition, LFA-1 blockade resulted in the increase of parasites in the tissues analyzed compared with immunized, infected mice. The spleen showed higher parasite increase, followed by hearts and livers respectively (**Figure 2C**). These results demonstrate that treatment with anti-LFA-1 increases blood parasitemia, which will reflect on increased tissue parasite burden.

LFA-1 Blockade Increases the Expression Level of the Fas/CD95 Molecule on the Surface of Effector $CD8^+$ T Cells

We analyzed whether LFA-1 blockade affects effector phenotype and activation of specific $CD8^+$ T cells. To this end, splenocytes were stained with anti-CD8 and $H2K^K$ TEWETQGI-multimer, and surface markers. In previous results obtained by our group, we demonstrated that immunization followed by infection induces specific $CD8^+$ T cells with the phenotype of effector cells (TE), which is characterized by the expression of $CD11a^{high}$, $CD44^{high}$, $CD62L^{low}$, and $CD127^{low}$ (25, 26). Anti-LFA-1 treatment increased

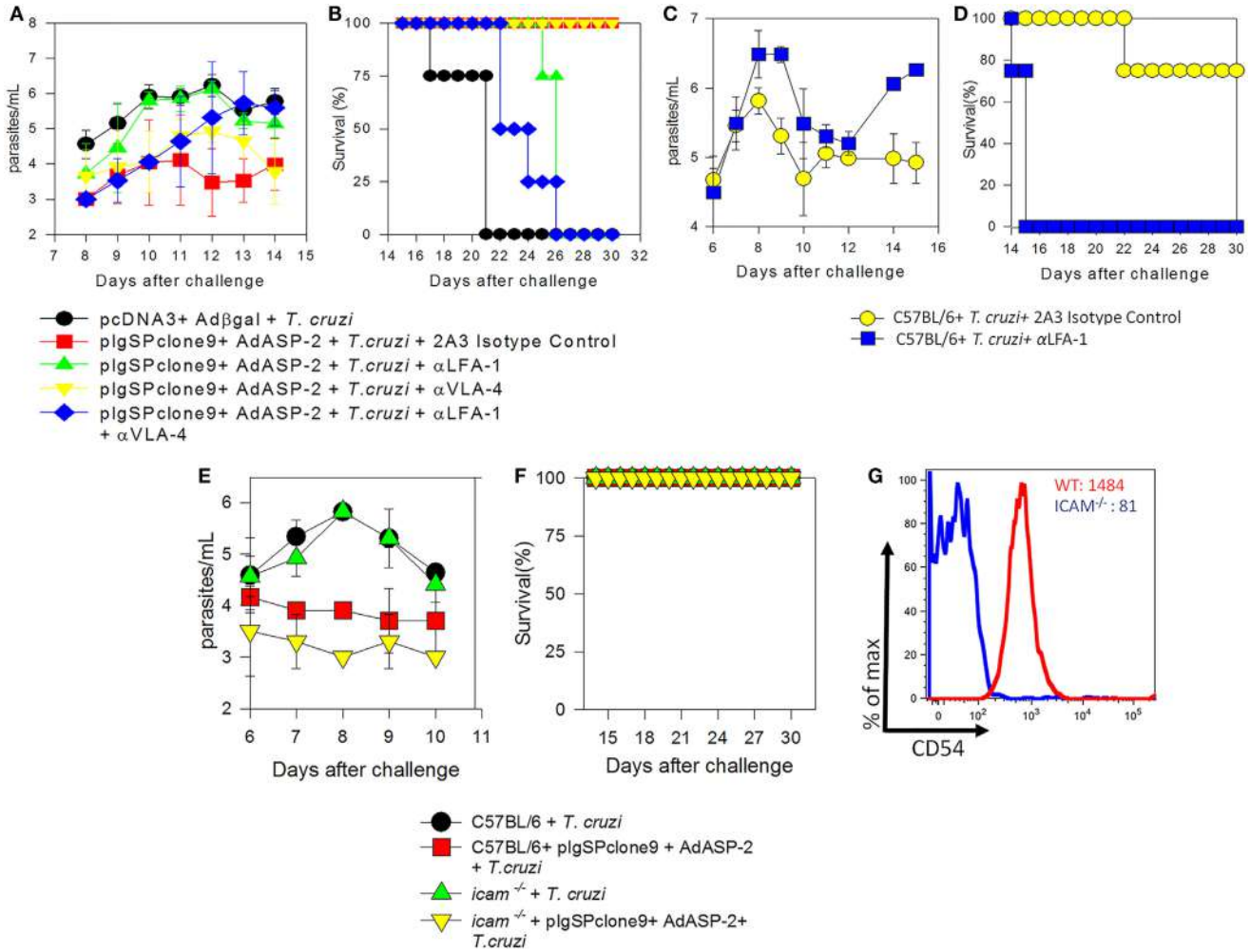

FIGURE 1 | LFA-1 blockade increases blood parasitemia and culminates in the death of A/Sn and C57BL/6 mice. A/Sn-, C57BL/6-, and intercellular adhesion molecule (ICAM)-deficient mice were immunized with plasmids pcDNA3 and/or pIgSPclone9 and adenoviral vectors Adβgal and AdASP-2. Fifteen days after the last immunization dose, mice were infected with 150 (A/Sn) and/or 10^4 (C57BL/6 and ICAM mice) blood trypomastigotes of the Y strain of *Trypanosoma cruzi*. Anti-VLA-4 and/or LFA-1 treatment was performed every 48 h after infection until the 20th days after infection. **(A)** Blood parasitemia was assessed, and values were log transformed and parasitemia data for each mice group are represented as mean ± SD for each group ($n = 4$). Values from peak parasitemia (day 12) were compared by one-way ANOVA and Tukey's HSD tests, and the results were as follows: Significant differences were found between the red in green groups ($P < 0.05$). There were no significant differences between the blue group and the green group ($P > 0.05$). **(B)** Kaplan–Meier curves for survival of the different groups were compared using the log-rank test. The results of the comparisons were as follows: The mice in red group survived longer than the mice in green group. The survival rate of mice in the blue group was similar to the mice in the green group. **(C)** Log parasitemia data for each mice group (C57BL/6 mice infected and/or treated with anti-LFA-1) are represented as mean ± SD for each group ($n = 4$). Values from peak parasitemia (day 9) were no significantly different across the groups ($P > 0.05$). On day 14, significant difference was found between the infected and treated with anti-LFA-1 mice and infected and treated with the anti-2A3 isotype control mice ($P < 0.05$). **(D)** Kaplan–Meier curves for survival of the different groups were compared using the log-rank test. The results of the comparisons were as follows: the mice in yellow group survived longer than the mice in blue group. **(E)** Log parasitemia data for each mice group (ICAM-deficient and C57BL/6 mice) are represented as mean ± SD for each group ($n = 4$). Peak parasitemia values (day 9) were significantly different across C57BL/6 groups and in ICAM-deficient mice groups ($P > 0.05$). **(F)** Kaplan–Meier curves for survival of the different groups were compared, and there were no differences across groups. **(G)** MFI of CD54 (ICAM-1) on $CD8^+$ T cells from C57BL/6 and ICAM-deficient mice: the red line indicates MFI of naïve C57BL/6 mice, whereas the blue line indicates MFI of naïve ICAM-deficient mice. One out of two individual experiments is shown.

the frequency and the absolute number of specific $CD8^+$ T cells in the spleen (**Figures 3A,B**). In addition, as there is competition between the antibodies used for *in vivo* blockade and flow cytometric labeling, we observed a decrease in CD11a MFI in the anti-LFA-1-treated groups (**Figure 3C**). In general, the markers whose expression levels increased in the anti-LFA-1-treated group (Gr.3) in comparison with the infected group (Gr.1) or the immunized and infected group (Gr.2) were as follows: CD27, CD43, CD69, and CD95 (**Figure 3C**). Our group has also demonstrated that the cells generated by immunization followed by infection expressed lower levels of CD95 on the surface compared with infected only group, and these cells were also resistant to death induced by anti-CD95 (12). Moreover, markers CD183, CD38, and PD-1 also displayed increased expression levels on the

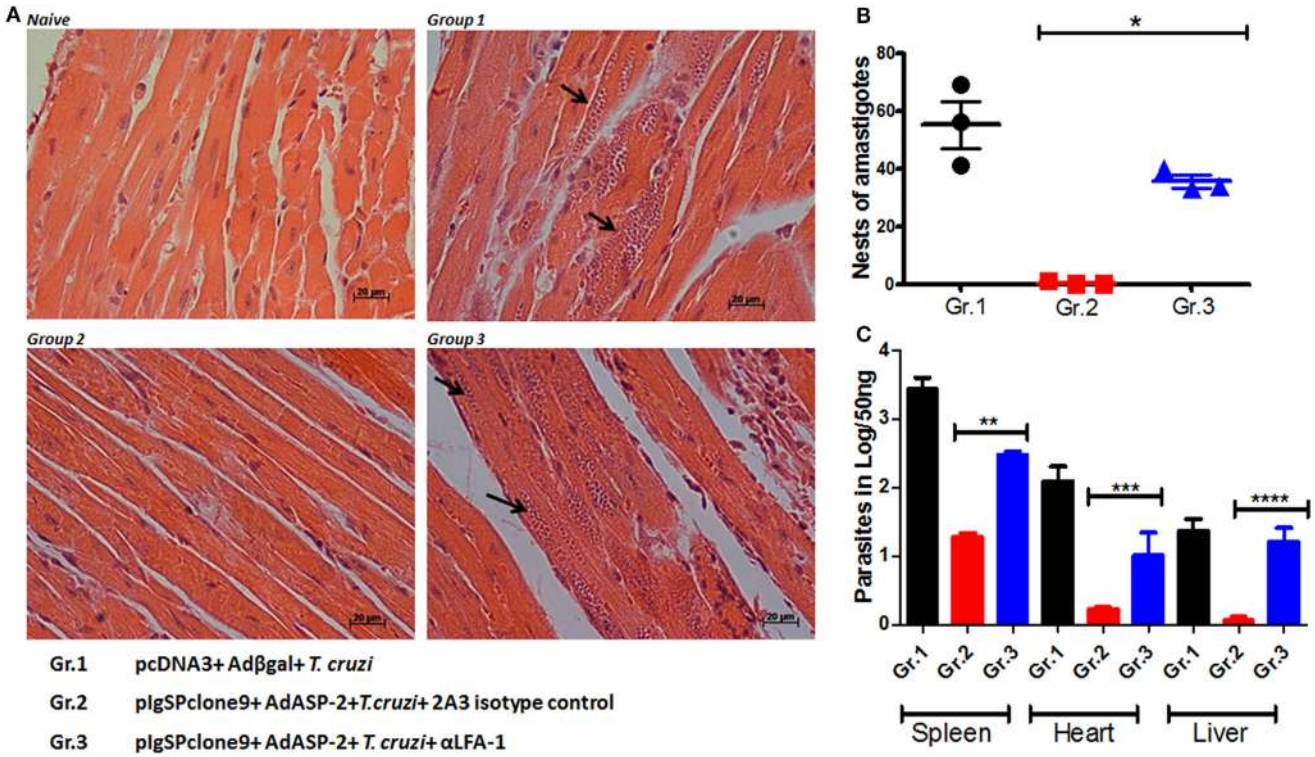

FIGURE 2 | Treatment with anti-LFA-1 increases tissue parasitemia. A/Sn mice were immunized with ASP-2 using the heterologous "prime-boost" vaccination regimen, infected with 150 trypomastigotes forms of *Trypanosoma cruzi* and treated with anti-LFA-1 or isotype control until the 20th after infection. In this day, spleens, hearts, and livers of this mice were taken for quantification of the parasite DNA and count of amastigote nests in the heart. **(A)** Histological section of the heart; the arrows indicate the amastigote nests in each group. **(B)** Quantification of heart amastigote nests performed from 50 fields/group. **(C)** Quantification of the parasite DNA by real-time PCR in the different groups (Log) obtained from 50 ng of tissue DNA. Results represent mean ± SD for each group ($n = 4$) and to a single experiment. Asterisks represent statistical differences among the groups. Statistical analysis was performed using one-way ANOVA (*$P < 0.001$, **$P = 0.000331$, ***$P = 0.006602$, and ****$P < 0.01$).

surface of specific CD8+ T cells after treatment with anti-LFA-1 (Gr.3) compared with Gr.2 (**Figure 3C**). KLRG1, however, had similar MFI among the three groups, and these groups showed low expression of markers CD122, BTLA, CTLA-4, and CD25. These results suggest that anti-LFA-1 treatment does not impair specific CD8+ T cells in the spleen. Instead, there is a greater frequency and absolute number of these cells. In addition, the treatment did not alter the phenotype of effector CD8+ T cells (TE); however, we found in the spleen of treated mice that those CD8+ T cells expressed high levels of CD95.

Specific CD8+ T Cells Accumulate in Secondary Lymphoid Organs and Decrease Migration into the Heart after LFA-1 Blockade

After demonstrating that anti-LFA-1 treatment increases blood and tissue parasitemia and leads to mice death, our hypothesis was that specific CD8+ T cells cannot migrate into the infected tissues since LFA-1 is associated with leukocyte migration. To test our hypothesis, we measured in the spleen, lymph, blood, liver, and heart the frequency of specific CD8+ T cells. For that propose, the cells were labeled with anti-CD8 and $H2K^K$-TEWETGQI multimer. We found higher frequency and increment in the absolute numbers of specific CD8+ T cells in spleens and lymph nodes, but not in the blood and liver of the anti-LFA-1-treated group when compared with the infected and immunized group (**Figures 4A–F**). A dramatic influx reduction of specific CD8+ T cells after anti-LFA-1 treatment (**Figure 4A**) was observed in group 3 hearts. In addition, we found that specific CD8+ T cells in the spleen, blood, and heart of the infected group (Gr.1) and the immunized and infected group (Gr.2) expressed high levels of CD11a, whereas the cells in the immunized, infected, and anti-LFA-1-treated group (Gr.3) showed decreased CD11a MFI due to the competition described earlier (**Figure 4G**). We also evaluated the frequency of total CD8+ T cells in the spleen, blood, and heart and, as shown in Figure S2 in Supplementary Material, there was a reduction in the frequency of CD8+ T cells in the heart of the anti-LFA-1-treated group (Figures S2A–D in Supplementary Material). Furthermore, by immunohistochemistry, there is a decrease in the number of CD8+ T cells in the heart of animals treated with anti-LFA-1 (Figures S2E,F in Supplementary Material). The number of CD8+ T cells in the heart of the treated group was similar to the infected group, and in relation to the immunized group, treatment with anti-LFA-1 decreased the migration of CD8+ T cells to the heart, observed

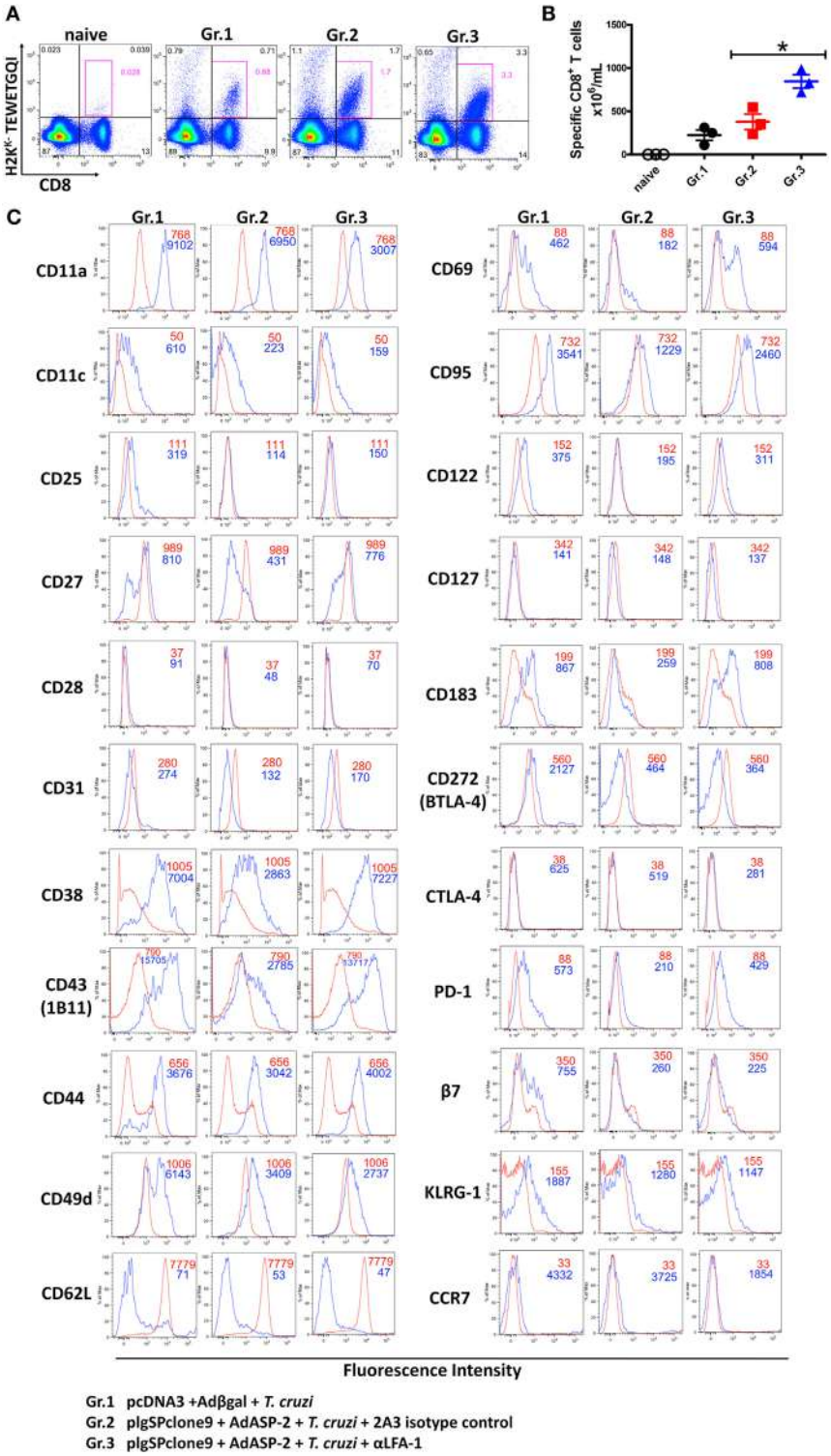

FIGURE 3 | Effector CD8+ T lymphocytes express high levels of CD95 on the surface after anti-LFA-1 treatment. A/Sn mice were immunized with ASP-2 using the heterologous "prime-boost" vaccination regimen, infected with 150 trypomastigotes forms of *Trypanosoma cruzi* and treated with anti-LFA-1 or isotype control until the 20th after infection. In this day, the splenic cells were labeled with H2K^{K}-TEWETGQI multimer, anti-CD8 and surface markers. **(A)** The frequency of specific CD8+ T cells in the spleen. **(B)** Absolute number of specific CD8+ T cells in the spleen. **(C)** Histograms with MFI of each marker analyzed in different groups. The red line represents the *naive* group, whereas the blue line represents groups 1, 2, and 3. Results in panels **(A,B)** are individual values with the mean ± SD of groups ($n = 4$), while in panel **(C)** representative analyses are shown for four mice per experiment. The experiment was performed two or more times with similar results. Statistical analysis was performed using the one-way ANOVA. Asterisks denote statistically significant differences between the groups 2 and 3 ($P < 0.05$).

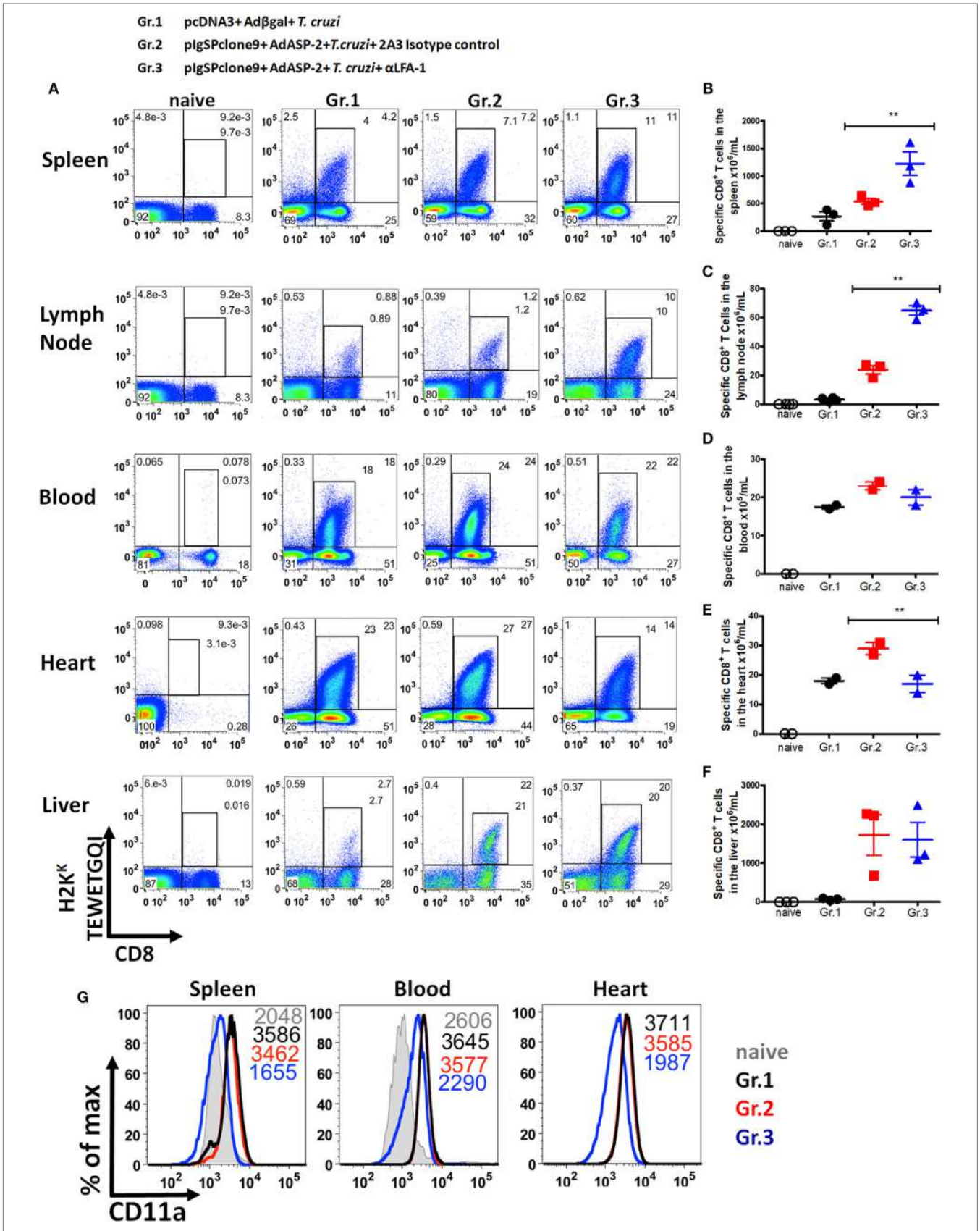

FIGURE 4 | Continued

FIGURE 4 | Continued
Specific CD8+ T cells accumulate in the spleen and lymph node and do not migrate into the heart after anti-LFA-1 treatment. A/Sn mice were immunized with ASP-2 using the heterologous "prime-boost" vaccination regimen, infected with 150 trypomastigotes forms of *Trypanosoma cruzi* and treated with anti-LFA-1 or isotype control until the 20th after infection. In this day, spleen, heart, liver, lymph nodes, and blood cells of the immunized, infected, and treated or not with anti-LFA-1 were labeled with anti-CD8 and H2K^K-TEWETGQI multimer. **(A)** Frequency of specific CD8+ T cells in the spleen, lymph node, blood, heart, and liver, respectively. **(B–F)** Absolute number of specific CD8+ T cells in the spleen, lymph node, blood, heart, and liver, respectively. The results for the spleen, lymph node, and liver are representative values of an individual in each group ($n = 4$) with mean ± SD. While the results for the blood and heart were taken from a pool of five individuals per group, values of an individual of each repetition ($n = 2$) with mean ± SD. Statistical analysis was performed using the one-way ANOVA. **(G)** Histograms represent MFI of specific CD8+ T cells that express CD11a onto the surface in the spleen, blood, and heart, respectively, and the group *naïve* the MFI of CD11a was analyzed onto the surface of CD8+ T cells. Asterisks denote statistically significant differences between groups 2 and 3 (**$P < 0.001$).

by the low number of these cells in the cardiac tissue. These results corroborate the decrease in specific CD8+ T cells in those organs. Therefore, during LFA-1 blockade, specific CD8+ T cells accumulate in the secondary lymphoid organs, such as spleen and lymph node, and cannot migrate into the heart, as observed by the lower frequency of these cells in that organ.

Specific CD8+ T Cells Degranulate and Produce IFN-γ and TNF-α after Anti-LFA-1 Treatment

Having in mind the important role of IFN-γ during infection by *T. cruzi* (2), we analyzed whether the anti-LFA-1 treatment may alter production of IFN-γ by specific CD8+ T cells. We also analyzed the effector function of specific CD8+ T cells in the spleen, liver, and lymph nodes regarding TNF-α production and indirect cytotoxicity involving cell surface mobilization of CD107a. The gate strategy used to evaluate the production of cytokines and the polyfunctionality of specific CD8+ T cells is illustrated in Figures S3A,B in Supplementary Material. In the spleen of the anti-LFA-1-treated group, compared with the immunized and infected group, there was an increase in the percentage of polyfunctional specific CD8+ T cells, that is, cells that are capable of degranulating and, at the same time, producing IFN-γ and TNF-α. Such increase in polyfunctionality of specific CD8+ T cells after anti-LFA-1 treatment was also observed in lymph nodes and liver (**Figures 5A,B**). In addition, anti-LFA-1 treatment also culminated in an increase in the amplitude of the immune response, i.e., the percentage of specific CD8+ T cells producing IFN-γ or TNF-α or degranulating, in the spleen, lymph node, and liver (**Figure 5C**). The number of specific CD8+ T cells producing IFN-γ was higher in the anti-LFA-1-treated group (Gr.3), when compared with Gr.2, and this increase occurred in the spleen, the lymph node, and liver (**Figure 5D**). Altogether, these results show that LFA-1 blockade does not affect the effector function of specific CD8+ T cells regarding IFN-γ and TNF-α secretion and degranulation. The increase in the effector function is probably due to the accumulation of specific cells in spleen and lymph node after treatment with anti-LFA-1.

Specific CD8+ T Cells Reduce Direct Cytotoxicity against Target Cells after Treatment with Anti-LFA-1

First, we tested whether treatment had impaired the frequency and absolute numbers of specific CD8+ T cells. As we can see, there was an increase in the frequency and absolute numbers of specific CD8+ T cells in the anti-LFA-1-treated group (**Figures 6A,B**). We concluded that the treatment did not interfere with specific CD8+ T cell expansion. Since specific CD8+ T cells are capable of secreting IFN-γ and TNF-α after LFA-1 blockade in the spleen, we assessed whether the treatment had impaired specific CD8+ T cells proliferative capacity. The proliferation of specific CD8+ T cells in the spleen was analyzed *in vivo* by thymidine BrdU analog incorporation. We found that a similar proportion of the H2K^K-TEWETGQI CD8+ cells incorporated BrdU *in vivo* in non-treated or treated mice indicating that the proliferative capacity of these cells was not significantly different (Gr. 2 and Gr. 3, **Figure 6C**). However, the infected mice have a greater proliferation in comparison with groups 2 and 3 (**Figures 6C,D**).

Another effector function triggered by specific CD8+ T cells is the direct cytotoxicity against the target cells. Here, we analyzed whether this function had been affected by the treatment. For that purpose, we used *in vivo* cytotoxicity assay. **Figure 7A** shows representative histograms containing two populations P1 (CFSE^{low}) and P2 (CFSE^{high}) showing the specific lysis of H2K^K-TEWETGQI peptide-labeled CFSE^{high} cells from Gr.1, Gr.2, and Gr.3 groups (**Figure 7A**). Surprisingly, we observed that the immunized mice treated with anti-LFA-1 had significantly decreased cytotoxicity when compared with the immunized group (**Figure 7B**). The specific CD8+ T cells from the immunized mice have 80% cytotoxicity whereas the anti-LFA-1-treated cells showed a 29% percentage drop. **Figure 7C** shows that the numbers of CFSE^{low} cells were similar across groups 1, 2, and 3, while the number of cells CFSE^{high} decreased in groups 2 (non-treated) and 3 (treated) compared with group 1 (**Figure 7D**).

The reduction of cytotoxicity did not affect the amount of granzyme B produced by specific CD8+ T cells in the anti-LFA-1-treated group. We observed that MFI and the percentage of specific CD8+ T cells that produce granzyme B were similar across the groups (**Figures 7E,F**). These results demonstrate that treatment with LFA-1 directly affects the cytotoxicity of specific CD8+ T cells and the impairment of this function may be one of the factors responsible for the reversal protection generated by immunization observed after LFA-1 blockade.

DISCUSSION

Our group previously demonstrated that the recirculation of specific CD8+ T cells generated by heterologous prime-boost immunization and *T. cruzi* infection is of paramount importance to the protection of A/Sn mice, which are highly susceptible to infection by *T. cruzi* (12, 13). Given that integrins play an important role

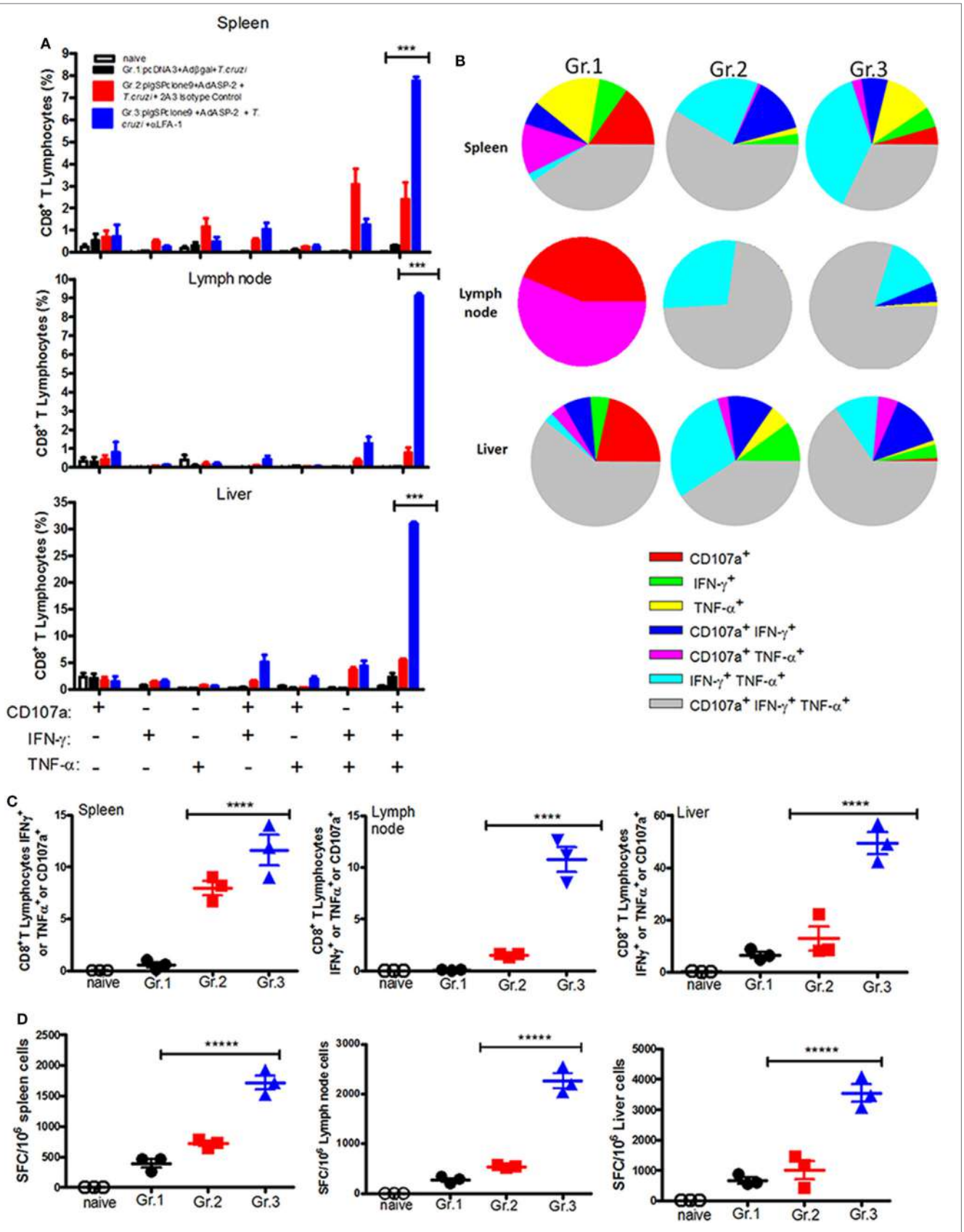

FIGURE 5 | Continued

FIGURE 5 | Continued
Anti-LFA-1 treatment increases the polyfunctionality of specific CD8+ T cells in the spleen, liver, and lymph node, and the number of IFN-γ-producing cells. A/Sn mice were immunized with ASP-2 using the heterologous "prime-boost" vaccination regimen, infected with 150 trypomastigotes forms of *Trypanosoma cruzi*, and treated with anti-LFA-1 or isotype control until 20th days after infection. In this day, splenocytes and cells of inguinal lymph nodes were collected. Furthermore, leukocytes from the liver were isolated by Percoll. These cells were restimulated *in vitro* in the presence of the peptide TEWETGQI at a final concentration of 10 mM. After 12 h, cells were stained for CD8, IFN-γ, and TNF-α. Frequencies were initially estimated for any CD8+ that expressed surface CD107a, IFN-γ, or TNF-α after stimulation *in vitro* with peptide TEWETGQI. **(A)** Percentage of specific CD8+ T cells performing each of the functions shown in the graph combinations; (+) indicates presence, while (–) indicates absence of CD107a/IFN-γ/TNF-α. **(B)** Pie chart represents the fraction of specific CD8+ T cells that carry each of the combinations shown in the legend. **(C)** Amplitude of the immune response, i.e., the percentage of CD8+ T cells that are performing at least one of the functions indicated. **(D)** ELISPOT graph of the IFN-γ-producing cells. Results are representative of two independent experiments with the mean ± SD of each individual shown in the graphs ($n = 4$). Asterisks show statistical difference between the groups. Statistical analysis was performed using one-way ANOVA ($P < 0.05$). Boolean analysis was performed using FlowJo software. SFC, spot-forming cell.

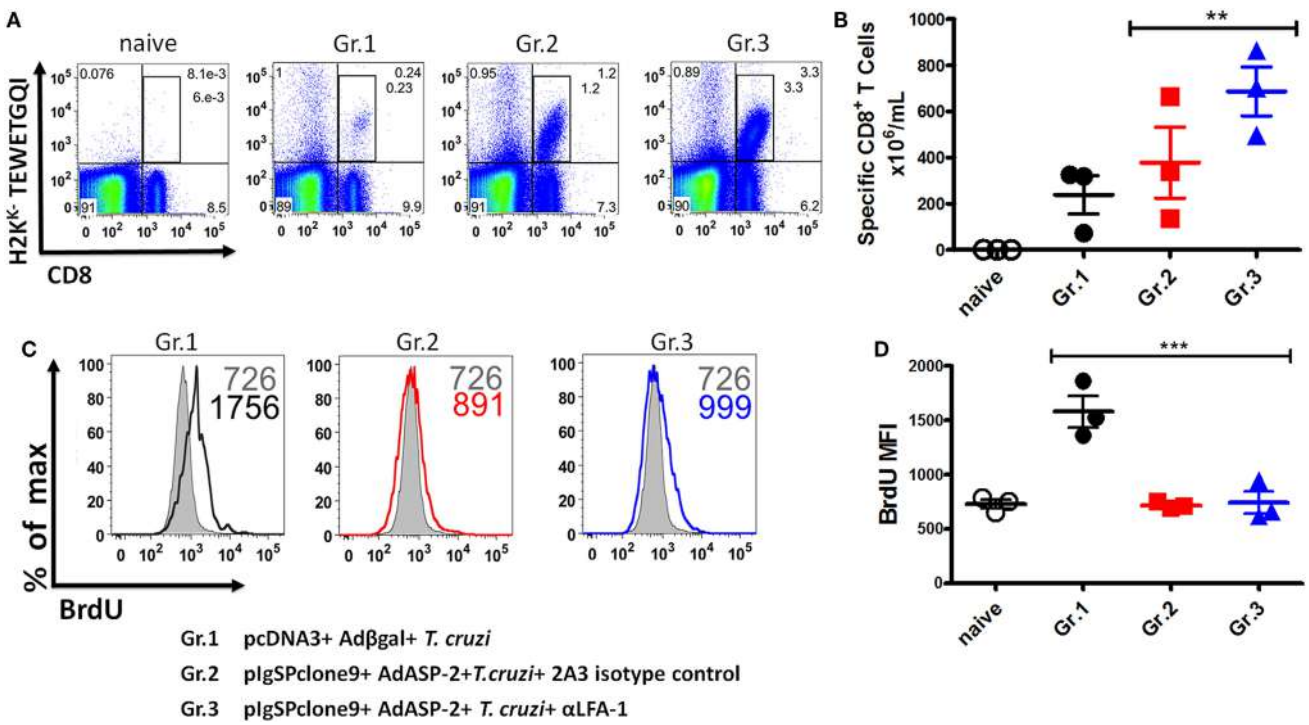

FIGURE 6 | Specific CD8+ T cells can proliferate after the treatment with anti-LFA-1. A/Sn mice were immunized with ASP-2 using the heterologous "prime-boost" vaccination regimen, infected with 150 trypomastigotes forms of *Trypanosoma cruzi*, and treated with anti-LFA-1 or isotype control until 20th days after infection. Mice received 2 mg of 5-bromo-2′-deoxyuridine (BrdU) every 48 h. In this day, spleen was harvested for the proliferation assay. 2 × 10^6 splenocytes were labeled with H2K^K-TEWETGQI multimer, anti-CD8 and anti-BrdU. **(A,B)** The frequency and absolute number of specific CD8+ T cells in the spleen, respectively. **(C,D)** Histograms with MFI of BrdU in the groups and graph of the MFI mean of the specific CD8 T cells expressing BrdU. The graphs represent the mean ± SD for each individual ($n = 3$). Representative results of two independent experiments. Statistical analysis was performed using one-way ANOVA test (**$P < 0.01$; ***$P < 0.005$).

in cell–cell and cell–extracellular matrix interactions, and that these interactions are responsible for the intracellular signal transduction that culminates in cell migration (14) and formation of the immunological synapse (15), the aim of this study was to analyze the role of LFA-1 and VLA-4 integrins in specific CD8+ T cells migration. During activation of specific CD8+ T cells, there was an increase in the expression level of CD11a (LFA-1) and CD49d (VLA-4) chains (12). In addition, an increase in effector CD8+ T cells that express molecules LFA-1/ICAM-1 and VLA-4/VCAM-1 occurred in the hearts of mice infected with *T. cruzi*, suggesting the role of these molecules in the migration of specific CD8+ T cells into infected tissues (22, 23, 32). Here, we investigated the hypothesis that these molecules participate in the migration of specific CD8+ T cells generated by immunization and infection. LFA-1 blockade, but not VLA-4, makes vaccinated A/Sn and infected C57BL/6 mice susceptible to infection with *T. cruzi*. The increased susceptibility of A/Sn mice was accompanied by increased parasitemia and tissue parasite burden, as well as rapid death of these mice. Even though VLA-4 does not play any role in our model, it participates in the migration of specific CTLs into the heart of C3H/He mice when infected with the Colombian strain of *T. cruzi* (22). Because we did not see any role of VLA-4 in the mice parasitemia and survival our study was conducted toward LFA-1 role.

To analyze the role of ICAM-1, a major ligand for LFA-1, we used ICAM-1 KO mice and challenged them with blood

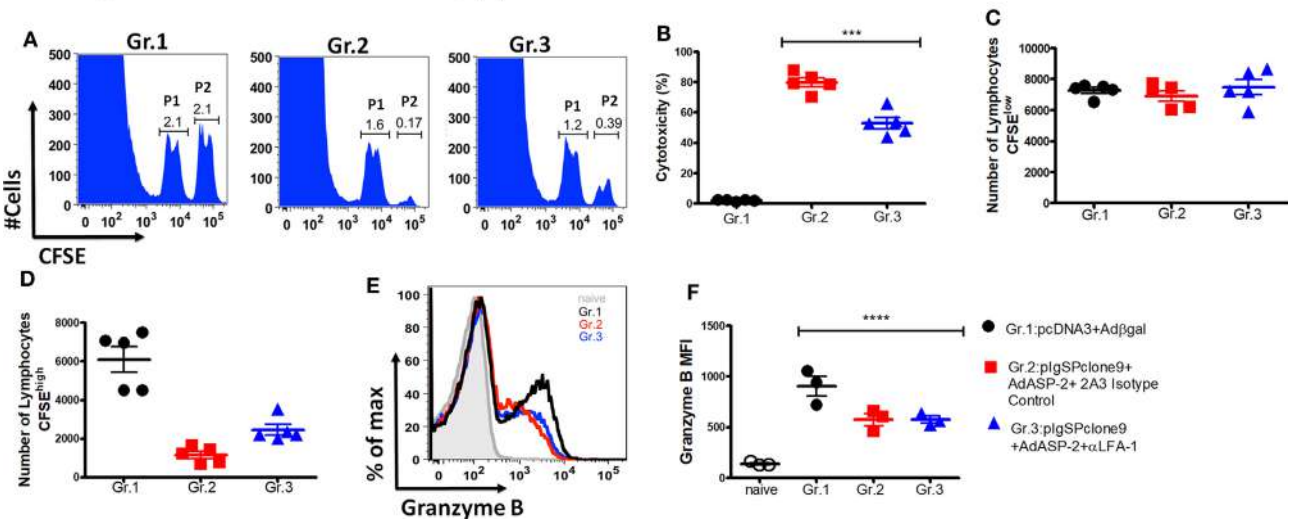

FIGURE 7 | Anti-LFA-1 treatment affects the *in vivo* cytotoxicity of specific CD8+ T cells. A/Sn mice were immunized with ASP-2 using the heterologous "prime-boost" vaccination regimen, infected with 150 trypomastigotes forms of *Trypanosoma cruzi*, and treated with anti-LFA-1 or isotype control until 20th days after infection. After that, the spleen was harvested for the cytotoxicity assay. Splenocytes from *naive* mice were used for labeling with $CFSE^{low}$ (1 μM) and $CFSE^{high}$ (10 μM); the $CFSE^{high}$ population was pulsed with the 2.5 μM of peptide TEWETGQI. The mice immunized and anti-LFA-1 treated or untreated received 10×10^6 cells from each population *via* retro-orbital route. In addition, for analysis of granzyme B expression by the specific CD8+ T cells, 2×10^6 splenocytes were stimulated *in vitro* with 10 μM TEWETGQI peptide. After 12 h, the splenocytes were collected for intracellular labeling of granzyme B. **(A)** The histograms represent the evens of $CFSE^{low}$ (P1) and $CFSE^{high}$ (P2) cells in each group. **(B)** Percentage of the cytotoxicity of specific CD8+ lymphocytes with the mean ± SD for each individual ($n = 6$). **(C,D)** The graphs with the mean cells $CFSE^{low}$ and $CFSE^{high}$ in the spleen of mice. **(E,F)** Histograms and the graph represent MFI and the percentage of specific CD8+ T cells that express granzyme B, respectively. The graphs represent the mean ± SD for each individual ($n = 3$). Representative results of two independent experiments. Statistical analysis was performed using one-way ANOVA test (***$P < 0.01$; ****$P = 0.0047$).

trypomastigotes of the Y strain of *T. cruzi*, which did not affect the susceptibility of these mice to infection. This may be related to the redundancy of ligands by which a receptor can connect to alternate ligands without complete loss of functions performed by a receptor (33–35).

LFA-1 acts as a co-stimulatory molecule participating in the activation of T lymphocytes (36), and it has been shown that this molecule activates CD4+ T cells and induces secretion of cytokines such as IFN-γ and IL-17 (37). Therefore, we evaluated whether LFA-1 blockade impairs the activation of specific CD8+ T cells or interferes with phenotype of effector CD8+ T cells (TE). Our group has characterized the profile of CD8+ T cells induced by immunization that displays a phenotype of effector CD8+ T cells (TE). TE cells are characterized by expression of $CD44^{high}$, $CD62L^{low}$, and $CD127^{low}$ (26), and we evaluated this profile and other activation markers on the cells from anti-LFA-1-treated mice. The anti-LFA-1 blockade decreased the CD11a MFI on specific CD8+ T cells surface by approximately 50%. In addition, treatment did not affect the phenotype of effector CD8+ T cells as well as the expression of early and late activation markers, such as CD69 and CD44, respectively. Results obtained by Gérard and colleagues also showed that the absence of LFA-1 does not reduce the expression of CD69 on CD8+ T cells (38).

The lower expression of CD95 in the cells induced upon vaccination was the main difference to CD8+ T cells generated by the infection, which had higher levels of CD95 (25). There is an increase in the expression of Fas/CD95 on some specific CD8+ T cells after immunization and treatment with anti-LFA-1. This result suggests that specific CD8+ T cells in mice treated with anti-LFA-1 may be more susceptible to programmed cell death by the extrinsic pathway. Similar results were shown by Borthwick and colleagues, who found that LFA-1 blockade reduces the survival of T lymphocytes, thus suggesting the important role of LFA-1 in survival signals during the process of T cells migration (39). Otherwise, reduction of migration to tissues upon LFA-1 blockade might increase effector CD8 T-cells expressing Fas in the secondary lymphoid organs.

Indeed, there is an impaired migration of specific CD8+ T cells after LFA-1 blockade. The number of these cells was quantified in the spleen, heart, liver, lymph nodes, and blood after anti-LFA-1 treatment. The treatment led to an increase in the frequency and absolute number of specific CD8+ T cells in the spleen and lymph node, and a decreased frequency mainly in the heart. However, despite the apparent decrease in the overall number of CD8 T cells in blood, this decrease was not statistically significant (Figure S2 in Supplementary Material). We have previous described that specific-peptide CD8+ activation occurs in the lymph nodes after subcutaneous infection by *T. cruzi* and also in vaccinated model (12, 13). We approached this subject by administering the immunosuppressive drug FTY720 (12, 13). In both models, this drug reduced lymphocyte recirculation by interfering with T cell signaling *via* S1Pr1. This

interference resulted in inhibition of S1Pr1 signaling, effectively trapping T cells within the lymph node without inhibiting T cell activation. FTY720 administration significantly impaired protective immunity supporting the hypothesis that T cell recirculation is critical for the protective immunity they mediate (12, 13). Here, we have not addressed how these cells accumulate more in the lymph after treatment with anti-LFA-1. However, our data confirm that recirculation of these cells is necessary to exert their effector function in the peripheral tissues. Thus, blocking the integrin LFA-1, we observed the same accumulation not only in the lymph node but also in the spleen. However, in our immunization, infection, and treatment model, there was no change in the number of specific $CD8^+$ T cells in the peripheral blood (Figure S2 in Supplementary Material), probably because of the increased accumulation of $CD8^+$ T cells in the spleen and lymph node. This phenomenon may be specific to our immunization and infection model but has not yet been explored in details or found in another model. One explanation might be that the blockage of LFA-1 integrin expressed by $CD8^+$ T cells prevents the interactions with its ligand might be required to exit from lymph node. Another explanation might be due the decreased speed or movement of these cells (40). These issues need to be further addressed in our vaccination and infection model. These results confirm that LFA-1 is important to the migration of specific $CD8^+$ T cells into infected tissues such as the heart, and the decline of these cells should be one of the causes for increased parasitemia in that organ. Recent studies have shown that LFA-1 blockade, and not VLA-4, reduces migration speed of T lymphocytes, leading to decreased antigen scanning by T cells (41) and, hence, lower immune response and higher parasitemia.

We also evaluated whether anti-LFA-1 treatment would affect the effector function of specific $CD8^+$ T cells, since these cells accumulated in the spleen are incapable of controlling the number of parasites. We analyzed the production of pro-inflammatory cytokines, crucial for controlling *T. cruzi* multiplication, such as IFN-γ and TNF-α, and observed that there was accumulation of polyfunctional specific $CD8^+$ T cells capable of degranulating and simultaneously producing TNF-α and IFN-γ in the spleen, lymph node and liver. As the LFA-1 blockade retained $CD8^+$ T cells in the spleen and lymph node, we believe that this accumulation led to increased effector function of these cells. In the liver, in which there was no accumulation of such cells, the increase in intracellular cytokine production can be explained by the fact that LFA-1 blockade does not affect the production of those cytokines. In addition, it has been shown that high doses of anti-LFA-1 were required for impairing the production of those mediators (42). Finally, specific $CD8^+$ T cells proliferated after LFA-1 blockade, and this result was consistent with the data obtained by Gérard et al. (38).

Another important function triggered by specific $CD8^+$ T cells is the direct cytotoxicity against target cells. NK cytotoxic cells and CTLs of chagasic patients express perforin and granzyme B, suggesting the importance of these mediators to the host immune response (43). In addition, specific $CD8^+$ T cells induced by immunization are cytotoxic and can produce perforin (2). Anti-LFA-1 treatment decreased the 80% cytotoxicity of specific $CD8^+$ T cells in the immunized group to 60% after treatment. Similar results were obtained by Petit et al., whereas LFA-1 blockade was responsible for a 50% decrease of direct cytotoxicity triggered by $CD8^+$ T cells (42). In addition, the decrease in cytotoxicity is independent of cytotoxic granule production and degranulation because there was no decrease in the amount of granzyme B and CD107a in specific $CD8^+$ T cells treated with anti-LFA-1. We believe that cytotoxicity is impaired not because of the reduction of cytotoxic granules but because LFA-1 is important to maintain stability between target and cytotoxic cells. The role of LFA-1 in maintaining a stable contact between the cells was demonstrated by blocking β2 chain of LFA-1, since absence of such molecule impaired the formation time of cell protrusions, as well as the stability of the immunological synapse (44–47). Also, it has been shown that LFA-1 blockade impairs close contact between effector T cells and antigen-presenting cells (48).

The reduction of direct cytotoxicity may explain why specific $CD8^+$ T cells cannot control the number of parasites in the spleen even if accumulation of these cells occurs during LFA-1 blockade. In addition, our results suggest that LFA-1 plays an important role in the migration of specific $CD8^+$ T cells into the heart and the survival of these cells. Finally, we believe that impairment of direct cytotoxicity and lower migration of specific $CD8^+$ T cells into the heart are the major causes of lack of protection to *T. cruzi* infection upon immunization and treatment with anti-LFA-1.

ETHICS STATEMENT

This study was carried out in strict accordance with the recommendations in the Guide for the Care and Use of Laboratory mice of the Brazilian National Council of Animal Experimentation (http://www.cobea.org.br/). The protocol was approved by the Committee on the Ethics of Animal Experiments of the Institutional Animal Care and Use Committee at the Federal University of Sao Paulo (Id # CEP 7559051115).

AUTHOR CONTRIBUTIONS

CF, LC, and JV conceived and designed the experiments. CF, LC, FV, BM, CM, PR, and DA performed the experiments. CF and LC analyzed the data and prepared the figures. AM, RG, O-BR, and MR contributed with reagents and materials. CF and JV wrote the manuscript. ML, JL-V, CM, and BM performed the final review of the article. All the authors read and approved the final article.

ACKNOWLEDGMENTS

This work is a tribute to the memory of Professor Mauricio Martins Rodrigues.

FUNDING

This research was supported by the Fundação de Amparo à Pesquisa do Estado de São Paulo (FAPESP, programa Jovem Pesquisador Processo: 2012/22514-3), CF (processo FAPESP: 2015/08814-2); LC (Processo FAPESP: 2017/11499-7); BM (2014/19422-5). CF, LC, and BM were recipients of fellowship from FAPESP. JV, O-BR, ML, AM, RG, JL-V, DA, and

MR are recipients of fellowships from CNPq. CM and BCA are recipients of fellowships from Coordenação de Aperfeiçoamento de Pessoal de Nível Superior (CAPES). JL-V is recipient of fellowships from UFRJ. RG is supported by a grant from the US National Institutes of Health (NIAID R01AI116577).

SUPPLEMENTARY MATERIAL

The Supplementary Material for this article can be found online at http://www.frontiersin.org/article/10.3389/fimmu.2017.01291/full#supplementary-material.

REFERENCES

1. World Health Organization. *Chagas Disease (American trypanosomiasis)*. World Health Organization (2016). Available from: http://www.who.int/chagas/epidemiology/en/
2. De Alencar BCG, Persechini PM, Haolla FA, Oliveira G, Silverio JC, Lannes-Vieira J, et al. Perforin and gamma interferon expression are required for CD4(+) and CD8(+) T-cell-dependent protective immunity against a human parasite, *Trypanosoma cruzi*, elicited by heterologous plasmid DNA prime-recombinant adenovirus 5 boost vaccination. *Infect Immun* (2009) 77(10):4383–95. doi:10.1128/IAI.01459-08
3. Vasconcelos JRC, Hiyane MI, Marinho CRF, Claser C, Machado AV, Gazzinelli RT, et al. Protective immunity against *Trypanosoma cruzi* infection in a highly susceptible mouse strain after vaccination with genes encoding the amastigote surface protein-2 and trans-sialidase. *Hum Gene Ther* (2004) 15(9):878–86. doi:10.1089/hum.2004.15.878
4. Machado AV, Cardoso JE, Claser C, Rodrigues MM, Gazzinelli RT, Bruna-Romero O. Long-term protective immunity induced against *Trypanosoma cruzi* infection after vaccination with recombinant adenoviruses encoding amastigote surface protein-2 and trans-sialidase. *Hum Gene Ther* (2006) 17(9):898–908. doi:10.1089/hum.2006.17.898
5. Freel SA, Lamoreaux L, Chattopadhyay PK, Saunders K, Zarkowsky D, Overman RG, et al. Phenotypic and functional profile of HIV-inhibitory CD8 T cells elicited by natural infection and heterologous prime/boost vaccination. *J Virol* (2010) 84(10):4998–5006. doi:10.1128/JVI.00138-10
6. Jaoko W, Karita E, Kayitenkore K, Omosa-Manyonyi G, Allen S, Than S, et al. Safety and immunogenicity study of multiclade HIV-1 adenoviral vector vaccine alone or as boost following a multiclade HIV-1 DNA vaccine in Africa. *Plos One* (2010) 5(9):e12873. doi:10.1371/journal.pone.0012873
7. Koup RA, Roederer M, Lamoreaux L, Fischer J, Novik L, Nason MC, et al. Priming immunization with DNA augments immunogenicity of recombinant adenoviral vectors for both HIV-1 specific antibody and T-cell responses. *Plos One* (2010) 5(2):e9015. doi:10.1371/journal.pone.0009015
8. Hill AV, Reyes-Sandoval A, O'Hara G, Ewer K, Lawrie A, Goodman A, et al. Prime-boost vectored malaria vaccines: progress and prospects. *Hum Vaccin* (2010) 6:78–83. doi:10.4161/hv.6.1.10116
9. Schooley RT, Spritzler J, Wang H, Lederman MM, Havlir D, Kuritzkes DR, et al. AIDS clinical trials group 5197: a placebo-controlled trial of immunization of HIV-1-infected persons with a replication-deficient adenovirus type 5 vaccine expressing the HIV-1 core protein. *J Infect Dis* (2010) 202(5):705–16. doi:10.1086/655468
10. De Rosa SC, Thomas EP, Bui J, Huang Y, deCamp A, Morgan C, et al. HIV-DNA priming alters T cell responses to HIV-adenovirus vaccine even when responses to DNA are undetectable. *J Immunol* (2011) 187(6):3391–401. doi:10.4049/jimmunol.1101421
11. Chuang I, Sedegah M, Cicatelli S, Spring M, Polhemus M, Tamminga C, et al. DNA prime/adenovirus boost malaria vaccine encoding *P. falciparum* CSP and AMA1 induces sterile protection associated with cell-mediated immunity. *PLoS One* (2013) 8(2):e55571. doi:10.1371/journal.pone.0055571
12. Vasconcelos JR, Dominguez MR, Neves RL, Ersching J, Araújo A, Santos LI, et al. Adenovirus vector-induced CD8+ T effector memory cell differentiation and recirculation, but not proliferation, are important for protective immunity against experimental *Trypanosoma cruzi* infection. *Hum Gene Ther* (2014) 25(4):350–63. doi:10.1089/hum.2013.218
13. Dominguez MR, Ersching J, Lemos R, Machado AV, Bruna-Romero O, Rodrigues MM, et al. Re-circulation of lymphocytes mediated by sphingosine-1-phosphate receptor-1 contributes to resistance against experimental infection with the protozoan parasite *Trypanosoma cruzi*. *Vaccine* (2012) 30(18):2882–91. doi:10.1016/j.vaccine.2012.02.037
14. Hogg N, Laschinger M, Giles K, McDowall A. T-cell integrins: more than just sticking points. *J Cell Sci* (2003) 1(116):4695–705. doi:10.1242/jcs.00876
15. Dustin ML. The cellular context of T cell signaling. *Immunity* (2009) 30(4):482–92. doi:10.1016/j.immuni.2009.03.010
16. Shamri R, Grabovsky V, Gauguet JM, Feigelson S, Manevich E, Kolanus W, et al. Lymphocyte arrest requires instantaneous induction of an extended LFA-1 conformation mediated by endothelium-bound chemokines. *Nat Immunol* (2005) 6(5):497–506. doi:10.1038/ni1194
17. Woolf E, Grigorova I, Sagiv A, Grabovsky V, Feigelson SW, Shulman Z, et al. Lymph node chemokines promote sustained T lymphocyte motility without triggering stable integrin adhesiveness in the absence of shear forces. *Nat Immunol* (2007) 8(10):1076–85. doi:10.1038/ni1499
18. Glatigny S, Duhen R, Arbelaez C, Kumari S, Bettelli E. Integrin alpha L controls the homing of regulatory T cells during CNS autoimmunity in the absence of integrin alpha 4. *Sci Rep* (2015) 16(5):7834. doi:10.1038/srep07834
19. Kwun J, Farris AB, Song H, Mahle WT, Burlingham WJ, Knechtle SJ. Impact of leukocyte function-associated antigen-1 blockade on endogenous allo-specific T cells to multiple minor histocompatibility antigen mismatched cardiac allograft. *Transplantation* (2015) 99(12):2485–93. doi:10.1097/TP.0000000000000805
20. Harning R, Pelletier J, Lubbe K, Takei F, Merluzzi VJ. Reduction in the severity of graft-versus-host disease and increased survival in allogenic mice by treatment with monoclonal antibodies to cell adhesion antigens LFA-1 alpha and MALA-2. *Transplantation* (1991) 52:842–5. doi:10.1097/00007890-199111000-00017
21. Kariya T, Ueta H, Xu XD, Koga D, Ezaki T, Yu E, et al. Direct evidence for activated CD8+ T cell transmigration across portal vein endothelial cells in liver graft rejection. *J Gastroenterol* (2016) 51(10):985–98. doi:10.1007/s00535-016-1169-1
22. Dos Santos PV, Roffê E, Santiago HC, Torres RA, Marino AP, Paiva CN, et al. Prevalence of CD8(+) alpha beta T cells in *Trypanosoma cruzi*-elicited myocarditis is associated with acquisition of CD62Llow LFA-1 highVLA-4 high activation phenotype and expression of IFN-gamma-inducible adhesion and chemoattractant molecules 1. *Microbes Infect* (2001) 3:971–84. doi:10.1016/S1286-4579(01)01461-7
23. Silverio JC, Pereira IR, Cipitelli Mda C, Vinagre NF, Rodrigues MM, Gazzinelli RT, et al. CD8+ T-cells expressing interferon gamma or perforin play antagonistic roles in heart injury in experimental *Trypanosoma cruzi*-elicited cardiomyopathy. *PLoS Pathog* (2012) 8(4):e1002645. doi:10.1371/journal.ppat.1002645
24. Michailowsky V, Celes MR, Marino AP, Silva AA, Vieira LQ, Rossi MA, et al. Intercellular adhesion molecule 1 deficiency leads to impaired recruitment of T lymphocytes and enhanced host susceptibility to infection with *Trypanosoma cruzi*. *J Immunol* (2004) 1:463–70. doi:10.4049/jimmunol.173.1.463
25. Vasconcelos JR, Bruña-Romero O, Araújo AF, Dominguez MR, Ersching J, de Alencar BC, et al. Pathogen-induced proapoptotic phenotype and high CD95 (Fas) expression accompany a suboptimal CD8+ T-cell response: reversal by adenoviral vaccine. *PLoS Pathog* (2012) 8(5):e1002699. doi:10.1371/journal.ppat.1002699
26. Rigato PO, de Alencar BC, Vasconcelos JR, Dominguez MR, Araújo AF, Machado AV, et al. Heterologous plasmid DNA prime-recombinant human adenovirus 5 boost vaccination generates a stable pool of protective long-lived CD8+T effector memory cells specific for a human parasite, *Trypanosoma cruzi*. *Infect Immun* (2011) 79(5):2120–30. doi:10.1128/IAI.01190-10
27. Tzelepis F, de Alencar BC, Penido ML, Gazzinelli RT, Persechini PM, Rodrigues MM. Distinct kinetics of effector CD8+ cytotoxic T cells after infection with *Trypanosoma cruzi* in naïve or vaccinated mice. *Infect Immun* (2006) 74(4):2477–81. doi:10.1128/IAI.74.4.2477-2481.2006

28. Reisman N, Floyd T, Wagener M, Kirk A, Larsen C, Ford M. LFA-1 blockade induces effector and regulatory T-cell enrichment in lymph nodes and synergizes with CTLA-4lg to inhibit effector function. *Blood* (2011) 118(22):5851–61. doi:10.1182/blood-2011-04-347252
29. Piron M, Fisa R, Casamitjana N, López-Chejade P, Puig L, Vergés M, et al. Development of a real-time PCR assay for *Trypanosoma cruzi* detection in blood samples. *Acta Trop* (2007) 103(3):195–200. doi:10.1016/j.actatropica.2007.05.019
30. Hintermann E, Ehser J, Christen U. The CYP2D6 animal model: how to induce autoimmune hepatitis in mice. *J Vis Exp* (2012) 3(60):3644. doi:10.3791/3644
31. Gutierrez F, Mariano F, Oliveira C, Pavanelli W, Guedes P, Silva G, et al. Regulation of *Trypanosoma cruzi*-induced myocarditis by programmed death cell receptor 1. *Infect Immun* (2011) 79:1873–81. doi:10.1128/IAI.01047-10
32. Zhang L, Tarleton RL. Persistent production of inflammatory and anti-inflammatory cytokines and associated MHC and adhesion molecule expression at the site of infection and disease in experimental *Trypanosoma cruzi* infections. *Exp Parasitol* (1996) 84(2):203–13. doi:10.1006/expr.1996.0106
33. Martin SD, Spinger TA. Intercellular adhesion de-1 (CAM-l) is a ligand for lymphocyte function-associated antigen 1 (LFA-1). *Cell* (1987) 51:813–9. doi:10.1016/0092-8674(87)90104-8
34. Rahman A, Fazal F. Hug tightly and say goodbye: role of endothelial ICAM-1 in leukocyte transmigration. *Antioxid Redox Signal* (2009) 11(4):823–39. doi:10.1089/ARS.2008.2204
35. Ley K. Pathways and bottlenecks in the web of inflammatory adhesion molecules and chemoattractants. *Immunol Res* (2001) 24(1):87–95. doi:10.1385/IR:24:1:87
36. Bachmann MF, McKall-Faienza K, Schmits R, Bouchard D, Beach J, Speiser DE, et al. Distinct roles for LFA-1 and CD28 during activation of naive T cells: adhesion versus costimulation. *Immunity* (1997) 7:549–57. doi:10.1016/S1074-7613(00)80376-3
37. Mori M, Hashimoto M, Matsuo T, Fujii T, Furu M, Ito H, et al. Cell-contact-dependent activation of CD4+ T cells by adhesion molecules on synovial fibroblasts. *Mod Rheumatol* (2017) 27(3):448–56. doi:10.1080/14397595.2016.1220353
38. Gérard A, Khan O, Beemiller P, Oswald E, Hu J, Matloubian M, et al. Secondary T cell–T cell synaptic interactions drive the differentiation of protective CD8+ T cells. *Nat Immunol* (2013) 14(4):356–63. doi:10.1038/ni.2547
39. Borthwick NJ, Akbar AA, Buckley C, Pilling D, Salmon M, Jewell AP, et al. Transendothelial migration confers a survival advantage to activated T lymphocytes: role of LFA-1/ICAM-1 interactions. *Clin Exp Immunol* (2003) 134:246–52. doi:10.1046/j.1365-2249.2003.02298.x
40. Reichardt P, Patzak I, Jones K, Etemire E, Gunzer M, Hogg N. A role for LFA-1 in delaying T-lymphocyte egress from lymph nodes. *EMBO J* (2013) 32(6):829–43. doi:10.1038/emboj.2013.33
41. Katakai T, Habiro K, Kinashi T. Dendritic cells regulate high-speed interstitial T cell migration in the lymph node via LFA-1/ICAM-1. *J Immunol* (2013) 191(3):1188–99. doi:10.4049/jimmunol.1300739
42. Petit AE, Demotte N, Scheid B, Wildmann C, Bigirimana R, Gordon-Alonso M, et al. A major secretory defect of tumour-infiltrating T lymphocytes due to galectin impairing LFA-1-mediated synapse completion. *Nat Commun* (2016) 22(7):12242. doi:10.1038/ncomms12242
43. Dotiwala F, Mulik S, Polidoro RB, Ansara JA, Burleigh BA, Walch M, et al. Killer lymphocytes use granulysin, perforin and granzymes to kill intracellular parasites. *Nat Med* (2016) 22(2):210–6. doi:10.1038/nm.4023
44. Hivrozand C, Saitaki M. Biophysical aspects of T lymphocyte activation at the immune synapse. *Front Immunol* (2016) 15(7):46. doi:10.3389/fimmu.2016.00046
45. Kinashi T. Intracellular signalling controlling integrin activation in lymphocytes. *Nat Rev Immunol* (2005) 5(7):546–59. doi:10.1038/nri1646
46. Sigal A, Bleijs DA, Grabovsky V, van Vliet SJ, Dwir O, Figdor CG, et al. The LFA-1 integrin supports rolling adhesions on ICAM-1 under physiological shear flow in a permissive cellular environment. *J Immunol* (2000) 165:442–52. doi:10.4049/jimmunol.165.1.442
47. Morgan MM, Labno CM, Van Seventer GA, Denny MF, Straus DB, Burkhardt JK. Superantigen-induced T cell: B cell conjugation is mediated by LFA-1 and requires signaling through Lck, but not ZAP-70. *J Immunol* (2001) 167:5708–18. doi:10.4049/jimmunol.167.10.5708
48. Friedman RS, Jacobelli J, Krummel MF. Surface-bound chemokines capture and prime T cells for synapse formation. *Nat Immunol* (2006) 7(10):1101–8. doi:10.1038/ni1384

Conflict of Interest Statement: The authors declare that the research was conducted in the absence of any commercial or financial relationships that could be construed as a potential conflict of interest.

PLOS | NEGLECTED TROPICAL DISEASES

RESEARCH ARTICLE

CXCR3 chemokine receptor guides *Trypanosoma cruzi*-specific T-cells triggered by DNA/adenovirus ASP2 vaccine to heart tissue after challenge

Camila Pontes Ferreira[1], Leonardo Moro Cariste[2], Barbara Ferri Moraschi[1], Bianca Ferrarini Zanetti[3], Sang Won Han[3], Daniel Araki Ribeiro[2], Alexandre Vieira Machado[4], Joseli Lannes-Vieira[5], Ricardo Tostes Gazzinelli[4,6], José Ronnie Carvalho Vasconcelos[1,2]*

1 Department of Microbiology, Immunology and Parasitology, Federal University of São Paulo, São Paulo, Brazil, **2** Department of Biosciences, Federal University of São Paulo, Santos, Brazil, **3** Department of Biophysics, Federal University of São Paulo, São Paulo, Brazil, **4** René Rachou Research Center, Fiocruz, Minas Gerais, Brazil, **5** Laboratory of Biology of the Interactions, Oswaldo Cruz Institute/Fiocruz, Rio de Janeiro, Brazil, **6** Division of Infectious Diseases and Immunology, University of Massachusetts Medical School, Worcester, United States ofAmerica

* jrcvasconcelos@gmail.com

OPEN ACCESS

Citation: Pontes Ferreira C, Cariste LM, Ferri Moraschi B, Ferrarini Zanetti B, Won Han S, Araki Ribeiro D, et al. (2019) CXCR3 chemokine receptor guides *Trypanosoma cruzi*-specific T-cells triggered by DNA/adenovirus ASP2 vaccine to heart tissue after challenge. PLoS Negl Trop Dis 13 (7): e0007597. https://doi.org/10.1371/journal.pntd.0007597

Editor: Juan M. Bustamante, University of Georgia, UNITED STATES

Received: March 14, 2019

Accepted: July 2, 2019

Published: July 29, 2019

Data Availability Statement: All relevant data are within the manuscript and its Supporting Information files.

Funding: This work was supported by grant from Fundação de Amparo à Pesquisa do Estado de São Paulo (http://www.fapesp.br/) (JRCV: 2012/22514-3; 2018/15607-1 CF: 2015/08814-2; LC: 2017/11499-7; BM: 2016/02840-4), Instituto Nacional de Ciência e Tecnologia em Vacinas (http://inct.cnpq.

Abstract

$CD8^+$ T lymphocytes play an important role in controlling infections by intracellular pathogens. Chemokines and their receptors are crucial for the migration of $CD8^+$ T-lymphocytes, which are the main IFNγ producers and cytotoxic effectors cells. Although the participation of chemokine ligands and receptors has been largely explored in viral infection, much less is known in infection by *Trypanosoma cruzi*, the causative agent of Chagas disease. After *T. cruzi* infection, CXCR3 chemokine receptor is highly expressed on the surface of $CD8^+$ T-lymphocytes. Here, we hypothesized that CXCR3 is a key molecule for migration of parasite-specific $CD8^+$ T-cells towards infected tissues, where they may play their effector activities. Using a model of induction of resistance to highly susceptible A/Sn mice using an ASP2-carrying DNA/adenovirus prime-boost strategy, we showed that CXCR3 expression was upregulated on $CD8^+$ T-cells, which selectively migrated towards its ligands CXCL9 and CXCL10. Anti-CXCR3 administration reversed the vaccine-induced resistance to *T. cruzi* infection in a way associated with hampered cytotoxic activity and increased proapoptotic markers on the $H2K^K$-restricted TEWETGQI-specific $CD8^+$ T-cells. Furthermore, CXCR3 receptor critically guided TEWETGQI-specific effector $CD8^+$ T-cells to the infected heart tissue that express CXCL9 and CXCL10. Overall, our study pointed CXCR3 and its ligands as key molecules to drive *T. cruzi*-specific effector $CD8^+$ T-cells into the infected heart tissue. The unveiling of the process driving cell migration and colonization of infected tissues by pathogen-specific effector T-cells is a crucial requirement to the development of vaccine strategies.

br/), Coordenação de Aperfeiçoamento de Pessoal de Nível Superior (http://www.capes.gov.br/) and Conselho Nacional de Desenvolvimento Científico e Tecnológico (http://cnpq.br/). RTG: Fapemig and National Institutes of Health (1R01AI116577). The funders had no role in study design, data collection and analysis, decision to publish, or preparation of the manuscript.

Competing interests: The authors declare that the research was conducted in the absence of any commercial or financial relationships that could be construed as a potential conflict of interest.

Author summary

Chemokine receptors and cell adhesion molecules are essential for T lymphocytes migration into infected tissues. Previously, our group demonstrated that CXCR3 receptor was highly expressed on specific $CD8^+$ T-cells surface after immunization and infection by *T. cruzi*. Also, recirculation of specific $CD8^+$ T-cells was more important than proliferation to control the infection by *T cruzi*. As $CD8^+$ T lymphocytes are responsible for controlling *T. cruzi* infection by releasing IFN-γ or by direct cytotoxicity against infected target cells, our aim was to analyze the role of the chemokine receptor CXCR3 in the migration of specific $CD8^+$ T-cells towards infected tissues. Our results revealed that intervention on CXCR3 by administration of a blocking anti-CXCR3 antibody decreased $CD8^+$ T-cell migration, hampering the access of parasite-specific effector cell into the heart tissue of mice infected by *T. cruzi*. Therefore, to induce the appropriate migration footmarks is crucial for drive the pathogen-specific effector to sites of infection and, therefore, to clarify this requirement is a crucial strategy for vaccine development.

Introduction

The causative agent of Chagas disease *Trypanosoma cruzi* is an intracellular parasite that infects a variety of cells of the mammalian host [1,2]. The activation of adaptive immune response occurs by recruiting T lymphocytes to the infection sites after the presentation of trypomastigote/amastigote-related proteins via MHC-I or MHC-II [3,4]. $CD8^+$ T lymphocytes are the cells primarily responsible for controlling intracellular pathogens such as *T. cruzi* [5–7]. Their relevance to the control of *T. cruzi* infection was demonstrated during the infection of CD8-deficient mice, or by the blockade of this molecule using monoclonal antibodies; in both cases, animals did not survive to infection [8]. The multiple antiparasitic mechanisms mediated by these cells include secretion of cytokines and direct cytotoxicity against infected cells [9,10].

The importance of the immune response mediated by $CD8^+$ T lymphocytes, which promote resistance to *T. cruzi* infection, has led several groups to investigate different vaccine strategies [11]. Our group has been studying the prime-boost protocol that uses plasmid vector for priming and a replication-defective human adenovirus type 5 (AdHu5 vector) [9,12] for boosting, both containing an insertion of the amastigote surface protein 2 (ASP2) gene ASP2. That immunization protocol can induce a strong CD8-mediated response able to protect the highly susceptible A/Sn mice to experimental *T. cruzi* infection [13,14]. Recently, we have shown that more than proliferative response, the specific $CD8^+$ T-cells need to recirculate to exert protection against infection in A/Sn mice [9,13].

Chemokine molecules are small chemotactic molecules responsible for the guidance of leukocyte migration during homeostasis and inflammation [15]. In addition to cell migration, chemokines acting as costimulatory molecules involved in T-lymphocytes activation, differentiation and proliferation [16,17]. Pro-inflammatory chemokines are induced by infection with different pathogens and molecular inflammatory stimuli [18]. Chemokines expression are induced by an IFN-γ- and TNF-enriched Th1-type immune response triggered by infection with intracellular pathogens [19,20] such as *T. cruzi* [21–23]. Naive T cells differentiate into cytokine-producing cells such as IFN-γ, IL-2 and TNF; this differentiation occurs through the expression of interleukin IL-12 and the T-bet transcription factor [24].

Differentiated effector T cells express high levels of the CXC-chemokine receptor CXCR3, whereas its ligands CXCL10 (IP-10), CXCL11, and CXCL9 (MIG) are produced by antigen

presenting cells present in the infected tissues [25]. The role of CXCR3 receptor and the migration of effector T lymphocytes during Th1 type responses have already been demonstrated in a murine model infected by the protozoan *Toxoplasma gondii*. This receptor was highly expressed on $CD4^+$ T cells and was responsible for the migration of T lymphocytes to the intestine, enabling the control of parasite load and tissue damage, and consequently the survival of infected mice [26]. In addition to cell migration, chemokine receptors such as CXCR3 affect the differentiation of T lymphocytes. Indeed, recently published studies have shown that the absence of CXCR3 favors the differentiation of memory effector $CD8^+$ T cells [27,28].

Considering that CXCL10 and CXCL9 are expressed in heart tissue of acute and chronically *T. cruzi*-infected mice presenting a $CD8^+$ T-cell-enriched myocarditis [21,29], here we hypothesized that CXCR3 is a key molecule for migration of specific $CD8^+$ T-cells towards infected tissues. Using a model of prime-boost immunization in highly susceptible to *T. cruzi* infection A/Sn mice, we analyzed the role of CXCR3 receptor present on pathogen-specific $CD8^+$ T-cells migration, compartmentalization and effector functions. Further, we used an anti-CXCR3 blocking antibody as a tool to interfere in the migration process of $CD8^+$ T-cells and analyzed susceptibility to infection, migration pattern, tissue colonization and effector activity. Therefore, we aimed to shed light on the importance of CXCR3-driven cell migration, and its role to protection and tissue injury in *T. cruzi* infected hosts. This knowledge may contribute to the strategies of vaccine development against intracellular pathogens.

Methods

Ethics statement and mice

This study was carried out in strict accordance with the recommendations in the Guide for the Care and Use of Laboratory Animals of the Brazilian National Council of Animal Experimentation (http://www.cobea.org.br). The protocol was approved by the Ethical Committee for Animal Experimentation at the Federal University of Sao Paulo (Id # CEP 7559051115). Eight-weeks-old female mice, A/Sn, C57BL/6 or CD8-deficient mice (*cd8*$^{-/-}$), were purchased from the Federal University of São Paulo (CEDEME). CCR2 deficient mice (*ccr2*$^{-/-}$) were kindly supplied by Dr. João Santana, Ribeirão Preto School of Medicine-FMPR. Blood trypomastigotes of Y strain of *T. cruzi* were maintained by weekly passages in A/Sn mice at the Xenodiagnosis Laboratory of Dante Pazzenese Cardiology Institute. For *in vivo* experiments, each mouse was inoculated with 150 (A/Sn) or 10^4 trypomastigotes forms from blood (C57BL/6) diluted in 0.2 mL PBS and administered subcutaneously (s.c.) at the base of the tail. Parasitemia was determined by the examination of 5 μL of blood, and parasites were counted with a light microscope.

Immunization protocol

Heterologous prime-boost immunization protocol with plasmid pIgSPCl.9 and the human replication-defective adenovirus type 5 containing the ASP2 gene, as described previously [12,30], was used. Briefly, the immunization consists of a dose of plasmid DNA (100 μg) as a prime (pcDNA3 control or pIgSPClone9) and three weeks later, mice were boosted with $2x10^8$ plaque-forming units (pfu) of the adenoviral vectors Adβ-gal or AdASP2. Both injections were performed via intramuscular route (*Tibialis anterior* muscle). After 15 days of boosting mice were infected with *T. cruzi*.

Treatments

Blocking monoclonal antibodies anti-CXCR3 (clone CXCR3-173, BioXcell), anti-CCL2 (clone 2H5, BioXcell) and isotype control antibody Rat IgG2a (clone 2A3, BioXcell), were

administered via i.p route on the same day of infection and every 48 hours until 20 days after infection. The quantity of antibodies administered was 250 μg of mAb/mouse. The dose was the same used in previously studies [31]. The groups were divided as shown below:

1. βgal+*T.cruzi*: Immunized with controls plasmid pcDNA3/Adβgal and challenged with *T.cruzi*;
2. ASP2+*T.cruzi*: Immunized with pIgSPclone9/AdASP2, challenged with *T.cruzi* and treated with isotype control antibody.
3. ASP2+αCXCR3+*T.cruzi*: Immunized with pIgSPclone9/AdASP2, challenged with *T. cruzi* and treated with anti-CXCR3 antibody.

Peptide

TEWETGQI immunodominant peptide described earlier [32], was synthesized by GenScript (Piscataway, New Jersey) and used for *in vitro* and *ex vivo* stimulation of splenocytes. The multimer $H2K^{K}$-TEWETGQI (Immudex Copenhagen, Denmark) was used for specific $CD8^{+}$ T cell detection.

Quantification of parasite burden

Hearts and spleens from βgal+*T.cruzi*, ASP2+*T.cruz*i and ASP2+αCXCR3+*T.cruzi* were used for DNA extraction. The DNA extraction, the specific primers for a satellite DNA region of the parasite (*T. cruzi*) and the qPCR reaction using TaqMan Universal Master Mix II with UNG were adapted from Piron and colleagues [33].

ELISpot

Briefly, $1x10^{6}$ responder cells from spleen were incubated with $3x10^{5}$ antigen-presenting cells in complete medium (1% NEAA, 1% L-glutamine, 1% vitamins and 1% pyruvate, 0,1% 2-ME, 10% FBS (HyClone), 20 U/mL mouse recombinant IL-2 (SIGMA) and on a plate previously coated with capture antibody those cells were incubated in the presence or absence of 10 μM of peptide TEWETGQI. After 24 hours the plates were washed with PBS and PBS-Tween 20 (0.05% Tween). Each well received 2 μg/mL of biotinylated anti-mouse monoclonal antibody (clone XMG1.2, Pharmingen). The plates were incubated with streptavidin-peroxidase (BD) and developed by adding peroxidase substrate (50mM Tris-HCl, pH 7.5, containing 1 mg/ml DAB and 1 μL/ml 30% hydrogen peroxide, both from SIGMA). The number of IFN-γ-producing cells was determined using a stereoscope.

Intracellular cytokine staining and flow cytometry

Two million cells from spleen were treated with ACK buffer (NH_4Cl, 0.15 M; $KHCO_3$, 10 mM; Na_2-EDTA 0.1 mM; pH = 7.4). Both spleen and heart cells were stained with $H2K^{k}$-TEWETGQI multimer for 10 minutes at RT. The splenocytes cell surface was stained for 30 min at 4˚C. The following antibodies were used for surface staining: anti-CD3 APCcy7 (clone 145-2C11, BD), anti-CD8 PERCP or anti-CD8 PACIFIC BLUE (clone 53–67, BD), anti-CD11a FITC (clone 2D7, BD), anti-CD11c APCcy7 (clone HL3, BD), anti-CD44 FITC (clone IM7, BD), anti-CD62L PE (clone MEL-14, BD), anti-CXCR3 PERCP/Cy5.5 (clone 173, BioLegend), anti-CD27 FITC (clone LG3A10, BD), anti-CD4 PEcy7 (clone RM4-5, BD) anti-KLRG1 FITC (clone 2F1, eBioscience), anti-CD49d PEcy7 (clone R1-2, BD), anti-CD69 PERCP (clone H1.2F3, BD), anti-CD43 PEcy7 (1B11, BioLegend), anti-CD95 PEcy7 (clone JO2, BD), anti-CD25 FITC (clone LG3A10, BD), anti-CD127 PE (clone SB/199, BD), anti-

CD122 FITC (clone TM-β1, BD), anti-CD38 PE (clone 90, BD), anti-β7 PERCP (clone FIB27, BioLegend), anti-CD31 FITC (clone MEC 13.3, BD), anti-CD272 PE (clone 8F4, eBioscience), anti-PD-1 FITC (clone J43, eBioscience), anti-CTLA-4 PE (clone UC10-4B9, eBioscience), and anti-CCR7 PE (clone 4B12, BD). For annexin V and 7-AAD assays, $2x10^6$ of spleen cells were labeled with multimer, subsequently, the cells were stained according to the Annexin-PE Kit protocol (BD Pharmingen).

To detect IFN-γ, TNF or granzyme B by intracellular staining, $2x10^6$ cells/mL in cell culture medium containing CD107a FITC antibody (clone 1D4B, BD), anti-CD28 (clone 37.51, BD), BD Golgi-Plug (1 μL/mL) and monensin (5 μg/mL) were incubated in presence or absence of 10 μM of peptide TEWETGQI, no longer than 12 hours in V-bottom 96-well plates with a final volume of 200 μL at 37˚C and containing 5% CO_2. Cells were washed and stained for surface markers with anti-CD8 PERCP antibody (clone 53–6.7, BD) on ice for 30 min. Cells were then double washed in buffer containing PBS, 0.5% BSA, and 2 mM EDTA, fixed and permeabilized with BD perm/wash buffer. After the double wash procedure with BD perm/wash buffer, cells were stained for intracellular markers using APC-labeled anti-IFN-γ (clone XMG1.2, BD), PE-labeled anti-TNF (clone MP6-XT22, BD) and PE-labeled anti-granzyme B (clone GB11, Invitrogen) for 20 minutes on ice. Finally, cells were washed twice with BD perm/wash buffer and fixed in 1% PBS-paraformaldehyde. At least 700,000 cells were acquired on a BD FACS Canto II flow cytometer and then analyzed with FlowJo.

Purification of heart lymphocytes

For isolating lymphocytes in the heart, we used the protocol described by Gutierrez and colleagues [34]. Briefly, hearts collected from 5 mice at day 20 dpi were minced, pooled, and incubated for 1h at 37˚C with RPMI 1640, supplemented with $NaHCO_3$, penicillin-streptomycin gentamicin, and 0.05 g/mL of liberase blendzyme CI (Roche, Basel, Switzerland). The tissues were processed in Medimachine (BD Biosciences) with phosphate buffered saline (PBS) containing 0.01% bovine serum albumin (BSA). After tissue digestion and washes the lymphocytes were isolated by Ficoll gradient (Sigma).

In vivo BrdU incorporation

On the same day of infection mice were treated with 2 mg of BrdU (5-bromo-2'-deoxiuridine, SIGMA) via i.p route and every 48 hours, until 20 days after challenge. Then, $2x10^6$ splenocytes were stained with $H2K^k$-TEWETGQI multimer; BrdU staining was performed according to the BrdU-FITC Kit protocol (BD Pharmingen). At least 700,000 cells were acquired on a BD FACS Canto II flow cytometer and analyzed with FlowJo 8.7.

In vitro proliferation

Splenocytes from βgal+*T.cruzi*, ASP2+*T.cruzi*, and ASP2+αCXCR3+*T.cruzi* were stained with 1,25 μM of carboxyfluorescein diacetate succinimidyl diester (CFSE; Molecular Probes, Eugene, OR, USA), stimulated with TEWETGQI peptide, and incubated during 6 days at 37˚C. Following, splenocytes were stained with $H2K^k$-TEWETGQI multimer and the percentage of CFSE dilution was analyzed. At least 700,000 cells were acquired on a BD FACS Canto II flow cytometer and analyzed with FlowJo 8.7.

In vivo cytotoxicity assay

We used the protocol described by Silverio et al [10]. Briefly, splenocytes collected from naive A/Sn mice were treated with ACK buffer to lyse the red blood cells. Those cells were divided

into two populations and were labeled with the fluorogenic dye CFSE (Molecular Probes, Eugene, OR, USA) at a final concentration of 10 μM ($CFSE^{high}$) or 1 μM ($CFSE^{low}$). $CFSE^{high}$ cells were coated with 2.5 μM of the TEWETGQI ASP2 peptide for 40 minutes at 37˚C. $CFSE^{low}$ cells remained uncoated. Subsequently, $CFSE^{high}$ cells were washed and mixed with equal numbers of $CFSE^{low}$ cells before intravenous injection ($2x10^7$ cells per mouse) into recipient mice. Spleen cells from the recipient mice were collected at 20 hours after adoptive cell transfer and fixed with 1.0% paraformaldehyde. At least 100,000 cells were acquired on a BD FACS Canto II flow cytometer and analyzed with FlowJo 8.7. The percentage of specific lysis was determined using the following formula:

$$\%\text{lysis} = \frac{1 - (\%CFSE^{high}\ \text{infected}/\%CFSE^{low}\ \text{infected})}{(\%CFSE^{high}\ \text{naive}/\%CFSE^{low}\ \text{naive})\ \text{x}\ 100.}$$

Quantification of chemokine genes by RT-PCR

Total RNA from hearts of naïve, βgal+*T.cruzi*, ASP2+*T.cruzi* and ASP2+αCXCR3+*T.cruzi* groups, was extracted by using TRIzol and complementary DNA prepared using SuperScript IV VILO (Applied Biosystems). Quantitative PCR was performed with TaqMan Universal Master Mix II (Applied Biosystems) using a StepOne thermocycler (Applied Biosystems). We used a customized plate—TaqMan Array 96-well Mouse Chemokines Plate targets genes.

Histology and immunohistochemistry analysis

Hearts were fixed in 10% formalin, and then dehydrated, embedded in paraffin blocks, and sectioned in microtome. Staining was obtained with hematoxylin and eosin, and the number of amastigotes nests was quantified using a light microscope with 40x objective lens. Overall, 25 fields/group were counted. For immunohistochemistry the mice's hearts were removed and frozen in Tissue-Tek O.C.T (Sakura Fineteck). The blocks were sectioned in cryostat (7 μm thickness) and then fixed in ice-cold acetone for 15 minutes. The samples were stained with 20 μg of the biotinylated anti-CD8 antibody (clone 53–6.7, RD systems) for 12 hours. After incubation, samples were labeled with streptavidin Alexa Fluor 488 (Thermo Fischer) at the concentration of 0.5 mg/mL, diluted 1:100 for 1 hour at room temperature. The DAPI (4',6-diamidino-2-phenylindole, Sigma) dye was used for labeling the cell nucleus, the concentration used was 5 mg/mL. The images were acquired in Confocal Leica TCS SP8 CARS microscope from Institute of Pharmacology and Molecular Biology (INFAR). The images were obtained using the 63x objective and processed in ImageJ software.

Luminex assay

Mice's serum was collected on days 0, 6, 8, 10, 12 and 14 after infection in order to quantify the ligands of CXCR3, IP-10 (CXCL10), MIG (CXCL9), also, MCP-1 (CCL2) and RANTES (CCL5). The quantification was performed according to the MCYTOMAG-70K Kit protocol (Merck Millipore). Luminex xMAP in the Institute of Pharmacology and Molecular Biology (INFAR) was used to read the plates.

Adoptive transfer to CD8 deficient mice

$CD8^+$T cells from spleens of βgal+*T.cruzi*, ASP2+*T.cruzi*, and ASP2+αCXCR3+*T.cruzi* groups were purified using $CD8a^+$ T cell isolation kit (Miltenyi) and labeled with 10 μM of CFSE. $1x10^6$ $CD8^+$ T cells were transferred via i.v. route to infected CD8 deficient mice (day 6 of infection) and 6 days afterwards, the number of $CD8^+$ CFSE cells on recipient mice's hearts were analyzed by fluorescent microscopy.

Migration index

$CD8^+$ T-cells from mice were purified using a negative selection kit (Miltenyi Biotec). A transwell microplate (Corning) with 5μm membrane pore was used to carry out the migration assay. For each condition tested, lower chambers of transwell were filled with 600 μL in the absence or presence of 100ng/mL CXCL9, CXC10 and/or CXCL11 (RD systems). $CD8^+$ T-cells ($5x10^4$ in 300 μL) were deposited in the upper chamber of transwell and incubated for 3h at 37˚C. $CD8^+$ T-cells were harvested from the lower chamber and counted using cytometer. The migration index was calculated through the ratio of cells that migrated in the presence of medium and ligands.

Statistical analysis

Parasitemia, number of IFN-γ-producing cells (ELISpot), and absolute number of $CD8^+$ T-cells were compared by analysis of unidirectional variance (ANOVA); subsequently, the Tukey's HSD test was used (http://vassarstats.net/). The survival rate was compare using the Log-rank test using GraphPad Prism 7. The expression of molecules was compared using MFI (Mean Fluorescence Intensity), and the *naive* group MFI was taken as the baseline. MFI was determined by the FlowJo software (version 9.9). The Kaplan-Meier method was employed to compare survival rates of the studied groups. All statistical tests were performed with GraphPad Prism 5.0 (La Jolla, CA, USA). Differences were considered statistically significant when $P < 0.05$.

Results

CXCR3 receptor is highly expressed on T lymphocyte surface after immunization and *T. cruzi* infection

To investigate whether T lymphocytes expressed CXCR3 receptor on T cells surface after immunization and/or infection with *T. cruzi*, splenic parasite antigen-specific $CD8^+$ and activated $CD4^+$ T-cells of A/Sn mice were labeled on day 20 after infection. The dot-plot graphs show the frequency of specific $CD8^+$ T cells, gated as positive for $H2K^K$-TEWETGQI (Fig 1A). In infected group, immunized with the control DNA/adenovirus encoding the βgal (βgal+*T. cruzi* group), the frequency of $H2K^K$-restricted TEWETGQI-specific $CD8^+$ T-cells was lower (Q2: 0.49%) when compared to that found in mice immunized with DNA/adenovirus encoding the ASP-2 (Q2: 5.91%) and further infected with *T. cruzi* (ASP2+*T.cruzi*), as shown in Fig 1A. Also, during the infection, the Mean of Fluorescence Intensity (MFI) of CXCR3 receptor was higher in βgal+*T.cruzi* than in ASP2+*T.cruzi* group (Fig 1B). When $CD44^{high}$ and $CD62L^{low}$ activated $CD4^+$ T-cells were gated (Fig 1C), we observed that differently in specific $CD8^+$ T cells, CXCR3 expression was higher expressed and similar in both experimental groups (βgal+*T.cruzi* and ASP2+*T.cruzi*) (Fig 1D). In addition to enhanced CXCR3 expression, we evaluated the concentrations of the CXCR3 ligands IP-10/CXCL10 and MIG/CXCL9 in the serum of mice at days 0, 6, 8, 10, 12, and 14 after infection. As shown in Fig 1E and 1F, the concentrations of CXCL9 and CXCL10 increased on day 10 after challenge in both groups, βgal+*T.cruzi* and ASP2+*T.cruzi* and reaching the maximum concentration on day 14 after infection. Importantly, the levels of IP-10 and MIG were higher in the serum of mice of the group βgal+*T.cruzi* when compared to the ASP2+*T.cruzi* group. We also measured the levels of the chemokines CCL2/MCP-1 and CCL5/RANTES, but no differences were observed in those chemokine levels when compared to those found in the serum of naïve group (S1A and S1B Fig). Interestingly, purified $CD8^+$ T cells from spleen of ASP2+*T.cruzi* mice group had higher migration index after chemotaxis induced by the recombinant proteins CXCL9 and

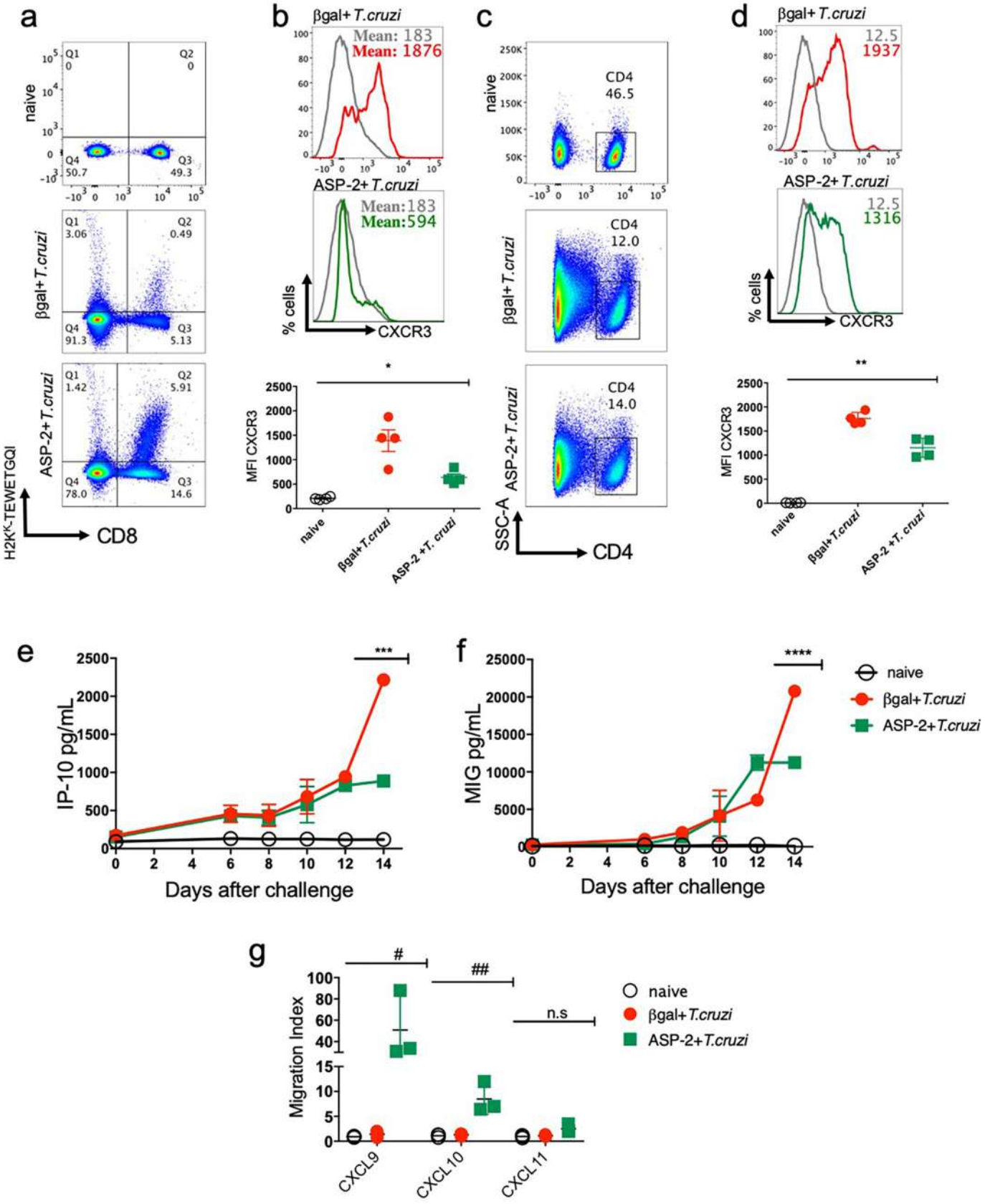
a
naive
βgal+ T.cruzi
ASP-2+ T.cruzi
H2K-TEWETGQI
CD8
b
βgal+ T.cruzi
Mean: 183
Mean: 1876
ASP-2+ T.cruzi
Mean:183
Mean:594
% cells
CXCR3
MFI CXCR3
naive
βgal+T.cruzi
ASP-2 +T. cruzi
c
CD4
46.5
CD4
12.0
CD4
14.0
SSC-A
CD4
d
βgal+ T.cruzi
12.5
1937
ASP-2+ T.cruzi
12.5
1316
% cells
CXCR3
MFI CXCR3
e
IP-10 pg/mL
Days after challenge
f
MIG pg/mL
Days after challenge
naive
βgal+T.cruzi
ASP-2+T.cruzi
g
Migration Index
CXCL9
CXCL10
CXCL11
naive
βgal+T.cruzi
ASP-2+T.cruzi
n.s

Fig 1. Specific $CD8^+$ and activated $CD4^+$ T-cells expressed CXCR3 receptor and CXCR3 ligands in the serum of *T. cruzi* infected mice. A/Sn mice were immunized with heterologous prime-boost protocol as described in the methods section. Thirty-six days after the first immunization, mice were challenged with 150 blood trypomastigotes forms of Y strain of *T. cruzi*. The experimental groups are mice immunized with a control vector and infected (βgal+*T. cruzi*) and mice immunized with ASP2 gene and infected (ASP2+*T.cruzi*). a-The dot-plot graphs represent the frequency of specific $H2K^k$-TEWETGQI $CD8^+$ T cells in the spleen of βgal+*T.cruzi* and ASP2+*T.cruzi* groups. b-The histograms and graph indicate the MFI (mean fluorescence intensity) of CXCR3 expression on specific $H2K^K$-TEWETGQI $CD8^+$ T cells surface. Each line corresponds to a group: naïve (grey), βgal+*T.cruzi* (red) or ASP2+*T.cruzi* (green). c-Dot-plots graphs show the frequency of $CD4^+$ T cells gated as $CD44^{high}$ and $CD62L^{low}$ population. d-The histograms and graph indicate the MFI (mean fluorescence intensity) of CXCR3 expression on activated $CD4^+$ T cells surface. Each line corresponds to a group: naïve (grey), βgal+*T.cruzi* (red) or ASP2+*T.cruzi* (green) groups. e-Quantity of IP-10 (CXCL10) and (f) MIG (CXCL9) chemokines in pg/mL in serum of naïve, βgal+*T.cruzi* and ASP2+*T.cruzi* groups. Chemokines were measured on days zero, 6, 8,10, 12 and 14 after infection, but the statistical analysis was performed only on day 14. g-Graph represents the migration index of $CD8^+$ T cells from the spleen of naïve, βgal+*T.cruzi* and ASP2+*T.cruzi* groups after stimulation with CXCL9, CXCL10, and CXCL11 chemokines. Results are shown as individual values and the mean ± SEM for each group (n = 4). One of two independent experiments is presented. Statistical analysis was performed using the One-Way ANOVA. Symbols indicate that the values observed were significantly different between the groups ($^*p = 0{,}0005$; $^{**}p = 0{,}0001$; $^{***}p<0{,}0001$; $^{****}p<0{,}0001$; $^{\#}p<0{,}05$; $^{\#\#}p<0{,}01$) and n.s means no significant.

https://doi.org/10.1371/journal.pntd.0007597.g001

CXCL10, when compared to cells harvested from mice of βgal+*T.cruzi* group (Fig 1G). No significant migration was detected under stimulation with CXCL11, supporting the selective effect of CXCL9 and CXCL10 to induce *ex vivo* chemotaxis of $CD8^+$ T-cells. These results showed that CXCR3 is highly expressed on T cell surface as well as CXCR3 ligands (CXCL9 and CXCL10), especially in the infected group; however, the immunized group's $CD8^+$ T cells showed more migration capacity after stimulation with CXCL9 and CXCL10 recombinant proteins.

CXCR3, but not CCR2 chemokine receptor is important to survival of A/Sn mice challenged with *T. cruzi*

Since we have previously shown that the recirculation of $CD8^+$ T lymphocytes was more important than their proliferative response to control *T. cruzi* infection [13], we evaluated which chemokine receptors could be important to drive the migration and to the effector functions of ASP2-specific $CD8^+$ T-cells after vaccination of highly susceptible A/Sn mouse lineage [9] challenged with the virulent *T. cruzi* Y strain. In order to analyze that, immunized and infected mice were treated with chemokine-specific blocking monoclonal antibodies to the Th1-related chemokines CXCR3 and CCL2. On the same day of challenge with the Y strain infection, A/Sn mice were treated with the anti-CXCR3 or anti-CCL2 monoclonal antibodies. This procedure was repeated every 48 hours until day 20 after infection. We observed that the treatment with anti-CCL2 antibody had no impact on the protective effect of ASP2 vaccination, as parasitemia levels remained lower compared to the ASP2+*T.cruzi* group, whereas, as expected, higher parasitemia levels were observed in mice of group βgal+*T.cruzi* (Fig 2A). Further, all mice from untreated and anti-CCL2-injected ASP2+*T.cruzi* groups survived, while mice from βgal+*T.cruzi* group succumbed to infection (Fig 2B). To approach the participation of CCR2, which has as ligands CCL2 and other CC-chemokines [35], we used CCR2-deficient ($ccr2^{-/-}$) mice. As previously described [36], *T. cruzi*-infected CCR2-deficient mice died due to infection, while wild-type resistant C57BL/6 mice survived. However, all CCR2-deficient mice immunized with the DNA/adenovirus ASP2 vaccine survived after to be challenged with *T. cruzi* (S2A and S2B Fig). After anti-CXCR3 administration into ASP2-vaccinated and challenged mice, we observed a trend in parasitemia increase only on day 12 after infection, when the peak of parasitemia was noticed, when compared to the immunized and isotype-treated control group (ASP2+*T.cruzi*), as shown in Fig 2C. At 20 days after infection, the quantification of parasite load in spleen by real time qPCR supported that trend in the treated group, showing that the number of parasites in the spleen of anti-CXCR3-treated vaccinated and challenged mice (ASP2+αCXCR3+*T.cruzi* group) was similar to the βgal+*T.cruzi* group and it contrasted with the low parasite load found in the spleen of mice of the isotype-treated ASP2+*T. cruzi* group (Fig 2D). The survival rate was followed for a 45-day period after infection and all

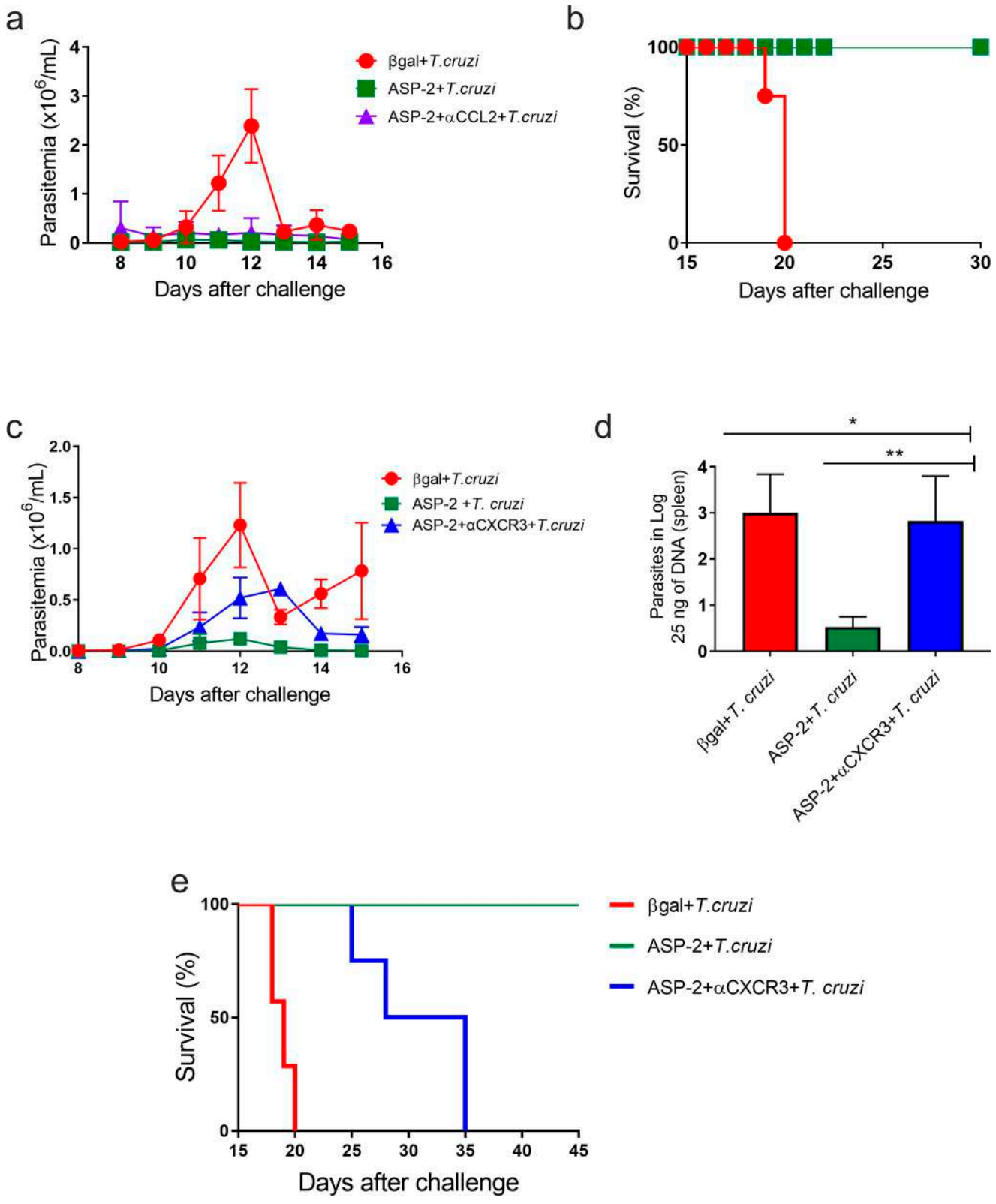

Fig 2. Parasitemia and survival of mice treated with anti-CCL2 or anti-CXCR3 antibody. A/Sn mice were immunized with the heterologous prime-boost protocol described earlier, and 15 days after the last dose of immunization, mice were challenged with 150 blood forms of Y strain of *T. cruzi* and treated, on the same day, with anti-CCL2 or anti-CXCR3 monoclonal antibodies. a-Linear parasitemia scale of βgal+*T.cruzi* (red), ASP2+*T.cruzi* (green)

and ASP2+αCCL2+*T.cruzi* (purple) groups. In A/Sn mice, the peak of parasitemia was on day 12 after infection. b-Survival rate curve of mice was followed up until 30 days of infection. Kaplan–Meier curves for survival of the different groups were compared using the Log-Rank test (all groups $p<0,002$; groups ASP2+*T.cruzi* and ASP2+αCCL2+*T.cruzi* $p>0,9$). c-Linear parasitemia scale of βgal+*T.cruzi* (red), ASP2+*T.cruzi* (green) and ASP2+αCXCR3+*T.cruzi* (blue) groups. d-Number of parasites in the spleen, measured by Real time qPCR. Asterisks indicate that the values were statistically different after analysis using One-Way ANOVA and Tukey's HSD tests ($^{*}p<0.002$ and $^{**}p<0.01$). e-Survival rate curve of mice was followed up until 45 days after infection. Kaplan–Meier curves for survival of the different groups were compared using the log-rank test (all groups $p<0,0001$; groups ASP2+*T.cruzi* and ASP2 +αCXCR3+*T.cruzi* $p = 0,0091$). Results are shown as individual values and the mean ± SEM for each group (n = 4). One of two independent experiments is presented.

https://doi.org/10.1371/journal.pntd.0007597.g002

mice from the ASP2+αCXCR3+*T.cruzi* group died due to infection while 100% of mice of the ASP2+*T.cruzi* group survived (Fig 2E). Taken together, these data indicate that the CXC-chemokine CXCR3 is important to control parasite dissemination and mice survival after challenge of ASP2-vaccinated mice.

Anti-CXCR3 treatment did not alter the number of cytokine-producing specific CD8$^+$ T cell in spleen

Next, we analyzed the number of antigen-specific CD8$^+$ T-cells after the treatment with anti-CXCR3 antibody. To perform that, we measured the number of specific CD8$^+$ T-cells in spleen using the H-2K^k-restricted TEWETGQI multimer, characterized as an immunodominant epitope of the ASP2 protein in A/Sn mice [3]. As expected, after immunization and infection, the frequency of TEWETGQI-specific CD8$^+$ T-cells was higher in mice of ASP2+*T.cruzi* group than in mice of βgal+*T.cruzi* control group. After treatment with anti-CXCR3, we observed a decrease in the frequency of TEWETGQI-specific CD8$^+$ T-cells in the anti-CXCR3 treated group, but no statistical differences in absolute numbers of TEWETGQI-specific CD8$^+$ T-cells were observed in ASP2+αCXCR3+*T.cruzi* group when compared to the ASP2+*T.cruzi* group (Fig 3A and 3B), suggesting that the treatment with anti-CXCR3 antibody did not influence in the number of TEWETGQI-specific CD8$^+$ T-cells in the A/Sn mice's spleen. To investigate whether anti-CXCR3 treatment affected the polyfunctionality and cytokines production by TEWETGQI-specific CD8$^+$ T-cells, we performed an Intracellular Staining assay (ICS) to measure the percentage of epitope-specific CD8$^+$ T-cells producing IFN-γ and TNF cytokines as well as the degranulation marker CD107a molecule (LAMP-1), an indirect indicator of cytotoxicity activity, after *ex vivo* stimulation with TEWETGQI peptide. The gate strategy used to evaluate the polyfunctionality of TEWETGQI-specific CD8$^+$ T-cells is in S3A and S3B Fig. After immunization and infection (ASP2+*T. cruzi*), the number of splenic polyfunctional (IFN-γ$^+$TNF$^+$CD107a$^+$) TEWETGQI-specific CD8$^+$ T-cells increased (5.17 ± 0.68), when compared to βgal+*T.cruzi* control group (3.55 ± 1.19) (Fig 3C). Also, we observed that the treatment with anti-CXCR3 did not alter the frequency of polyfunctional TEWETGQI-specific CD8$^+$ T-cells (4.25 ± 1.82) in comparison to the isotype-treated ASP2+*T.cruzi* group (Fig 3C). Using the ELISpot assay to detect IFN-γ-secreting cells, we observed that the number of IFN-γ-producing CD8$^+$ T-cells in βgal+*T. cruzi* group was lower than in the immunized and infected groups (Fig 3D). In addition, the number of IFN-γ-producing CD8$^+$ T-cells decreased in ASP2+αCXCR3+*T.cruzi* when compared to ASP2+*T.cruzi* group. Collectively, these data provide evidence that the polyfunctionality capacity of TEWETGQI-specific CD8$^+$ T-cells, characterized by the capacity of producing cytokines and degranulation at the same time, was not altered after anti-CXCR3 administration.

Increased proapoptotic phenotype on TEWETGQI-specific CD8$^+$ T-cells after anti-CXCR3 treatment

Previously, we have described that TEWETGQI-specific CD8$^+$ T-cells generated by prime-boost heterologous immunization are effectors (TE), characterized by the CD44^{high},

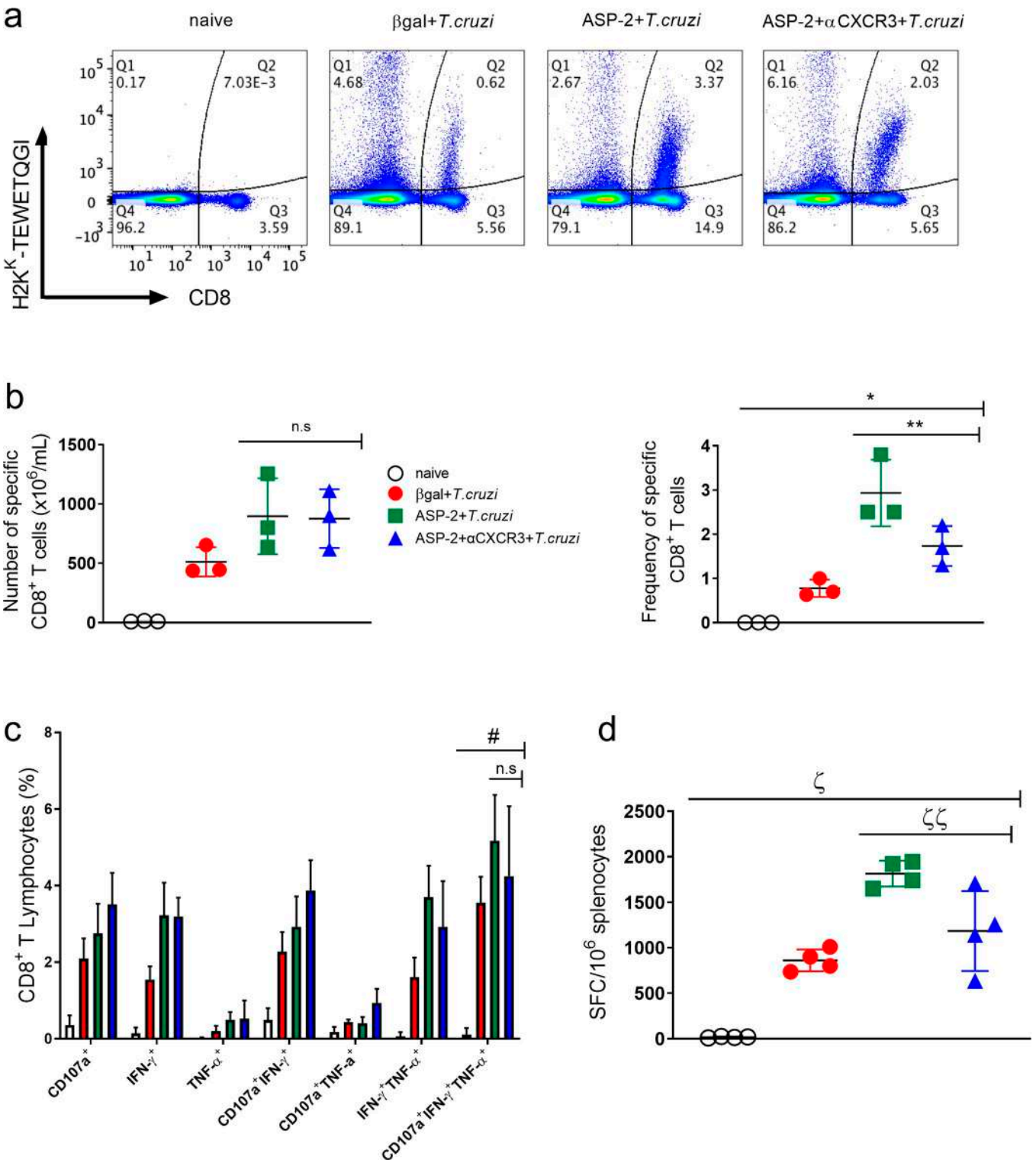

Fig 3. Anti-CXCR3 treatment did not alter the cytokine production by specific CD8$^+$ T cells. Specific CD8$^+$ T cells from the spleen were labeled using the dextramer H2K^K-TEWETGQI and anti-CD8$^+$ antibody. To measure cytokine production, splenocytes from βgal+*T.cruzi*, ASP2+*T.cruzi*, and ASP2+αCXCR3 +*T.cruzi* were stimulated for 12 hours with TEWETGQI peptide of *T. cruzi*. a-Dot-plots show the frequency of specific H2K^K-TEWETGQI CD8$^+$ T cells in the spleen from each group. b-The frequency and absolute number of specific CD8$^+$ T cells in the spleen of βgal+*T.cruzi*, ASP2+*T.cruzi*, and ASP2+αCXCR3+*T. cruzi* groups were quantified. c-The bar graph represents the percentage of CD8$^+$ T cells expressing each individual molecule or the combinations after *ex vivo* stimulation (CD107a, IFN-γ and/or TNF-α). Boolean analysis was performed using FlowJo software, version 8.4. d-ELISpot graph with the number of IFN-γ

producing cells. SFC = Spot-Forming Cell. Results are representative of two independent experiments with the mean ± SD of each individual group (n = 3). Statistical analysis was performed using the One-Way ANOVA and Tukey's HSD tests. Symbols indicate that the values observed were significantly different between the groups ($^{*}p = 0{,}0002$; $^{**}p<0.05$; $^{\#}p = 0{,}001$; $^{\zeta}p<0{,}0001$; $^{\zeta\zeta}p<0{,}05$) and n.s means no significant.

https://doi.org/10.1371/journal.pntd.0007597.g003

CD11a^{high}, CD62L^{low}, CD127^{low}, and KLRG-1^{high} phenotype [12]. These cells play a crucial role in the control of infection by producing cytokines and killing the target cells by direct cytotoxicity [9]. Here, we evaluated whether anti-CXCR3 treatment affects the function-linked phenotypes of TEWETGQI-specific CD8^{+} T-cells in the spleen. In order to analyze that, TEWETGQI-specific CD8^{+} T-cells were labeled with tetramer and markers associated with cell activation and differentiation. Overall, we observed that anti-CXCR3 treatment did not alter the phenotype of TEWETGQI-specific CD8^{+} T-cells when compared to the isotype-treated ASP2+*T.cruzi* group. Indeed, TEWETGQI-specific CD8^{+} T-cells from the ASP2 +αCXCR3+*T.cruzi* group had effector phenotype characterized as CD44^{high}, CD11a^{high}, CD62L^{low} and KLRG-1^{high}, comparable to the epitope-specific CD8^{+} T-cells found in the ASP2+*T.cruzi* group (S4 Fig). Interestingly, we observed that the expression of the CD95 molecule was increased in the specific CD8^{+} T cells from spleen of ASP2+αCXCR3+*T.cruzi* group, when compared to the βgal+*T.cruzi* and ASP2+*T.cruzi* groups (Fig 4A and 4B). Previously, our group showed that the reason of a suboptimal CD8^{+} T-cell response profile during infection with *T. cruzi* was associated with an upregulation of CD95 expression and a proapoptotic phenotype, that was reversible with ASP2 vaccination which prevented that phenotyping observed only during infection [37]. Taking into account those findings, we evaluated the proapoptotic phenotyping by labeling specific CD8^{+} T cells with annexin V and 7-AAD molecules. We observed in ASP2+αCXCR3+*T.cruzi* group an increase in annexin V levels when compared to the βgal+*T.cruzi* and ASP2+*T.cruzi* groups, however, the percentage of cells expressing 7-AAD was similar in all groups (Fig 4C), indicating that anti-CXCR3 treatment increased the apoptotic phenotype in specific CD8^{+} T cells, but not necrosis. Next, we assessed the proliferative response of the TEWETGQI-specific CD8^{+} T-cells *in vivo* by BrdU incorporation assay and by CFSE-labeling after *ex-vivo* re-stimulation with TEWETGQI peptide. The number of epitope-specific CD8^{+} T-cells that incorporated BrdU was similar in all infected groups (Fig 4D). Similar results were also observed in *ex vivo* CFSE-labeled cell proliferation assay (Fig 4E). Together, these results suggest that anti-CXCR3 treatment of vaccinated and challenged mice increased the proapoptotic phenotype of TEWETGQI-specific CD8^{+} T-cells in the spleen.

CXCR3 is important to cytotoxicity of specific CD8^{+} T cells

One of the effector functions of the CD8^{+} T-cells is to kill infected cells by direct cytotoxicity, which is crucial for controlling infection by *T. cruzi* [9]. Here, we evaluated the cytotoxicity activity of TEWETGQI-specific CD8^{+} T-cells after treatment with anti-CXCR3 antibody after immunization and infection. The cytotoxicity assay was performed using transference of $1x10^{7}$ CFSE^{low} (not pulsed) and CFSE^{high} (pulsed with TEWETGQI peptide) to experimental groups. After 12 hours, the percentage of CFSE^{high} lysis was measured. We demonstrated that the percentage of cytotoxicity in immunized mice treated with the anti-CXCR3 blocking antibody (ASP2+αCXCR3) decreased when compared to isotype-treated ASP2-immunized mice (Fig 5A and 5B). After infection, however, no differences were observed in the cytotoxicity activity of CD8^{+} T-cells in the spleen of mice from βgal+*T.cruzi*, ASP2+*T.cruzi*, and ASP2+αCXCR3 +*T.cruzi* experimental groups (Fig 5C). Moreover, granzyme B production by TEWETGQI-specific CD8^{+} T-cells was similar in these three experimental groups (Fig 5D). Overall, the

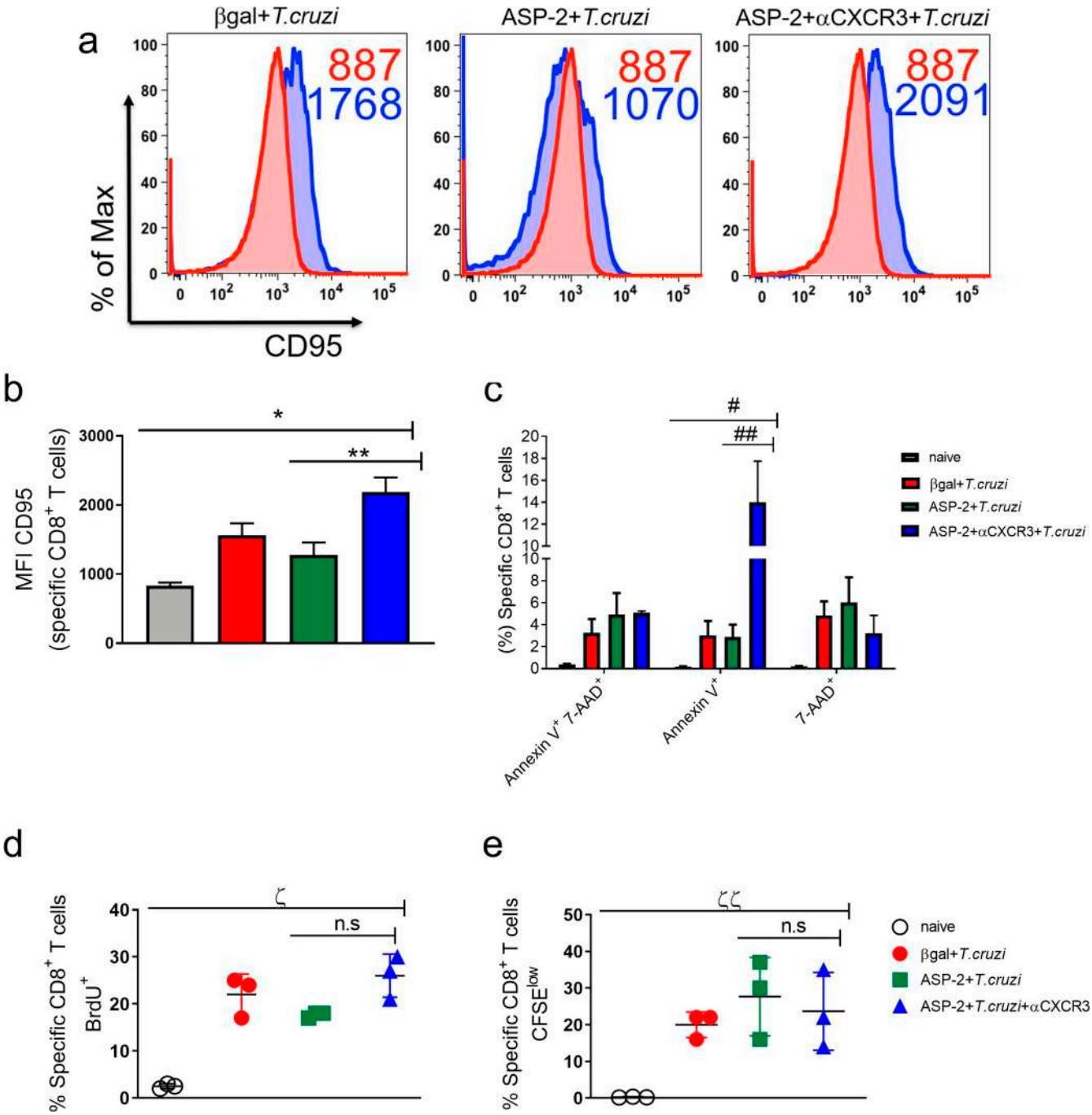

Fig 4. Anti-CXCR3 treatment increased the proapoptotic phenotype of specific CD8$^+$ T cells, but those cells could proliferate. Specific CD8$^+$ T cells from βgal+*T.cruzi*, ASP2+*T.cruzi*, and ASP2+ αCXCR3+*T.cruzi* groups were labeled to check proapoptotic profile. a-Histograms represent the MFI of CD95 (Fas) molecule on specific CD8$^+$ T cells surface (from spleen). The red histogram represents the naïve group and the blue are: βgal+*T.cruzi*, ASP2+*T.cruzi* and ASP2+αCXCR3+*T.cruzi* groups. b-Bar graph shows the average of CD95 MFI on specific CD8$^+$ T cells. c- Boolean analysis with the frequency of specific CD8$^+$ T cells positive for annexin V$^+$ and/or 7-AAD$^+$. d-The percentage of specific CD8$^+$ T cells that incorporated the BrdU molecule. The BrdU administration was done in the same day after infection (2mg of BrdU, via i.p route) and every 48 hours until 20 days after infection. e-Percentage of specific CD8$^+$ T cells expressing CFSE^{low}. The splenocytes from βgal+*T.cruzi*, ASP2+*T.cruzi* and ASP2+αCXCR3+*T.cruzi* groups were labeled with CFSE and stimulated for 5 days with TEWETGQI peptide. Afterword the specific CD8$^+$ T cells were labeled with H2K^k-TEWETGQI dextramer. Results are shown as individual values and as the mean ± SEM for each group (n = 3). Statistical analysis was performed using the One-Way ANOVA and Tukey's HSD tests. Symbols indicate that the values observed were significantly different between the groups ($^*p < .0001$; $^{**}p < .01$; $^{\#}p < .0001$; $^{\#\#}p<0.01$; $^{\zeta}p < .0001$ and $^{\zeta\zeta}p = 0.0105$) and n.s means no significant.

https://doi.org/10.1371/journal.pntd.0007597.g004

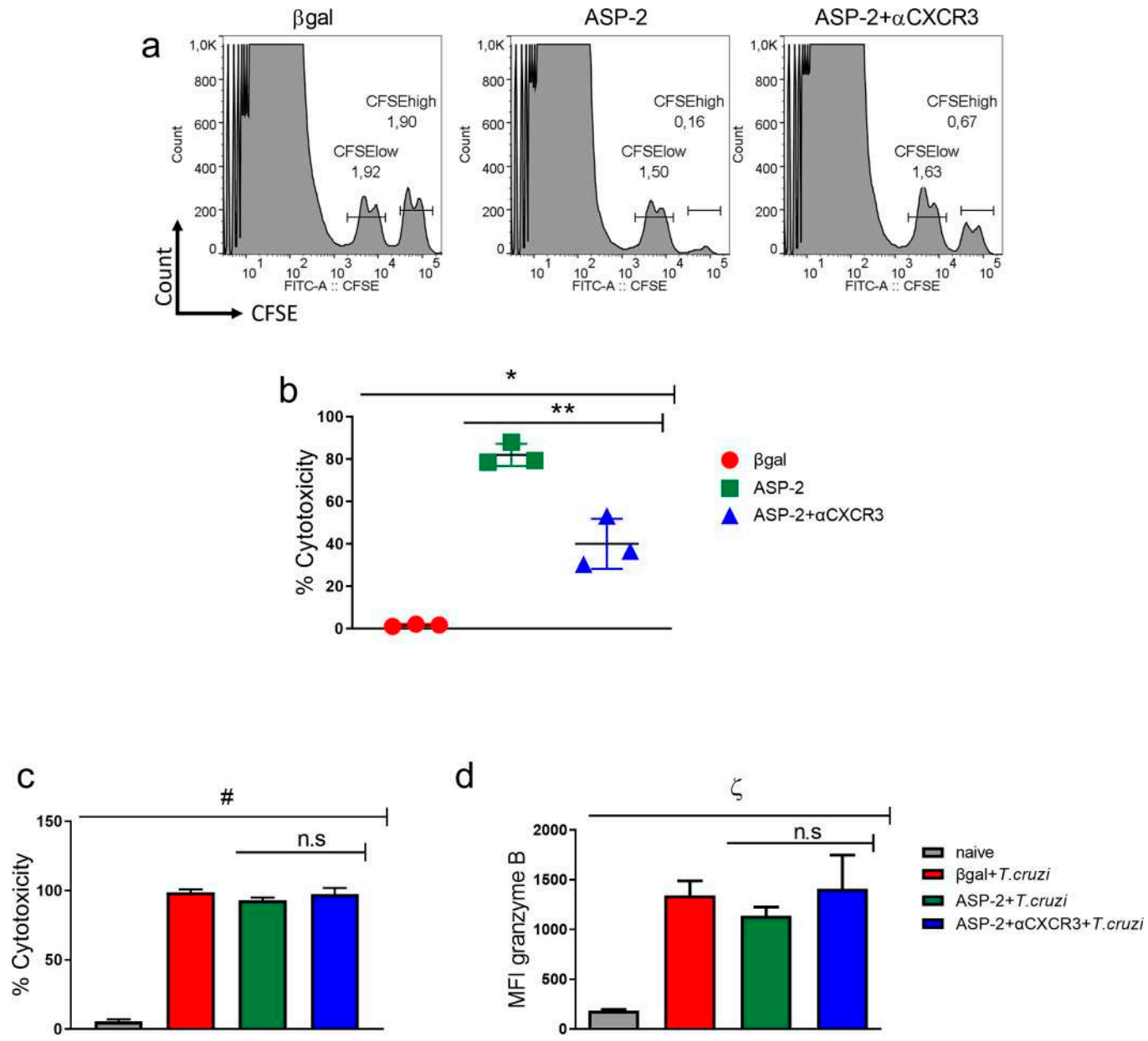

Fig 5. CXCR3 receptor is important to cytotoxicity of specific CD8$^+$ T cells during the immunization. a-Histograms represent the frequency of CFSE^{low} and CFSE^{high} population that were transferred to βgal, ASP2, and ASP2+αCXCR3 groups. After 12 hours of transference, the percentage of CFSE^{high} cell lyses was calculated as described in the methods section. b-Cytotoxicity percentage of specific CD8$^+$ T cells during immunization and treatment with anti-CXCR3. c-Percentage of cytotoxicity of specific CD8$^+$ T cells during immunization, infection and treatment with anti-CXCR3 d-Granzyme B MFI on specific CD8$^+$ T cells from βgal+*T.cruzi*, ASP2+*T.cruzi*, and ASP2+αCXCR3+*T.cruzi* groups. Results are shown as individual values and as the mean ± SEM for each group (n = 3). One of three independent experiments is presented. Statistical analysis was performed using the One-Way ANOVA and Tukey's HSD tests. Symbols indicate that the values observed were significantly different between the groups ($^*p < .0001$; $^{**}p < .01$; $^{\#}p < .0001$; $^{\zeta}p = 0.0001$) and n.s means no significant.

https://doi.org/10.1371/journal.pntd.0007597.g005

CXC-chemokine receptor CXCR3 indicates to be important to the cytotoxicity activity of TEWETGQI-specific CD8$^+$ T-cells generated after prime-boost immunization protocol in A/Sn mice.

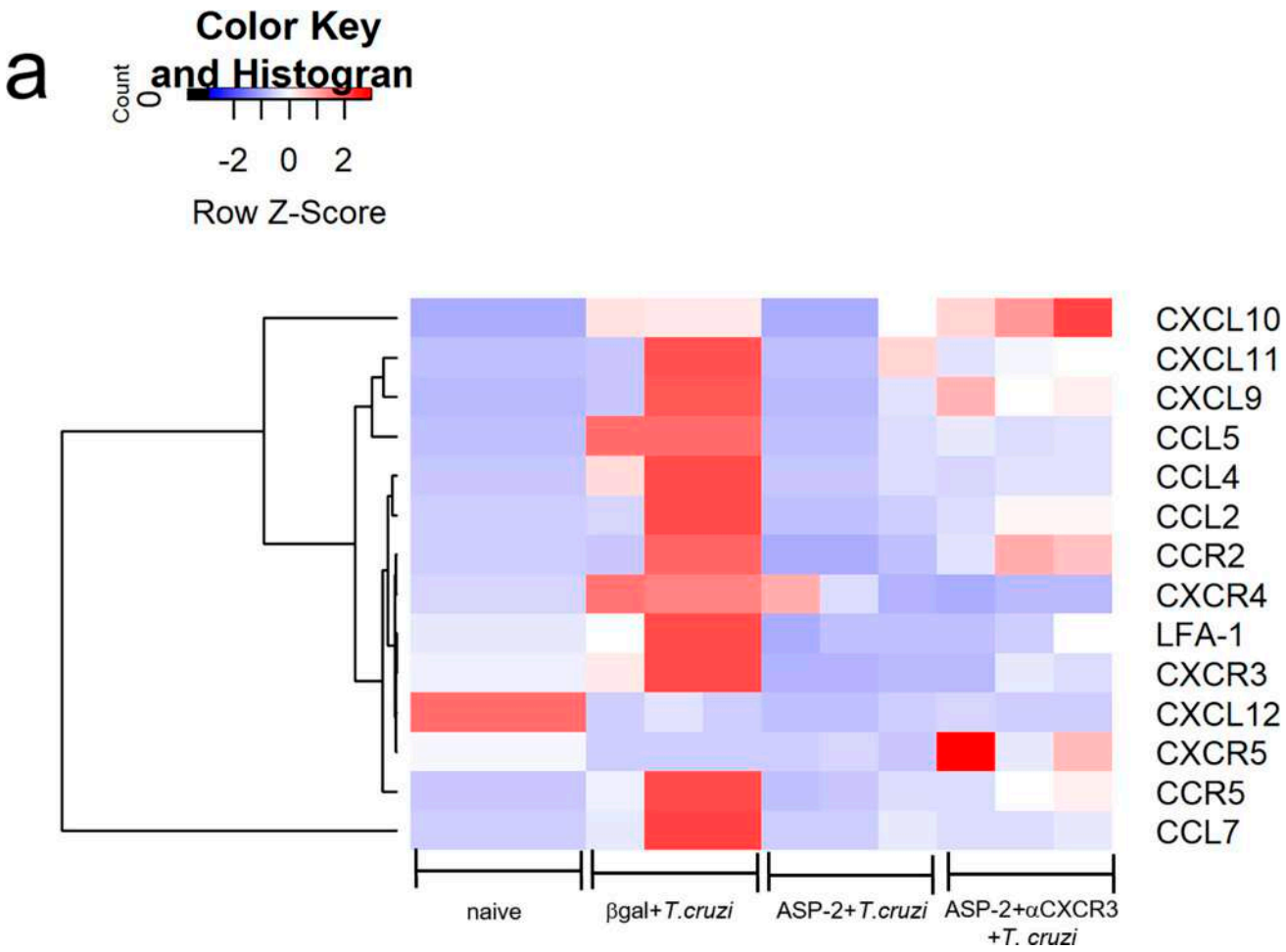

Fig 6. CXCR3 ligands were expressed in heart of infected mice. a-The heatmap graph represents the fold change of chemokine genes in heart of βgal+*T. cruzi*, ASP2+*T.cruzi*, and ASP2+αCXCR3+*T.cruzi* groups. The quantification of chemokines gene expression in heart was on day 20 after infection and we used a customized plate (Mouse Chemokines Plate targets genes). Results are shown as individual values and the mean ± SEM for each group (n = 3).

https://doi.org/10.1371/journal.pntd.0007597.g006

CXCR3 ligands are selectively expressed in the heart tissue of vaccinated and challenged mice

Having shown the high expression of CXCR3 chemokine receptor in TEWETGQI-specific $CD8^+$ T-cells, we evaluated the expression of CXCR3 ligands in heart, as well as other molecules involved in cell migration (CC-chemokines and their receptors and cell adhesion molecules). In heart of naïve mice, all genes had low expression, except CXCL12 gene that was downregulated in infected groups. In general, we observed that in infected heart of mice from βgal+*T.cruzi* group only CXCL12 and CXCR5 were low expressed, while the other genes were highly expressed, including CXCR3 ligands such as: CXCL11, CXCL10 and CXCL9. In ASP2 +*T.cruzi* experimental group, we observed a low expression of inflammatory cell migration genes, whereas in heart of mice from ASP2+αCXCR3+*T.cruzi* group, CXCR3 ligands CXCL10 and CXCL9 were high expressed, as well as CCR2 and CXCR5 (Fig 6A). These results suggest that CXCR3 ligands, CXCL10 and CXCL9 were selectively high expressed in heart of infected mice, supporting that vaccination prevented the expression of most of the genes involved in cell migration here studied.

CXCR3 guides specific CD8$^+$ T cells into infected heart tissue

T. cruzi infects the cardiac tissue [38] triggering an inflammatory response associated with tissue injury, leading to cardiomyopathy in 30% of the infected patients in the chronic phase of Chagas disease [11,39]. Thus, we evaluated the migration of CD8$^+$ T-cells to heart after anti-CXCR3 treatment. For that propose, CFSE-labeled CD8$^+$ T-cells obtained from βgal+*T.cruzi*, ASP2+*T.cruzi*, or ASP2+αCXCR3+*T.cruzi* groups were transferred to groups of CD8-deficient mice (*cd8*$^{-/-}$) as shown in the experimental scheme in Fig 7A. The number of CFSE$^+$CD8$^+$ T-cells was quantified, and we observed a statistical decreased in the number of CFSE$^+$CD8$^+$ T-cells that migrated in the heart tissue of CD8-deficient mice who received CD8$^+$ T-cells from ASP2+αCXCR3+*T. cruzi* mice, when compared to the recipient mice that received cells from the ASP2+*T.cruzi* donors (Fig 7B and 7C).

To endorse these results, we measured parasite burden and migration of TEWETGQI-specific CD8$^+$ T-cells into the heart, after vaccination, challenge and anti-CXCR3 antibody administration. Firstly, we quantified the number of amastigote nests in the heart tissue by HE (hematoxylin and eosin) staining, and we observed that both βgal+*T.cruzi* and ASP2 +αCXCR3+*T.cruzi* experimental groups had higher number of amastigote nests when compared to the ASP2+*T.cruzi* group (Fig 8A and 8B). Also, we estimated the parasite load using qPCR, and again both βgal+*T.cruzi* and ASP2+αCXCR3+*T.cruzi* groups had an increased number of parasites in heart tissue when compared to the ASP2+*T.cruzi* group (Fig 8C). Considering the results described above and the increased numbers of parasite nests seen in the heart after treatment with anti-CXCR3 antibody, we evaluated whether TEWETGQI-specific CD8$^+$ T-cells migrate into the heart tissue after anti-CXCR3 treatment. For that propose, we purified parasite-specific CD8$^+$ T-cells from cardiac tissue using a pool of dissociated hearts (n = 5 mice/group) and those cells were labeled with the H-2K^k-restricted TEWETGQI multimer. Curiously, the frequency of TEWETGQI-specific CD8$^+$ T-cells decreased in the heart tissue of ASP2+αCXCR3+*T.cruzi* group when compared to ASP2+*T.cruzi* group (Fig 8D and 8E), whereas the βgal+*T.cruzi* group had the lowest frequency of TEWETGQI-specific CD8$^+$ T-cells. Additionally, we quantified the number of CD8$^+$ T-cells in heart using confocal microscopy. Again, anti-CXCR3 decreased the number of CD8$^+$ T cells in the heart (Fig 8F and 8G). Altogether, these results show that CXCR3 guides TEWETGQI-specific CD8$^+$ T-cells toward the *T. cruzi*-infected heart tissue, and these cells play an important role controlling the infection.

Discussion

The recirculation of T lymphocytes into infected and, frequently, injured sites is essential for controlling infection by *T. cruzi* [13]. As chemokine receptors are pivotal for T-cell migration, we hypothesized that CXCR3 receptor might play an important role in parasite-specific CD8$^+$ T-cells migration into infected tissues after immunization and challenge by *T. cruzi*. Firstly, we evaluated CCR2 and CXCR3 role during immunization and infection and both CXCR3 and CCR2 receptors are highly expressed in the heart of *T. cruzi* infected mice [22]. Other studies using the Colombian strain of *T. cruzi* have shown that CCR2-deficiency leads to increase in parasitemia [36]. The CC-chemokine receptor CCR2 is responsible for monocytes migration during the inflammation [40], being CCL2 (MCP-1) its main ligand. However, in our experiments the treatment with anti-CCL2 did not impact in parasitemia or survival rate. As CCR2-deficient mice were high susceptible and CCR2 has other ligands than CCL2 [41], we immunized CCR2-deficient mice, and all vaccinated mice survived to the challenge with *T. cruzi* infection. Moreover, after anti-CXCR3 treatment, all mice had an increased parasitemia and burden of tissue parasitism, and died due to infection, showing that CXCR3, but not

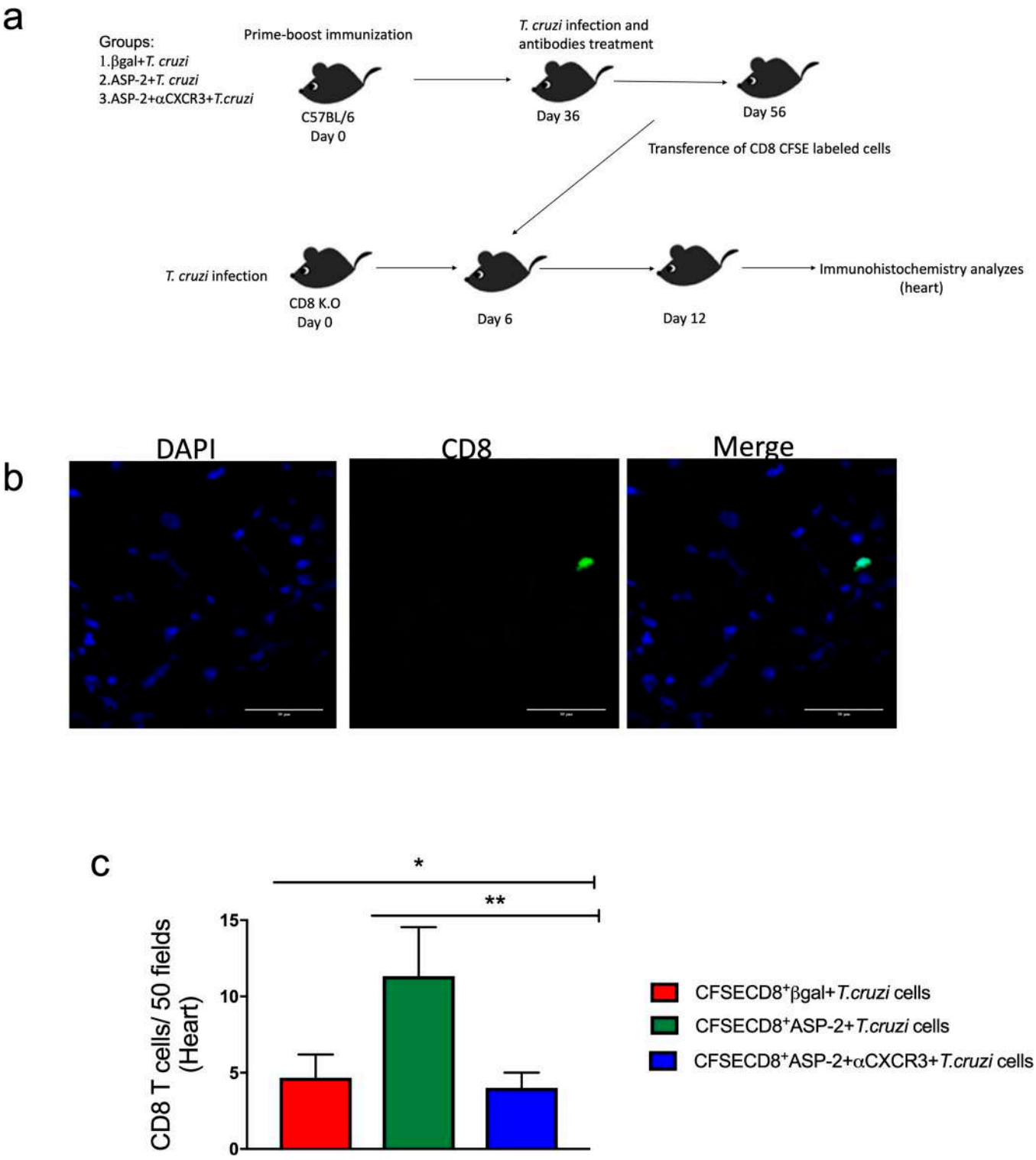

Fig 7. The treatment with anti-CXCR3 decreases the number of CD8$^+$ T cells in the heart. a-Experimental design showing the immunization, infection, treatment with anti-CXCR3 antibody and adoptive transference of CD8$^+$ CFSE labeled cells to CD8 deficient mice (infected). Briefly, C57BL/6 mice were immunized with prime-boost heterologous protocol, the first dose of immunization was with pCDNA3/pIgSPclone9 after 21 days of prime the mice received Adβgal/AdSP-2 and after 15 days were infected with *T. cruzi* and treated with 250 μg of CXCR3 antibody, and on day 20 after infection, CD8$^+$ T cells from spleen were purified, labeled with CFSE, and transferred into CD8 K.O mice previously infected (on day 6 after infection). After 6 days of transference, the number of CD8$^+$ T cells in heart from βgal+*T.cruzi*, ASP2+*T.cruzi* and ASP2+αCXCR3+*T.cruzi* groups was quantified. b-IHC in heart showing the CFSE$^+$CD8$^+$ T cells (green). The DAPI staining was used to label the nucleus of the cells. c-Number CFSE$^+$CD8$^+$ T cells that migrated to CD8 K.O mice hearts.

The cells were counted using the fluorescent microscopy and 50 fields were counted. Results are shown as individual values and the mean ± SEM for each group (n = 3). Statistical analysis was performed using the One-Way ANOVA and Tukey's HSD tests. Symbols indicate that the values observed were significantly different between the groups ($^{*}p = 0.010$; $^{**}p < .05$).

https://doi.org/10.1371/journal.pntd.0007597.g007

CCR2, had a pivotal role in *T. cruzi* resistance. The role of CXCR3 in the resistance against infections by virus and other pathogens has been shown [42,26], reinforcing that CXCR3 is essential to control infection by intracellular pathogens.

CXCR3 is highly expressed in murine Th-1 $CD4^+$ and $CD8^+$ T-cells [43], and the CXC-chemokine receptor CXCR3 plays a role in the regulation of leukocyte migration into inflammatory sites in mice and human [44]. Here, we have shown that CXC-chemokine receptor CXCR3 is more highly expressed on TEWETGQI-specific $CD8^+$ cells of *T. cruzi* challenged mice than in ASP2 immunized animals; however, the expression on effector $CD4^+$ T-cells was similar between the groups. In addition, we found increased levels of ligands CXCL9 and CXCL10 in the serum of those mice. Although specific $CD8^+$ T cells infected expressed higher levels of CXCR3 on cell surface, $CD8^+$ T-cells from the immunized group had a higher migration index compared to specific $CD8^+$ T cells generated only by infection, after the *ex vivo* stimulation with CXCL9 and CXCL10, but not with CXCL11. These three ligands are all induced by IFN-γ [45], but are differently expressed [46] and that may explain the differential role played by the CXC-chemokine receptor CXCR3 in several diseases [47].

Concerning the *in vitro* high migration capacity of $CD8^+$ T cells of the immunized group, CXCR3 low expression in those cells may be explained because specific $CD8^+CXCR3^+$ cells from the spleen migrated to the non-lymphoid peripheral tissue, for example, the heart tissue. We observed a higher number of specific $CD8^+$ T cells in the immunized group compared to the infected group. Another explanation might be that CXCR3 receptor from the immunized group is more responsive to CXCR3 ligands and the receptor is activated and internalized [48], which decreases the number of cells positive for CXCR3 receptor.

Additionally, we evaluated the effector function of the TEWETGQI-specific $CD8^+$ T-cells after anti-CXCR3 antibody administration. We observed that these parasite-specific $CD8^+$ T-cells present in the spleen can release cytokines in the ELISpot assay, in which we observed a decrease in the number of IFN-γ producing cells. However, in ICS assay, the percentage of IFN-γ $CD8^+$ producing cells was similar in the ASP2 immunized group, indicating that the decrease was due to a technique variation. In addition, TEWETGQI-specific $CD8^+$ T-cells after anti-CXCR3 antibody administration showed proliferative response. Similar results were observed during infection by virus and during anti-CXCR3 treatment [42,49–50]. However, during autoimmune diseases and infection by *Leishmania major*, CXCR3 is important for cytokine production and proliferation by $CD8^+$ T-cells [51–53]. In addition to cytokine production, we evaluated the cytotoxicity of these TEWETGQI-specific $CD8^+$ T-cells and during infection these cells show high cytotoxicity [32]; therefore, we decided to perform the analyzes in parasite-specific $CD8^+$ T-cells generated only by immunization because during the infection the cells are very cytotoxic and it is difficult observed differences among the groups [3]. Our results showed that the treatment with anti-CXCR3 also decreased cytotoxicity of TEWETGQI-specific $CD8^+$ T-cells in ASP2 immunized mice, corroborating the results observed by Thapa and colleagues [54]. Unlike this study, however, we did not observe a decrease in granzyme B production by these TEWETGQI-specific $CD8^+$ T-cells. The decreased cytotoxicity activity may be explained because the CXC chemokine receptor CXCR3 is important to the contact between infected target cells and specific $CD8^+$ T-cells [50].

The role of CXCR3 in the differentiation of $CD8^+$ T-cells in memory subtypes has been shown in other studies [28]. The receptor CXCR3 is important for the intranodal positioning

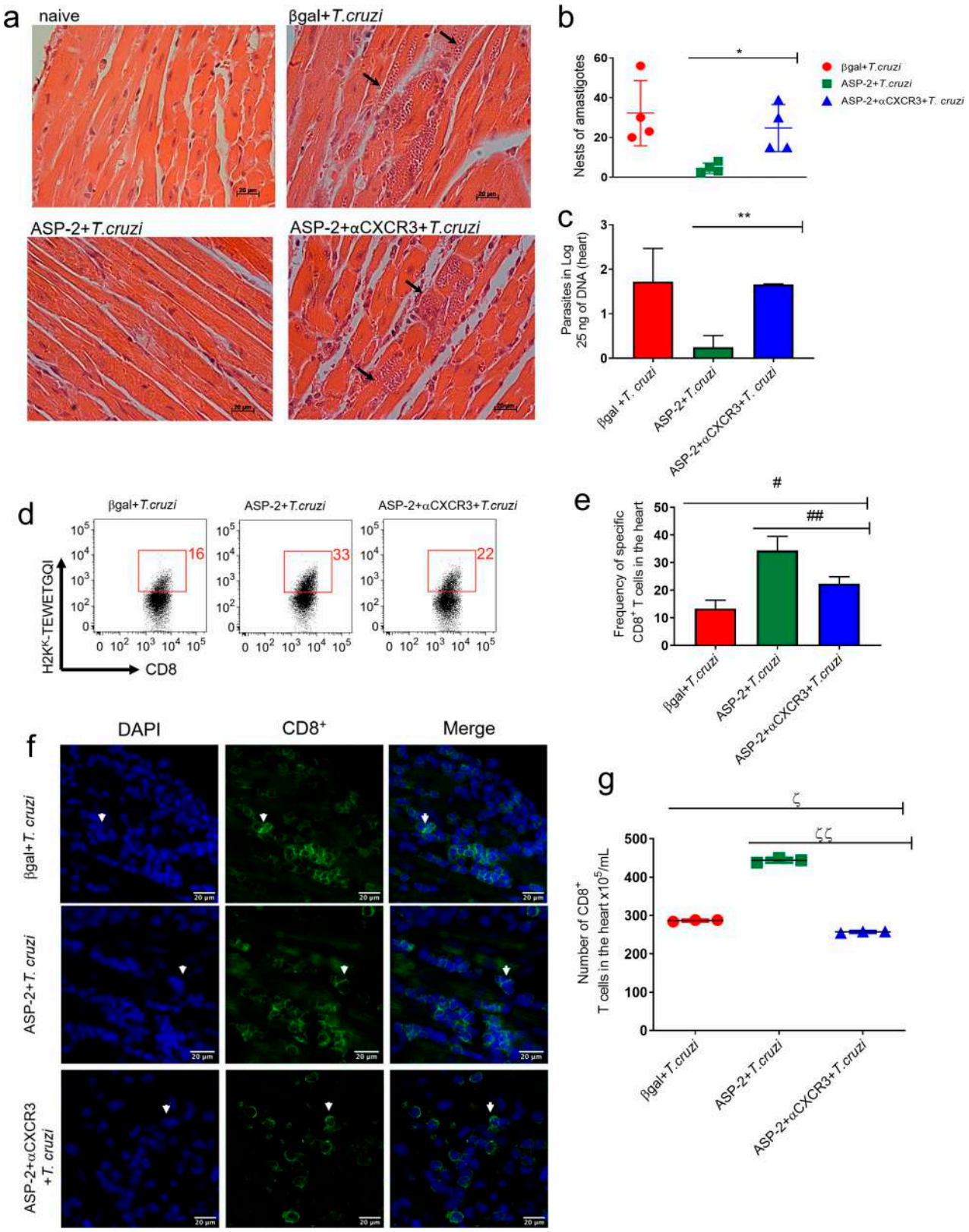

Fig 8. The migration of specific CD8$^+$ T cells to heart was impaired after treatment with anti-CXCR3 antibody. a-Histological section from heart tissue: the black arrows show the amastigotes nests in βgal+*T.cruzi*, ASP2+*T.cruzi*, and ASP2+αCXCR3+*T.cruzi* groups. b-Graph represents the

number of amastigotes nests in the heart, measured in 25 fields using light microscopy. c-Number of parasites in heart tissue quantified by Real time PCR from 25 ng of DNA sample. d-The dot-plot show the frequency of specific $CD8^+$ T cells in the heart tissue. e-The frequency average of specific $CD8^+$ T cells in heart. f-IHC section showing $CD8^+$ T cells (in green) in cardiac tissue on day 20 after infection. The DAPI was used to reveal the $CD8^+$ T cell nucleus. g-Number of $CD8^+$ T cells in cardiac tissue. Results are shown as individual values and the mean ± SEM for each group (n = 3). Statistical analysis was performed using the t-test, One-Way ANOVA, and Tukey's HSD tests. Symbols indicate that the values observed were significantly different between the groups ($^{*}p = 0.0251$; $^{**}p < .0001$; $^{\#}p = 0.001$; $^{\#\#}p = 0.001$; $^{\zeta}p < .0001$ and $^{\zeta\zeta}p < .01$).

https://doi.org/10.1371/journal.pntd.0007597.g008

of T-cells and Th cell polarization [55] and facilitates $CD8^+$ T-cell differentiation into short-lived effector cells and memory generation [27]. The TEWETGQI-specific $CD8^+$ T-cells generated by heterologous immunization and challenge by *T. cruzi* infection are effector cells characterized by the expression of these molecules and levels: $CD11a^{high}$, $CD62L^{low}$, $CD44^{high}$ and $CD127^{low}$ and $KLRG1^{high}$ [12]. The treatment with anti-CXCR3 did not alter the effector phenotype of the TEWETGQI-specific $CD8^+$ T-cells but increased the levels of CD95 expression on cell surface of those cells. Previously, our group showed that TEWETGQI-specific $CD8^+$ T-cells generated by immunization had lower CD95 expression when compared to cells generated after infection [37]. As CD95 is a cell death-promoting molecule [56], we analyzed the apoptosis in TEWETGQI-specific $CD8^+$ T-cells and we observed an increase in annexin V expression, suggesting that anti-CXCR3 treatment increased the proapoptotic phenotype of TEWETGQI-specific $CD8^+$ T-cells. The protection of cell death during immunization with ASP2 ensures that TEWETGQI-specific $CD8^+$ T-cells trigger the effector function and control parasites replication. We have also demonstrated that CXCR3 molecule expression protected TEWETGQI-specific $CD8^+$ T-cells from cell death.

CXCR3 receptor is also essential for $CD8^+$ T-cell migration after immunization and, particularly, for parasite-specific $CD8^+$ T-cell migration into the heart tissue after immunization and challenge with *T. cruzi* infection. Indeed, after anti-CXCR3 treatment, we observed a reduced number of $CD8^+$ T-cells infiltrating the heart tissue. Consistently with the reduced number of $CD8^+$ T-cells in the heart tissue of anti-CXCR3-treated mice, we found a significant increase in the number of amastigote nests and parasite load in the heart tissue of these mice. Furthermore, we demonstrated that several chemokines genes in infected mice hearts were highly expressed, indicating a high inflammation/migration to heart tissue. The high expression of CCL5/RANTES, CCL3/MIP-1a, CCL4/MIP-1b, CCL2/MCP-1 and the CXC chemokines CXCL10/IP-10 and CXCL9/MIG mRNA also have been detected in the heart tissue of acutely and chronically *T. cruzi*-infected mice [29].

The high expression of chemokines genes in the infected group did not guarantee a high migration of specific $CD8^+$ T cells. Studies have shown that a pro-inflammatory environment in the heart tissue is sufficient to activate autoreactive T cells and cause cardiomyopathy during Chagas disease [57]. Immunization with ASP2 prevents the expression of most of the analyzed chemokines; however, expression of CXCR3 ligands CXCL9 and CXCL10 was observed in two animals. Also, both chemokines were detected in the mice's serum, suggesting that parasite-specific $CD8^+$ T-cells expressing CXCR3 can be attracted to the heart tissue. In fact, the number of TEWETGQI-specific $CD8^+$ T-cells in the ASP2 immunized heart tissue is higher than in the infected group. In addition, in the ASP2 immunized group, the number of amastigote nests and parasite burden is lower than in the infected mice group, suggesting that the higher number of TEWETGQI-specific $CD8^+$ T cells participate in the infection control. After anti-CXCR3 administration, we observed a high expression of CXCR3 ligands, which may be explained for the competition between anti-CXCR3 and the ligands to CXCR3 ligation, resulting in CXCR3 ligands accumulation.

The importance of CXCR3 in T cells migration has been demonstrated in several studies and shown that anti-CXCR3 treatment is effective at preventing acute and chronic heart

rejection after transplantation [58]. Although previous studies have shown CXCR3 role in the migration of effector lymphocytes involved in the control of viral, protozoan and bacterial infection [49–60], our study reveals for the first time that CXCR3 receptor is pivotal for the migration and positioning of pathogen-specific $CD8^+$ T-cells directly involved in the clearance of *T. cruzi* after the prime-boost immunization and challenge. Therefore, our data support that prime-boost vaccination protocol was effective in the selective CXC-chemokine-mediated CXCR3-driven activation, migration and positioning in a target tissue that is drastically affected during the chronic phase of *T. cruzi* infection. Moreover, our work places CXCR3 as a powerful molecule able to address specific cell to target tissue of infection and, therefore, to be included as a key requirement for design of vaccines against intracellular pathogens. The potential use of chemokines receptor as an adjuvant in vaccines strategies has been demonstrated in the dengue model [61]. In Chagas disease, CXCR3 receptor may be used to guide specific $CD8^+$ T cells to the heart and prevent cell death. Consequently, it might control parasites replication.

In general, we have demonstrated that anti-CXCR3 treatment increased the susceptibility of immunized A/Sn mice, which died very quickly due to infection. Moreover, specific $CD8^+$ T-cells decreased the migration into the heart tissue, and those cells displayed a pro-apoptotic profile. Taken together, those results show that CXCR3 has a critical role in the protective immune response and understanding its migratory role might support the development of vaccines against intracellular parasites such as *Trypanosoma cruzi*.

Supporting information

S1 Fig. During infection and/or immunization with ASP2 gene the levels of MCP-1 and RANTES chemokines were low. a-Quantity of MCP-1 and (b) RANTES chemokines in pg/mL in serum of naïve, βgal+*T.cruzi* and ASP-2+*T.cruzi*. The chemokines were measured on days zero, 6, 8,10, 12 and 14 after infection by Luminex assay. Results are shown as individual values and the mean ± SEM for each group (n = 4). One independent experiment is presented. (TIF)

S2 Fig. Prime-boost immunization protected CCR2 deficient mice against infection with *T. cruzi*. C57BL/6 or CCR2 deficient mice were immunized with heterologous prime-boost protocol, and 15 days after the last dose of immunization, mice were challenged with $1x10^4$ blood forms of Y strain of *T. cruzi*. a-Parasitemia in log of C57BL/6 and CCR2 deficient mice infected or immunized as described in the figure. b-Survival rate curve of mice was followed up until 30 days of infection. Results are shown as individual values and the mean ± SEM for each group (n = 4). One of two independent experiments is presented. The n.s means no differences on parasitemia levels between C57BL/6 and CCR2 K.O infected mice were found. (TIF)

S3 Fig. Gates strategy used for intracellular staining of cytokines analysis. A/Sn mice were immunized with ASP2 using the heterologous prime-boost vaccination regimen, infected with 150 tripomastigotes forms of *T. cruzi* and treated with anti-CXCR3 until the day 20^{th} after infection. At this point, the splenic cells were re-stimulated *ex vivo* in the presence of peptide TEWETGQI at a final concentration of 10 μM. After 12h, cells were stained with anti-CD8, anti-IFN-γ, and anti-TNF-α antibodies. a-Gate strategy was made as follows: SSC-A/Time, SSC-A/FSC-A, FSC-H/FSC-A and SSC-A/CD8. b-Dot-plot graphs represent the gate strategy used to analyze the production of intracellular cytokines in peptide-stimulated $CD8^+$ T cells. (TIF)

S4 Fig. Treatment with anti-CXCR3 monoclonal antibody did not alter the effector phenotype of specific CD8+ T cells. Specific $CD8^+$ T cells were labeled in the spleen using the

dextramer H2K^K-TEWETGQI with APC-fluorophore and all markers showed in the histograms. a-Histograms represent one animal of each group (βgal+*T.cruzi*, ASP-2+*T.cruzi*, and ASP-2+αCXCR3+*T.cruzi*). The MFI of each marker expressed on the surface of specific CD8$^+$ T cells in the spleen were shown in the histograms. The markers that we choose are related with the activation and stimulation of T lymphocytes. Previously, our group described the effector phenotype on specific CD8$^+$ T cells, as CD44^{high}, CD62L^{low} and CD11a^{high}. The red histogram represents the naïve group and the blue the groups βgal+*T.cruzi*, ASP-2+*T.cruzi*, and ASP-2+αCXCR3+*T.cruzi*. Results are shown as individual values and as the mean ± SEM for each group (n = 4).
(TIF)

Acknowledgments

We gratefully acknowledge Dr. Ricardo Gazzinelli, Dr. Joseli Lannes-Vieira for discussions and all supporting. This study is a tribute in memory of Professor Mauricio Martins Rodrigues.

Author Contributions

Conceptualization: Camila Pontes Ferreira, Sang Won Han, Daniel Araki Ribeiro, Alexandre Vieira Machado, Joseli Lannes-Vieira, Ricardo Tostes Gazzinelli, José Ronnie Carvalho Vasconcelos.

Data curation: Barbara Ferri Moraschi, Bianca Ferrarini Zanetti, Sang Won Han, Daniel Araki Ribeiro, Alexandre Vieira Machado, Joseli Lannes-Vieira, Ricardo Tostes Gazzinelli, José Ronnie Carvalho Vasconcelos.

Formal analysis: Camila Pontes Ferreira, Leonardo Moro Cariste, Bianca Ferrarini Zanetti, Daniel Araki Ribeiro, Alexandre Vieira Machado, Joseli Lannes-Vieira, Ricardo Tostes Gazzinelli, José Ronnie Carvalho Vasconcelos.

Funding acquisition: José Ronnie Carvalho Vasconcelos.

Investigation: Camila Pontes Ferreira.

Methodology: Camila Pontes Ferreira, Leonardo Moro Cariste, Barbara Ferri Moraschi, Bianca Ferrarini Zanetti, Sang Won Han, Alexandre Vieira Machado, Joseli Lannes-Vieira, José Ronnie Carvalho Vasconcelos.

Resources: José Ronnie Carvalho Vasconcelos.

Supervision: José Ronnie Carvalho Vasconcelos.

Validation: Camila Pontes Ferreira, Leonardo Moro Cariste, Barbara Ferri Moraschi, Bianca Ferrarini Zanetti, José Ronnie Carvalho Vasconcelos.

Visualization: Sang Won Han.

Writing – original draft: Camila Pontes Ferreira.

Writing – review & editing: Joseli Lannes-Vieira, José Ronnie Carvalho Vasconcelos.

References

1. Machado FS, Dutra WO, Esper L, Gollob K, Teixeira M, Factor SM, et al. Current understanding of immunity to Trypanosoma cruzi infection and pathogenesis os Chagas disease. Semin Immunopathol. 2013; 34(6):753–70.

2. Vega-Royero SP, Sibona GJ. Who benefits from cellular immune response during the Chagas disease? Biosystems [Internet]. 2018 Sep; 171(July):66–73. Available from: https://doi.org/10.1016/j.biosystems.2018.07.005

3. Tzelepis F, de Alencar BCG, Penido MLO, Claser C, Machado A V., Bruna-Romero O, et al. Infection with Trypanosoma cruzi Restricts the Repertoire of Parasite-Specific CD8+ T Cells Leading to Immunodominance. J Immunol [Internet]. 2008; 180(3):1737–48. Available from: https://doi.org/10.4049/jimmunol.180.3.1737 PMID: 18209071

4. Junqueira C, Caetano B, Bartholomeu DC, Melo MB, Ropert C, Rodrigues MM, et al. The endless race between Trypanosoma cruzi and host immunity: lessons for and beyond Chagas disease. Expert Rev Mol Med [Internet]. 2010; 12(September):e29. Available from: http://www.journals.cambridge.org/abstract_S1462399410001560 https://doi.org/10.1017/S1462399410001560 PMID: 20840799

5. Tarleton RL, Koller BH, Latour A, Postan M. Susceptibility of β2-microglobulin-deficient mice to Trypanosoma cruzi infection. Nature [Internet]. 1992 Mar; 356(6367):338–40. Available from: http://www.nature.com/articles/356338a0 https://doi.org/10.1038/356338a0 PMID: 1549177

6. Brener Z, Gazzinelli RT. Immnunological Control of Trypanosoma cruzi Infection and Pathogenesis of Chagas' Disease. Vol. 114, International Archives of Allergy and Immunology. 1997. p. 103–10. https://doi.org/10.1159/000237653 PMID: 9338602

7. Tarleton RL. CD8+ T cells in Trypanosoma cruzi infection. Semin Immunopathol [Internet]. 2015 May 29; 37(3):233–8. Available from: https://doi.org/10.1007/s00281-015-0481-9 PMID: 25921214

8. Martin DL, Weatherly DB, Laucella SA, Cabinian MA, Crim MT, Sullivan S, et al. CD8+ T-cell responses to Trypanosoma cruzi are highly focused on strain-variant trans-sialidase epitopes. Immunol Rev. 2006; 201(8):304–17.

9. De Alencar BCG, Persechini PM, Haolla FA, De Oliveira G, Silverio JC, Lannes-Vieira J, et al. Perforin and gamma interferon expression are required for CD4+ and CD8+ T-cell-dependent protective immunity against a human parasite, Trypanosoma cruzi, elicited by heterologous plasmid DNA prime-recombinant adenovirus 5 boost vaccination. Infect Immun. 2009; 77(10):4383–95. https://doi.org/10.1128/IAI.01459-08 PMID: 19651871

10. Silverio JC, Pereira IR, Cipitelli M da C, Vinagre NF, Rodrigues MM, Gazzinelli RT, et al. CD8+ T-cells expressing interferon gamma or perforin play antagonistic roles in heart injury in experimental trypanosoma cruzi-elicited cardiomyopathy. PLoS Pathog. 2012; 8(4).

11. Dos F, Virgilio S, Pontes C, Dominguez MR, Ersching J, Rodrigues MM, et al. Infection: A Path for Vaccine Development? 2014;2014.

12. Rigato PO, de Alencar BC, de Vasconcelos JRC, Dominguez MR, Araújo AF, Machado A V., et al. Heterologous plasmid DNA prime-recombinant human adenovirus 5 boost vaccination generates a stable pool of protective long-lived CD8+T effector memory cells specific for a human parasite, Trypanosoma cruzi. Infect Immun. 2011; 79(5):2120–30. https://doi.org/10.1128/IAI.01190-10 PMID: 21357719

13. Vasconcelos JR, Dominguez MR, Neves RL, Ersching J, Araújo A, Santos LI, et al. Adenovirus Vector-Induced CD8 $^{+}$ T Effector Memory Cell Differentiation and Recirculation, But Not Proliferation, Are Important for Protective Immunity Against Experimental *Trypanosoma cruzi* Infection. Hum Gene Ther [Internet]. 2014; 25(4):350–63. Available from: https://doi.org/10.1089/hum.2013.218 PMID: 24568548

14. Ferreira CP, Cariste LM, Virgílio FDS, Moraschi BF, Monteiro CB, Machado AMV, et al. LFA-1 mediates cytotoxicity and tissue migration of specific CD8+T cells after heterologous prime-boost vaccination against Trypanosoma cruzi infection. Front Immunol. 2017; 8(OCT).

15. Zlotnik a, Yoshie O. Chemokines: a new classification system and their role in immunity. Immunity. 2000; 12(2):121–7. PMID: 10714678

16. Campbell DJ, Kim CH, Butcher EC. Chemokines in the systemic organization of immunity. Immunol Rev. 2003; 195:58–71. PMID: 12969310

17. Groom JR, Luster AD. CXCR3 in T cell function. Exp Cell Res. 2011; 317(5):620–31. https://doi.org/10.1016/j.yexcr.2010.12.017 PMID: 21376175

18. Bachmann MF, Kopf M, Marsland BJ. Chemokines: more than just road signs. Nat Rev Immunol [Internet]. 2006 Feb 1; 6(2):159–64. Available from: http://www.nature.com/articles/nri1776 https://doi.org/10.1038/nri1776 PMID: 16491140

19. Zlotnik A, Yoshie O. The Chemokine Superfamily Revisited. Immunity [Internet]. 2012; 36(5):705–12. Available from: https://doi.org/10.1016/j.immuni.2012.05.008 PMID: 22633458

20. Iwata S, Mikami Y, Sun HW, Brooks SR, Jankovic D, Hirahara K, et al. The Transcription Factor T-bet Limits Amplification of Type I IFN Transcriptome and Circuitry in T Helper 1 Cells. Immunity [Internet]. 2017;1–9. Available from: http://dx.doi.org/10.1016/j.immuni.2017.05.005

21. Dos Santos PVA, Roffê E, Santiago HC, Torres RA, Marino APMP, Paiva CN, et al. Prevalence of CD8+αβ T cells in Trypanosoma cruzi-elicited myocarditis is associated with acquisition of CD62LLowLFA-

1HighVLA-4Highactivation phenotype and expression of IFN-γ-inducible adhesion and chemoattractant molecules. Microbes Infect. 2001; 3(12):971–84. PMID: 11580984

22. Teixeira MM, Gazzinelli RT, Silva JS. Chemokines, inflammation and Trypanosoma cruzi infection. Trends Parasitol. 2002; 18(6):262–5. PMID: 12036740

23. Gomes JAS, Bahia-Oliveira LMG, Rocha MOC, Martins-Filho OA, Gazzinelli G, Correa-Oliveira R. Evidence that development of severe cardiomyopathy in human Chagas' disease is due to a Th1-specific immune response. Infect Immun. 2003; 71(3):1185–93. https://doi.org/10.1128/IAI.71.3.1185-1193.2003 PMID: 12595431

24. Zhu J, Yamane H, Paul WE. Differentiation of Effector CD4 T Cell Populations. Annu Rev Immunol [Internet]. 2010 Mar; 28(1):445–89. Available from: http://www.annualreviews.org/doi/10.1146/annurev-immunol-030409-101212

25. Moser B, Wolf M, Walz A, Loetscher P. Chemokines: Multiple levels of leukocyte migration control. Trends Immunol [Internet]. 2004 Feb; 25(2):75–84. Available from: http://linkinghub.elsevier.com/retrieve/pii/S1471490603003867 https://doi.org/10.1016/j.it.2003.12.005 PMID: 15102366

26. Cohen SB, Maurer KJ, Egan CE, Oghumu S, Satoskar AR, Denkers EY. CXCR3-Dependent CD4+ T Cells Are Required to Activate Inflammatory Monocytes for Defense against Intestinal Infection. PLoS Pathog. 2013; 9(10).

27. Hu JK, Kagari T, Clingan JM, Matloubian M. Expression of chemokine receptor CXCR3 on T cells affects the balance between effector and memory CD8 T-cell generation. Proc Natl Acad Sci [Internet]. 2011; 108(21):E118–27. Available from: https://doi.org/10.1073/pnas.1101881108 PMID: 21518913

28. Kurachi M, Kurachi J, Suenaga F, Tsukui T, Abe J, Ueha S, et al. Chemokine receptor CXCR3 facilitates CD8 $^{+}$ T cell differentiation into short-lived effector cells leading to memory degeneration. J Exp Med [Internet]. 2011; 208(8):1605–20. Available from: https://doi.org/10.1084/jem.20102101 PMID: 21788406

29. Talvani A, Ribeiro CS, Aliberti JCS, Michailowsky V, Santos PVA, Murta SMF, et al. Kinetics of cytokine gene expression in experimental chagasic cardiomyopathy: Tissue parasitism and endogenous IFN-γ as important determinants of chemokine mRNA expression during infection with Trypanosoma cruzi. Microbes Infect. 2000; 2(8):851–66. PMID: 10962268

30. Vasconcelos JR, Hiyane MI, Marinho CRF, Claser C, Machado AMV, Gazzinelli RT, et al. Protective Immunity Against Trypanosoma cruzi Infection in a Highly Susceptible Mouse Strain After Vaccination with Genes Encoding the Amastigote Surface Protein-2 and Trans-Sialidase. Hum Gene Ther [Internet]. 2004; 15(9):878–86. Available from: https://doi.org/10.1089/hum.2004.15.878 PMID: 15353042

31. Uppaluri R, Sheehan KCF, Wang L, Bui JD, Brotman JJ, Lu B, et al. Prolongation of Cardiac and Islet Allograft Survival by a Blocking Hamster Anti-Mouse CXCR3 Monoclonal Antibody. Transplantation [Internet]. 2008 Jul; 86(1):137–47. Available from: https://insights.ovid.com/crossref?an=00007890-200807150-00024 https://doi.org/10.1097/TP.0b013e31817b8e4b PMID: 18622291

32. Tzelepis F, de Alencar B, Penido M, Gazzinelli R, Persechini P, Rodrigues M. Distinct kinetics of effector CD8+ cytotoxic T cells after infection with Trypanosoma cruzi in Naıve or vaccinated mice. Infect Immun. 2006; 74(4):2477–81. https://doi.org/10.1128/IAI.74.4.2477-2481.2006 PMID: 16552083

33. Piron M, Fisa R, Casamitjana N, López-Chejade P, Puig L, Vergés M, et al. Development of a real-time PCR assay for Trypanosoma cruzi detection in blood samples. Acta Trop. 2007; 103(3):195–200. https://doi.org/10.1016/j.actatropica.2007.05.019 PMID: 17662227

34. Gutierrez FRS, Mariano FS, Oliveira CJF, Pavanelli WR, Guedes PMM, Silva GK, et al. Regulation of Trypanosoma cruzi-induced myocarditis by programmed death cell receptor 1. Infect Immun. 2011; 79(5):1873–81. https://doi.org/10.1128/IAI.01047-10 PMID: 21357717

35. Allen SJ, Crown SE, Handel TM. Chemokine:Receptor Structure, Interactions, and Antagonism. Annu Rev Immunol [Internet]. 2007; 25(1):787–820. Available from: http://www.annualreviews.org/doi/10.1146/annurev.immunol.24.021605.090529

36. Hardison JL, Kuziel WA, Manning JE, Lane TE. Chemokine CC Receptor 2 Is Important for Acute Control of Cardiac Parasitism but Does Not Contribute to Cardiac Inflammation after Infection with Trypanosoma cruzi. J Infect Dis [Internet]. 2006. Jun; 193(11):1584–8. Available from: http://www.ncbi.nlm.nih.gov/pubmed/16652288 https://doi.org/10.1086/503812 PMID: 16652288

37. Vasconcelos JR, Bruña-Romero O, Araújo AF, Dominguez MR, Ersching J, de Alencar BCG, et al. Pathogen-induced proapoptotic phenotype and high CD95 (Fas) expression accompany a suboptimal CD8+T-cell response: Reversal by adenoviral vaccine. PLoS Pathog. 2012; 8(5).

38. Melo RC, Brener Z. Tissue tropism of different Trypanosoma cruzi strains. J Parasitol [Internet]. 1978 Jun; 64(3):475–82. Available from: http://www.ncbi.nlm.nih.gov/pubmed/96243 PMID: 96243

39. Bilate AMB, Cunha-Neto E. Chagas disease cardiomyopathy: current concepts of an old disease. Rev Inst Med Trop Sao Paulo [Internet]. 50(2):67–74. Available from: http://www.ncbi.nlm.nih.gov/pubmed/18488083 https://doi.org/10.1590/s0036-46652008000200001 PMID: 18488083

40. Serbina N V., Pamer EG. Monocyte emigration from bone marrow during bacterial infection requires signals mediated by chemokine receptor CCR2. Nat Immunol. 2006; 7(3):311–7. https://doi.org/10.1038/ni1309 PMID: 16462739

41. Jia T, Serbina N V., Brandl K, Zhong MX, Leiner IM, Charo IF, et al. Additive Roles for MCP-1 and MCP-3 in CCR2-Mediated Recruitment of Inflammatory Monocytes during Listeria monocytogenes Infection. J Immunol [Internet]. 2008; 180(10):6846–53. Available from: https://doi.org/10.4049/jimmunol.180.10.6846 PMID: 18453605

42. Thapa M, Carr DJJ. CXCR3 Deficiency Increases Susceptibility to Genital Herpes Simplex Virus Type 2 Infection: Uncoupling of CD8+ T-Cell Effector Function but Not Migration. J Virol [Internet]. 2009; 83 (18):9486–501. Available from: https://doi.org/10.1128/JVI.00854-09 PMID: 19587047

43. Groom JR, Luster AD. CXCR3 ligands: Redundant, collaborative and antagonistic functions. Immunol Cell Biol [Internet]. 2011; 89(2):207–15. Available from: https://doi.org/10.1038/icb.2010.158 PMID: 21221121

44. Garcia-Lopez MA, Sanchez-Madrid F, Rodriguez-Frade JM, Mellado M, Acevedo A, Garcia MI, et al. CXCR3 chemokine receptor distribution in normal and inflamed tissues: expression on activated lymphocytes, endothelial cells, and dendritic cells. Lab Invest. 2001; 81(3):409–18. PMID: 11310833

45. Colvin RA, Campanella GSV, Sun J, Luster AD. Intracellular domains of CXCR3 that mediate CXCL9, CXCL10, and CXCL11 function. J Biol Chem. 2004; 279(29):30219–27. https://doi.org/10.1074/jbc.M403595200 PMID: 15150261

46. Zhang Z, Kaptanoglu L, Haddad W, Ivancic D, Alnadjim Z, Hurst S, et al. Donor T cell activation initiates small bowel allograft rejection through an IFN-γ-inducible protein-10-dependent mechanism. J Immunol. 2002; 168(7).

47. Lacotte S, Brun S, Muller S, Dumortier H. CXCR3, inflammation, and autoimmune diseases. Ann N Y Acad Sci. 2009; 1173:310–7. https://doi.org/10.1111/j.1749-6632.2009.04813.x PMID: 19758167

48. Sauty A, Colvin RA, Wagner L, Rochat S, Spertini F, Luster AD. CXCR3 Internalization Following T Cell-Endothelial Cell Contact: Preferential Role of IFN-Inducible T Cell Chemoattractant (CXCL11). J Immunol. 2014; 167(12):7084–93.

49. Kohlmeier JE, Cookenham T, Miller SC, Roberts AD, Christensen JP, Thomsen AR, et al. CXCR3 Directs Antigen-Specific Effector CD4+ T Cell Migration to the Lung During Parainfluenza Virus Infection. J Immunol [Internet]. 2009; 183(7):4378–84. Available from: https://doi.org/10.4049/jimmunol.0902022 PMID: 19734208

50. Hickman HD, Reynoso G V., Ngudiankama BF, Cush SS, Gibbs J, Bennink JR, et al. CXCR3 chemokine receptor enables local CD8+T cell migration for the destruction of virus-infected cells. Immunity [Internet]. 2015; 42(3):524–37. Available from: https://doi.org/10.1016/j.immuni.2015.02.009 PMID: 25769612

51. Stiles LN, Hosking MP, Edwards RA, Strieter RM, Lane TE. Differential roles for CXCR3 in CD4+ and CD8+ T cell trafficking following viral infection of the CNS. [Internet]. Vol. 36, European Journal of Immunology. 2006. p. 613–22. Available from: http://www.ncbi.nlm.nih.gov/pubmed/16479546 https://doi.org/10.1002/eji.200535509 PMID: 16479546

52. Liu L, Huang D, Matsui M, He TT, Hu T, DeMartino J, et al. Severe Disease, Unaltered Leukocyte Migration, and Reduced IFN- Production in CXCR3-/- Mice with Experimental Autoimmune Encephalomyelitis. J Immunol [Internet]. 2006; 176(7):4399–409. Available from: https://doi.org/10.4049/jimmunol.176.7.4399 PMID: 16547278

53. Rosas LE, Barbi J, Lu B, Fujiwara Y, Gerard C, Sanders VM, et al. CXCR3-/- mice mount an efficient Th1 response but fail to control Leishmania major infection. Eur J Immunol. 2005; 35(2):515–23. https://doi.org/10.1002/eji.200425422 PMID: 15668916

54. Thapa M, Welner RS, Pelayo R, Carr DJJ. CXCL9 and CXCL10 expression are critical for control of genital herpes simplex virus type 2 infection through mobilization of HSV-specific CTL and NK cells to the nervous system. J Immunol [Internet]. 2008 Jan 15; 180(2):1098–106. Available from: http://www.ncbi.nlm.nih.gov/pubmed/18178850 https://doi.org/10.4049/jimmunol.180.2.1098 PMID: 18178850

55. Groom JR, Richmond J, Murooka TT, Sorensen EW, Sung JH, Bankert K, et al. CXCR3 Chemokine Receptor-Ligand Interactions in the Lymph Node Optimize CD4+T Helper 1 Cell Differentiation. Immunity [Internet]. 2012; 37(6):1091–103. Available from: https://doi.org/10.1016/j.immuni.2012.08.016 PMID: 23123063

56. Schwaderer J, Gaiser AK, Phan TS, Delgado Me, Brunner T. Liver receptor homolog-1 (NR5a2) regulates CD95/Fas ligand transcription and associated T-cell effector functions. Cell Death Dis. 2017; 8 (4):1–12.

57. Leon JS, Engman DM. Autoimmunity in Chagas heart disease. Int J Parasitol. 2001; 31(5–6):555–61. PMID: 11334942

58. Schnickel GT, Bastani S, Hsieh GR, Shefizadeh A, Bhatia R, Fishbein MC, et al. Combined CXCR3/CCR5 blockade attenuates acute and chronic rejection. J Immunol [Internet]. 2008; 180(7):4714–21. Available from: http://www.ncbi.nlm.nih.gov/pubmed/18354195 https://doi.org/10.4049/jimmunol.180.7.4714 PMID: 18354195

59. Wadwa M, Klopfleisch R, Adamczyk A, Frede A, Pastille E, Mahnke K, et al. IL-10 downregulates CXCR3 expression on Th1 cells and interferes with their migration to intestinal inflammatory sites. Mucosal Immunol. 2016; 9(5):1263–77. https://doi.org/10.1038/mi.2015.132 PMID: 26732675

60. Hildebrandt GC, Corrion LA, Olkiewicz KM, Lu B, Lowler K, Duffner UA, et al. Blockade of CXCR3 Receptor:Ligand Interactions Reduces Leukocyte Recruitment to the Lung and the Severity of Experimental Idiopathic Pneumonia Syndrome. J Immunol [Internet]. 2004; 173(3):2050–9. Available from: https://doi.org/10.4049/jimmunol.173.3.2050 PMID: 15265940

61. Rivino L, Kumaran EA, Thein TL, Too CT, Gan VCH, Hanson BJ, et al. Virus-specific T lymphocytes home to the skin during natural dengue infection. Sci Transl Med. 2015; 7(278):1126.

PLOS NEGLECTED TROPICAL DISEASES

RESEARCH ARTICLE

CXCR3 chemokine receptor contributes to specific CD8$^+$ T cell activation by pDC during infection with intracellular pathogens

Camila Pontes Ferreira[1], Leonardo de Moro Cariste[2], Isaú Henrique Noronha[1], Danielle Fernandes Durso[3], Joseli Lannes-Vieira[4], Karina Ramalho Bortoluci[5], Daniel Araki Ribeiro[2], Douglas Golenbock[3], Ricardo Tostes Gazzinelli[3], José Ronnie Carvalho de Vasconcelos[1,2]*

1 Department of Microbiology, Immunology and Parasitology, Federal University of São Paulo, São Paulo, Brazil, **2** Department of Biosciences of the Federal University of São Paulo, Santos, Brazil, **3** Department of Medicine, University of Massachusetts Medical School, Worcester, Massachusetts, United States of America, **4** Laboratory of Biology of the Interactions, Oswaldo Cruz Institute, Fiocruz, Rio de Janeiro, Brazil, **5** Department of Biology Sciences, Federal University of São Paulo, São Paulo, Brazil

* jrcvasconcelos@gmail.com

Citation: Pontes Ferreira C, Moro Cariste Ld, Henrique Noronha I, Fernandes Durso D, Lannes-Vieira J, Ramalho Bortoluci K, et al. (2020) CXCR3 chemokine receptor contributes to specific CD8$^+$ T cell activation by pDC during infection with intracellular pathogens. PLoS Negl Trop Dis 14(6): e0008414. https://doi.org/10.1371/journal.pntd.0008414

Editor: Abhay R. Satoskar, Ohio State University, UNITED STATES

Received: January 31, 2020

Accepted: May 22, 2020

Published: June 23, 2020

Data Availability Statement: All relevant data are within the manuscript and its Supporting Information files.

Funding: This work was supported by grant from Fundação de Amparo à Pesquisa do Estado de São Paulo (http://www.fapesp.br/) (JRCV: 2012/22514-3; 2018/15607-1 CF: 2015/08814-2; LC: 2019/17994-5; BM: 2016/02840-4), Instituto Nacional de Ciência e Tecnologia em Vacinas (http://inct.cnpq.

Abstract

Chemokine receptor type 3 (CXCR3) plays an important role in CD8$^+$ T cells migration during intracellular infections, such as *Trypanosoma cruzi*. In addition to chemotaxis, CXCR3 receptor has been described as important to the interaction between antigen-presenting cells and effector cells. We hypothesized that CXCR3 is fundamental to *T. cruzi*-specific CD8$^+$ T cell activation, migration and effector function. Anti-CXCR3 neutralizing antibody administration to acutely *T. cruzi*-infected mice decreased the number of specific CD8$^+$ T cells in the spleen, and those cells had impaired in activation and cytokine production but unaltered proliferative response. In addition, anti-CXCR3-treated mice showed decreased frequency of CD8$^+$ T cells in the heart and numbers of plasmacytoid dendritic cells in spleen and lymph node. As CD8$^+$ T cells interacted with plasmacytoid dendritic cells during infection by *T. cruzi*, we suggest that anti-CXCR3 treatment lowers the quantity of plasmacytoid dendritic cells, which may contribute to impair the prime of CD8$^+$ T cells. Understanding which molecules and mechanisms guide CD8$^+$ T cell activation and migration might be a key to vaccine development against Chagas disease as those cells play an important role in *T. cruzi* infection control.

Author summary

Inflammatory chemokine receptors such as CXCR3 play an important role in T lymphocytes migration into an infected tissue during Th1 response. Recently, the role of CXCR3 as a co-stimulatory molecule was demonstrated, and T lymphocytes from CXCR3 deficient mice had impaired effector function. CXCR3 receptor was highly expressed on specific CD8$^+$ T cells after challenge with *T. cruzi*, and the hypothesis of that molecule is important for CD8$^+$ T cells activation, migration and functionality was raised. We used

br/), Coordenação de Aperfeiçoamento de Pessoal de Nível Superior (http://www.capes.gov.br/), Conselho Nacional de Desenvolvimento Científico e Tecnológico (http://cnpq.br/), and NIH 1R01AI116577 to RTG. The funders had no role in study design, data collection and analysis, decision to publish, or preparation of the manuscript.

Competing interests: The authors have declared that no competing interests exist.

the anti-CXCR3 neutralizing antibody approach and demonstrated that C57BL/6 treated mice died very quickly due to *T. cruzi* infection, and specific $CD8^+$ T cells had decreased effector phenotyping, cytokine production, and cytotoxicity. In addition, anti-CXCR3 treatment decreased the number of dendritic plasmacytoid cells in the lymphoid tissues. The lower quantity of dendritic plasmacytoid cells in those tissues might contribute to the decrease in $CD8^+$ T cells activation. Overall, CXCR3 molecule seems to be an important molecule to be explored during vaccine against Chagas disease strategies.

Introduction

Chemokine receptors play an important role in T lymphocytes migration during homeostasis and inflammation. Inflammatory chemokines control the recruitment of effector leukocytes into infected tissues, and different types of these chemoattractant cytokines are preferentially expressed in innate and adaptive immune responses [1,2]. CXCR3 receptor, a G protein-coupled cell surface receptor (GPCR) with seven transmembrane α-helical domains, is expressed during Th1 adaptive response and it is an inflammatory chemokine inducible by CXCL9/MIG, CXCL10/IP-10 and CXCL11/I-TAC [3,4]. T-bet is a transcription factor that directly activates transcription of a set of genes which are important for Th1 cell function, including those encoding IFN-γ and the chemokine receptor CXCR3 [5].

CXCR3 receptor has been reported to be expressed in several immune cell types such as: T effector lymphocytes, $CD4^+$ $Foxp3^+$ T cells, natural killer (NK) and B cells [3,6]. We have demonstrated that CXCR3 is expressed in specific $CD8^+$ T cells after *Trypanosoma cruzi* infection, which induced Th1 responses with high levels of IFN-γ cytokine [7]. In *T. cruzi* infection, it was demonstrated that patients with cardiomyopathy also had an increase in the expression of CXCR3 ligands [8,9].

The role of CXCR3 in T cell migration has been demonstrated during infection by *Toxoplasma gondii*: $CXCR3^+$ $CD4^+$ T migrated into infected tissues and controlled the infection [10]. In cardiac allografts rejection, T lymphocytes expressing CXCR3 are responsible for recruiting cytokine-producing T cells that cause inflammation, culminating with the allograft rejection [11]. During infection with parainfluenza, CXCR3 guides $CD4^+$ T cells to the lungs [12]. Also, we demonstrated that CXCR3 is essential to specific $CD8^+$ T cell migration into infected hearts and infection control during immunization with ASP-2-based anti-*T. cruzi* vaccine [13].

In addition to chemotaxis, CXCR3 signaling may influence the development of effector T cells because $CD8^+$ T cells have reduced proliferative and cytotoxic ability in receptor- or ligand-deficient mice [14]. During infection with HSV-2, T cells from CXCR3-deficient mice exhibited impaired $CD8^+$ T cell cytotoxicity and reduced expression of T-bet, IFN-γ, perforin and granzyme B [15].

Hickman and colleagues demonstrated that CXCR3-deficient $CD8^+$ T cells had impaired cytotoxicity and suggested that CXCR3 plays a role in the contact between antigen-presenting cells and $CD8^+$ T cells, allowing priming and activation of T cells [16]. In fact, CXCL10-expressing dendritic cells (DCs) actively interacted with T cells, indicating a role of CXCL10/CXCR3 in the interactions between the cells [17]. Recently, it was demonstrated that CXCL9 produced by allograft DCs promotes priming towards cytotoxic $CD8^+$ T cells (CTL) and Th1 $CD4^+$ IFN-γ producing T cells [18].

T. cruzi-specific $CD8^+$ T cells, which are responsible for controlling parasite load via cytokine release and cytotoxic activity, express high levels of CXCR3 on the surface [19,20]. Therefore,

we hypothesized that CXCR3 is pivotal for CD8$^+$ T cell activation and effector function guiding those cells toward antigen-presenting cells, such as plasmacytoid dendritic cells (pDCs). We used the anti-CXCR3 neutralizing antibody approach to understand the role of CXCR3 in the CD8$^+$ T cell function. For that propose, C57BL/6 mice were infected with *T*. *cruzi* and treated with anti-CXCR3 antibody every 48 hours, first, we evaluated the parasitemia and survival rate, also, we investigated the function, activation and migration of specific CD8$^+$ T cells.

Methods

Ethics statement, mice, infection and treatments

We followed the recommendations in the Guide for the Care and Use of Laboratory Animals of the Brazilian National Council of Animal Experimentation to develop this study. The protocol (CEUA 7559051115) was approved by the Ethical Committee for Animal Experimentation at the Federal University of São Paulo. Eight-weeks-old female, C57BL/6, OT-I and Foxp3-GFP reporter mice were purchased from the Federal University of São Paulo (CEDEME). The REX3 lineage was provided by Dr. Ricardo Tostes Gazzinelli (University of Massachusetts). For infection of C57BL/6 (or background) mice, blood trypomastigotes forms of the Y strain of *T*. *cruzi* were maintained by weekly passages in A/Sn mice at the Xenodiagnosis Laboratory of Dante Pazzenese Cardiology Institute. For *in vivo* experiments using C57BL/6, each mouse was inoculated with 10^4 trypomastigotes forms from blood (Y strain of *T*. *cruzi*) and OT-I mice were infected with $1x10^6$ Y-OVA transgenic parasites that were maintained in culture (LLCMK2 cells). Both parasites were diluted in 0.2 mL PBS and administered subcutaneously (s.c.) at the base of the tail. We used anti-mouse CXCR3 monoclonal antibodies (CXCR3-173, BioXcell) and Rat IgG2a isotype control antibody (clone 2A3, BioXcell). Both were administered via the intraperitoneal route on the same day of infection and every 48 hours until day 15 of infection. The quantity of antibodies administered was 250 μg of mAb/mouse, the same amount used by Uppaluri *et al* [21]. Parasitemia was determined by the examination of 5 μL of blood, and parasites were counted using a light microscope.

Quantification of parasites burden and relative expression of CXCL10, CXCL9 and CD8 molecules

On day 15 after infection, hearts from the Isotype Control group and the anti-CXCR3 group were harvested, and DNA extraction was performed using phenol-chloroform-isoamyl alcohol (SIGMA). For Real Time PCR reaction, we used specific primers for a satellite DNA sequence of the parasite (*T*. *cruzi*) and TaqMan Universal Master Mix II with UNG, adapted from Piron and colleagues [22]. For quantification of chemokines, the RNA from mice's heart was extracted using TRIzol and complementary DNA was prepared using Multiscript RT (Applied Biosystems). PCR was performed with SYBR Green Master Mix (Applied Biosystems) and the primer sequences used to measure chemokines and CD8 expression were: CXCL9, 5′-AATGC ACGATGCTCCTGCA-3′ and 5′-AGGTCTTTGAGGGATTTGTAGTGG-3′; CXCL10, 5′-GC CGTCATTTTCTGCCTCA-3′ and 5′-CGTCCTTGCGAGAGGGATC-3′, CD8, 5′-GACGAA GCTGACTGTGGTTGA-3′ CD8, 5′-GCAGGCTGAGGGTGGTAAG-3′. The samples were normalized using GAPDH gene, 5′-GTGGTGAAGCAGGCATCTGA-3′ and 5′-GGGAGTCA CTGTTGAAGTCGC-3′ primers.

Image flow cytometry analyses

For the *in vivo* interaction experiment, C57BL/6 mice (CD45.1) were irradiated at 900 Rads. Each irradiated animal received $10{\times}10^6$ bone marrow cells by i.v route, isolated from GREAT

IFN-γ GFP reporter mice and REX3 CXCL10-BFP and CXCL9-RFP reporter mice (CD45.2). Twelve weeks after the transference, mice were infected with *T*. *cruzi* and, on day 12 after infection, spleens were harvested, then fixed with 1% of PFA, and labeled with DRAQ5 (BD, Pharmingen) and anti-CD8 (clone 53–67, BD). For experiments with REX3 mice, spleen cells were harvested on day 12 after infection, then fixed with 1% of PFA and labeled with: anti-CD8 (clone 53–67, BD), anti-CD11b (clone M1/70, ebioscience), anti-CD209a (clone MMD3, ebioscience), anti-CD317 (pDCA-1, Miltenyi Biotec), anti-CD11c (clone HL3, BD), and DRAQ5 (BD, Pharmingen). The samples were acquired from ImageStream Ammis, and we used the Ideas software to perform the analysis. The double cells were selected based on aspect ratio versus cell area [23].

Immunological assays

The immunodominant peptide VNHRFTLV (pA8) from GenScript described earlier [24] was used for *ex vivo* stimulation splenocytes. For surface labeling, two million splenocyte cells were treated with lysis buffer and specific $CD8^+$ T cells were labeled using $H2K^b$-VNHRFTLV multimer (Immudex) for 10 minutes at RT. After that, the other surface antigens were labeled for 30 min at 4˚C. The antibodies used were: anti-CD3 (clone 145-2C11, BD), anti-CD8 (clone 53–67, BD), anti-CD11a (clone 2D7, BD), anti-CD11c (clone HL3, BD), anti-CD44 (clone IM7, BD), anti-CD62L (clone MEL-14, BD), anti-CXCR3 (clone 173, BioLegend), anti-CD27 (clone LG3A10, BD), anti-CD4 (clone RM4-5, BD) anti-KLRG1 (clone 2F1, eBioscience), anti-CD49d (clone R1-2, BD), anti-CD69 (clone H1.2F3, BD), anti-CD43 (1B11, BioLegend), anti-CD95 (clone JO2, BD), anti-CD25 (clone LG3A10, BD), anti-CD127 (clone SB/199, BD), anti-CD122 (clone TM-β1, BD), anti-CD38 (clone 90, BD), anti-β7 (clone FIB27, BioLegend), anti-CD31 (clone MEC 13.3, BD), anti-CD272 (clone 8F4, eBioscience), anti-PD-1 (clone J43, eBioscience) and anti-CTLA-4 (clone UC10-4B9, eBioscience). For annexin V and 7-AAD assays, $2x10^6$ of splenocytes were stained according to the Annexin Kit protocol (BD Pharmingen). To measure cytokine profile, splenocytes were stimulated with peptide (pA8) for 12 hours, the supernatant was collected, and the cytokines were measured using the Cytometric Bead Array Mouse Th1/Th2/Th17 Cytokines Kit (BD).

For Intracellular Staining (ICS), $2x10^6$ of splenocytes were incubated during 12 hours with medium containing CD107a FITC antibody (clone 1D4B, BD), anti-CD28 (clone 37.51, BD), BD Golgi-Plug (1 μL/mL) and monensin (5 μg/mL) BD Golgi-Plug (1 μL/mL) and stimulated with 10 μM of peptide pA8. To detect IFN-γ, TNF or granzyme B, splenocytes were labeled with multimer and anti-CD8 PERCP antibody (clone 53–6.7, BD) on ice for 30 min. Following, the cells were fixed and permeabilized with BD perm/wash buffer. For intracellular staining, we used anti-IFN-γ (clone XMG1.2, BD), anti-TNF (clone MP6-XT22, BD), and anti-granzyme B (clone GB11, INVITROGEN). At least 700,000 cells were acquired on a BD FACS Canto II flow cytometer and then analyzed with FlowJo software.

For the ELISPOT assay, $1x10^6$ responder cells from the spleen were incubated with $3x10^5$ antigen-presenting cells in complete cell culture medium (1% NEAA, 1% L-glutamine, 1% vitamins and 1% pyruvate, 0,1% 2-ME, 10% FBS (HyClone), 20 U/ml mouse IL-2 recombinant (SIGMA) and, on a plate previously coated with 10 μg/ml of anti-IFN-γ capture antibody (clone R4-6A2, Pharmingen), those cells were incubated in the presence or absence of 10 μM of peptide pA8. After 24 hours, the plates were washed and incubated with 2 μg/ml of biotinylated anti-IFN-γ antibody (clone XMG1.2, Pharmingen). Subsequently, the plates were incubated with streptavidin-peroxidase (BD) and developed by adding peroxidase substrate (50mM Tris-HCl, pH 7.5, containing 1 mg/ml DAB and 1 μL/ml 30% hydrogen peroxide, both from SIGMA). The number of IFN-γ-producing cells was determined using a stereoscope.

In vivo BrdU incorporation

BrdU (5-bromo-2'-deoxiuridine, SIGMA) administration was performed on the same day of infection; 2mg of BrdU were injected via i.p route every 48 hours until 15 days after infection. Then, $2x10^6$ splenocytes were stained according to the BrdU-FITC Kit protocol (BD Pharmingen) in order that the percentage of specific $CD8^+$ T cells that incorporated BrdU could be analyze. At least 700,000 cells were acquired on a BD FACS Canto II flow cytometer and analyzed with FlowJo software.

In vivo cytotoxicity assay

The protocol described by Silverio *et al* [25] was used. Splenocytes from naïve mice were divided into two populations labeled with CFSE (Molecular Probes) at a final concentration of 10 μM ($CFSE^{high}$) or 1 μM ($CFSE^{low}$). $CFSE^{high}$ cells were coated with 2.5 μM of pA8 peptide for 40 minutes at 37˚C. Subsequently, $CFSE^{high}$ cells were mixed with equal numbers of $CFSE^{low}$ cells before intravenous injection ($2x10^7$ cells per mouse) into recipient mice. Spleen cells from the recipient mice were collected 18 hours after adoptive cell transfer and the events were acquired on a BD FACS Canto II flow cytometer and analyzed with FlowJo 8.7. The percentage of specific lysis was determined using the following formula:

$$\%\text{lysis} = 1 - \frac{(\%\text{CFSE}^{\text{high}}\ \text{infected}/\%\text{CFSE}^{\text{low}}\ \text{infected})}{(\%\text{CFSE}^{\text{high}}\ \text{naive}/\%\text{CFSE}^{\text{low}}\ \text{naive})} \times 100$$

Histology and immunohistochemistry

Hearts from naïve, Isotype Control and anti-CXCR3 groups were fixed in 10% formalin, and then dehydrated, embedded in paraffin blocks, and sectioned in a microtome. Staining was performed using hematoxylin and eosin. The number of amastigote nests was quantified using a light microscope with a 40x objective lens. Overall, 50 fields/group were counted. For immunohistochemistry the mice's hearts were frozen in Tissue-Tek O.C.T (Sakura Fineteck); the blocks were sectioned in cryostat (7μm thickness) and fixed in ice-cold acetone for 15 minutes. The samples were stained with 20 μg of the biotinylated anti-CD8 antibody (clone 53–6.7, RD systems) overnight, and labeled with streptavidin Alexa Fluor 488 (Thermo Fischer) at a concentration of 0.5 mg/mL for 1 hour at room temperature. The DAPI (SIGMA) dye was used for labeling the cell nucleus at a concentration of 5 mg/ml. The images were acquired on Confocal Leica TCS SP8 CARS microscope from the Institute of Pharmacology and Molecular Biology (INFAR). The images were obtained using a 63x objective lens and processed on ImageJ software.

Statistical analysis

The data was presented as mean ± Standard Deviation (SD). Unidirectional Variance (ANOVA), the Tukey's HSD posthoc and Student's t-test (http://vassarstats.net/) were used to compare parasitemia, the number of IFN-γ-producing cells (ELISPOT), and absolute number of $CD8^+$ T-cells. The survival rate was compared using the Log-rank test using GraphPad Prism 7. Molecule expression was compared using MFI (Mean Fluorescence Intensity), determined by the FlowJo software (version 10.5.3). Differences were considered statistically significant when $P < 0.05$.

Results

T. cruzi infection upregulates CXCR3 on T lymphocytes in lymphoid tissues and its ligands CXCL10 and CXCL9 in the heart tissue

Here, we checked whether specific $CD8^+$ and activated $CD4^+$ T cells generated by *T. cruzi* infection expressed CXCR3 receptor. For that propose, we labeled specific $CD8^+$ T cells in the

spleen and lymph nodes with multimer H2K^b-restricted VNHRFTLV, an immunodominant peptide of ASP-2 *T. cruzi* surface amastigote protein [26,27]. To label CD4$^+$ T cells, we first gated those cells as CD44^{high}CD62L^{low} and then for CD4$^+$ T cells. On the bar graphs, it can be observed the frequency of specific CD8$^+$ T cells in the spleen and lymph nodes in infected mice on day 15 after infection (Fig 1A and 1B).

Likewise, VNHRFTLV specific CD8$^+$ and activated CD4$^+$ T cells were gated as showed in dot-plots graph and we observed that those cells expressed high levels of CXCR3 molecule on the surface of both spleen and lymph node, as shown by an increase in MFI numbers in comparison to naïve group (Fig 1A and 1B). Furthermore, CXCR3 expression was evaluated in the spleen and lymph nodes on days 5, 10, 15, 20, and 30 after infection. In specific CD8$^+$ and activated CD4$^+$ T cells, we observed that CXCR3 expression was high in both T cells and tissues on each day of analysis (Fig 1C and 1D).

In addition, CXCR3 ligand (CXCL10/IP-10 and CXCL9/MIG) expressions were evaluated in infected hearts by RT-PCR (Fig 1E and 1F). We noticed an increase in CXCL10 and CXCL9 expressions during infection compared to *naïve* hearts. Further, the relative expression of CXCL10 was higher than CXCL9 in infected mice. Collectively, these data showed that CXCR3 and their CXCL10 and CXCL9 ligands were highly expressed during acute *T. cruzi* infection.

Anti-CXCR3 treated mice increased parasitemia and susceptibility to *T. cruzi* infection in C57BL/6 mice

Here, we assessed whether CXCR3 receptor is important to control *T. cruzi* infection in C57BL/6 mice. For that intend, C57BL/6 mice were infected and on the same day treated with 250 μg of anti-CXCR3 or IgG2a isotype control antibodies. The treatment was repeated every 48 hours and for two weeks. On day 15 after infection, we performed immune responses and survival rate analyses as shown in the experimental scheme (Fig 2A). During the infection with the Y strain of *T. cruzi*, the peak of parasite levels in the blood of C57BL/6 mouse usually occurs on day 9 after infection. After that, this mouse strain controls the acute phase and the number of parasites drastically decreased after the peak as we described previously [28]. As we can see in the Fig 2B, mice treated with isotype control antibody displayed low levels of parasitemia and did not change the already described parasitemia profile after infection with the Y strain of *T. cruzi*. Interestingly, on day 9 after infection (the peak), the anti-CXCR3 treated group had higher parasitemia compared to the Isotype control group (Fig 2B). After the peak, parasitemia in isotype control and anti-CXCR3 treated groups decreased, and on day 13, the parasitemia levels increased again only in anti-CXCR3 treated group (Fig 2B). The parasitemia level in the anti-CXCR3 group remained high until day 15 after infection in contrast with the Isotype control group (Fig 2B). These results indicate that anti-CXCR3 treated mice could not control the parasite multiplication. In addition, all anti-CXCR3 treated mice which presented high parasitemia became susceptible and died very quickly due to infection when compared to controls, which had a 100% survival rate (Fig 2C). Together, those results indicate that CXCR3 receptor is important to control *T. cruzi* infection in C57BL/6 mice.

The number of H2K^b-restricted VNHRFTLV-specific CD8$^+$ T cells decreased as well as polyfunctionality and cytotoxicity after anti-CXCR3 treatment

Specific CD8$^+$ T cells play an important role in controlling *T. cruzi* infection by cytokine production and cytotoxicity against infected cells [20]. Initially, we evaluated the number of specific CD8$^+$ T cells in spleen after anti-CXCR3 treatment on day 15 after infection. We

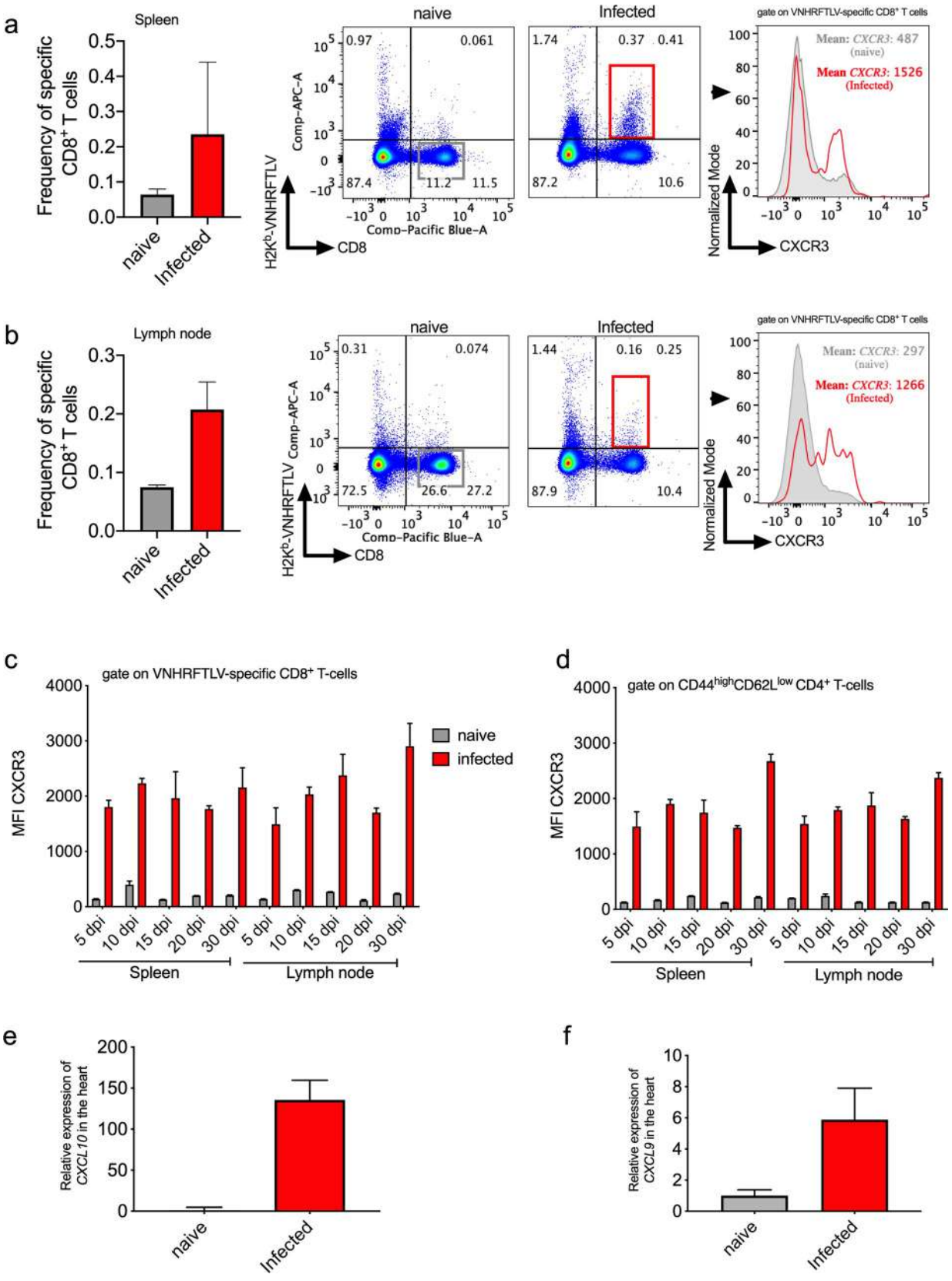
a
Spleen
Frequency of specific CD8+ T cells
naive
Infected
naive
Infected
gate on VNHRFTLV-specific CD8+ T cells
Mean: CXCR3: 487 (naive)
Mean CXCR3: 1526 (Infected)
H2Kb-VNHRFTLV
Comp-APC-A
Comp-Pacific Blue-A
CD8
Normalized Mode
CXCR3
b
Lymph node
Frequency of specific CD8+ T cells
Mean: CXCR3: 297 (naive)
Mean: CXCR3: 1266 (Infected)
c
gate on VNHRFTLV-specific CD8+ T-cells
MFI CXCR3
naive
infected
5 dpi
10 dpi
15 dpi
20 dpi
30 dpi
Spleen
Lymph node
d
gate on CD44highCD62Llow CD4+ T-cells
e
Relative expression of CXCL10 in the heart
f
Relative expression of CXCL9 in the heart

Fig 1. CXCR3 chemokine receptor is highly expressed on specific CD8$^+$ and activated CD4$^+$ T cell surfaces as well as the CXCR3 ligands in the heart of infected mice. C57BL/6 mice were infected with 1x10^4 blood forms of the Y strain of *Trypanosoma cruzi*. a-The bar graph indicates the frequency of VNHRFTLV specific CD8$^+$ T cells and the representative dot-plot graphs show the frequency of specific CD8$^+$ T cells in the spleen. The histogram showed CXCR3 expression on specific CD8$^+$ T in the spleen of naïve and infected mice. b-The bar graph indicates the frequency of VNHRFTLV specific CD8$^+$ T cells and the representative dot-plot graphs show the frequency of specific CD8$^+$ T cells in lymph node. The histogram showed CXCR3 expression on specific CD8$^+$ T in the lymph node of naïve and infected mice 15 days post infection. The grey line represents the naïve animals while the red line represents the infected ones. c-The graphs represent MFI of CXCR3 in specific CD8$^+$ and (d) activated CD4$^+$ T cells. CXCR3 expression was evaluated on days 5, 10, 15, 20 and 30 post infection (dpi) in the spleen and lymph node. e-Relative expression of CXCL10 and (f) CXCL9 chemokines in naïve and infected mice hearts 15 days post infection. Data are mean ± SD and are representative of one independent experiment with n = 4.

https://doi.org/10.1371/journal.pntd.0008414.g001

observed a percentage 0.2% of specific CD8$^+$ T cells in isotype control treated mice whereas the anti-CXCR3 treated mice group showed 0.09% of specific CD8$^+$ T cells (Fig 3A). Consequently, the absolute number of specific CD8$^+$ T cells in the anti-CXCR3 treated group drastically decreased compared to the isotype control group (Fig 3B). Additionally, we analyzed the number of total CD4$^+$ T cells and we could observe that the treatment with anti-CXCR3 antibody did not alter the absolute number of CD4$^+$ T cells in the spleen when compared to the isotype control group (S1A Fig). Moreover, we evaluated the number of CD4$^+$ T cells Foxp3$^+$ in the spleen using Foxp3-GFP reporter mice and, despite the decrease in frequency of

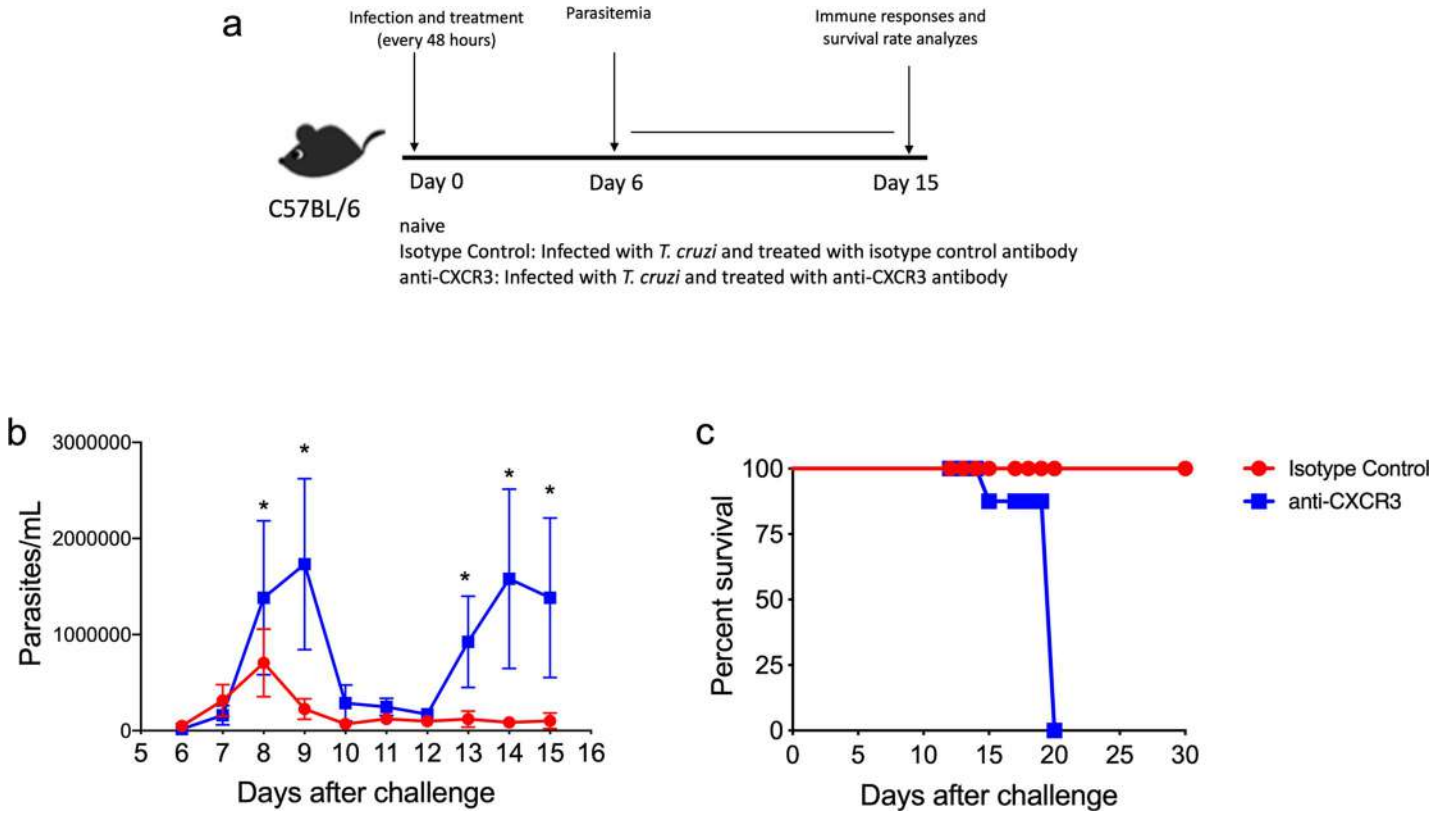

Fig 2. CXCR3 receptor is important to parasitemia and survival of C57BL/6 infected with *Trypanosoma cruzi*. a-Experimental scheme showing the model used in this study. Both Isotype control and anti-CXCR3 antibody treated groups were infected with 1x10^4 blood trypomastigotes of the Y strain of *T. cruzi*. On the same day of infection, anti-CXCR3 group was treated with 250 μg of anti-CXCR3 antibody while the isotype control group was treated with the same concentration of anti-IgG of Rat antibody. The treatment was performed every 48 hours until 15 days after infection by intraperitoneal route. b-Graph of parasitemia showed in linear scale of Isotype Control and anti-CXCR3 groups. c-The Kaplan–Meier curves for survival of Isotype control and anti-CXCR3 groups. The statistical differences between the groups were compared using the log-rank test (p = 0.0091). Data are mean ± SD and are representative of 3 independent experiments with n = 4. *values are significantly different between isotype Control and anti-CXCR3 groups in indicated days (*p>0.001). The statistical analysis was performed using the Student's t-test.

https://doi.org/10.1371/journal.pntd.0008414.g002

$CD4^+Foxp3^+$ cells in the isotype control (0.19%) and anti-CXCR3 (0.23%) groups when compared to naïve cells (2.23%), we did not observe any statistical differences in the absolute number of $CD4^+Foxp3^+$ cells among naïve, isotype control and anti-CXCR3 groups (S1B and S1C Fig). The $CD4^+$ $Foxp3^+$ cells from infected groups expressed high levels of CD25 molecule on the surface (S1 Fig). Furthermore, CXCR3 receptor was highly expressed on the surface of $CD4^+$ $Foxp3^+$ cells during infection when compared to naïve cells (S1E Fig).

Next, we examined whether specific $CD8^+$ T cells could proliferate after the anti-CXCR3 antibody treatment. To perform that, we administered BrdU molecule (thymidine analogues) on the same day of infection and quantified the incorporation of that molecule by flow cytometry. We observed that, after infection with *T*. *cruzi*, the percentage of specific $CD8^+$ T cell $BrdU^+$ increased when compared to naïve $CD8^+$ T cells (Fig 3C). Also, the percentages of specific $CD8^+$ T cells that were BrdU positive from Isotype control and anti-CXCR3 groups were similar (Fig 3D), indicating that the anti-CXCR3 treatment did not alter the proliferation of specific $CD8^+$ T cells in the spleen. Furthermore, we measured the pro-apoptotic profile of specific $CD8^+$ T cells after anti-CXCR3 treatment by using annexin V labeling. There was an increase of specific $CD8^+$ T cells positive for annexin V after infection when compared to $CD8^+$ T cells from naïve group. However, we did not observe any differences between the percentage of specific $CD8^+$ T cells positive for annexin V between isotype control and anti-CXCR3 groups (Fig 3E).

Another important function triggered by $CD8^+$ T cells is the directed cytotoxicity against infected cells. It is known that during *T*. *cruzi* infection there is an induction of cytotoxic $CD8^+$ T cells. Silverio and colleagues demonstrated two populations of anti-*T*. *cruzi* $CD8^+$ T cells segregated into a group showing the capacity for producing interferon-gamma (IFN-γ) and another one that performed specific cytotoxicity [25]. Thus, we performed the *in vivo* cytotoxicity of specific $CD8^+$ T cells on day 12 after infection and observed that those cells from the Isotype control mice had almost 50% of cytotoxicity, while the percentage in the anti-CXCR3 group was 27% (Fig 3F). Surprisingly, on day 15 after infection, the cytotoxicity of infected specific $CD8^+$ T cells was 100% in the isotype control group and in the anti-CXCR3 group the cytotoxicity decreased almost 50% percent when compared to the isotype control group (Fig 3G). We also examined granzyme B production, which is one of the important cytotoxic granules produced and released by $CD8^+$ T cells. After infection, specific $CD8^+$ T cells increase granzyme B expression when compared to $CD8^+$ T cells from naïve group. In the anti-CXCR3 group we detected a decrease in MFI of granzyme B compared to isotype control group, but that decrease was not statistically different (Fig 3H).

In addition, cytokine production by specific $CD8^+$ T cells was analyzed by ELISPOT, CBA and ICS assays. Using ELISPOT assay, harvested splenocytes from naïve, isotype control and anti-CXCR3 groups were stimulated with pA8 peptide and the number of $CD8^+$ IFN-γ producing cells was counted. We observed that the anti-CXCR3 group had a decrease in the number of IFN-γ $CD8^+$-producing cells in the spleen when compared to the isotype control group (Fig 3I). Additionally, using CBA assay, we measured Th1/Th2/Th17 cytokine profile from splenocytes supernatant and observed a high quantity of cytokines related to Th1 response in the infected groups, such as IFN-γ and TNF, however, we noticed that in the anti-CXCR3 group it was a trend in IFN-γ decrease (Fig 3J).

We also checked the polyfunctionality of specific $CD8^+$ T cells measured by ICS. We quantified the percentage of specific $CD8^+$ T that were degranulating (CD107a) and/or producing TNF and/or IFN-γ. Those cells were subdivided into groups of cells that were triggered 3, 2 or 1 function. We observed that the percentage of specific $CD8^+$ T triple positive cells in the Isotype Control group was 3.83% while that percentage dropped to 0.47% in the anti-CXCR3 group, indicating that the anti-CXCR3 treatment diminished the polyfunctionality of specific

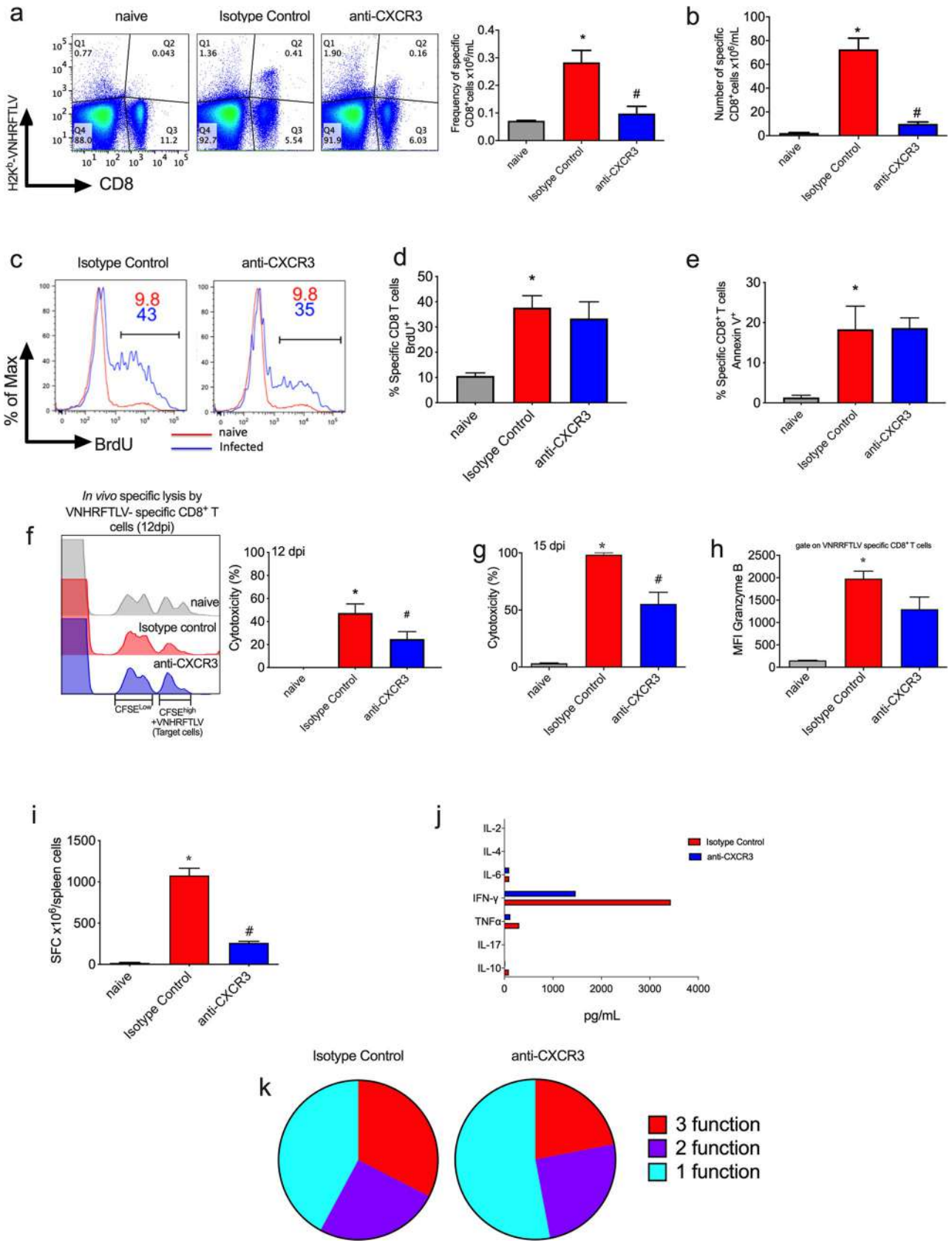
a
naive
Isotype Control
anti-CXCR3
Q1 0.77
Q2 0.043
Q4 88.0
Q3 11.2
Q1 1.36
Q2 0.41
Q4 92.7
Q3 5.54
Q1 1.90
Q2 0.16
Q4 91.9
Q3 6.03
H2Kb-VNHRFTLV
CD8
Frequency of specific CD8+cells x10^6/mL
b
Number of specific CD8+cells x10^6/mL
c
Isotype Control
anti-CXCR3
9.8
43
9.8
35
% of Max
BrdU
naive
Infected
d
% Specific CD8 T cells BrdU+
e
% Specific CD8+ T cells Annexin V+
f
In vivo specific lysis by VNHRFTLV- specific CD8+ T cells (12dpi)
naive
Isotype control
anti-CXCR3
CFSELow
CFSEhigh +VNHRFTLV (Target cells)
12 dpi
Cytotoxicity (%)
g
15 dpi
Cytotoxicity (%)
h
gate on VNRRFTLV specific CD8+ T cells
MFI Granzyme B
i
SFC x10^6/spleen cells
j
IL-2
IL-4
IL-6
IFN-γ
TNFα
IL-17
IL-10
Isotype Control
anti-CXCR3
pg/mL
k
Isotype Control
anti-CXCR3
3 function
2 function
1 function

Fig 3. Anti-CXCR3 group decreased number of specific CD8$^+$ T cells as well as polyfunctionality after infection with *T. cruzi*. a-Representative dot-plot graphs of each group show the frequency of specific CD8$^+$ T cells (in Q2 quadrant) in the spleen and the bar graph represents the mean of specific CD8$^+$ T cells frequency on day 15 after infection. Those cells were labeled with H2K^b-VNHRFTLV multimer. b-The bar graph with absolute numbers of specific CD8$^+$ T cells in the spleen on day 15 after infection. c-Histograms represent the gate on specific CD8$^+$ T cells positive for BrdU; the red line represents one mouse from the naïve group while the blue one refers to the *T. cruzi* infected mice (Isotype control and anti-CXCR3 groups, respectively). d-Percentage of specific CD8$^+$ T cells positive for BrdU (thymidine analogues) in the spleen. The *in vivo* proliferation assay was performed by BrdU administration (5mg/mouse). e-Percentage of specific CD8$^+$ T cells in the spleen positive for Annexin V. f-The histogram represents the gate for CFSE^{Low} and CFSE^{high} (target cells) population in the spleen from naïve, Isotype control and anti-CXCR3 groups on day 12 post infection (12 dpi) and the bar graph represents the cytotoxicity percentage of specific CD8$^+$ T cells from naïve, Isotype control and anti-CXCR3 groups. g-The percentage of cytotoxicity of specific CD8$^+$ T cells from the spleen on day 15 post infection. h-The Mean Intensity of Fluorescence (MFI) of granzyme B on specific CD8$^+$ T cells surface. i-Number of IFN-γ producing cells quantified by ELISPOT assay. j-Quantity of cytokines (pg/mL) from splenocytes supernatants. CBA mouse Th1/Th2/Th17 cytokine kit was used. k-Pie graphs show the percentage of specific CD8$^+$ T cells that performed each combination as shown in legends (3, 2 or 1 function). The polyfunctionality of specific CD8$^+$ T cells was performed after ICS staining and Boolean analyses. Data are mean ± SD and represent 3 independent experiments with n = 3. $^*P<0.05$ comparing noninfected controls (naïve), Isotype control and anti-CXCR3 groups. # $P<0.01$ comparing Isotype control and anti-CXCR3 groups.

https://doi.org/10.1371/journal.pntd.0008414.g003

CD8$^+$ T cells (Fig 3K). In order to confirm the decrease in polyfunctionality of specific CD8$^+$ T cells during the anti-CXCR3 treatment, we infected OT-I mice with a transgenic parasite, Y strain which expresses OVA protein. On the same day of infection, we treated the mice with anti-CXCR3 antibody. Subsequently, splenocytes were stimulated with SIINFEKL peptide for 12 hours and after that using ICS technique, IFN-γ, TNF and CD107a were labeled. Once again we observed that specific CD8$^+$ T cells from mice treated with anti-CXCR3 antibody (OT-I+Y-OVA+anti-CXCR3 group) had a decrease in the percentage of specific CD8$^+$ T cells triple positive when compared to mice treated with isotype control (OT-I+Y-OVA+isotype control group) (S2A and S2B Fig). Altogether those results indicate that CXCR3 receptor is important to cytotoxicity and cytokine production by specific CD8$^+$ T cells.

CXCR3 molecule contributes to anti-*T. cruzi* CD8$^+$ T cells activation

After activation, effector anti-*T. cruzi* CD8$^+$ T cells upregulated the expression of CD11a, CD44, and KLRG-1 molecules and downregulated the expression of CD62L compared to naïve cells [29]. Since CXCR3 molecule is important to T cells differentiation [30], we examined the expression of activation, homing, or memory markers on specific CD8$^+$ T cells after *T. cruzi* infection and anti-CXCR3 treatment. Those markers and expression levels are critical for the activation of specific CD8$^+$ T cells, their migration into infection sites, and elimination of parasites. We compared the expression of molecules using the MFI (Mean of Fluorescence Intensity) and found that several molecules analyzed, such as CD11c, CD25, CD27, CD31, and CD122, did not change the expression levels both in the Isotype control group and anti-CXCR3 group (S3 Fig). However, some molecules were expressed differently by specific CD8$^+$ T cells from those groups. Specific CD8$^+$ T cells from the Isotype Control group highly expressed CD11a (LFA-1), CD38, CD44, CD49d, KLRG-1 and the transcription factor T-bet, and downregulated CD62L molecule when compared to naïve CD8$^+$ T cells. On the other hand, specific CD8$^+$ T cells from the anti-CXCR3 group downregulated CD11a (LFA-1), CD38, CD44, CD49d, KLRG-1 and T-bet, and upregulated CD62L molecule when compared to the Isotype Control group (Fig 4A and 4B).

Altogether, those results suggest that CXCR3 receptor may have a role in CD8$^+$ T cell activation after *T. cruzi* infection.

CXCR3 guides the migration of specific CD8$^+$ T cells into infected hearts

Previously, our group described that CXCR3 is critical for migration of specific CD8$^+$ T cells into the heart during vaccination with ASP-2 and infection with *T. cruzi* [13]. Firstly, we analyzed the presence of CD8$^+$ T cells in the heart using confocal microscopy, and differently

from naïve hearts, we observed $CD8^+$ T cells (green) in the heart of Isotype Control and anti-CXCR3 groups (Fig 5A). However, in anti-CXCR3 group, we found fewer cells. In order to quantify the number of $CD8^+$ T cells in the heart of both infected groups, we measured the relative expression of CD8 molecule by RT-PCR and observed a statistical decrease in CD8 expression in the heart of anti-CXCR3 treated mice when compared to the Isotype Control group (Fig 5B).

To confirm those data, we quantified the number of specific $CD8^+$ T cells in the heart by flow cytometry; the specific $CD8^+$ T cells were labeled with VNHRFTLV multimer. In the heart of the Isotype Control group, we observed 1.31% of specific $CD8^+$ T cells while the percentage of specific $CD8^+$ T cells in the anti-CXCR3 group was 0,32% (Fig 5C).

We investigated the tissue burden in the heart of infected mice and as expected, due the lower number of $CD8^+$ T cells in the heart of anti-CXCR3, we observed an increase of amastigote nests in the anti-CXCR3 group when compared to the Isotype Control group (Fig 5D and 5E). In addition, the number of parasites (on day 15 after infection) in the heart was quantified by qPCR. We observed higher parasite numbers in the anti-CXCR3 group when compared to the Isotype Control group (Fig 5F).

Altogether, these results indicate that CXCR3 is important to specific $CD8^+$ T cells migration into the heart of *T. cruzi* infected mice and to control the infection.

pDCs produced CXCL10 chemokine and interacted with $CD8^+$ T cells after infection with *T. cruzi*

CXCR3 ligands are produced by antigen-presenting cells (APCs) [30]. During cerebral malaria, the monocyte-derived dendritic cells (MO-DCs) produce CXCL10 and CXCL9 [31], but it is still unclear which APCs are responsible for producing CXCR3 ligands during *T. cruzi* infection. Previously, our group demonstrated that dendritic plasmacytoid cells (pDCs) have a role in *T. cruzi* antigen presentation [32]. Here, we investigated whether pDCs and MO-DCs produced CXCR3 ligands. In order to analyze that, REX3 reporter mice (CXCL10-BFP and CXCL9-RFP) were infected and, on days 4, 9, 12, and 20 after infection, we quantified the number of those cells by flow cytometry. We observed that the number of MO-DCs increased on day 4 after infection only. However, in the pDCs population, we observed a higher number on day 12 after infection (Fig 6A). In addition, both MO-DCs and pDCs produced CXCL10 chemokine on days 4, 9, 12, and 20 after infection (Fig 6B and 6C), but only MO-DCs produced CXCL9 and CXCL10 at the same time (Fig 6C). To investigate which $CXCL10^+$ antigen-producing cells might interact *in vivo* with IFN-γ–producing cells after *T. cruzi* infection, we generated bone marrow chimeras. Irradiated WT mice were reconstituted with bone marrow from Great IFN-γ GFP reporter mice and REX3 CXCL10-BFP and CXCL9-RFP reporter mice. After 12 weeks, those mice were infected with *T. cruzi* and, on day 12 after infection, the spleens were harvested. The interaction was evaluated using Image Flow Cytometry (ImageStream). To quantify the interaction among those cells, we gated the double cells labeled with DRAQ5 (nucleus marker) and then we gated for IFN-γ^+/$CXCL10^+$ or $CD8^+$/$CXCL10^+$ positive cells. As expected, the cells from naïve chimera mice did not produce IFN-γ and CXCL9/CXCL10; however, in the infected group, we could observe an interaction between CXCL10-producing cells and IFN-γ-producing cells (Fig 6D).

Next, we examined the interaction between MO-DCs and pDCs with $CD8^+$ T cells after infection. The REX3 reporter mice were infected and, on day 12 after infection, the numbers of MO-DC^+/$CD8^+$ and pDC^+/$CD8^+$ double cells were calculated. The pDC population was gated as pDCA-1^+ and $CD11c^+$, and MO-DC population was gated first to $CD11b^+F4/80^+$ and then to DC-$SIGN^+$ and MHC-II^+. We observed that both pDCs and MO-DCs produced

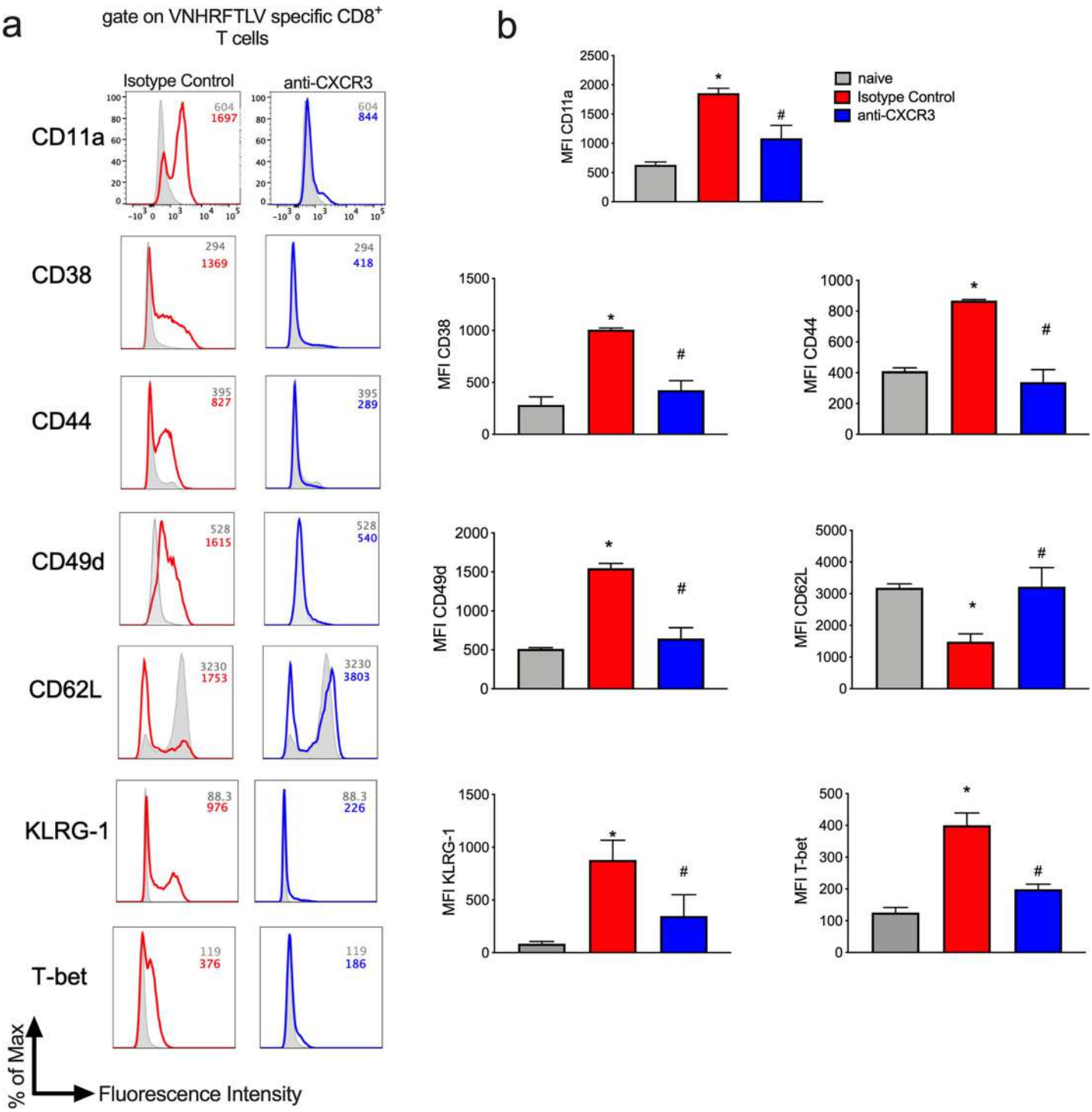

Fig 4. CXCR3 contributes to specific CD8+ T cells activation. The immunophenotyping of specific CD8+ T cells was performed in the spleen. We evaluated the expression of markers associated with activation, homing and memory. a-The histogram graphs represent each molecule analyzed from naïve (grey line), Isotype Control (red line) and anti-CXCR3 (blue line) groups. b-The bar graphs show MFI of each molecule analyzed in specific CD8+ T cells from naïve, Isotype Control and anti-CXCR3 groups. Data are mean ± SD and represent 2 independent experiments with n = 3. *P<0.05 comparing noninfected controls (naïve), Isotype Control and anti-CXCR3 groups. #P < .01 comparing Isotype control and anti-CXCR3 groups. The statistical analysis was performed using One-way ANOVA, followed by Tukey post-hoc test.

https://doi.org/10.1371/journal.pntd.0008414.g004

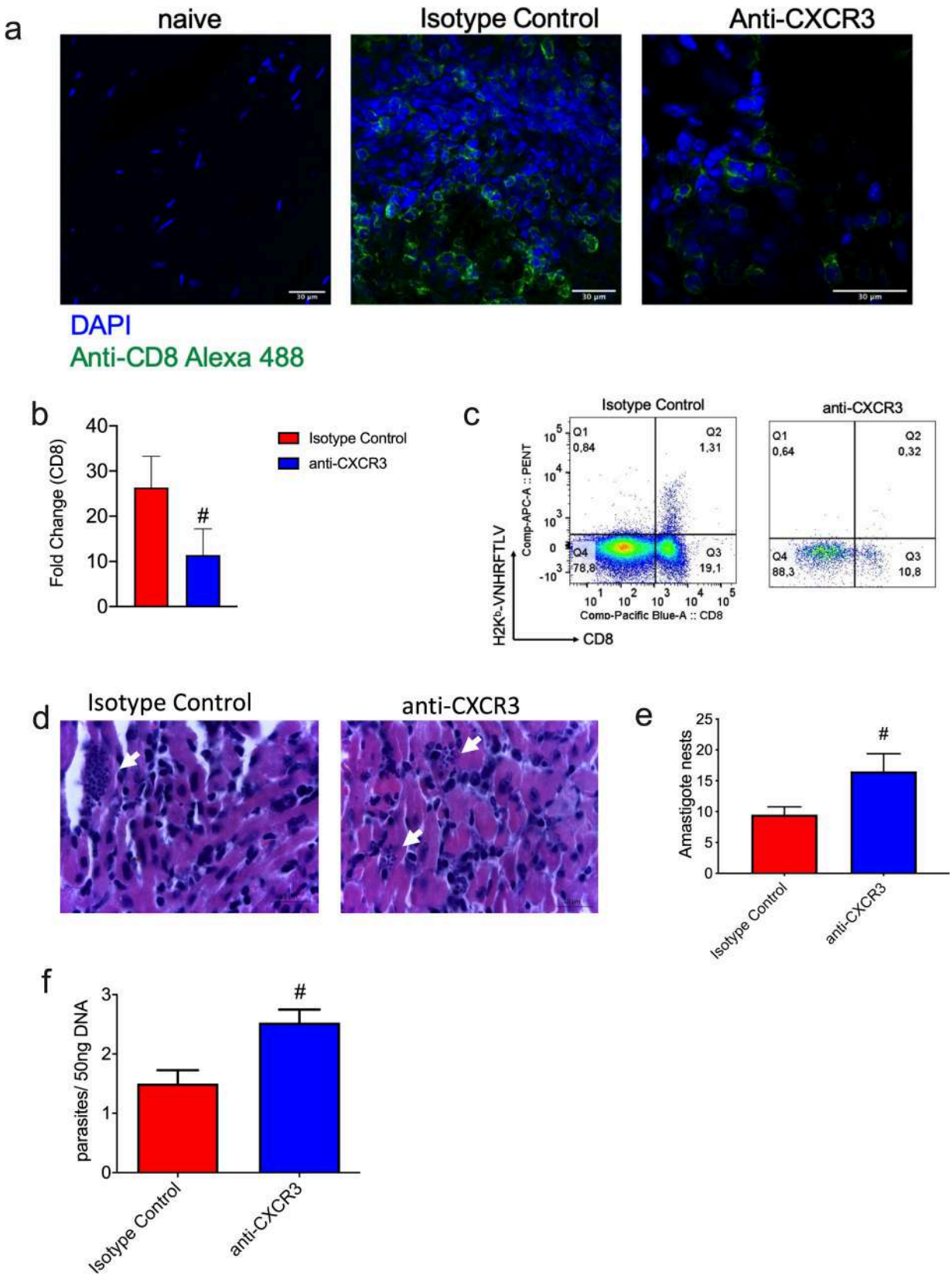
a
naive
Isotype Control
Anti-CXCR3
DAPI
Anti-CD8 Alexa 488
b
Fold Change (CD8)
Isotype Control
anti-CXCR3
#
c
Isotype Control
anti-CXCR3
Q1 0,84
Q2 1,31
Q4 78,8
Q3 19,1
Q1 0,64
Q2 0,32
Q4 88,3
Q3 10,8
Comp-APC-A :: PENT
Comp-Pacific Blue-A :: CD8
H2Kb-VNHRFTLV
CD8
d
Isotype Control
anti-CXCR3
e
Amastigote nests
#
Isotype Control
anti-CXCR3
f
parasites/ 50ng DNA
#
Isotype Control
anti-CXCR3

Fig 5. CXCR3 guides CD8$^+$ T cells migration into *T. cruzi* infected heart. a-Immunohistochemistry staining of hearts from naïve, Isotype Control and anti-CXCR3 groups; CD8$^+$ T cells were labeled in green. b-The relative expression of CD8$^+$ T cells in the heart of Isotype Control and anti-CXCR3 groups. c-The dot-plot graphs represent the frequency of specific CD8$^+$ T cells (pool of 3 mice/group) in the heart of Isotype Control and anti-CXCR3 groups. d-Histological section from infected hearts; the white arrows indicate the amastigote nests. e-Number of amastigote nests from Isotype Control and anti-CXCR3 groups counted in 50 fields. f-The parasite burden quantification by qPCR from infected hearts. The qPCR was performed from 50 ng of the heart's DNA. Data are mean ± SD and represent 2 independent experiments. #P < .01 comparing Isotype control and anti-CXCR3 groups. The statistical analysis was performed using Student's t-test.

https://doi.org/10.1371/journal.pntd.0008414.g005

CXCL10 chemokine (in purple) and interacted with CD8$^+$ T cells (in red) during the infection with *T. cruzi* (Fig 6E and 6F); however, the number of pDCs interacting with CD8$^+$ T cells was higher than MO-DCs (Fig 6G).

Additionally, we analyzed the number of pDCs after the anti-CXCR3 treatment. We analyzed those cells on day 12 after infection because we observed a high number of pDCs in the spleen on that day. Interestingly, we observed that the number of pDCs in the spleen and lymph node decreased after infection and treatment with anti-CXCR3 antibody when we compared to the isotype control group (Fig 7A and 7B); also, pDCs expressed CXCR3 receptor on the surface after infection (Fig 7C and 7D).

Discussion

Chemokine receptors guide T lymphocytes during homeostasis and infection. Also, may play a role in the activation and functionality of T lymphocytes [33,34]. CXCR3 chemokine receptor is highly expressed on T lymphocytes surface during Th1 responses against intracellular infection, such as with *Trypanosoma cruzi*. Previously, our group demonstrated that CXCR3 chemokine receptor was important to protect A/Sn vaccinated mice against death after *T. cruzi* infection [13]. Here, we aimed to examine whether CXCR3 chemokine contributes to specific CD8$^+$ T cells migration, activation, and functionality. We used a neutralizing monoclonal antibody (anti-CXCR3) treatment approach. Our results show the increase in parasitemia and precocious mortality in anti-CXCR3-treated *T. cruzi*-infected mice. Our finding corroborate with the studies performed with *Toxoplasma gondii* and Herpes virus models, where, CXCR3-deficient mice die after infections with those pathogens [10,15].

The role of CXCR3 chemokine receptor guiding T lymphocytes to lymphoid tissues has been demonstrated in several models that included: allografts, autoimmune diseases, *T. gondii* infections, and the genital herpes virus [11,15,35]. In fact, we demonstrated that CXCR3 guides CD8$^+$ T cells to the heart after infection with *T. cruzi*, since we observed a decreased in the frequency of those cells after anti-CXCR3 antibody treatment. In addition, the decrease numbers of CD8$^+$ T cells lead to the increased parasite burden in the heart, which show the importance of CD8$^+$ T cells in control *T. cruzi* infection.

Furthermore, we analyzed the number of specific CD8$^+$ T cells in the spleen and we observed that CXCR3 mAb treatment decreased the number of specific CD8$^+$ T cells in that tissue. However, the treatment did not alter significantly the absolute number of CD4$^+$ and CD4$^+$Foxp3$^+$ T cells in the spleen, suggesting that the anti-CXCR3 treatment did not alter the migration of those cells. In spite of our result, the role of CXCR3 in CD4$^+$ T cells migration has been shown in infection by *Plasmodium chabaudi* [36], however, in our model we believe that others chemokine might be involved in CD4$^+$ T cells migration to spleen.

Regardless of the decrease in VNHRFTLV-specific CD8$^+$ T cells in the spleen, we did not observe a decrease in specific CD8$^+$ T cell proliferation or any changes in pro-apoptotic profile after the anti-CXCR3 treatment, indicating that the decrease in the number of specific CD8$^+$ T cells was not due to the impaired proliferation or death pathways. Conversely, Thapa and colleagues have shown that CXCR3 is important to the T lymphocytes proliferation, however,

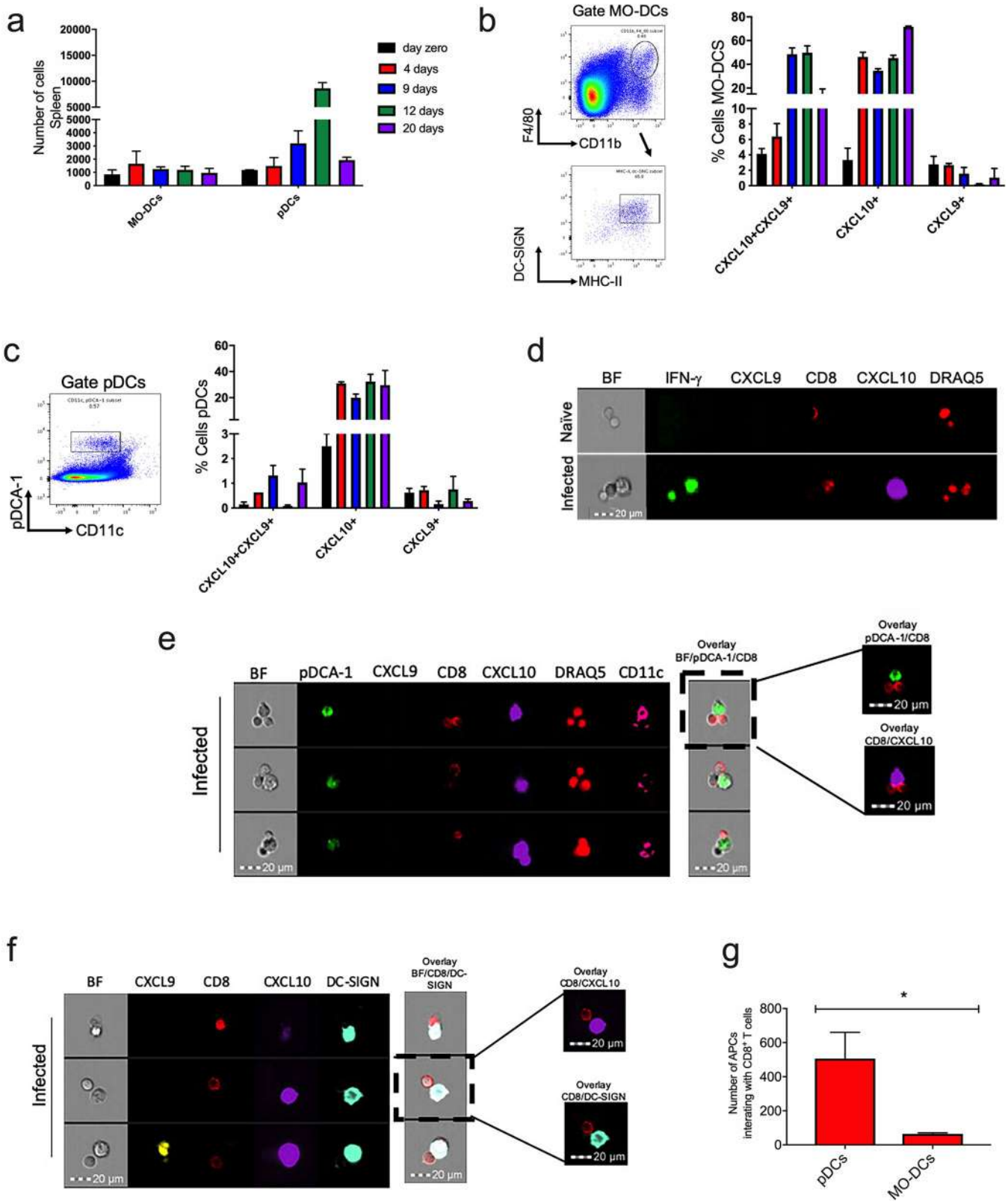

Fig 6. Plasmacytoid dendritic cells (pDCs) produced CXCL10 chemokine and interacted *in vivo* with CD8⁺ T cells during *T. cruzi* infection. To analyze which antigen-presenting cells (APCs) produced CXCR3 ligands, a REX3 linage mouse (CXCL10-BFP and CXCL9-RFP reporter) was infected on days 4, 9, 12,

and 20 and we analyzed the number of MO-DCs, pDCs and chemokine production. a-The graphs represent the number of MO-DCs and pDCs on days 0, 4, 9, 12, and 20 after infection. b-The MO-DCs were gated as $F4/80^{+}CD11b^{+}$ and $DC\text{-}SIGN^{+}MHC\text{-}II^{+}$; the graph represents the percentage of MO-DCs-producing chemokines—CXCL9 and/or CXCL10. c-The pDCs were gated as $CD11c^{low}$ and $pDCA\text{-}1^{+}$ and the graph represents the percentage of pDCs producing chemokines—CXCL9 and/or CXCL10. d-Image Flow Cytometry of chimera mice that received IFN-γ GFP, CXCL9-RFP and CXCL10-BFP cells; the double cells were gated using DRAQ5 labeling. e-Image Flow Cytometry of REX3 infected mice shows the markers used as well as the interaction between CXCL10 pDC-producing cells and $CD8^{+}$ T cells. f-Image Flow Cytometry of REX3 infected mice shows the markers used as well as the interaction between CXCL10 MO-DC-producing cells and $CD8^{+}$ T cells. g-The number of pDCs and MO-DCs interacting with $CD8^{+}$ T cells after *T. cruzi* infection. Data are mean ± SD and represent one experiment with n = 3. *indicates statistical differences between the number of pDCs and MO-DCs interacting with $CD8^{+}$ T cells (*P = 0.001515, statistical analysis was performed using Student's t-test).

https://doi.org/10.1371/journal.pntd.0008414.g006

CXCR3 was important to T cell proliferation in early days of infection by HSV-2 virus and here we evaluated the proliferation on day 15 after infection [37].

In addition, we observed a decrease in the number of IFN-γ producing $CD8^{+}$ T cells and polyfunctionality in the anti-CXCR3 treated group. The lower polyfunctionality in anti-CXCR3 treated group was confirmed using OT-I infected mice with a transgenic parasite

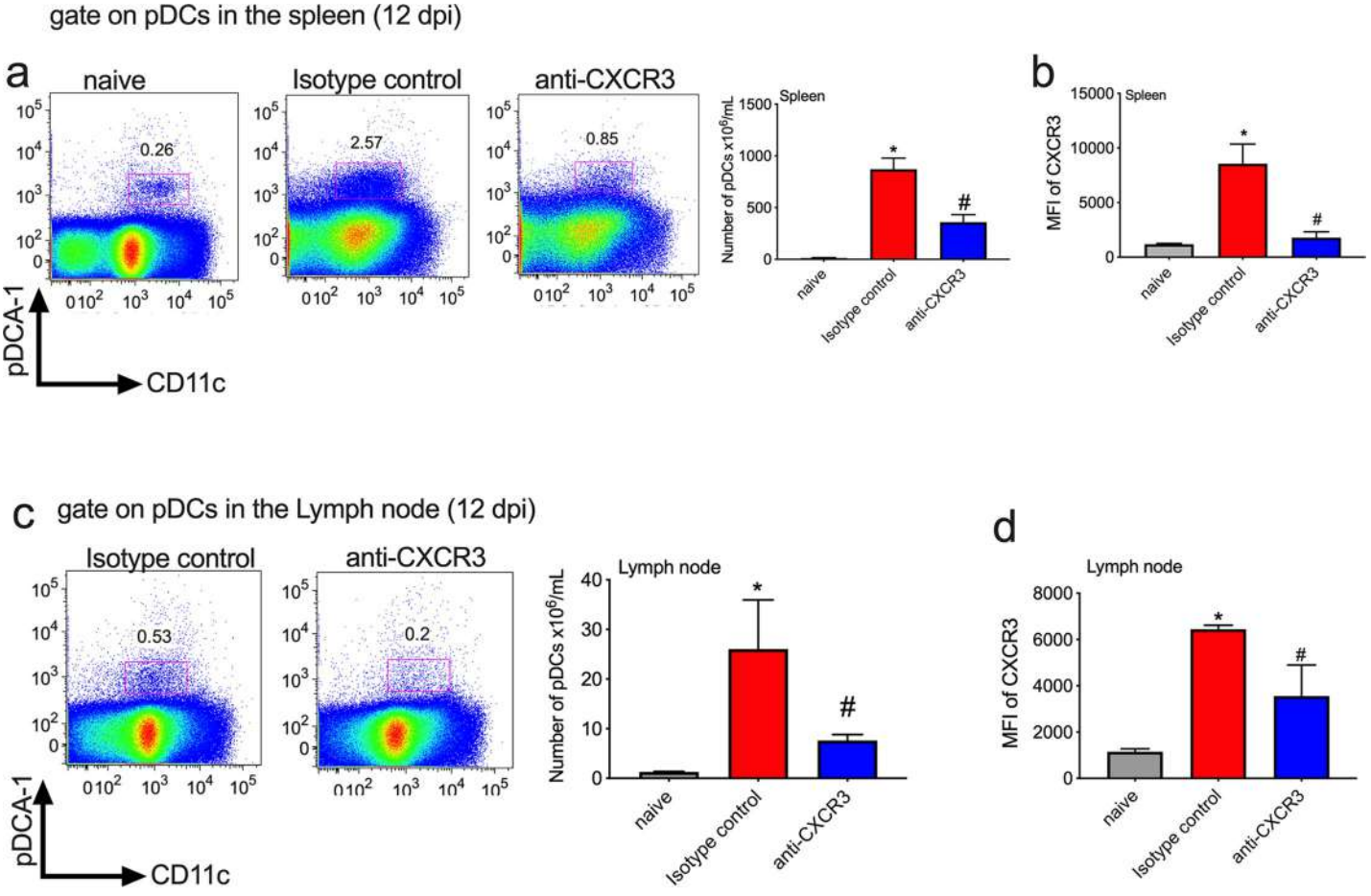

Fig 7. The number of plasmacytoid dendritic cells (pDCs) decreased after anti-CXCR3 treatment and *T. cruzi* infection. The number of pDCs after anti-CXCR3 treatment was quantified on day 12 after infection in the spleen and lymph node. a-The dot-plots represent the gate strategy used to measure the frequency of pDCs in the spleen and the bar graph represents the number of pDCs in the spleen of naïve, Isotype control and anti-CXCR3 groups. b-The MFI of CXCR3 receptor on pDCs surface in the spleen of naïve, Isotype control and anti-CXCR3 groups. c-The dot-plots represent the gate strategy used to measure the frequency of pDCs in the lymph node and the bar graph represents the number of pDCs in the lymph node. d-The MFI of CXCR3 receptor on pDCs surface on the lymph node of naïve, Isotype control and anti-CXCR3 groups. Data are mean ± SD and represent one experiment with n = 3. *P<0.05 comparing noninfected controls (naïve), Isotype control and anti-CXCR3 groups. #P < .01 comparing Isotype control and anti-CXCR3 groups.

https://doi.org/10.1371/journal.pntd.0008414.g007

carrying OVA protein model. Once again, the anti-CXCR3 treatment decreased the number of polyfunctional SIINFEKL-CD8$^+$ T cells. Corroborating with our results, T lymphocytes from CXCR3 deficient mice exhibited reduced IFN-γ production during viral and *Leishmania donovani* infection models [15,38].

Another important function triggered by CD8$^+$ T cells is the directed cytotoxicity against infected cells [20,39,40]. That function was analyzed *in vivo* and anti-CXCR3 treated mice showed impairment in that function. However, we did not observe reduced production of granzyme B. Similarly, Hickman and colleagues, showed that specific CD8$^+$ T cells from CXCR3-deficient mice had reduced cytotoxicity when compared to control group during the infection with vaccinia virus model. The authors suggested that that reduction in the cytotoxicity could be explained by the role of CXCR3 receptor in establish contact between CD8$^+$ cytotoxic and infected antigen presenting cells [16].

We also evaluated the activation pattern of specific CD8$^+$ T cells. After infection, those cells upregulated the expression of CD11a, CD44 and KLRG-1 and downregulated the expression of CD62L when compared to naïve CD8$^+$ T cells [29]. However, specific CD8$^+$ T cells from the anti-CXCR3 treated group downregulated the expression of CD11a, CD44, and KLRG-1 and upregulated CD62L molecule as well, when compared to specific CD8$^+$ T cells from the isotype control group (Infected). Hu and collaborators demonstrated that mice infected with lymphocytic choriomeningitis virus (LCV), the colocalization of virus-specific CD8$^+$ T cells with antigen in the spleen was dependent on CXCR3 expression [41], and we raised the hypothesis that the decreased in effector function of CD8$^+$ T cells could be due to the lower prime by APCs. To address that, we evaluated which APCs were responsible for producing CXCL9 (MIG) and CXCL10 (IP-10) chemokines, the ligands for CXCR3. We observed that both plasmacytoid cells (pDCs) and Monocytes—Derived Dendritic cells (MO-DCs) produced CXCR3 ligands, however the pDCs expressed only CXCL10. The CXCL10 expression by MO-DCs and pDCs started very early and remained until day 20 after infection, which is consistent with the high expression of CXCR3 in specific CD8$^+$ T cells, observed from day 5 to 30 after infection. We also observed a higher expression of CXCL10 in the heart of infected mice on day 15 after infection.

Furthermore, we observed that CXCL10-producing cells can interact with IFN-γ $^+$ cells after *T. cruzi* infection, and CXCL10$^+$ produced by pDCs showed a higher interaction with CD8$^+$ T cells than MO-DCs. Interestingly, the anti-CXCR3 treatment reduced the number of pDCs in the spleen and lymph node, and those cells also expressed CXCR3 receptor on the surface. Similarly, the reduction in the number of pDCs in the lymph node of CXCR3-deficient mice was observed during herpes virus type 2 infection [15]. In addition, expression of CXCR3 in pDCs was also demonstrated by other groups [42,43].

We believe that CXCR3 receptor is essential promote the encounter between pDCs and CD8$^+$ T cells. The lower activation phenotyping and effector function of specific CD8$^+$ T cells observed during anti-CXCR3 treatment can be explained by the lower quantity of pDCs in spleen and lymph node. Previously, our group demonstrated that during *T. cruzi* infection pDCs express co-stimulatory molecules and are responsible for activating anti-*T. cruzi* CD8$^+$ T cells [44].

Overall, we have demonstrated that C57BL/6 mice died very quickly due to infection during the anti-CXCR3 treatment. Moreover, the number of specific CD8$^+$ T-cells decreased as well as activation and polyfunctionality. We showed that pDCs and CD8$^+$ T cells interacted *in vivo* and we believe that CXCR3 is important to pDCs and anti-*T.cruzi* CD8$^+$ T cells encounter and subsequently, to antigen presentation by pDCs to CD8$^+$ T cells. After priming, CD8$^+$ T cells produce cytokines and kill the infected cells by cytotoxicity.

Altogether, our results indicate that CXCR3 plays a critical role in specific CD8$^+$ T cells activation and migration. Understanding its role might help to promote the development of vaccines against intracellular parasites such as *Trypanosoma cruzi*.

Supporting information

S1 Fig. CD4 Foxp3$^+$ T cells expressed CXCR3 after infection. a-Graph with the absolute number of CD4$^+$ T cells in the spleen of naïve, isotype control and anti-CXCR3 groups. The number of total CD4$^+$ T cells was calculated on day 15 after infection. b-Dot-plots represent the gate and the frequency of CD4$^+$ Foxp3$^+$ T cells in naïve, isotype control and anti-CXCR3 groups on day 15 after infection. c-Bar graph with the absolute number of CD4 Foxp3$^+$ T cells. d-Histogram shows CD4 Foxp3$^+$ T cells expressing CD25 molecule and bar graph with the MFI quantification of CD25 molecule expressed in CD4 Foxp3$^+$ T cells, respectively. e-Histogram represents CD4 Foxp3$^+$ T expressing CXCR3 molecule, and bar graph with MFI quantification of CXCR3 molecule on the surface of CD4 Foxp3$^+$ T cells, respectively. Data are mean ± SD and are representative of 2 independent experiments with n = 3. The symbols indicate values that are statistically differences between the groups ($\zeta P = 0.000661$, $\zeta\zeta P < .01$). The statistical analyses were carried out using One-way ANOVA, followed by Tukey post-hoc test).
(TIF)

S2 Fig. SIINFEKL-specific CD8$^+$ T cells treated with anti-CXCR3 decreased the polyfunctionality. OT-I mice were infected with 1x10^6 forms of Y-OVA transgenic *T. cruzi* strain and treated with anti-CXCR3. On day 10 after infection, spleens were harvested and splenocytes were stimulated for 6 hours with SIINFEKL peptide. ICS staining was performed to quantify the cytokine production and degranulation by CD8$^+$ T cells; we subdivided CD8 T cells that had performed 3, 2, or 1 function (s) at same time. a-Dot-plots graph show the frequency of specific CD8$^+$ T cells from naïve, OT-I+Y-OVA+Isotype Control and OT-I+Y-OVA+anti-CXCR3 groups, double positive for: IFN-γ^+ TNF-α^+; CD107a$^+$ and TNF-α^+; IFN-γ^+ and/or CD107a$^+$IFN-γ^+. b-The graph represents the percentage of specific CD8$^+$ T cells that performed 3, 2, or 1 function. Boolean data were performed using FlowJo Software version 9.0. Data are mean ± SD and are representative of 2 independent experiments with n = 3.
(TIF)

S3 Fig. CXCR3 antibody treatment did not alter the expression of some molecules on CD8$^+$ T cells surface. The immunophenotyping of VNHRFTLV specific CD8$^+$ T cells was performed in the spleen of naïve, Isotype control and anti-CXCR3 groups. We evaluated the expression of markers related to activation, homing and memory. a-The histogram graphs represent each molecule analyzed in specific CD8$^+$ T cells in the spleen of naïve (grey line), Isotype Control (red line) and anti-CXCR3 (blue line) groups. Data are mean ± SD and are representative of 2 independent experiments with n = 3.
(TIF)

Acknowledgments

We gratefully acknowledge the Xenodiaginóstico laboratory from Institute Dante Pazzanese for the parasites. Also, Dr. Maria Bellio for the Y-OVA parasites.

Author Contributions

Conceptualization: Camila Pontes Ferreira, Karina Ramalho Bortoluci, Ricardo Tostes Gazzinelli.

Data curation: Camila Pontes Ferreira, Leonardo de Moro Cariste, Isaú Henrique Noronha, Joseli Lannes-Vieira, Karina Ramalho Bortoluci, Daniel Araki Ribeiro, Douglas Golenbock, Ricardo Tostes Gazzinelli, José Ronnie Carvalho de Vasconcelos.

Formal analysis: Camila Pontes Ferreira, Leonardo de Moro Cariste, Isaú Henrique Noronha, Danielle Fernandes Durso, Joseli Lannes-Vieira, Karina Ramalho Bortoluci, Daniel Araki Ribeiro, Ricardo Tostes Gazzinelli, José Ronnie Carvalho de Vasconcelos.

Funding acquisition: Ricardo Tostes Gazzinelli, José Ronnie Carvalho de Vasconcelos.

Investigation: Camila Pontes Ferreira, Joseli Lannes-Vieira, Karina Ramalho Bortoluci, Ricardo Tostes Gazzinelli, José Ronnie Carvalho de Vasconcelos.

Methodology: Camila Pontes Ferreira, Leonardo de Moro Cariste, Isaú Henrique Noronha, Danielle Fernandes Durso, Joseli Lannes-Vieira, Karina Ramalho Bortoluci, Daniel Araki Ribeiro, Ricardo Tostes Gazzinelli.

Project administration: José Ronnie Carvalho de Vasconcelos.

Resources: José Ronnie Carvalho de Vasconcelos.

Supervision: Joseli Lannes-Vieira, José Ronnie Carvalho de Vasconcelos.

Validation: Camila Pontes Ferreira, José Ronnie Carvalho de Vasconcelos.

Visualization: Camila Pontes Ferreira.

Writing – original draft: Camila Pontes Ferreira.

Writing – review & editing: Joseli Lannes-Vieira, Karina Ramalho Bortoluci, Douglas Golenbock, Ricardo Tostes Gazzinelli, José Ronnie Carvalho de Vasconcelos.

References

1. Zlotnik A, Yoshie O. The Chemokine Superfamily Revisited. Immunity [Internet]. 2012; 36(5):705–12. Available from: https://doi.org/10.1016/j.immuni.2012.05.008 PMID: 22633458
2. Moser B, Wolf M, Walz A, Loetscher P. Chemokines: Multiple levels of leukocyte migration control. Trends Immunol [Internet]. 2004 Feb; 25(2):75–84. Available from: http://linkinghub.elsevier.com/retrieve/pii/S1471490603003867 https://doi.org/10.1016/j.it.2003.12.005 PMID: 15102366
3. Groom JR, Luster AD. CXCR3 ligands: redundant, collaborative and antagonistic functions. Immunol Cell Biol [Internet]. 2011 Feb [cited 2019 Jul 22]; 89(2):207–15. Available from: https://doi.org/10.1038/icb.2010.158 PMID: 21221121
4. Campbell DJ, Kim CH, Butcher EC. Chemokines in the systemic organization of immunity. Immunol Rev. 2003; 195:58–71. https://doi.org/10.1034/j.1600-065x.2003.00067.x PMID: 12969310
5. Koch MA, Tucker-Heard G, Perdue NR, Killebrew JR, Urdahl KB, Campbell DJ. The transcription factor T-bet controls regulatory T cell homeostasis and function during type 1 inflammation. Nat Immunol. 2009; 10(6):595–602. https://doi.org/10.1038/ni.1731 PMID: 19412181
6. Mackay CR. Chemokines: immunology ' s high impact factors. 2010; 2(2).
7. Teixeira MM, Gazzinelli RT, Silva JS. Chemokines, inflammation and Trypanosoma cruzi infection. Trends Parasitol. 2002; 18(6):262–5. https://doi.org/10.1016/s1471-4922(02)02283-3 PMID: 12036740
8. Nogueira LG, Santos RHB, Ianni BM, Fiorelli AI, Mairena EC, Benvenuti LA, et al. Myocardial Chemokine Expression and Intensity of Myocarditis in Chagas Cardiomyopathy Are Controlled by Polymorphisms in CXCL9 and CXCL10. PLoS Negl Trop Dis. 2012; 6(10).
9. Cunha-Neto E, Chevillard C. Chagas disease cardiomyopathy: Immunopathology and genetics. Mediators Inflamm. 2014;2014.
10. Cohen SB, Maurer KJ, Egan CE, Oghumu S, Satoskar AR, Denkers EY. CXCR3-Dependent CD4+ T Cells Are Required to Activate Inflammatory Monocytes for Defense against Intestinal Infection. PLoS Pathog. 2013; 9(10).
11. Hancock WW, Lu B, Gao W, Csizmadia V, Faia K, King JA, et al. Requirement of the Chemokine Receptor CXCR3 for Acute Allograft Rejection. J Exp Med. 2002; 192(10):1515–20.

12. Kohlmeier JE, Cookenham T, Miller SC, Roberts AD, Christensen JP, Thomsen AR, et al. CXCR3 Directs Antigen-Specific Effector CD4+ T Cell Migration to the Lung During Parainfluenza Virus Infection. J Immunol [Internet]. 2009; 183(7):4378–84. Available from: https://doi.org/10.4049/jimmunol.0902022 PMID: 19734208

13. Ferreira CP, Cariste LM, Moraschi BF, Zanetti BF, Han SW, Ribeiro DA, et al. CXCR3 chemokine receptor guides Trypanosoma cruzi-specific T-cells triggered by DNA/adenovirus ASP2 vaccine to heart tissue after challenge. 2019 [cited 2019 Aug 5]; Available from: https://doi.org/10.1371/journal.pntd.0007597 PMID: 31356587

14. Lacotte S, Brun S, Muller S, Dumortier H. CXCR3, Inflammation, and Autoimmune Diseases. Ann N Y Acad Sci [Internet]. 2009 Sep; 1173(1):310–7. Available from: http://doi.wiley.com/10.1111/j.1749-6632.2009.04813.x

15. Thapa M, Carr DJJ. CXCR3 Deficiency Increases Susceptibility to Genital Herpes Simplex Virus Type 2 Infection: Uncoupling of CD8+ T-Cell Effector Function but Not Migration. J Virol [Internet]. 2009; 83(18):9486–501. Available from: https://doi.org/10.1128/JVI.00854-09 PMID: 19587047

16. Hickman HD, Reynoso G V., Ngudiankama BF, Cush SS, Gibbs J, Bennink JR, et al. CXCR3 chemokine receptor enables local CD8+T cell migration for the destruction of virus-infected cells. Immunity [Internet]. 2015; 42(3):524–37. Available from: https://doi.org/10.1016/j.immuni.2015.02.009 PMID: 25769612

17. Yoneyama H, Narumi S, Zhang Y, Murai M, Baggiolini M, Lanzavecchia A, et al. Pivotal Role of Dendritic Cell–derived CXCL10 in the Retention of T Helper Cell 1 Lymphocytes in Secondary Lymph Nodes. J Exp Med. 2002; 195(10):1257–66. https://doi.org/10.1084/jem.20011983 PMID: 12021306

18. Groom JR, Richmond J, Murooka TT, Sorensen EW, Sung JH, Bankert K, et al. CXCR3 Chemokine Receptor-Ligand Interactions in the Lymph Node Optimize CD4+T Helper 1 Cell Differentiation. Immunity [Internet]. 2012; 37(6):1091–103. Available from: https://doi.org/10.1016/j.immuni.2012.08.016 PMID: 23123063

19. Tarleton RL. CD8+ T cells in Trypanosoma cruzi infection. Semin Immunopathol [Internet]. 2015 May 29; 37(3):233–8. Available from: https://doi.org/10.1007/s00281-015-0481-9 PMID: 25921214

20. De Alencar BCG, Persechini PM, Haolla FA, De Oliveira G, Silverio JC, Lannes-Vieira J, et al. Perforin and gamma interferon expression are required for CD4+ and CD8+ T-cell-dependent protective immunity against a human parasite, Trypanosoma cruzi, elicited by heterologous plasmid DNA prime-recombinant adenovirus 5 boost vaccination. Infect Immun. 2009; 77(10):4383–95. https://doi.org/10.1128/IAI.01459-08 PMID: 19651871

21. Uppaluri R, Sheehan KCF, Wang L, Bui JD, Brotman JJ, Lu B, et al. Prolongation of Cardiac and Islet Allograft Survival by a Blocking Hamster Anti-Mouse CXCR3 Monoclonal Antibody. Transplantation [Internet]. 2008 Jul; 86(1):137–47. Available from: https://insights.ovid.com/crossref?an=00007890-200807150-00024 https://doi.org/10.1097/TP.0b013e31817b8e4b PMID: 18622291

22. Piron M, Fisa R, Casamitjana N, López-Chejade P, Puig L, Vergés M, et al. Development of a real-time PCR assay for Trypanosoma cruzi detection in blood samples. Acta Trop. 2007; 103(3):195–200. https://doi.org/10.1016/j.actatropica.2007.05.019 PMID: 17662227

23. Ahmed F, Friend S, George TC, Barteneva N, Lieberman J. Numbers matter: Quantitative and dynamic analysis of the formation of an immunological synapse using imaging flow cytometry. J Immunol Methods [Internet]. 2009; 347(1–2):79–86. Available from: https://doi.org/10.1016/j.jim.2009.05.014 PMID: 19524586

24. Ersching J, Vasconcelos JR, Ferreira CP, Caetano BC, Machado A V., Bruna–Romero O, et al. The Combined Deficiency of Immunoproteasome Subunits Affects Both the Magnitude and Quality of Pathogen- and Genetic Vaccination-Induced CD8+T Cell Responses to the Human Protozoan Parasite Trypanosoma cruzi. PLoS Pathog. 2016; 12(4):1–23.

25. Silverio JC, Pereira IR, Cipitelli M da C, Vinagre NF, Rodrigues MM, Gazzinelli RT, et al. CD8+ T-cells expressing interferon gamma or perforin play antagonistic roles in heart injury in experimental trypanosoma cruzi-elicited cardiomyopathy. PLoS Pathog. 2012; 8(4).

26. Tzelpis F, de Alencar B, Penido M, Gazzinelli R, Persechini P, Rodrigues M. Distinct kinetics of effector CD8+ cytotoxic T cells after infection with Trypanosoma cruzi in Naıve or vaccinated mice. Infect Immun. 2006; 74(4):2477–81. https://doi.org/10.1128/IAI.74.4.2477-2481.2006 PMID: 16552083

27. Dominguez MR, Silveira EL V, de Vasconcelos JRC, de Alencar BCG, Machado A V, Bruna-Romero O, et al. Subdominant/cryptic CD8 T cell epitopes contribute to resistance against experimental infection with a human protozoan parasite. PLoS One [Internet]. 2011; 6(7):e22011. Available from: http://www.ncbi.nlm.nih.gov/pubmed/21779365%0Ahttp://www.pubmedcentral.nih.gov/articlerender.fcgi?artid=PMC3136500 https://doi.org/10.1371/journal.pone.0022011 PMID: 21779365

28. Dos F, Virgilio S, Pontes C, Dominguez MR, Ersching J, Rodrigues MM, et al. CD8+ T Cell-Mediated Immunity during Trypanosoma cruzi Infection: A Path for Vaccine Development? Mediators Inflamm. 2014; 2014:12.

29. Vasconcelos JR, Bruñ A-Romero O, Araú Jo AF, Dominguez MR, Ersching J, De Alencar BCG, et al. Pathogen-Induced Proapoptotic Phenotype and High CD95 (Fas) Expression Accompany a Suboptimal CD8 + T-Cell Response: Reversal by Adenoviral Vaccine. 2012 [cited 2019 Jul 2]; Available from: www.plospathogens.org https://doi.org/10.1371/journal.ppat.1002699 PMID: 22615561

30. Groom JR, Luster AD. CXCR3 in T cell function. Exp Cell Res [Internet]. 2011; 317(5):620–31. Available from: https://doi.org/10.1016/j.yexcr.2010.12.017 PMID: 21376175

31. Hirako IC, Ataide MA, Faustino L, Assis PA, Sorensen EW, Ueta H, et al. Splenic differentiation and emergence of CCR5+CXCL9+CXCL10+ monocyte-derived dendritic cells in the brain during cerebral malaria. Nat Commun [Internet]. 2016; 7:13277. Available from: https://doi.org/10.1038/ncomms13277 PMID: 27808089

32. Vasconcelos JR, Dominguez MR, Neves RL, Ersching J, Araújo A, Santos LI, et al. Adenovirus Vector-Induced CD8 + T Effector Memory Cell Differentiation and Recirculation, But Not Proliferation, Are Important for Protective Immunity Against Experimental *Trypanosoma cruzi* Infection. Hum Gene Ther [Internet]. 2014; 25(4):350–63. Available from: https://doi.org/10.1089/hum.2013.218 PMID: 24568548

33. Lacotte S, Brun S, Muller S, Dumortier H. CXCR3, inflammation, and autoimmune diseases. Ann N Y Acad Sci. 2009; 1173:310–7. https://doi.org/10.1111/j.1749-6632.2009.04813.x PMID: 19758167

34. Kurachi M, Kurachi J, Suenaga F, Tsukui T, Abe J, Ueha S, et al. Chemokine receptor CXCR3 facilitates CD8 + T cell differentiation into short-lived effector cells leading to memory degeneration. J Exp Med [Internet]. 2011; 208(8):1605–20. Available from: https://doi.org/10.1084/jem.20102101 PMID: 21788406

35. Sporici R, Issekutz TB. CXCR3 blockade inhibits T-cell migration into the CNS during EAE and prevents development of adoptively transferred, but not actively induced, disease. Eur J Immunol. 2010;

36. Berretta F, Piccirillo CA, Stevenson MM. Plasmodium chabaudi AS Infection Induces CD4+ Th1 Cells and Foxp3+T-bet+ Regulatory T Cells That Express CXCR3 and Migrate to CXCR3 Ligands. Front Immunol [Internet]. 2019 Mar 11; 10. Available from: https://www.frontiersin.org/article/10.3389/fimmu.2019.00425/full

37. Thapa M, Carr DJJ. CXCR3 deficiency increases susceptibility to genital herpes simplex virus type 2 infection: Uncoupling of CD8+ T-cell effector function but not migration. J Virol. 2009; 83(18):9486–501. https://doi.org/10.1128/JVI.00854-09 PMID: 19587047

38. Barbi J, Oghumu S, Rosas LE, Carlson T, Lu B, Gerard C, et al. Lack of CXCR3 Delays the Development of Hepatic Inflammation but Does Not Impair Resistance to Leishmania donovani. J Infect Dis. 2007;

39. Ferreira CP, Cariste LM, Virgílio FDS, Moraschi BF, Monteiro CB, Machado AMV, et al. LFA-1 mediates cytotoxicity and tissue migration of specific CD8+T cells after heterologous prime-boost vaccination against Trypanosoma cruzi infection. Front Immunol. 2017; 8(OCT).

40. Dotiwala F, Mulik S, Polidoro RB, Ansara JA, Burleigh BA, Walch M, et al. Killer lymphocytes use granulysin, perforin and granzymes to kill intracellular parasites. Nat Med. 2016;

41. Hu JK, Kagari T, Clingan JM, Matloubian M. Expression of chemokine receptor CXCR3 on T cells affects the balance between effector and memory CD8 T-cell generation. Proc Natl Acad Sci [Internet]. 2011; 108(21):E118–27. Available from: https://doi.org/10.1073/pnas.1101881108 PMID: 21518913

42. Martín-Fontecha A, Thomsen LL, Brett S, Gerard C, Lipp M, Lanzavecchia A, et al. Induced recruitment of NK cells to lymph nodes provides IFN-γ for TH1 priming. Nat Immunol. 2004;

43. Yoneyama H, Matsuno K, Zhang Y, Nishiwaki T, Kitabatake M, Ueha S, et al. Evidence for recruitment of plasmacytoid dendritic cell precursors to inflamed lymph nodes through high endothelial venules. Int Immunol. 2004;

44. Dominguez MR, Ersching J, Lemos R, Machado A V., Bruna-Romero O, Rodrigues MM, et al. Re-circulation of lymphocytes mediated by sphingosine-1-phosphate receptor-1 contributes to resistance against experimental infection with the protozoan parasite Trypanosoma cruzi. Vaccine. 2012

frontiers in Cellular and Infection Microbiology

ORIGINAL RESEARCH
published: 25 May 2021
doi: 10.3389/fcimb.2021.676183

Rapamycin Improves the Response of Effector and Memory CD8$^+$ T Cells Induced by Immunization With ASP2 of *Trypanosoma cruzi*

Barbara Ferri Moraschi[1,2], Isaú Henrique Noronha[1,2], Camila Pontes Ferreira[1,2], Leonardo M. Cariste[3], Caroline B. Monteiro[3], Priscila Denapoli[1], Talita Vrechi[4], Gustavo J. S. Pereira[4], Ricardo T. Gazzinelli[5,6], Joseli Lannes-Vieira[7], Maurício M. Rodrigues[1,2†], Karina R. Bortoluci[1,4] and José Ronnie C. Vasconcelos[1,2,3]*

[1] Molecular Immunology Laboratory, Center of Molecular and Cellular Therapy, Federal University of São Paulo (UNIFESP), São Paulo, Brazil, [2] Department of Microbiology, Immunology and Parasitology, Federal University of São Paulo (UNIFESP), São Paulo, Brazil, [3] Recombinant Vaccines Laboratory, Department of Biosciences, Federal University of São Paulo, Santos, Brazil, [4] Department of Pharmacology, Federal University of São Paulo, (UNIFESP), São Paulo, Brazil, [5] René Rachou Research Center, Fiocruz, Belo Horizonte, Brazil, [6] Division of Infectious Disease and Immunology, Department of Medicine, University of Massachusetts Medical School, Worcester, MA, United States, [7] Laboratoy of Biology of the Interactions, Oswaldo Cruz Institute, Fiocruz, Rio de Janeiro, Brazil

OPEN ACCESS

Edited by:
Giovane R. Sousa,
Harvard Medical School,
United States

Reviewed by:
Karina Andrea Gomez,
CONICET Instituto de Investigaciones en Ingeniería Genética y Biología Molecular Dr. Héctor N. Torres (INGEBI), Argentina
Marcos Damasio,
Massachusetts General Hospital and Harvard Medical School,
United States

***Correspondence:**
José Ronnie C. Vasconcelos
jrcvasconcelos@gmail.com

[†]*In memoriam*

Specialty section:
This article was submitted to Parasite and Host, a section of the journal Frontiers in Cellular and Infection Microbiology

Received: 04 March 2021
Accepted: 20 April 2021
Published: 25 May 2021

Citation:
Moraschi BF, Noronha IH, Ferreira CP, Cariste LM, Monteiro CB, Denapoli P, Vrechi T, Pereira GJS, Gazzinelli RT, Lannes-Vieira J, Rodrigues MM, Bortoluci KR and Vasconcelos JRC (2021) Rapamycin Improves the Response of Effector and Memory CD8$^+$ T Cells Induced by Immunization With ASP2 of Trypanosoma cruzi. Front. Cell. Infect. Microbiol. 11:676183. doi: 10.3389/fcimb.2021.676183

Deficiency in memory formation and increased immunosenescence are pivotal features of *Trypanosoma cruzi* infection proposed to play a role in parasite persistence and disease development. The vaccination protocol that consists in a prime with plasmid DNA followed by the boost with a deficient recombinant human adenovirus type 5, both carrying the ASP2 gene of *T. cruzi*, is a powerful strategy to elicit effector memory CD8$^+$ T-cells against this parasite. In virus infections, the inhibition of mTOR, a kinase involved in several biological processes, improves the response of memory CD8$^+$ T-cells. Therefore, our aim was to assess the role of rapamycin, the pharmacological inhibitor of mTOR, in CD8$^+$ T response against *T. cruzi* induced by heterologous prime-boost vaccine. For this purpose, C57BL/6 or A/Sn mice were immunized and daily treated with rapamycin for 34 days. CD8$^+$ T-cells response was evaluated by immunophenotyping, intracellular staining, ELISpot assay and *in vivo* cytotoxicity. In comparison with vehicle-injection, rapamycin administration during immunization enhanced the frequency of ASP2-specific CD8$^+$ T-cells and the percentage of the polyfunctional population, which degranulated (CD107a$^+$) and secreted both interferon gamma (IFNγ) and tumor necrosis factor (TNF). The beneficial effects were long-lasting and could be detected 95 days after priming. Moreover, the effects were detected in mice immunized with ten-fold lower doses of plasmid/adenovirus. Additionally, the highly susceptible to *T. cruzi* infection A/Sn mice, when immunized with low vaccine doses, treated with rapamycin, and challenged with trypomastigote forms of the Y strain showed a survival rate of 100%, compared with 42% in vehicle-injected group. Trying to shed light on the biological mechanisms involved in these beneficial effects on CD8$^+$ T-cells by mTOR inhibition after immunization, we showed that *in vivo* proliferation was higher after rapamycin treatment compared with vehicle-injected group. Taken

together, our data provide a new approach to vaccine development against intracellular parasites, placing the mTOR inhibitor rapamycin as an adjuvant to improve effective CD8+ T-cell response.

Keywords: rapamycin, mTOR, CD8+ T-cells, vaccine, *Trypanosoma cruzi*, effector CD8+ T cells, memory CD8+ T cells

INTRODUCTION

The immunization regimen known as heterologous prime-boost vaccination uses two distinct vectors for priming and boosting, both carrying the target antigen. Different combinations of vectors have been tested and the application of this strategy has promoted an immune response against several experimental infections, such as simian immunodeficiency virus (SIV), malaria, Ebola, tuberculosis, Chagas disease, toxoplasmosis and COVID-19 (Li et al., 1993; McConkey et al., 2003; Wilson et al., 2006; Zhang et al., 2007; De Alencar et al., 2009; Elvang et al., 2009; Hensley et al., 2010; Hill et al., 2010; Martins et al., 2010; Chuang et al., 2013; Graham et al., 2020). This regimen began to be studied more than 20 years ago and has shown excellent protective responses both to intracellular pathogens and neoplastic cells due to the induction of cytotoxic $CD8^+$ T-cells (Zavala et al., 2001; Gilbert et al., 2002; Ranasinghe and Ramshaw, 2009).

Chagas disease, caused by the intracellular protozoan *Trypanosoma cruzi*, is an endemic disease in Latin America and considered a neglected one by the World Health Organization (WHO), as it affects approximately 6-7 million people worldwide (World Health Organization, 2016). The clinical course of Chagas disease generally comprises acute and chronic phases and affects mainly the heart and the digestive system. Currently, the treatment consists of administering the chemotherapeutic benznidazole or nifurtimox, but these drugs have limited efficacy when started late, and there are still no vaccines for the disease (Pérez-Molina and Molina, 2017).

The heterologous prime-boost vaccination protocol, capable of conferring a significant degree of protection against experimental *T. cruzi* infection, consists of priming immunization with plasmid DNA, followed by boosting with replication-defective human recombinant adenovirus type 5, both vectors expressing the amastigote surface protein-2 (ASP2) (De Alencar et al., 2009; Haolla et al., 2009; Dominguez et al., 2011; Rigato et al., 2011; Vasconcelos et al., 2012; Ferreira et al., 2017). Previously, we demonstrated that this prime-boost protocol generates a high frequency of effector $CD8^+$ T cells ($CD44^{High}$, $CD11a^{High}$, $CD62L^{Low}$, $CD127^{Low}$ and $KLRG1^{High}$), which subsequently acquire an effector memory phenotype ($CD44^{High}$, $CD11a^{High}$, $CD62L^{Low}$, $CD127^+$ and $KLRG1^{High}$) (Rigato et al., 2011). These phenotype and cytotoxic effector activity were long-lasting, being detected 98 days after boosting (De Alencar et al., 2009; Rigato et al., 2011). Moreover, the effector memory $CD8^+$ T-cells (TEM) induced by heterologous prime-boost immunization are polyfunctional, since express IFNγ , TNF and CD107a, and play cytotoxic activity simultaneously (De Alencar et al., 2009; Rigato et al., 2011).

During the specific immune response development, several signaling pathways are required to activate T-cells and initiate their differentiation. The highly conserved kinase called mammalian target of rapamycin (mTOR) is a key regulator of essential cellular processes such as cell growth, autophagy, survival, proliferation, and metabolism in response to environmental factors, including levels of cellular energy, insulin, cytokines and amino acids, through the complexes mTORC1 and mTORC2, that contain different scaffold associated proteins, Raptor and Rictor, respectively, which define their downstream targets pathways (Dennis et al., 2001; Wullschleger et al., 2006; Thomson et al., 2009; Powell et al., 2012). In $CD8^+$ T-cells, mTORC1 controls, for example, glucose uptake and glycolysis during activation and effector phases and also participates in the signaling generated by the antigen recognition receptor (TCR) and cytokines (Jacobs et al., 2008; Buck et al., 2015; Chang and Pearce, 2016). Even though rapamycin has been commonly used in organ transplantation to prevent graft rejection (Augustine et al., 2007), several studies have reported that mTOR inhibition by treatment with low and continuous doses of rapamycin during the immune challenge of $CD8^+$ T cells could improve the function and memory formation following viral infections or tumor challenges (Araki et al., 2009; Rao et al., 2010; Li et al., 2011; Turner et al., 2011; Bassett et al., 2012; Mattson et al., 2014; Shrestha et al., 2014).

The transcriptome of activated $CD8^+$ T cells treated with rapamycin revealed that most genes modulated by mTOR inhibitor are associated with apoptosis, survival, maintenance, and cell migration, which take part in the $CD8^+$ T cell programming after activation (Mattson et al., 2014; Borsa et al., 2019). Moreover, a clinical trial found that elderly people immunized against influenza and treated with rapamycin had a response 20% higher in antibody titer than the placebo group, paralleled by increased T cells life span, improving immune function and reducing infections (Mannick et al., 2014; Mannick et al., 2018).

Based on these findings, here we tested the role of the mTOR inhibitor rapamycin combined with heterologous prime-boost immunization against *T. cruzi* during $CD8^+$ T-cell activation. For this purpose, C57BL/6 and AS/n mice were immunized and daily treated with rapamycin. The inflammatory and cytolytic immune responses were analyzed. Additionally, mice were challenged with the highly infective trypomastigote forms of Y strain.

METHODS

Ethics Statement

This study was carried out in strict accordance with the recommendations in the Guide for the Care and Use of

Laboratory mice of the Brazilian National Council of Animal Experimentation (http://www.sbcal.org.br/) and Federal Law 11.794 (October 8, 2008). The project was approved by the Ethical Committee for Animal Experimentation at the Federal University of Sao Paulo, registered under number 9959021014.

Mice and Parasites

Male and female 8-week-old C57BL/6 and A/Sn mice were supplied by the Center for the Development of Experimental Models for Medicine and Biology (CEDEME) from the Federal University of São Paulo. Blood trypomastigotes of Y type II strain of *T. cruzi* were maintained by weekly passages in A/Sn mice at the Xenodiagnostic Laboratory of Dante Pazzanese Institute of Cardiology. For *in vivo* experiments, the challenge was performed with 150 or 1 x 10^4 trypomastigotes diluted in PBS (0.2 mL) in A/Sn and C57BL/6 mice, respectively, administered subcutaneously (s.c.) in the tail. Parasitemia was monitored after the 6^{th} day of infection until day 15. A blood sample (5 µl) was collected from the tail for parasite quantification on the light microscope.

Immunization Protocol

The heterologous prime-boost immunization protocol previously described by Rigato and group (Rigato et al., 2011) was used in this study. The protocol consists of a dose of plasmid DNA, with the vectors pcDNA3 (control) or pIgSPClone9, at 10 or 100 µg/mouse. Three weeks after the first immunization, mice were immunized with 2 x 10^7 or 2 x 10^8 pfu of the adenoviral vectors Adβ-Gal (control) or AdASP-2. Both immunizations were performed by intramuscular route in the Tibialis anterior muscle. Experimental groups were delineated as follows: 1) Control: immunized with the control vectors pcDNA3 and Adβ-Gal; 2) ASP2: immunized with pIgSPCl.9/AdASP-2 and vehicle-injected (PBS); 3) ASP2/rapamycin: immunized with pIgSPCl.9/AdASP-2 and rapamycin-treated.

Treatment With Rapamycin

Mice were treated every 24 hours with 2 µg rapamycin (Sigma Aldrich) per mouse (0.075 mg/kg/day), diluted in 0.2 mL PBS *via* intraperitoneal (i.p.) for 34 days, starting at priming (Li et al., 2011; Bassett et al., 2012). Control mice were treated with the vehicle (PBS). To assess mTOR inhibition, phospho-S6 ribosomal protein conjugate antibody (Ser235/236) from Cell Signaling Technology was used. This antibody binds to the PS6 protein only in its phosphorylated form, indicating whether mTOR was activated. For phospho-S6 ribosomal protein staining, the protocol was performed according to Ersching and group (Ersching et al., 2017).

Peptides and Multimers

The ASP2 synthetic peptides VNHRFTLV and TEWETGQI were synthesized by GenScript with purity greater than 95%. The peptides were used during *in vivo* and *ex vivo* assays to stimulate specific $CD8^+$ T-cells.

$H2K^b$-VNHRFTLV multimer was purchased from ProImmune Inc., and $H2K^K$-TEWETGQI multimer, labeled with allophycocyanin, was purchased from Immudex. Both were used for labeling TCR-specific $CD8^+$ T-cells.

Flow Cytometry Analysis

Splenocytes were treated with ACK buffer (NH_4Cl, 0.15 M, $KHCO_3$, 10 mM, 0.1 mM Na2-EDTA, pH 7.4) for osmotic lysis of red cells and washed with RPMI supplemented with 10% fetal bovine serum (FBS). After lysis, cells were labeled with the multimers for 10 minutes at room temperature. The cell surface was stained for 30 min at 4°C with the following antibodies: anti-CD8 (clone 53-67); anti-CD11a (clone 2D7), anti-CD11c (clone HL3), anti-CD25 (clone 7D4), anti-CD27 (clone LG.7F9), anti-CD31 (clone MEC13.3), anti-CD43 (clone Ly 48), anti-CD43 (clone 1B11), anti-CD44 (clone IM7), anti-CD49d (clone R-12), anti-CD62L (clone MEL-CD70 (clone FR70), anti-CD95 (clone Jo2), anti-CD95L (MFL3), anti-CD122 (clone TM-b1), anti-CD127 (Clone J43), anti-PDL-1 (clone MIH5), anti-CCR-5 (clone HM-CCR5), anti-CCR-7 (clone 4B12), anti-KLRG-1 (clone 2F1 and anti-CD183 (CXCR3-clone 173). At least 500,000 events were acquired on FACS Canto II flow cytometer (BD). The results were analyzed with FlowJo software version 9.9.6 (FlowJo, LLC).

Intracellular Cytokine Staining

Two million splenocytes were incubated in the presence or absence of the peptides VNHRFTLV or TEWETGQI (10 µg/mL or 10 µM) in supplemented RPMI medium with CD107a FITC antibody (clone 1D4B, BD), anti-CD28 (clone 37.51, BD Bioscience), BD Golgi-Plug (1 µL/mL, BD Bioscience) and monensin (5 µg/mL, Sigma Aldrich) no longer than 12 hours in V-bottom 96-well plates (Corning) in a final volume of 200 µL, at 37°C containing 5% CO_2. After incubation, cells were labeled with anti-CD8 antibody PerCP (clone 53-6.7, BD) for 30 minutes at 4°C. For cellular fixation and permeabilization, the Cytofix/Cytoperm kit (BD Biosciences) was used according to the supplier's instructions. For intracellular staining, was used the following antibodies: anti-IFNγ APC (clone XMG1.2, BD Biosciences) and anti-TNF PE (clone MPC-XT22, BD Biosciences). At least 700,000 events were acquired using a FACSCanto II flow cytometer (BD Biosciences).

Enzyme-Linked-Immunospot Assay (ELISpot)

The IFNγ secretion was measured by ELISpot as described previously (Ferreira et al., 2017). Briefly, 10^5 responder cells (represented by splenocytes from mice previously immunized) were incubated with 3 x 10^5 antigen-presenting cells (represented by splenocytes from naive mice) on nitrocellulose 96-wells flat-bottom plates (Millipore) in the presence or absence of the specific ASP2 peptides VNHRFTLV or TEWETGQI for $CD8^+$ T cells for 24 hours. The number of IFNγ-producing cells was determined using a stereoscope. The final value refers to the numeric average of spots of stimulated wells minus the numeric average of spots of unstimulated wells. The result is multiplied by 10 to display the data by spot forming cells (SFC) in million units.

Cytokine Determination

One million splenocytes were incubated for 48 hours in the presence or absence of the peptide VNHRFTLV in a final concentration of 10 μg/mL. Culture supernatants were harvested and stored at −80°C until analysis. IL-2, IL-4, IL-6, IL-10, IL-17, IFNγ, and TNF cytokines were detected simultaneously using mouse Th1/Th2/Th17 cytokine bead array (CBA) kit (BD Pharmingen), according to the manufacturer's instructions. After acquiring samples on a flow cytometer, the data were analyzed in FCAP Array™ software to generate results in graphical and tabular format. The data are expressed in pg/mL and the values correspond to the number of the value of stimulated samples minus the value of unstimulated ones.

In Vivo Cytotoxicity Assay

Splenocytes from naive mice were divided into two populations stained with carboxyfluorescein succinimidyl ester (CFSE - Molecular Probes) at a final concentration of 10 μM ($CFSE^{High}$) and 1 μM ($CFSE^{Low}$). PKH26 Red Fluorescent Cell Linker (Sigma-Aldrich) was also used at a final concentration of 20 μM. The target cells labeled with $CFSE^{High}$ or PKH were pulsed with peptide VNHRFTLV or TEWETGQI for 40 minutes at 37°C according to each experiment's concentration. $CFSE^{Low}$ cells remained uncoated. Subsequently, all stained populations were counted and mixed at the same proportion. 4 x 10^7 cells were transferred *via* intravenous into mice and after 14 hours, the spleens of recipient mice were collected to $CFSE^{Low}$, $CFSE^{High}$ and PKH^+ detection by flow cytometry using FACS Canto II. The percentage of specific lysis was determined by this formula:

$$\%Lysis = [1 - (\%CFSE^{high}immunized/\%CFSE^{low}immunized)/(\%CFSE^{high}naive/\%CFSE^{low}naive)] \times 100$$

BrdU Proliferation Assay

For *in vivo* proliferation, A/Sn mice were treated with 2 mg of BrdU (SIGMA) (i.p.) after boosting for 14 days every 48 hours. Then, the splenocytes were purified for staining with anti-CD8 and BrdU detection according to the manufacturer's instructions (BrdU Flow Kit APC or FITC - BD Pharmingen). At least 100,000 cells were obtained in low flow rate on a BD FACSCanto II flow cytometer (BD Bioscience), and then analyzed with FlowJo software (FlowJo, LLC).

BMDC Generation, Immunophenotyping Antigen-Presentation Capacity

Bone marrow dendritic cells (BMDC) were generated as described earlier (Ersching et al., 2016). Overall, cells removed from the femurs were cultured with 20 ng/ml of recombinant granulocyte–macrophage colony-stimulating factor (rGM-CSF-RD System) for 7 days. The medium was replaced on the fourth day. In some conditions, BMDC were matured with 200 ng/ml of LPS from *E. coli* (Sigma-Aldrich) for 3 hours, resulting in a population that comprises around 80% of $CD11c^+$ cells. For *in vitro* antigen presentation capacity assay, BMDC were incubated with AdASP-2 (MOI = 50) for 24 hours, or with VNHRFTLV peptide (10 μg/mL) for 1 hour. Rapamycin was used in a final concentration of 1 μM. The frequency of IFNγ-producing by $CD8^+$ T cells was detected by ELISpot. Additionally, BMDC were stained with the following antibodies for flow cytometry analysis: anti-CD11c, anti-CD40, anti-CD86 and anti-MHC class I ($H2K^b$).

Statistical Analysis

Groups were compared using One-way ANOVA followed by Tukey's HSD test on Vassarstats (http://vassarstats.net). Before performing parametric tests, the normal distribution was analyzed by Shapiro-Wilk test and residuals distribution in QQ-plots on GraphPad Prism 8.0. Survival analysis by Log-rank was also performed on GraphPad Prism 8.0. Because the variances were similar, values were expressed as mean ± standard deviations (SD). The expression of the receptors was compared by MFI (mean fluorescence intensity), and the MFI of naive group was taken as a baseline. Differences were considered significant when the p value was <0.05.

RESULTS

Rapamycin Treatment Enhances the Number and Quality of Specific $CD8^+$ T-Cells

Initially, the blockade of mTOR by rapamycin was confirmed by ribosomal protein S6 staining, which is a target of mTOR kinase. The detection antibody used binds to S6 ribosomal protein only in its phosphorylated form (Ser235/236), indicating whether there was mTOR activity. $CD8^+$ T cells from splenocytes of C57BL/6 mice incubated with rapamycin for 1 hour showed a lower expression of phosphorylated S6K than untreated or concavalin A stimulated cells (**Supplementary Figure 1**).

T lymphocytes perform a strong antiparasitic role mediated by the secretion of IFNγ and other mediators that also participate in the parasite dissemination control. The $CD8^+$ T-cells induced by heterologous prime-boost regimen are polyfunctional, as they exhibit cytotoxic activity and secrete the cytokines IFNγ and TNF simultaneously (De Alencar et al., 2009; Rigato et al., 2011). Based on these findings, we evaluated the production of cytokines IFNγ and TNF, as well as the degranulation by the expression of the CD107a molecule (LAMP-1) in VNHRFTLV peptide-specific $CD8^+$ T-cells obtained from splenocytes of immunized mice. Experimental groups were delineated as follows: 1) Control: immunized with the control vectors pcDNA3 and Adβ-Gal; 2) ASP2: immunized with pIgSPCl.9/AdASP-2 and vehicle-injected (PBS); 3) ASP2/rapamycin: immunized with pIgSPCl.9/AdASP-2 and rapamycin-treated.

After *ex vivo* stimulation with the peptide VNHRFTLV and intracellular staining (gates strategy showed in **Supplementary Figure 2**), the number of $CD8^+$ T-cells that simultaneously express IFNγ, TNF and CD107a, named polyfunctional subpopulation, were increased in rapamycin-treated mice (Gr.3), compared with vehicle-injected mice (Gr.2), after Boolean analysis (**Figures 1B, C**). In addition, the magnitude of responding $CD8^+$ T-cells (frequency of cells that express at least one of the three molecules IFNγ or TNF or CD107a after *ex*

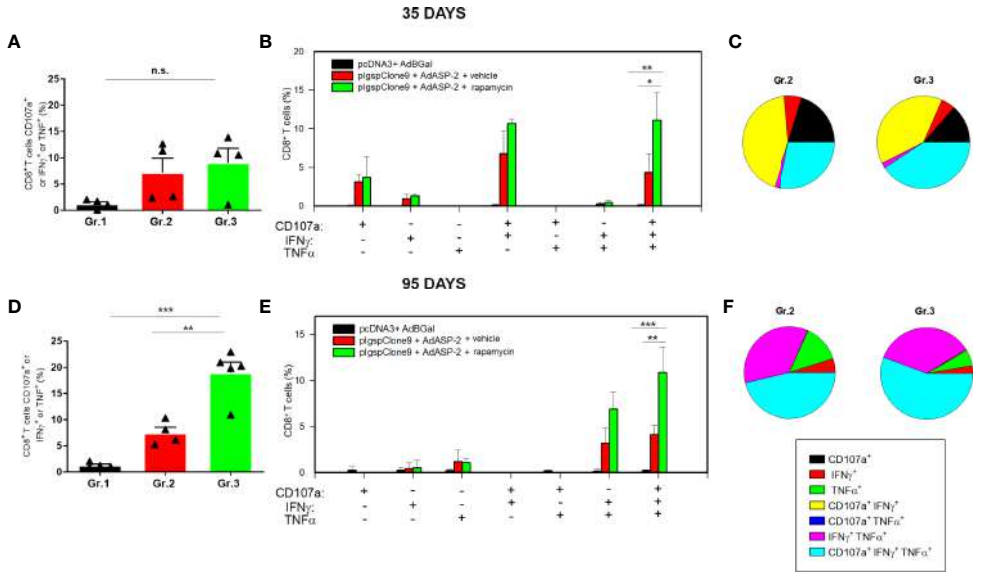

FIGURE 1 | Specific CD8+ T cell-mediated immune responses was higher in rapamycin-treated mice, after 35 or 95 days from priming. C57BL/6 mice were immunized *via* i.m. with plasmid (100 μg) and adenovirus (2 x 10^8 pfu) according to the experimental groups described in the *Methods* section. They were also treated daily with rapamycin or vehicle (i.p.) for 34 days. On days 35 or 95 after priming, splenic cells were collected and cultured *ex vivo* in the presence of anti-CD107a and anti-CD28, with or without the VNHRFTLV peptide. After 12 hours, the cells were labeled with anti-CD8, anti-IFNγ and anti-TNF antibodies. **(A, D)** Frequencies of CD8+ T cell that express CD107a or IFNγ or TNF after stimulation. **(B, E)** Subpopulations of CD8+ T cells expressing each individual molecule or the combinations between CD107a, IFNγ and TNF. **(C, F)** Pie charts show the fraction of specific cells expressing the indicated molecules. The results correspond to the mean values of 4 mice per group, with standard deviation. Statistical analysis was performed using the *One-Way* ANOVA and Tukey's HSD tests. Asterisks indicate significant differences among groups, defined as $^*P<0.05$, $^{**}P < 0.01$, and $^{***}P < 0.001$. The experiments were repeated four times, and representative results are shown. N.S, non-significant. Boolean analysis was performed using FlowJo Software.

vivo stimulus with the specific peptide) was also higher in Gr.3 (**Figure 1A**), at 35 days after priming. The differences between Gr.2 (vehicle-injected) and Gr.3 (rapamycin-treated) were more evident at 95 days after priming (**Figures 1D–F**).

In order to measure the frequency of ASP2 specific CD8+ T-cells, the splenocytes were labeled with the H2K^b-VNHRFTLV pentamer and anti-CD8. We found that the frequency and absolute number of specific CD8+ T-cells were significantly higher in Gr.3 after 35 days and sustained after 95 days after priming (**Figures 2A–C**). These results demonstrate that treatment with rapamycin enhances the response generated by immunization and memory formation, confirming that inhibition of mTOR modulates T-lymphocyte differentiation during adaptive immunity to *T. cruzi* antigens, as previously proposed in other conditions (Araki et al., 2009; Nam, 2009).

Specific CD8+ T-Cells Phenotype Remains Unchanged After Treatment With Rapamycin

Traditionally, antigen-specific CD8+ T-cells are divided into three major groups according to their markers of activation, homing, migration, proliferation capacity and effector functions: i) effectors (TE): effector cells that control the infection (CD44^{High}, CD11a^{High}, CD62L^{Low}, CD127$^-$, KLRG1^{High}); ii) central memory (TCM): long-lasting memory cells with high proliferative potential after antigen stimulation and reside in secondary lymphoid organs (CD44^{High}, CD11a^{High}, CD62L^{High}, CD127$^+$, KLRG1^{High}); iii) effector memory (TEM): transitional cells that exist for a shorter time, present high effector activity and express TE surface markers (CD44^{High}, CD11a^{High}, CD62L^{Low}, KLRG1^{High}) and a TCM marker (CD127$^+$). They home primarily in peripheral tissues and rapidly produce effector cytokines upon antigenic stimulation (Wherry et al., 2003; Lanzavecchia and Sallusto, 2005; Wirth et al., 2009; Wirth et al., 2010; Angelosanto and Wherry, 2010; Cui and Kaech, 2010; Ahmed and Akondy, 2011; Sheridan and Lefrançois, 2011).

Previously, it has been shown that heterologous prime-boost regimen induces a strong response of effector CD8+ T-cells, which develop into an effector memory (TEM) population (Rigato et al., 2011). Here, we challenged the hypothesis that mTOR inhibition changes the profile of CD8+ T-cells generated by vaccination as, for example, into a TCM phenotype, as described in other experimental models combined with rapamycin (Araki et al., 2009; Pearce et al., 2009; Turner et al., 2011). To this end, we performed the phenotypic characterization of specific CD8+ T-cells from the spleen of C57BL/6 mice immunized and treated with rapamycin or vehicle.

Specific CD8+ T-cells were stained with H2K^b-VNHRFTLV multimer and anti-CD8. The expression pattern of the molecules CD11a, CD44, CD62L, CD127, KLRG-1 and CCR7 on specific CD8+ T-cells was similar between Gr.2 and Gr.3, at 35 and 95 days after priming (**Figure 2D**), showing that rapamycin, all in all, did not modify the TE(M) profile of CD8+ T-cells generated by

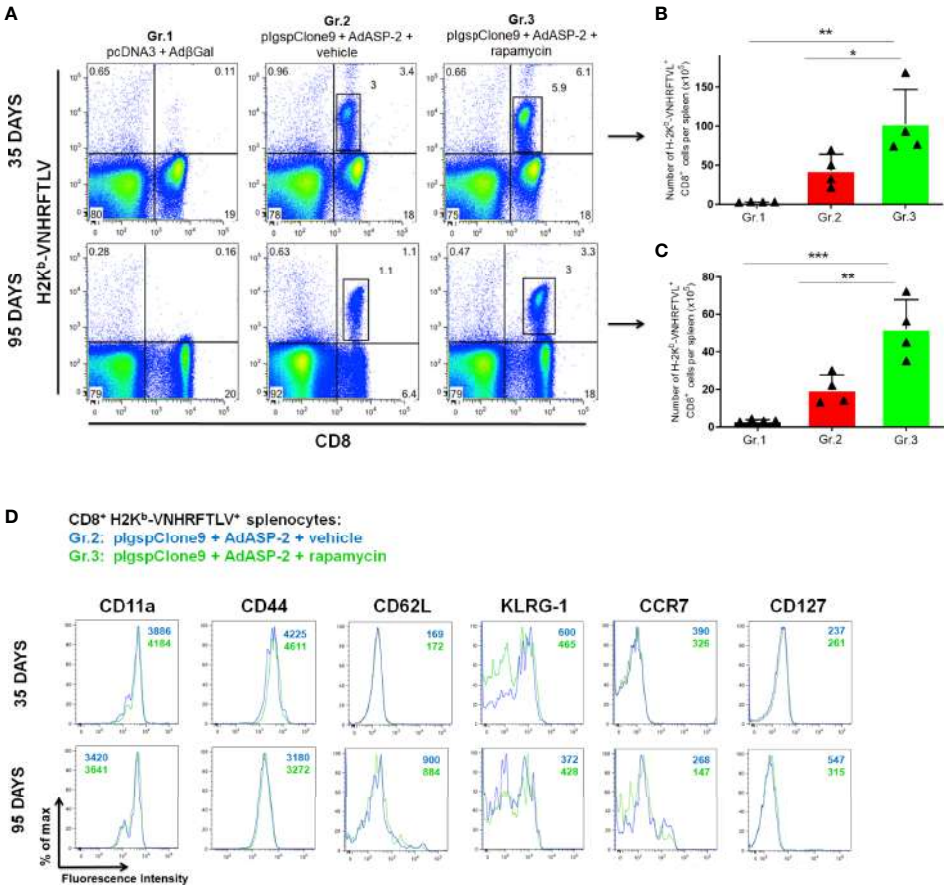

FIGURE 2 | Frequency and absolute number of specific CD8$^+$ T cells were higher in rapamycin-treated group, after 35 or 95 days from priming. C57BL/6 mice were immunized *via* i.m. with plasmid (100 μg) and adenovirus (2 x 10^8 pfu) according to the experimental groups described in the method section. They were also treated daily with rapamycin or vehicle (i.p.) for 34 days. After 35 or 95 days of priming, the splenic cells were labeled with anti-CD8 and H2K^b-VNHRFTLV pentamer for flow cytometry analysis. **(A)** Dot-plots charts correspond to the representative mouse (median) from 4 mice. Numbers represent frequencies of splenic cells. **(B, C)** The total number of specific lymphocytes was estimated. The bars indicate the group mean ± SD. Statistical analysis was performed using the One-Way ANOVA and Tukey's HSD tests. Asterisks indicate significant differences among groups, defined as *P < 0.05, **P < 0.01, and ***P < 0.001. Data referring to 4 mice per group and representing 4 independent experiments. **(D)** Splenic cells were labeled with anti-CD8, H2K^b-VNHRFTLV multimer and the molecules indicated above for flow cytometric analysis. Histograms show the expression of the markers in CD8$^+$ H2K^b-VNHRFTLV$^+$ cells in Gr.2 (blue lines) and Gr.3 (green lines). Analyses were performed using cells pools of 4 mice and they are representative of two independent experiments. The numbers indicate the mean fluorescence intensity (MFI). The individual analysis of mice from each group presented similar results.

vaccination. In both ASP2 immunized groups, differently from the expected, an increase in CD127 expression on specific memory CD8$^+$ T cells was not found after 95 days. Other markers involved with activation and migration were not altered either. The complete immunophenotyping, where twenty-four surface markers associated with activation, regulation, migration, and cell death were used, is shown in **Supplementary Figures 3** and **4**.

Cellular Response Remained High Even With Reduced Doses of Immunization in Rapamycin-Treated C57BL/6 Mice

Next, we evaluated the role of rapamycin during vaccination with reduced doses, to highlight the adjuvant effect of rapamycin. For that purpose, C57BL/6 mice were vaccinated with 10-fold lower doses of plasmid/adenovirus, treated with rapamycin or vehicle and the immune response was assessed by the standard protocol. On days 35 and 95, splenocytes were isolated, and specific CD8$^+$ T-cells were stained using H-2K^b-restricted VNHRFTLV multimer. Splenocytes were stimulated with VNHRFTLV specific ASP-2 peptide for ELISpot anti-IFNγ. The increase in the number of VNHRFTLV-specific CD8$^+$ T cells was replicated with 10-fold lower doses since the rapamycin-treated mice showed a higher frequency of specific CD8$^+$ T cells (Gr.3L), both on days 35 and 95 after priming (**Figures 3A, B**). Later, when we analyzed the IFNγ secretion by CD8$^+$ T-cells after *ex vivo* stimulation with the VNHRFTLV peptide, rapamycin-treated group (Gr.3L) was superior in both analyses (**Figures 3C–E**).

In addition, we determined the concentration of cytokines in the supernatant of VNHRFTLV-stimulated splenocytes from mice immunized 95 days after priming using Th1/Th2/Th17

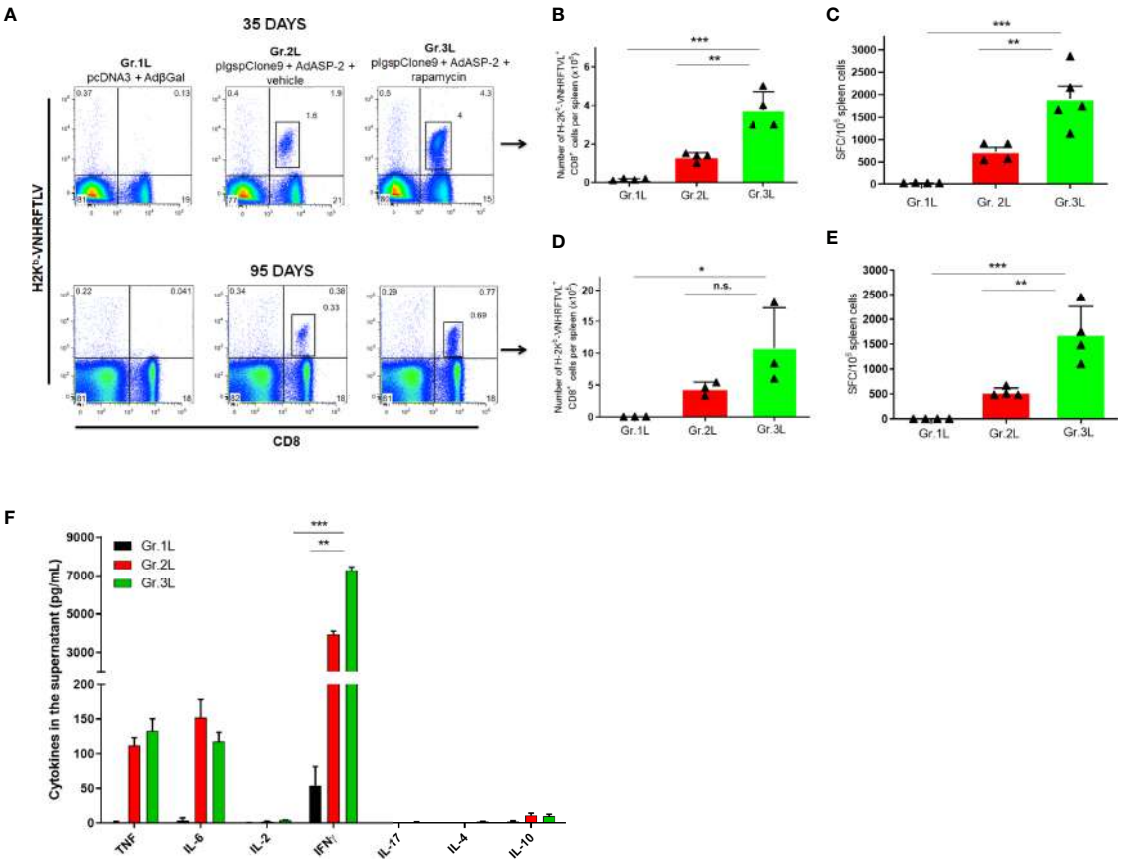

FIGURE 3 | Rapamycin increased the frequency of specific CD8$^+$ T cells and IFNγ production from mice immunized with reduced doses, after 35 or 95 days from priming. C57BL/6 mice were immunized *via* i.m. with plasmid (10 μg) and adenovirus (2 x 10^7 pfu) according to the experimental groups described in the method section. They were also treated daily with rapamycin or vehicle (i.p.) for 34 days. On days 35 or 95 after priming, splenic cells were collected for surface staining of anti-CD8 and H2K^b-VNHRFTLV$^+$ pentamer or cultured with the specific peptide VNHRFTLV for ELISpot or CBA assay. **(A)** FACS charts show the frequency of CD8$^+$ and H2K^b-VNHRFTLV$^+$ cells in the spleen. The dot-plots correspond to the representative mice (median) of the group. Numbers represent the frequencies of CD8$^+$ H2K^b-VNHRFTLV$^+$ cells in the spleen. **(B, D)** The total number of specific CD8$^+$ T cells was estimated. **(C, E)** Number of IFNγ producing cells by ELISpot. SFC: Spot-forming cells. **(F)** The supernatant of splenocytes from mice immunized for 95 days cultured for 48 hours was used to measure the indicated cytokines by flow cytometry. Statistical analysis was performed using the *One-Way* ANOVA and Tukey's HSD tests. Asterisks indicate significant differences among groups, defined as *$P < 0.05$, **$P < 0.01$, and ***$P < 0.001$. Data referring to 4 mice per group and representing 4 independent experiments. N.S, Non-significant.

CBA kit. IFNγ was the predominant cytokine after VNHRFTLV stimulation and the splenocytes from rapamycin-treated mice (Gr.3L) presented the highest IFNγ concentration in the supernatants (**Figure 3F**). As previously shown, heterologous prime-boost vaccination induces predominantly a Th1 profile response (De Alencar et al., 2009). Thus, the present findings enable us to adopt a protocol with reduced doses of vaccine formulation, which were able to induce a strong and potentially CD8$^+$ T response.

Higher *In Vivo* Cytotoxicity of Specific CD8$^+$ T After the Rapamycin Treatment

Another essential effector function involved in intracellular pathogens dissemination control is the direct cytotoxicity performed by NK and CD8$^+$ T cells, releasing cytotoxic granules, such as perforins, granzymes B and granulysin, which are responsible for forming pores on the plasma membrane of target infected cells as well as inducing apoptosis. Thus, the cytotoxic activity of VNHRFTLV-specific CD8$^+$ T-cells in C57BL/6 mice immunized with 10-fold lower doses of plasmid/adenovirus and treated with rapamycin or vehicle was analyzed at 35 days after priming. The *in vivo* cytotoxicity assay was evaluated using adoptive transfer of labeled cells with two concentrations of CFSE dye, CFSE^{High} and CFSE^{Low}. Only the CFSE^{High} population was pulsed with 2,5 μM of the VNHRFTLV ASP2 peptide. Both populations were transferred to recipient mice of the experimental groups (Gr.1L, Gr.2L and Gr.3L) and, after 15 hours, we analyzed the percentage of lysis in CFSE^{High} cells. The cytotoxic activity of VNHRFTLV-specific CD8$^+$ T-cells was similar in both immunized groups, e.g., 97,6% in Gr.2L and 95,07% in Gr.3L (**Supplementary Figure 5**), which corroborates with our previous findings showing a strong cytotoxic activity

induced by heterologous prime-boost immunization using the ASP2 (De Alencar et al., 2009).

Therefore, we performed another cytotoxicity assay lowering the concentrations of VNHRFTLV peptide, trying to reveal any beneficial effect of rapamycin treatment on cytotoxic activity. For that, two dyes were used to sort 3 different populations: $CFSE^{Low}$, $CFSE^{High}$ and PKH^{+}. Both $CFSE^{High}$ and PKH^{+} populations were pulsed with the peptide at a final concentration of 500 nM and 50 nM, respectively (**Figure 4**). After 15 hours, rapamycin-treated mice (Gr.3L) exhibited a higher percentage of cytotoxic activity against $VNHRFTLV^{+}$ target cells of $CFSE^{High}$ (500 nM peptide) and PKH^{+} (50 nM peptide) populations compared with the cytotoxic activity observed in vector control Gr.1L and vehicle-injected Gr.2L mice (**Figures 4A, B**). Similar results were found at 95 days after priming. As expected, the main difference between the two immunized groups was the cytotoxic activity of $CD8^{+}$ T-cells on the PKH^{+} target cell population, pulsed with the lowest concentration (50 nM) of the specific VNHRFTLV peptide (**Figure 4B**).

Treatment With Rapamycin Increased the Survival of the Highly Susceptible A/Sn Mice Immunized With Low Doses After Challenge

Once the putative protective profiles of $CD8^{+}$ T-cells induced by vaccination have been improved when combined with rapamycin treatment, we challenged highly susceptible A/Sn mice with *T. cruzi* and survival was registered. Since heterologous prime-boost immunization can induce a protective response, mice groups were immunized with 10-fold lower doses of plasmid/adenovirus and treated with rapamycin or vehicle. Thirty-five days after priming, mice were challenged with 150 trypomastigotes forms of the Y strain of *T. cruzi*. The parasitemia and survival ratio were monitored daily.

Parasitemia (**Figure 5A**) was followed from day 5 post infection, and no significant difference were detected between Gr.2L and Gr.3L. Suprisingly, as shown in the survival curve (**Figure 5B**), 42.8% of mice from Gr.2L survived, while the rapamycin-treated mice (Gr.3L) showed 100% of survival rate (Log-rank p = 0.0218). In an independent experiment, rapamycin alone was not able to protect A/Sn mice from the experimental challenge (**Supplementary Figure 6**). These results demonstrate the adjuvant effect of rapamycin when combined with the vaccination, even with 10-fold lower concentrations of plasmid/adenovirus, inducing a protective immune response generated by prime-boost ASP2 immunization.

Rapamycin Improved the Protective Immune Response Generated by Heterologous Prime-Boost Protocol in A/Sn Mice

To verify whether the $CD8^{+}$ T-cell response in A/Sn mice was also favored by the immunization combined with the rapamycin

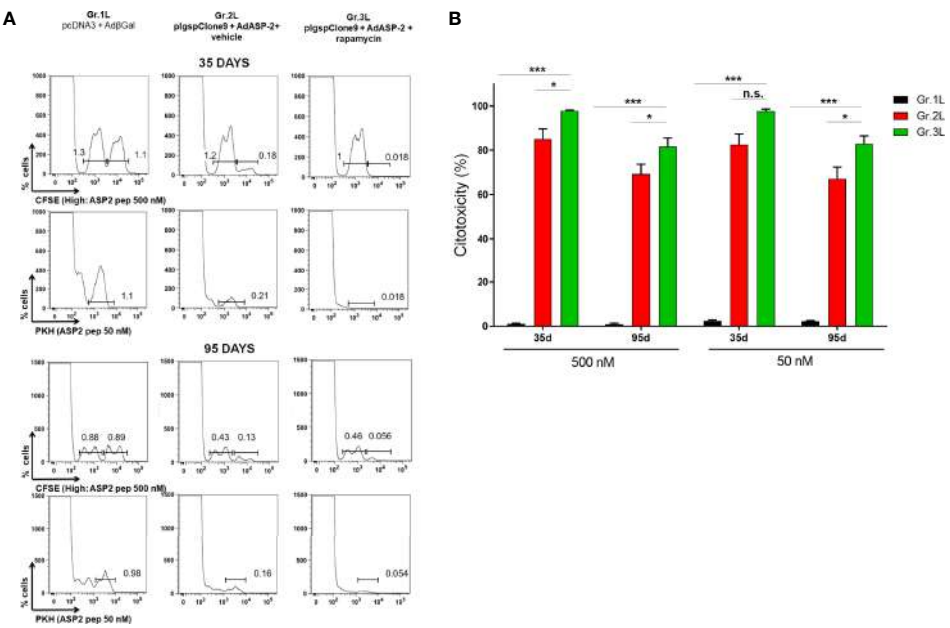

FIGURE 4 | *In vivo* cytotoxicity of specific $CD8^{+}$ T cells was higher in rapamycin-treated mice. C57BL/6 mice were immunized *via* i.m. with plasmid (10 μg) and adenovirus (2×10^{7} pfu) according to the experimental groups described in the method section. They were also treated daily with rapamycin or vehicle (i.p.) for 34 days. Splenocytes from naive mice were stained with CFSE or PKH. $CFSE^{High}$ and PKH^{+} populations were pulsed with peptide VNHRFTLV at a final concentration of 500 nM or 50 nM, respectively. $CFSE^{Low}$ was the negative control. Stained cells were transferred to the experimental groups and, after 14 hours, spleens were harvested to quantify the frequency of stained cells. Histograms represent the frequencies of $CFSE^{High}$, $CFSE^{Low}$ and PKH^{+} cells in each group, after 35 days **(A)** or 95 days from priming **(B)**. Percentage of cytotoxicity, with mean ± SD. Statistical analysis was performed using the One-Way ANOVA and Tukey's HSD tests. Asterisks indicate significant differences among groups, defined as *P < 0.05, and ***P < 0.001. Results from 2 experiment and 4 mice per group. N.S, Non-significant.

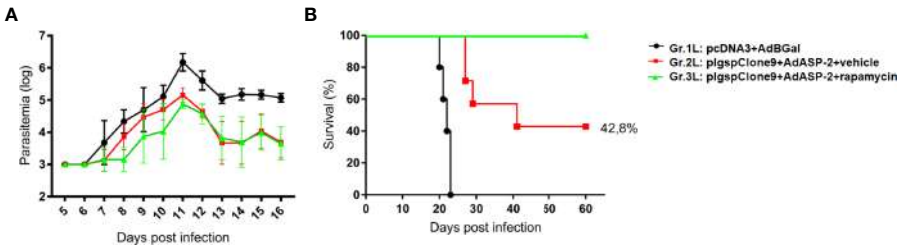

FIGURE 5 | Rapamycin improved the protection of A/Sn mice immunized with reduced doses in experimental challenge with *T. cruzi*. A/Sn mice were immunized *via* i.m. with plasmid (10 μg) and adenovirus (2 x 10^7 pfu) according to the experimental groups described in the method section. They were also treated daily with rapamycin or vehicle (i.p.) for 34 days. Fifteen days after boosting, mice were infected with 150 blood trypomastigotes of *Y* strain of *T. cruzi*. **(A)** Parasitemia was monitored daily between days 5 and 16 after challenge. The parasitemia values were log transformed and groups 2 and 3 were compared on day 11 (parasitemia peak) by *One-Way* ANOVA and Tukey's HSD tests (*p<0,0001). **(B)** The survival rate was also followed and analyzed by Log-rank (Mantel-Cox) test (all groups p = 0.0001; groups 2 and 3 p = 0.0218). Results from 7 mice per group.

treatment, we performed the *ex vivo* assays. Splenocytes from A/Sn mice, immunized with 10-fold lower doses and treated with rapamycin or vehicle, were collected on days 35 or 95 after priming to measure the number of specific $CD8^+$ cells labeled with the multimer $H2K^K$- restricted TEWETGQI peptide. In addition, we performed the intracellular staining to label CD107a, IFNγ and TNF, and ELISpot to measure the number of TEWETGQI-specific IFNγ producing $CD8^+$ T-cells.

Initially, to quantify TEWETGQI-specific $CD8^+$ T-cells, pools of splenocytes and lymph node cells from 4 mice per group were prepared. After labeling the cells with the multimer and anti-CD8, our data show that the frequency and absolute number of TEWETGQI-specific $CD8^+$ T-cells increased in the rapamycin-treated mice (Gr.3L) (**Figures 6A, B**). Further, 35 after priming both ASP2-immunized groups (Gr2.L and Gr3L) presented a population of TEWETGQI-specific $CD8^+$ T-cells with an activated phenotype, characterized by expression of the cell markers $CD44^{High}$, $CD62L^{Low}$, $KLRG1^{High}$ and $CD127^{Low}$ (**Figure 6C**). At 95 days after priming, the TEWETGQI-specific $CD8^+$ T-cells presented a reduced expression of CD127 and KLRG-1 (**Figure 6C**).

At 35 days and 95 days after priming, the frequencies of polyfunctional $CD8^+$ T cells ($CD107a^+$, $IFN\gamma^+$ and TNF) (**Figures 6D–E, G–H**), and the absolute number of $IFN\gamma^+$ $CD8^+$ T cells, as revealed by ELISpot assay (**Figures 6F, I**), were significantly higher in splenocytes obtained from Gr.3L mice, compared to Gr.1L and Gr.2L, after *ex vivo* stimulation with the specific peptide. Altogether, these findings corroborate the improvement of vaccination after rapamycin treatment and explain the protective profile found after the challenge with the virulent *T. cruzi* Y strain, as described above.

Treatment With Rapamycin Increased *In Vivo* $CD8^+$ T-Cell Proliferation

Since the number of ASP2-specific $CD8^+$ T-cells increased in the rapamycin-treated mice (Gr.3 and Gr3L), we hypothesized that $CD8^+$ T-cells might show a differential proliferate response and clonal expansion after activation. Hence, the proliferation of $CD8^+$ T-cells was analyzed *in vivo* using the BrdU incorporation approach. For that, A/Sn mice were immunized and treated with rapamycin or vehicle. After boosting, mice were treated every 48 hours with BrdU (2 mg/dose) until day 35 after priming.

According to **Figure 7**, ASP2-specific $CD8^+$ T-cells from rapamycin-treated mice (Gr.3L) showed a higher incorporation of BrdU compared to Gr.1L and Gr.2L, due to the number of precursors activated by the boost. Therefore, during the expansion phase induced by vaccination, rapamycin treatment potentiated proliferative response of ASP2-specific $CD8^+$ T-cells.

Dendritic Cells Activated in the Presence of Rapamycin Lack Improvement in the Antigenic Presentation Capacity of ASP2-Specific $CD8^+$ T-Cells

Dendritic cells are specialized in antigen processing and presentation, capable of inducing the initial activation of T lymphocytes. The study performed by Amiel et al. (2012) showed that inhibition of mTOR during activation of dendritic cells derived from bone marrow (BMDC) prolonged their useful life and increased the expression of costimulatory molecules, essential for the antigen presentation. In addition, a tuberculosis vaccine (BCG) study that employed the stimulation of dendritic cells in the presence of rapamycin led to an increase in T cell activation (Jagannath et al., 2009). Hence, analyzing the role of dendritic cells antigen presentation for $CD8^+$ T-cells during immunization appeared to be important. For that purpose, BMDC of C57BL/6 mice were generated *in vitro* for 7 days, incubated with the ASP2-carrying adenovirus vector (MOI = 50) or the VNHRFTLV peptide (10 μg/ml) in the presence or absence of rapamycin (1 μM). In some conditions, BMDC were primed/matured with LPS (200 ng/mL) for 3 hours. As shown in **Figures 8A, B**, the expression level of costimulatory molecules (CD86 and CD40) and MHC class I ($H2K^b$) in $CD11c^+$ cells were analyzed. We observed that expression levels of these markers were similar in dendritic cells stimulated in the presence or absence of rapamycin.

Next, we evaluated the antigenic presentation capacity of BMDC stimulated in the presence of rapamycin to activate ASP2-specific $CD8^+$ T-cells. Purified $CD8^+$ cells from mice previously immunized with AdASP-2 were co-cultured with antigen-loaded BMDC under the same conditions as described

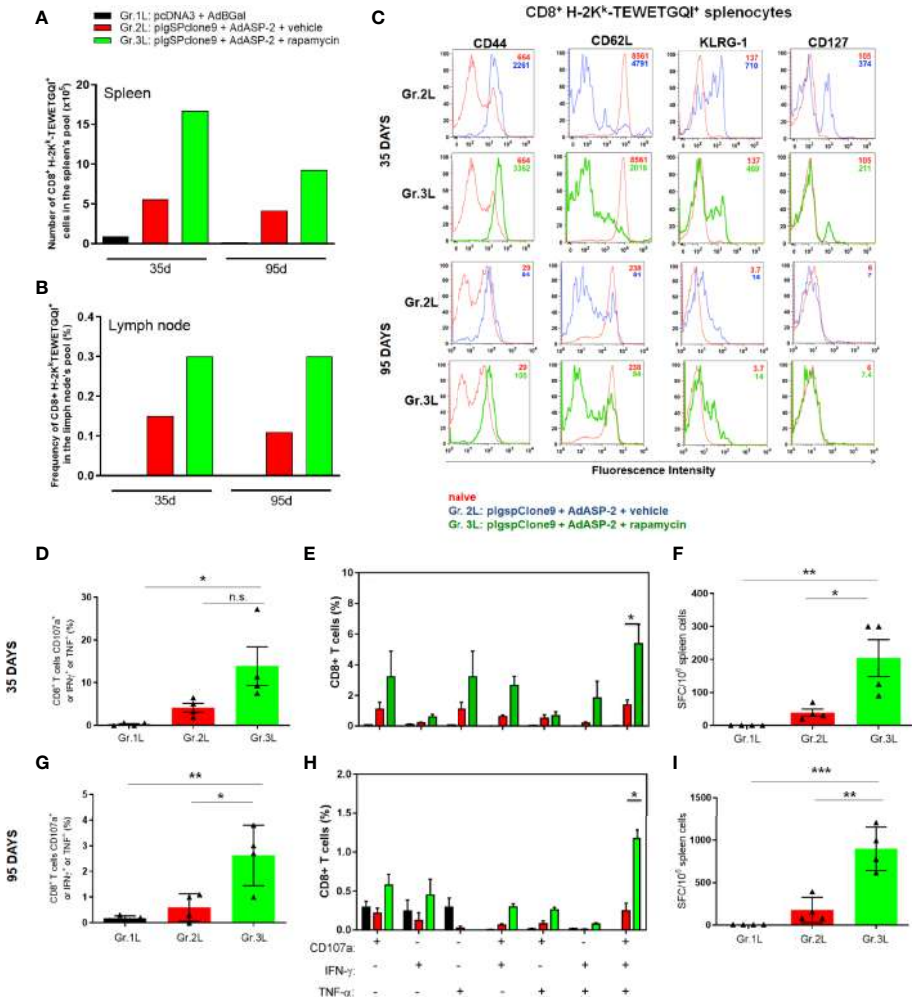

FIGURE 6 | Rapamycin increased the frequency of specific CD8+ T cell and immune responses from A/Sn mice, after 35 or 95 days after priming. A/Sn mice were immunized *via* i.m. with plasmid (10 μg) and adenovirus (2 x 10^7 pfu) according to the experimental groups described in the method section. They were also treated daily with rapamycin or vehicle (i.p.) for 34 days. 35 or 95 days from priming, cells from spleen or lymph nodes were collected for surface staining or *ex vivo* assays. **(A)** Absolut number of specific CD8+ T H2Kk-TEWETGQI+ cells from spleen's pool of each group. **(B)** Frequency of specific CD8+ T H2Kk-TEWETGQI+ cells from lymph node's pool of each group. **(C)** Histograms show the expression of the markers cited above in CD8+ H2Kk-TEWETGQI+ cells from Gr.2 (blue lines) and Gr.3 (green lines), or in CD8+ H2Kk-TEWETGQI- from naïve mice (red lines). **(D, G)** CD8+ T cell frequencies in percentage expressing CD107a, IFNγ or TNF after stimulation. **(E, H)** Subpopulations of CD8+ T cells expressing each individual molecule or combinations (CD107a, IFNγ and/or TNF). **(F, I)** ELISpot assay plots shows mean ± SD of IFNγ producing cells. SFC: Spot-forming cells. Statistical analysis was performed using the *One-Way* ANOVA and Tukey's HSD tests. Asterisks indicate significant differences among groups, defined as $^*P < 0.05$, $^{**}P < 0.01$, and $^{***}P < 0.001$. Data referring of 2 experiments and 4 mice per group. N.S., Non-significant.

above, for 24 hours. The frequency of IFNγ-producing cells was detected by ELISpot. Interestingly, unlike expected, the *in vitro* antigenic presentation by BMDC in the presence of rapamycin decreased CD8+ T-cell activation, since the number of IFNγ secreting cells was lower with the VNHRFTLV peptide or AdASP-2 and rapamycin (**Figure 8C**).

DISCUSSION

The heterologous prime-boost strategy is a well-established protocol capable of generating an effective response by inducing specific CD8+ T-cells against *T. cruzi*. The characterization of the phenotype and function of specific CD8+ T-lymphocytes show that these cells secrete IFNγ and TNF, express CD107a and are highly cytotoxic *in vivo* (De Alencar et al., 2009). Furthermore, this protocol was able to protect highly susceptible mice in experimental challenges with *T. cruzi* (De Alencar et al., 2009; Dominguez et al., 2011; Rigato et al., 2011). However, we showed here that treatment with rapamycin during immunization was able to potentiate the response of -specific CD8+ T-cells.

The number and frequency of immunization-specific CD8+ T-cells increased significantly in the rapamycin-treated mice,

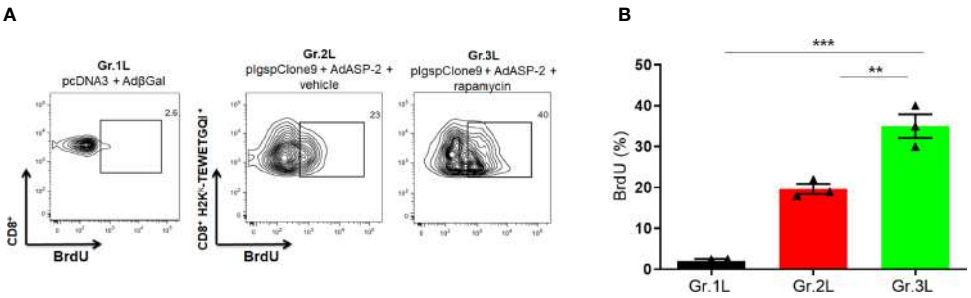

FIGURE 7 | *In vivo* proliferation of specific CD8+ T cells was higher in rapamycin-treated group during immunization. A/Sn mice were immunized *via* i.m. with plasmid (10 μg) and adenovirus (2 x 10^7 pfu) according to the experimental groups described in the method section. They were also treated daily with rapamycin or vehicle (i.p.) for 34 days. Mice were also treated with BrdU after boosting, every 48 hours (2 mg) *via* i.p. **(A)** Fifteen days after boosting, the splenocytes were collected and labeled with anti-CD8, $H2K^k$-TEWETGQI+ multimer and anti-BrdU to quantify the frequency of incorporating-BrdU cells during immunization. **(B)** Frequencies of BrdU incorporation in CD8+ $H2K^k$-TEWETGQI+ cells with mean ± SD. Statistical analysis was performed using the *One-Way* ANOVA and Tukey's HSD tests. Asterisks indicate significant differences among groups, defined as $^{**}P < 0.01$ and $^{***}P < 0.001$. Data referring of 3 mice per group.

even after 95 days after priming. It implies that cell contraction was delayed, and rapamycin treatment elicited memory precursor CD8+ T-cells rather than short-lived cells. In addition, specific CD8+ T-cells generated by immunization and rapamycin treatment showed a TE phenotype after 35 days from priming, and acquire subsequently a TEM profile, which was previously characterized in studies by our group (Rigato et al., 2011). Although rapamycin treatment has been reported to modulate the transition from effector to memory cells, especially to TCM after viral infections and tumors (Araki et al., 2009; Li et al., 2011; Turner et al., 2011; Li et al., 2012; Mattson et al., 2014; Shrestha et al., 2014), this modulation was not detected in our model. However, similar to our results, rapamycin combined with OX-40 stimulation induced a CD8+ memory population with a TEM profile following immunization with AdHu5 against LCMV (33), as well as found during the treatment with rapamycin in a carcinoma model (Jung et al., 2018).

The superiority between the TEM and TCM memory profiles is not yet fully established. Although TCM cells have been reported to provide superior long-term protection against systemic infections (Zaph et al., 2004; Klebanoff et al., 2005; Angelosanto and Wherry, 2010), this memory phenotype does not necessarily represent higher quality (Lanzavecchia and Sallusto, 2005). Indeed, CD8+ TEM cells generated by heterologous prime-boost immunization protocol confer immunity and protection against *T. cruzi* in acute and chronic infections (De Alencar et al., 2009; Haolla et al., 2009; Rigato et al., 2011; Araújo et al., 2014). TEM CD8+ T cells can respond fast during recall and this quality is crucial for protection of individuals in endemic areas.

Additionally, the analysis of the functional response performed by specific CD8+ T-cells showed that rapamycin-treated mice had an increased CD8+ T response, with greater magnitude and number of polyfunctional cells (IFNγ+, TNF+, CD107a+), especially 95 days after priming. Similar results in CD8+ T cell polyfunctionality improvement was found after rapamycin-treatment of rhesus macaques immunized against vaccinia, up to 140 days after immunization, as well as following infection with LCMV (Turner et al., 2011). These results were found here also in mice immunized with 10-fold lower doses of plasmid/adenovirus lasting up to 95 days after priming. Regarding the cytotoxic function, after *in vivo* challenge, CD8+ T-cells cytotoxic activity was higher in the rapamycin-treated mice with both peptides concentrations, which enriches the adjuvant potential of rapamycin treatment during the immune challenge of CD8+ T-cells, generating functional cells and memory precursors (Araki et al., 2009; Pearce et al., 2009; Mannick et al., 2014; de Souza et al., 2016).

We described for the first time the treatment with rapamycin was able to improve the protection of susceptible A/Sn mice immunized with 10-fold lower doses of plasmid/adenovirus in the experimental challenge with *T. cruzi*. Surprisingly, the rapamycin-treated mice resisted the experimental challenge and showed maximum survival, while only 42.8% of the vehicle-injected mice (Gr.2L) resisted. Immune response assays performed in A/Sn mice also showed that specific CD8+ T-cell frequency was higher in the rapamycin-treated group in the spleen and lymph node, as well as the production of IFNγ and the number of polyfunctional cells. Taken together, these results strongly confirm the positive effect of rapamycin during immunization, as differences were found in distinct mouse strains up to 95 days after the priming.

Related to the increase in specific CD8+ T population, the results obtained here suggest that rapamycin induced a higher proliferation rate of specific CD8+ T-cells during differentiation and expansion phase, which occurs concurrently with *in vivo* rapamycin treatment. Although it was reported by Araki (Araki et al., 2009) that after 30 days of viral challenge and rapamycin treatment there was minimal incorporation of BrdU into DNA of specific CD8+ T-cells in all groups, showing that the decrease in T-cell contraction was not due to increase of cell proliferation but probably by survival, our data indicate that modulation exerted by rapamycin may inhibit cell contraction by different mechanisms, depending on the infection model and vaccine protocol used.

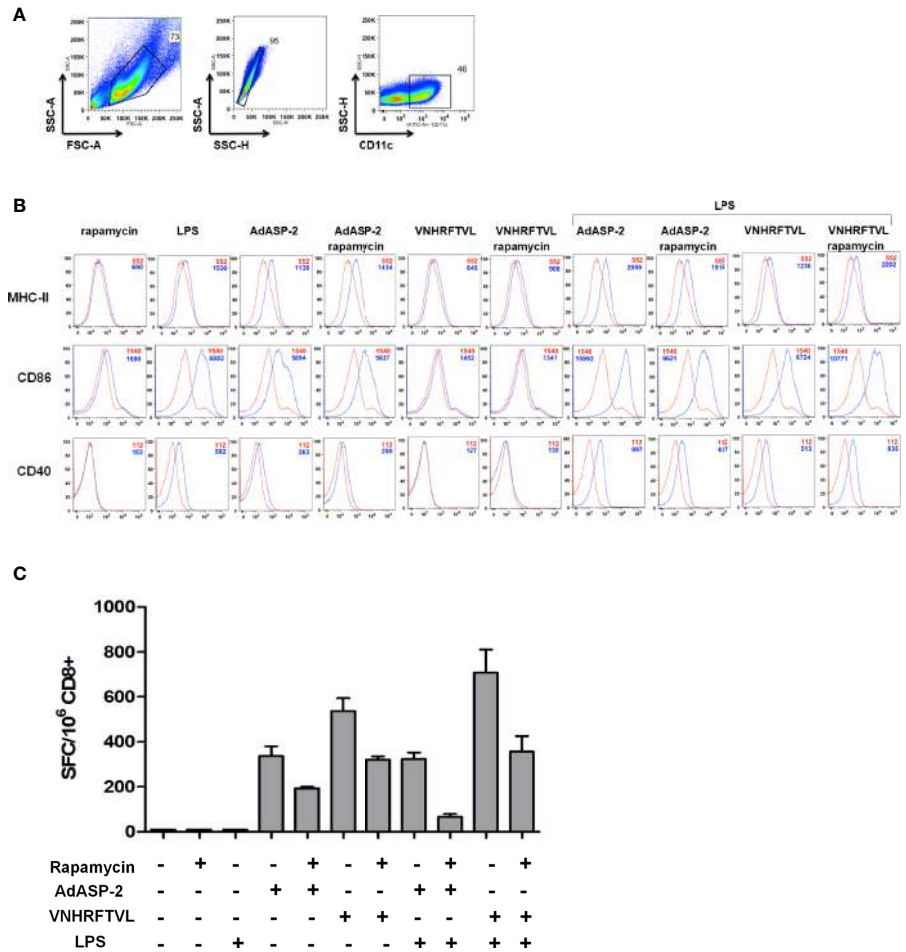

FIGURE 8 | Rapamycin did not affect the MHC-I expression and costimulatory molecules in BMDC, but impaired antigen presentation capacity to CD8+ T cells. *In vitro*-generated BMDC from C57BL/6 mice strain were incubated with VNHRFTLV peptide (1 hour), AdASP-2 (24 hours) (blue curves) or left untreated (red curves). Some conditions were treated with rapamycin (1 μM) during stimulation. The same experiment was performed with LPS-primed BMDC (200 ng/mL for 3 hours). The surface expression of CD40, CD86 and MHC class I ($H2K^b$) molecules were analyzed by flow cytometry. **(A)** Gate strategy used to select BMDCs $CD11c^+$. **(B)** Histograms with the fluorescence intensities (MFI) of the markers in $CD11c^+$ cells in unstimulated (red lines) or stimulated (blue lines). **(C)** Purified $CD8^+$ T cells were obtained from the spleens of C57BL/6 mice immunized with AdASP-2 ($2x10^7$ pfu) 15 days earlier. The purified $CD8^+$ T cells were co-cultured with loaded-BMDC and incubated overnight. The frequency of IFNγ-producing cells was detected by ELISpot. The results correspond to the mean ± SD of triplicate values of one experiment. For negative control, $CD8^+$ T cells from naive mice were also incubated, but did not produce spots.

By investigating the effect of rapamycin on dendritic cells and how it would influence cellular response, the treatment suppressed $CD8^+$ T-cell presentation and activation ability. This result corroborates previous studies showing that inhibition of mTOR appears to suppress DCs differentiation and maturation, so the cells exposed to rapamycin have an impaired ability to stimulate T-cells and cytokine production (Hackstein et al., 2003; Araki et al., 2010). Another *in vitro* study showed a suppressive effect on some aspects of DCs function at high doses of rapamycin, while at decreasing doses this effect was reversed, promoting the inflammatory function of cytokines (Gammon et al., 2017). Taken together, these data suggest that mTOR signaling has several effects on both inhibitory and stimulatory dendritic cells.

It is important to mention that our results presented some limitations, including the small sample size used in both *in vivo* and *in vitro* experiments as well as the use of splenocyte's pools instead of individual splenocytes in the multimer experiments with A/Sn mice. Despite that, our findings are exciting and open new approaches to understand and validate the modulation made by rapamycin in vaccine context.

By knowing this, it is not clear how the blockage by rapamycin and mTOR pathways may interact synergistically to improve $CD8^+$ T-cell memory. Several published studies have demonstrated that autophagy and metabolic switches are important for memory development (Araki et al., 2009; Pearce et al., 2009; Jagannath and Bakhru, 2012; Puleston et al., 2014; Xu et al., 2014; Chang and Pearce, 2016). Following activation, $CD8^+$

T-cells increase their glucose uptake and produce ATP by glycolysis through mTORC1 signaling. After the contraction phase, the memory population acquires a catabolic metabolism based on oxidative phosphorylation by the oxidation of fatty acids (FAO) and amino acids (Jones and Thompson, 2007). Pearce (Pearce et al., 2009) demonstrated that fat acid oxidation regulates memory development of $CD8^+$ T-cells. Additionally, autophagy has been also described as important to memory formation of $CD8^+$ T-cells due to the molecules recycling, damage repairing and product substrates for oxidative phosphorylation and FAO (Puleston et al., 2014; Xu et al., 2014). Since activation and other cellular processes lead to activation of mTOR, which induces glycolysis to support cell growth, proliferation and cell function (Chang and Pearce, 2016), it will be necessary to examine whether mTOR inhibition during immunization could interfere with T cell metabolism and bioenergetic capacity, polarizing the response to a metabolic profile similar to long-term memory cells.

The induction of memory cells is important due to long-lasting persistence, but also due to the ability to respond in the antigen recall. A catabolic capacity and greater mitochondrial mass confer the ability to respond fast and powerfully against the antigen, providing long-lasting protection (van der Windt et al., 2013). Therefore, the interest in generating a functional memory population through modulating their metabolic profile and energy capacity, will have more concern in the vaccine development field against chronic diseases and tumors.

Although rapamycin inhibition of mTOR has been reported to impair the differentiation of effector $CD8^+$ T-cells, lead to loss of function, failure to control viral infections and cellular anergy (Araki et al., 2010; Yao et al., 2013; Goldberg et al., 2014), this was not observed in this study. Indeed, it was evident that treatment with rapamycin in our vaccination model does not impair the differentiation of the specific $CD8^+$ T population, cytokine production and cytotoxic activity, both in the effector and memory phases, which culminates in increased protection after challenge with *T. cruzi*.

Importantly, the dose of rapamycin used in our study and others cited was suboptimal, since low doses were used compared to treatments aimed an immunosuppression effect (Araki et al., 2009; Araki et al., 2010; Gammon et al., 2017). *In vivo* drug's administration was unable to completely block mTOR signaling and this inhibition occurs in a dose-dependent manner (Araki et al., 2009; Gammon et al., 2017), as observed in $CD8^+$ T-cells when mTOR expression was decreased by RNAi, suggesting that rapamycin stimulates the formation of memory $CD8^+$ T-cells by incompletely inhibition of mTOR signaling. Higher doses of rapamycin may result in suppression of $CD8^+$ T cell expansion (Araki et al., 2009).

Given that mTOR signaling plays a central role in regulating cellular responses, this appears to be a potential pathway to be explored for modulating immune responses induced by vaccines (Sallusto et al., 2010). Here, we have shown for the first time the use of rapamycin improves functional qualities as well as the frequency of specific $CD8^+$ T-cells generated by heterologous prime-boost immunization against *T. cruzi*. This adjuvant effect was seen during the effector and memory phase, even with low immunogenic doses induced by the vaccination, besides promoting protection after experimental challenge. We speculate that mTOR inhibition by rapamycin is acting synergistically on $CD8^+$ T-cells, modulating their activation, proliferation, differentiation and possibly their metabolism. Although some mechanisms need to be further elucidated, these findings suggest that strategic rapamycin treatment may improve effector and memory cell development in response to vaccine protocols, offering a new method for adjusting the desired immune response as well as plasticity, phenotype and cellular function.

In order to induce a population with a phenotype that provides optimal protection and functional qualities of memory $CD8^+$ T-cells against the target pathogen, we provided herein a novel approach to upgrade the efficacy of genetic vaccines against intracellular infections, such as Chagas disease.

DATA AVAILABILITY STATEMENT

The raw data supporting the conclusions of this article will be made available by the authors, without undue reservation.

ETHICS STATEMENT

The animal study was reviewed and approved by Ethical Committee for Animal Experimentation at the Federal University of Sao Paulo, registered under number 9959021014.

AUTHOR CONTRIBUTIONS

BM, MR and JV conceived and designed the experiments. BM, IN, CF, LC, CM, PD, and TV performed the experiments. BM, IN, CF and JV analyzed the experiment data. RG, JL-V, KB, GP and JV contributed with reagents and materials, and additional experiments design. BM wrote the manuscript. BM, JL-V, KB and JV reviewed the manuscript. All authors contributed to the article and approved the submitted version.

FUNDING

This work was supported by grants from Fundação de Amparo à Pesquisa do Estado de São Paulo (http://www.fapesp.br/) (BM: 2014/19422-5, 2016/02840-4; CF: 2015/08814-2; JV: 2012/22514-3, 2018/15607-1), Instituto Nacional de Ciência e Tecnologia em Vacinas (http://inct.cnpq.br/), Coordenação de Aperfeiçoamento de Pessoal de Nível Superior (http://www.capes.gov.br/) and Conselho Nacional de Desenvolvimento Científico e Tecnológico (http://cnpq.br/).

ACKNOWLEDGMENTS

This work is a tribute to the memory of Dr. Mauricio Martins Rodrigues.

SUPPLEMENTARY MATERIAL

The Supplementary Material for this article can be found online at: https://www.frontiersin.org/articles/10.3389/fcimb.2021.676183/full#supplementary-material

Supplementary Figure 1 | Expression of Ribosomal Phospho-S6 (PS6) protein in $CD8^+$ T cells after treatment with rapamycin. Splenocytes from naïve mice were incubated with Concavalin A (2 mg/mL) or rapamycin (100 nM) for one hour. Then, cells were stained with anti-CD8, fixed and permeabilizated to anti-pS6K staining. **(A)** Dot-plots show the frequency of pS6K in singlets in each condition. **(B)** Histograms indicate the mean of fluorescence intensity of cells in medium (red line), treated with rapamycin (green line) or stimulated with ConA (blue line).

Supplementary Figure 2 | Strategy used for analysis of intracellular staining of cytokines in $CD8^+$ T cells. Splenocytes were treated conform described in the methods section. **(A)** Gate strategy used for positive selection of $CD8^+$ cells. **(B)** Dot-plots represent the frequencies of CD107a, IFNg and TNF in $CD8^+$ T cells from immunized mice after stimulation with the specific peptide in vitro. Data correspondent to a representative mouse.

Supplementary Figure 3 | Immunophenotyping of specific $CD8^+$ T cells from C57BL/6 mice immunized and treated with rapamycin or diluent after 35 days from priming. C57BL/6 mice were immunized via i.m. with plasmid (100 µg) and adenovirus (2×10^8 pfu) according to the experimental groups described in the method section. They were also treated daily with rapamycin or vehicle (i.p.) for 34 days. After 35 days from priming, splenocytes were labeled with anti-CD8, $H2K^b$-VNHRFTLV multimer and with the specific markers indicated above for flow cytometric analysis. Histograms show the expression of the markers in $CD8^+$ $H2K^b$-$VNHRFTLV^+$ cells (blue and green lines) or $CD8^+$ cells of naive as control (red lines). Analyses were performed using cells pools of 4 mice and they are representative of two independent experiments. The numbers indicate the mean fluorescence intensity (MFI). The individual analysis of mice from each group presented similar results.

Supplementary Figure 4 | Immunophenotyping of specific $CD8^+$ T cells of C57BL/6 mice immunized and treated with rapamycin or diluent after 95 from priming. C57BL/6 mice were immunized *via* i.m. with plasmid (100 µg) and adenovirus (2×10^8 pfu) according to the experimental groups described in the method section. They were also treated daily with rapamycin or vehicle (i.p.) for 34 days. After 35 days from priming, splenocytes were labeled with anti-CD8, $H2K^b$-VNHRFTLV multimer and with the specific markers indicated above for flow cytometric analysis. Histograms show the expression of the markers in $CD8^+$ $H2K^b$-$VNHRFTLV^+$ cells (blue and green lines) or $CD8^+$ cells of naive as control (red lines). Analyses were performed using cells pools of 4 mice and they are representative of two independent experiments. The numbers indicate the mean fluorescence intensity (MFI). The individual analysis of mice from each group presented similar results.

Supplementary Figure 5 | In vivo cytotoxicity of specific $CD8^+$ T cells of C57BL/6 mice immunized and treated with rapamycin or diluent. C57BL/6 mice were immunized *via* i.m. with plasmid (100 µg) and adenovirus (2×10^8 pfu) according to the experimental groups described in the method section. They were also treated daily with rapamycin or vehicle (i.p.) for 34 days. Splenocytes from naive mice were stained with CFSE in 2 different concentrations. $CFSE^{High}$ population was pulsed with peptide VNHRFTLV at a final concentration of 2 mM. $CFSE^{Low}$ was the negative control. Stained cells were transferred to the experimental groups and, after 14 hours, spleens were harvested to quantify the frequency of stained cells. **(A)** Histograms represent the frequencies of $CFSE^{High}$ and $CFSE^{Low}$ in each group. **(B)** Percentage of $CD8^+$ T mediated cytotoxicity, with mean ± SD. Results from one experiment and 4 mice per group. Statistical analysis was performed using the One-Way ANOVA and Tukey's HSD tests. Asterisks indicate significant differences among groups, defined as $^*P < 0.05$, $^{**}P < 0.01$, and $^{***}P < 0.001$. N.S., Non-significant.

Supplementary Figure 6 | Experimental challenge of A/sn mice after treatment with rapamycin or vehicle. A/Sn mice were treated daily with rapamycin or vehicle (PBS) for 34 days. On the last day, mice were infected with 150 blood trypomastigotes of Y strain of T. cruzi. **(A)** Parasitemia was monitored daily between days 6 and 15 after challenge. The parasitemia values were log transformed. **(B)** The survival rate was also followed and analyzed by Log-rank (Mantel-Cox) test (all groups p = 0,0285). Results from 4 mice per group.

REFERENCES

Ahmed, R., and Akondy, R. S. (2011). Insights Into Human CD8+ T-Cell Memory Using the Yellow Fever and Smallpox Vaccines. *Immunol. Cell Biol.* 89, 340–345. doi: 10.1038/icb.2010.155

Amiel, E., Everts, B., Freitas, T. C., King, I. L., Curtis, J. D., Pearce, E. L., et al. (2012). Inhibition of Mechanistic Target of Rapamycin Promotes Dendritic Cell Activation and Enhances Therapeutic Autologous Vaccination in Mice. *J. Immunol* 189 (5), 2151–2158. doi: 10.4049/jimmunol.1103741

Angelosanto, J. M., and Wherry, E. J. (2010). Transcription Factor Regulation of CD8+ T-Cell Memory and Exhaustion. *Immunol. Rev.* 236, 167–175. doi: 10.1111/j.1600-065X.2010.00927.x

Araki, K., Turner, A. P., Shaffer, V. O., Gangappa, S., Keller, S. A., Bachmann, M. F., et al. (2009). mTOR Regulates Memory CD8 T-Cell Differentiation. *Nature* 460, 108–112. doi: 10.1038/nature08155

Araki, K., Youngblood, B., and Ahmed, R. (2010). The Role of mTOR in Memory CD8+ T-Cell Differentiation. *Immunol. Rev.* 235 (1), 234–243. doi: 10.1111/j.0105-2896.2010.00898.x

Araújo, A. F., de Oliveira, G., Vasconcelos, J. F., Ersching, J., Dominguez, M. R., Vasconcelos, J. R., et al. (2014). Genetic Vaccination Against Experimental Infection With Myotropic Parasite Strains of Trypanosoma Cruzi. *Mediators Inflamm.* 2014, 1–13. doi: 10.1155/2014/605023

Augustine, J. J., Bodziak, K. A., and Hricik, D. E. (2007). Use of Sirolimus in Solid Organ Transplantation. *Drugs* 67 (3), 369–391. doi: 10.2165/00003495-200767030-00004

Bassett, J. D., Swift, S. L., Vanseggelen, H., Hammill, J. A., McGray, A. R., Evelegh, C., et al. (2012). Combined mTOR Inhibition and OX40 Agonism Enhances CD8 T Cell Memory and Protective Immunity Produced by Recombinant Adenovirus Vaccines. *Mol. Ther.* 20, 860–869. doi: 10.1038/mt.2011.281

Borsa, M., Barnstorf, I., Baumann, N. S., Pallmer, K., Yermanos, A., Gräbnitz, F., et al. (2019). Modulation of Asymmetric Cell Division as a Mechanism to Boost CD8+ T Cell Memory. *Sci. Immunol.* 4 (34), eaav1730. doi: 10.1126/sciimmunol.aav1730

Buck, M. D., O'Sullivan, D., and Pearce, E. L. (2015). T Cell Metabolism Drives Immunity. *J. Exp. Med.* 212 (9), 1345–1360. doi: 10.1084/jem.20151159

Chang, C. H., and Pearce, E. L. (2016). Emerging Concepts of T Cell Metabolism as a Target of Immunotherapy. *Nat. Immunol.* 17 (4), 364–368. doi: 10.1038/ni.3415

Chuang, I., Sedegah, M., Cicatelli, S., Spring, M., Polhemus, M., Tamminga, C., et al. (2013). Dna Prime/Adenovirus Boost Malaria Vaccine Encoding P. Falciparum CSP and AMA1 Induces Sterile Protection Associated With Cell-Mediated Immunity. *PloS One* 8 (2), e55571. doi: 10.1371/journal.pone.0055571

Cui, W., and Kaech, S. M. (2010). Generation of Effector CD8+ T Cells and Their Conversion to Memory T Cells. *Immunol. Rev.* 236, 151–166. doi: 10.1111/j.1600-065X.2010.00926.x

De Alencar, B. C. G., Persechini, P. M., Haolla, F. A., De Oliveira, G., Silverio, J. C., Lannes-Vieira, J., et al. (2009). Perforin and Gamma Interferon Expression are Required for CD4+ and CD8+ T-Cell-Dependent Protective Immunity Against a Human Parasite, Trypanosoma Cruzi, Elicited by Heterologous Plasmid DNA Prime-Recombinant Adenovirus 5 Boost Vaccination. *Infect. Immun.* 77, 4383–4395. doi: 10.1128/IAI.01459-08

Dennis, P. B., Jaeschke, A., Saitoh, M., Fowler, B., Kozma, S. C., and Thomas, G. (2001). Mammalian TOR: A Homeostatic ATP Sensor. *Sci. (80-)* 294 (5544), 1102–1105. doi: 10.1126/science.1063518

de Souza, A. P. D., de Freitas, D. N., Antuntes Fernandes, K. E., D'Avila da Cunha, M., Antunes Fernandes, J. L., Benetti Gassen, R., et al. (2016). Respiratory Syncytial Virus Induces Phosphorylation of mTOR At ser2448 in CD8 T Cells From Nasal Washes of Infected Infants. *Clin. Exp. Immunol.* 183, 248–257. doi: 10.1111/cei.12720

Dominguez, M. R., Silveira, E. L. V., de Vasconcelos, J. R. C., de Alencar, B. C. G., Machado, A. V., Bruna-Romero, O., et al. (2011). Subdominant/Cryptic CD8 T Cell Epitopes Contribute to Resistance Against Experimental Infection With a Human Protozoan Parasite. *PloS One* 6, e22011. doi: 10.1371/journal.pone.0022011

Elvang, T., Christensen, J. P., Billeskov, R., Thi Kim Thanh Hoang, T., Holst, P., Thomsen, A. R., et al. (2009). CD4 and CD8 T Cell Responses to the M. Tuberculosis Ag85B-TB10.4 Promoted by Adjuvanted Subunit, Adenovector or Heterologous Prime Boost Vaccination. *PloS One* 4, e5139. doi: 10.1371/journal.pone.0005139

Ersching, J., Basso, A. S., Kalich, V. L. G., Bortoluci, K. R., and Rodrigues, M. M. (2016). A Human Trypanosome Suppresses CD8+ T Cell Priming by Dendritic Cells Through the Induction of Immune Regulatory CD4+ Foxp3+ T Cells. *PloS Pathog.* 12, 1–23. doi: 10.1371/journal.ppat.1005698

Ersching, J., Efeyan, A., Mesin, L., Jacobsen, J. T., Pasqual, G., Grabiner, B. C., et al. (2017). Germinal Center Selection and Affinity Maturation Require Dynamic Regulation of mTORC1 Kinase. *Immunity* 46, 1045–1058.e6. doi: 10.1016/j.immuni.2017.06.005

Ferreira, C. P., Cariste, L. M., Virgílio, F. D. S., Moraschi, B. F., Monteiro, C. B., Machado, A. M. V., et al. (2017). LFA-1 Mediates Cytotoxicity and Tissue Migration of Specific CD8+ T Cells After Heterologous Prime-Boost Vaccination Against Trypanosoma Cruzi Infection. *Front. Immunol.* 8, 1291. doi: 10.3389/fimmu.2017.01291

Gammon, J. M., Gosselin, E. A., Tostanoski, L. H., Chiu, Y. C., Zeng, X., Zeng, Q., et al. (2017). Low-Dose Controlled Release of mTOR Inhibitors Maintains T Cell Plasticity and Promotes Central Memory T Cells. *J. Control Release* 263, 151–161. doi: 10.1016/j.jconrel.2017.02.034

Gilbert, S. C., Schneider, J., Hannan, C. M., Hu, J. T., Plebanski, M., Sinden, R., et al. (2002). Enhanced CD8 T Cell Immunogenicity and Protective Efficacy in a Mouse Malaria Model Using a Recombinant Adenoviral Vaccine in Heterologous Prime-Boost Immunisation Regimes. *Vaccine* 20, 1039–1045. doi: 10.1016/S0264-410X(01)00450-9

Goldberg, E. L., Smithey, M. J., Lutes, L. K., Uhrlaub, J. L., and Nikolich-Žugich, J. (2014). Immune Memory–Boosting Dose of Rapamycin Impairs Macrophage Vesicle Acidification and Curtails Glycolysis in Effector Cd8 Cells, Impairing Defense Against Acute Infections. *J. Immunol.* 193 (2), 757–763. doi: 10.4049/jimmunol.1400188

Graham, S. P., McLean, R. K., Spencer, A. J., Belij-Rammerstorfer, S., Wright, D., Ulaszewska, M., et al. (2020). Evaluation of the Immunogenicity of Prime-Boost Vaccination With the Replication-Deficient Viral Vectored COVID-19 Vaccine Candidate ChAdOx1 Ncov-19. *NPJ Vaccines* 5 (1), 69. doi: 10.1038/s41541-020-00221-3

Hackstein, H., Taner, T., Zahorchak, A. F., Morelli, A. E., Logar, A. J., Gessner, A., et al. (2003). Rapamycin Inhibits IL-4-Induced Dendritic Cell Maturation In Vitro and Dendritic Cell Mobilization and Function In Vivo. *Blood* 101 (11), 4457–4463. doi: 10.1182/blood-2002-11-3370

Haolla, F. A., Claser, C., de Alencar, B. C. G., Tzelepis, F., de Vasconcelos, J. R., de Oliveira, G., et al. (2009). Strain-Specific Protective Immunity Following Vaccination Against Experimental Trypanosoma Cruzi Infection. *Vaccine* 27, 5644–5653. doi: 10.1016/j.vaccine.2009.07.013

Hensley, L. E., Mulangu, S., Asiedu, C., Johnson, J., Honko, A. N., Stanley, D., et al. (2010). Demonstration of Cross-Protective Vaccine Immunity Against an Emerging Pathogenic Ebolavirus Species. *PloS Pathog.* 6 (5), e1000904. doi: 10.1371/journal.ppat.1000904

Hill, A. V. S., Reyes-Sandoval, A., O'Hara, G., Ewer, K., Lawrie, A., Goodman, A., et al. (2010). Prime-Boost Vectored Malaria Vaccines: Progress and Prospects. *Hum. Vaccin* 6, 78–83. doi: 10.4161/hv.6.1.10116

Jacobs, S. R., Herman, C. E., MacIver, N. J., Wofford, J. A., Wieman, H. L., Hammen, J. J., et al. (2008). Glucose Uptake is Limiting in T Cell Activation and Requires Cd28-Mediated Akt-Dependent and Independent Pathways. *J. Immunol.* 180 (7), 4476–4486. doi: 10.4049/jimmunol.180.7.4476

Jagannath, C., and Bakhru, P. (2012). Rapamycin-Induced Enhancement of Vaccine Efficacy in Mice. *Methods Mol. Biol.* 821, 295–303. doi: 10.1007/978-1-61779-430-8_18

Jagannath, C., Lindsey, D. R., Dhandayuthapani, S., Xu, Y., Hunter, R. L., and Eissa, N. T. (2009). Autophagy Enhances the Efficacy of BCG Vaccine by Increasing Peptide Presentation in Mouse Dendritic Cells. *Nat. Med.* 15 (3), 267–276. doi: 10.1038/nm.1928

Jones, R. G., and Thompson, C. B. (2007). Revving the Engine: Signal Transduction Fuels T Cell Activation. *Immunity* 27 (2), 173–178. doi: 10.1016/j.immuni.2007.07.008

Jung, J. W., Veitch, M., Bridge, J. A., Overgaard, N. H., Cruz, J. L., Linedale, R., et al. (2018). Clinically-Relevant Rapamycin Treatment Regimens Enhance CD8+ Effector Memory T Cell Function in The Skin and Allow Their Infiltration Into Cutaneous Squamous Cell Carcinoma. *Oncoimmunology* 7 (9), e1479627. doi: 10.1080/2162402X.2018.1479627

Klebanoff, C. A., Waldmann, T. A., Palmer, D. C., Torabi-Parizi, P., Restifo, N. P., Cardones, A. R., et al. (2005). Central Memory Self/Tumor-Reactive CD8+ T Cells Confer Superior Antitumor Immunity Compared With Effector Memory T Cells. *Proc. Natl. Acad. Sci.* 102, 9571–9576. doi: 10.1073/pnas.0503726102

Lanzavecchia, A., and Sallusto, F. (2005). Understanding the Generation and Function of Memory T Cell Subsets. *Curr. Opin. Immunol.* 17, 326–332. doi: 10.1016/j.coi.2005.04.010

Li, X., Garcia, K., Sun, Z., and Xiao, Z. (2011). Temporal Regulation of Rapamycin on Memory CTL Programming by IL-12. *PloS One* 6 (9), e25177. doi: 10.1371/journal.pone.0025177

Li, Q., Rao, R., Vazzana, J., Goedegebuure, P., Odunsi, K., Gillanders, W., et al. (2012). Regulating mTOR to Tune Vaccination Induced CD8+ T Cell Responses for Tumor Immunity. *J. Immunol.* 188, 3080–3087. doi: 10.4049/jimmunol.1103365.Regulating

Li, S., Rodrigues, M., Rodriguez, D., Rodriguez, J. R., Esteban, M., Palese, P., et al. (1993). Priming With Recombinant Influenza Virus Followed by Administration of Recombinant Vaccinia Virus Induces CD8+ T-Cell-Mediated Protective Immunity Against Malaria. *Proc. Natl. Acad. Sci.* 90 (11), 5214–5218. doi: 10.1073/pnas.90.11.5214

Mannick, J. B., Del Giudice, G., Lattanzi, M., Valiante, N. M., Praestgaard, J., Huang, B., et al. (2014). mTOR Inhibition Improves Immune Function in the Elderly. *Sci. Transl. Med.* 6 (268), 268ra179. doi: 10.1126/scitranslmed.3009892

Mannick, J. B., Morris, M., Hockey, H. U., Roma, G., Beibel, M., Kulmatycki, K., et al. (2018). TORC1 Inhibition Enhances Immune Function and Reduces Infections in the Elderly. *Sci. Transl. Med.* 10 (449), eaaq1564. doi: 10.1126/scitranslmed.aaq1564

Martins, M. A., Wilson, N. A., Reed, J. S., Ahn, C. D., Klimentidis, Y. C., Allison, D. B., et al. (2010). T-Cell Correlates of Vaccine Efficacy After a Heterologous Simian Immunodeficiency Virus Challenge. *J. Virol* 84 (9), 4352–4365. doi: 10.1128/jvi.02365-09

Mattson, E., Xu, L., Li, L., Liu, G. E., and Xiao, Z. (2014). Transcriptome Profiling of CTLs Regulated by Rapamycin Using RNA-Seq. *Immunogenetics* 66, 625–633. doi: 10.1007/s00251-014-0790-5

McConkey, S. J., Reece, W. H. H., Moorthy, V. S., Webster, D., Dunachie, S., Butcher, G., et al. (2003). Enhanced T-cell Immunogenicity of Plasmid DNA Vaccines Boosted by Recombinant Modified Vaccinia Virus Ankara in Humans. *Nat. Med.* 9, 729–735. doi: 10.1038/nm881

Nam, J. H. (2009). Rapamycin: Could it Enhance Vaccine Efficacy? *Expert Rev. Vaccines* 8, 1535–1539. doi: 10.1586/erv.09.115

Pearce, E. L., Walsh, M. C., Cejas, P. J., Harms, G. M., Shen, H., Wang, L. S., et al. (2009). Enhancing CD8 T-Cell Memory by Modulating Fatty Acid Metabolism. *Nature* 460 (7251), 103–107. doi: 10.1038/nature08097

Pérez-Molina, J. A., and Molina, I. (2017). Chagas Disease. *Lancet* 6736, 1–13. doi: 10.1016/S0140-6736(17)31612-4

Powell, J. D., Pollizzi, K. N., Heikamp, E. B., and Horton, M. R. (2012). Regulation of Immune Responses by Mtor. *Annu. Rev. Immunol.* 30, 39–68. doi: 10.1146/annurev-immunol-020711-075024

Puleston, D. J., Zhang, H., Powell, T. J., Lipina, E., Sims, S., Panse, I., et al. (2014). Autophagy is a Critical Regulator of Memory CD8(+) T Cell Formation. *Elife* 3, e03706. doi: 10.7554/eLife.03706

Ranasinghe, C., and Ramshaw, I. A. (2009). Genetic Heterologous Prime-Boost Vaccination Strategies for Improved Systemic and Mucosal Immunity. *Expert Rev. Vaccines* 8, 1171–1181. doi: 10.1586/erv.09.86

Rao, R. R., Li, Q., Odunsi, K., and Shrikant, P. A. (2010). The Mtor Kinase Determines Effector Versus Memory Cd8 + T Cell Fate by Regulating the Expression of Transcription Factors T-bet and Eomesodermin. *Immunity* 32 (1), 67–78. doi: 10.1016/j.immuni.2009.10.010

Rigato, P. O., de Alencar, B. C., de Vasconcelos, J. R. C., Dominguez, M. R., Araújo, A. F., Machado, A. V., et al. (2011). Heterologous Plasmid Dna Prime-Recombinant Human Adenovirus 5 Boost Vaccination Generates a Stable Pool of Protective Long-Lived CD8+ T Effector Memory Cells Specific for a Human Parasite, Trypanosoma Cruzi. *Infect. Immun.* 79, 2120–2130. doi: 10.1128/iai.01190-10

Sallusto, F., Lanzavecchia, A., Araki, K., and Ahmed, R. (2010). From Vaccines to Memory and Back. *Immunity* 33 (4), 451–463. doi: 10.1016/j.immuni.2010.10.008

Sheridan, B. S., and Lefrançois, L. (2011). Regional and Mucosal Memory T Cells. *Nat. Immunol.* 12, 485–491. doi: 10.1038/ni.2029

Shrestha, S., Yang, K., Wei, J., Karmaus, P. W. F., Neale, G., and Chi, H. (2014). Tsc1 Promotes the Differentiation of Memory CD8+ T Cells Via Orchestrating the Transcriptional and Metabolic Programs. *Proc. Natl. Acad. Sci. U S A* 111, 14858–14863. doi: 10.1073/pnas.1404264111

Thomson, A. W., Turnquist, H. R., and Raimondi, G. (2009). Immunoregulatory Functions of mTOR Inhibition. *Nat. Rev. Immunol* 9 (5), 324–337. doi: 10.1038/nri2546

Turner, A. P., Shaffer, V. O., Araki, K., Martens, C., Turner, P. L., Gangappa, S., et al. (2011). Sirolimus Enhances the Magnitude and Quality of Viral-Specific CD8 + T-cell Responses to Vaccinia Virus Vaccination in Rhesus Macaques. *Am. J. Transplant* 11, 613–618. doi: 10.1111/j.1600-6143.2010.03407.x

van der Windt, G. J. W., O'Sullivan, D., Everts, B., Huang, S. C.-C., Buck, M. D., Curtis, J. D., et al. (2013). CD8 Memory T Cells Have a Bioenergetic Advantage That Underlies Their Rapid Recall Ability. *Proc. Natl. Acad. Sci.* 110, 14336–14341. doi: 10.1073/pnas.1221740110

Vasconcelos, J. R., Dominguez, M. R., Araújo, A. F., Ersching, J., Tararam, C. A., Bruna-Romero, O., et al. (2012). Relevance of Long-Lived CD8+T Effector Memory Cells for Protective Immunity Elicited by Heterologous Prime-Boost Vaccination. *Front. Immunol.* 3, 1–11. doi: 10.3389/fimmu.2012.00358

Wherry, E. J., Teichgräber, V., Becker, T. C., Masopust, D., Kaech, S. M., Antia, R., et al. (2003). Lineage Relationship and Protective Immunity of Memory CD8T Cell Subsets. *Nat. Immunol.* 4, 225–234. doi: 10.1038/ni889

Wilson, N. A., Reed, J., Napoe, G. S., Piaskowski, S., Szymanski, A., Furlott, J., et al. (2006). Vaccine-Induced Cellular Immune Responses Reduce Plasma Viral Concentrations After Repeated Low-Dose Challenge With Pathogenic Simian Immunodeficiency Virus Sivmac239. *J. Virol* 80 (12), 5875–5885. doi: 10.1128/jvi.00171-06

Wirth, T. C., Badovinac, V. P., Zhao, L., Dailey, M. O., and Harty, J. T. (2009). Differentiation of Central Memory CD8 T Cells is Independent of CD62L-Mediated Trafficking to Lymph Nodes. *J. Immunol.* 182, 6195–6206. doi: 10.4049/jimmunol.0803315

Wirth, T. C., Xue, H.-H., Rai, D., Sabel, J. T., Bair, T., Harty, J. T., et al. (2010). Repetitive Antigen Stimulation Induces Stepwise Transcriptome Diversification But Preserves a Core Signature of Memory CD8(+) T Cell Differentiation. *Immunity* 33, 128–140. doi: 10.1016/j.immuni.2010.06.014

World Health Organization. (2016). *Chagas Disease (American trypanosomiasis)*. World Health Organization. Available from: http://www.who.int/chagas/epidemiology/en/.

Wullschleger, S., Loewith, R., and Hall, M. N. (2006). TOR Signaling in Growth and Metabolism. *Cell* 124 (3), 471–484. doi: 10.1016/j.cell.2006.01.016

Xu, X., Araki, K., Li, S., Han, J. H., Ye, L., Tan, W. G., et al. (2014). Autophagy is Essential for Effector CD8 + T Cell Survival and Memory Formation. *Nat. Immunol* 15 (12), 1152–1161. doi: 10.1038/ni.3025

Yao, S., Buzo, B. F., Pham, D., Jiang, L., Taparowsky, E. J., Kaplan, M. H., et al. (2013). Interferon Regulatory Factor 4 Sustains CD8+ T Cell Expansion and Effector Differentiation. *Immunity*. doi: 10.1016/j.immuni.2013.10.007

Zaph, C., Uzonna, J., Beverley, S. M., and Scott, P. (2004). Central Memory T Cells Mediate Long-Term Immunity to Leishmania Major in the Absence of Persistent Parasites. *Nat. Med.* 10, 1104–1110. doi: 10.1038/nm1108

Zavala, F., Rodrigues, M., Rodriguez, D., Rodriguez, J. R., Nussenzweig, R. S., and Esteban, M. (2001). A Striking Property of Recombinant Poxviruses: Efficient Inducers of In Vivo Expansion of Primed CD8+ T Cells. *Virology* 280 (2), 155–159. doi: 10.1006/viro.2000.0792

Zhang, G., Huong, V. T. T., Battur, B., Zhou, J., Zhang, H., Liao, M., et al. (2007). A Heterologous Prime-Boost Vaccination Regime Using DNA and a Vaccinia Virus, Both Expressing GRA4, Induced Protective Immunity Against Toxoplasma Gondii Infection in Mice. *Parasitology* 134, 1339. doi: 10.1017/S0031182007002892

Conflict of Interest: The authors declare that the research was conducted in the absence of any commercial or financial relationships that could be construed as a potential conflict of interest.

Hormones and Behavior 137 (2022) 105087

Contents lists available at ScienceDirect

Hormones and Behavior

journal homepage: www.elsevier.com/locate/yhbeh

High and fluctuating levels of ovarian hormones induce an anxiogenic effect, which can be modulated under stress conditions: Evidence from an assisted reproductive rodent model

Bianca Santos Martins Gonçalves [a], Flora França Nogueira Mariotti [a], Giovana Ponsone [a], Thalita Aparecida Avelino Soares [a], Paula Cristina Barbosa Garcia Perão [a], Marcos Mônico-Neto [a], Leonardo Moro Cariste [a], Auro Maluf [b], Gustavo da Silva Soares Nascimento [a], Hanna Karen Moreira Antunes [a], Isabel Cristina Céspedes [a,1], Milena de Barros Viana [a], Luciana Le Sueur-Maluf [a,*]

[a] Departamento de Biociências, Universidade Federal de São Paulo, UNIFESP, 11015-020 Santos, SP, Brazil
[b] Departamento de Ciências do Mar, Universidade Federal de São Paulo, UNIFESP, 11070-102 Santos, SP, Brazil

ARTICLE INFO

Keywords:
Superovulation
Female rats
Unpredictable chronic mild stress (UCMS)
Assisted reproduction
Ovarian hormones
Anxiety disorders
Resilience

ABSTRACT

Elevated levels of endogenous ovarian hormones are conditions commonly experienced by women undergoing assisted reproductive technologies (ART). Additionally, infertility-associated stress and treatment routines are factors that together may have a highly negative impact on female emotionality, which can be aggravated when several cycles of ART are needed to attempt pregnancy. This study aimed to investigate the effect of high and fluctuating levels of gonadal hormones induced by repeated ovarian stimulation on the stress response in rodents. To mimic the context of ART, female rats were exposed to an unpredictable chronic mild stress (UCMS) paradigm for four weeks. During this time, three cycles of ovarian stimulation (superovulation) (150 IU/Kg of PMSG and 75 IU/Kg of hCG) were applied, with intervals of two estrous cycles between them. The rats were distributed into four groups: Repeated Superovulation/UCMS; Repeated Superovulation/No Stress; Saline/UCMS; and Saline/No Stress. Anxiety-like and depressive-like behaviors were evaluated in a light-dark transition box and by splash test, respectively. Corticosterone, estradiol, progesterone, and biometric parameters were assessed. Data were analyzed using a two-way Generalized Linear Model (GzLM). Our results showed that repeated ovarian stimulation exerts by itself an expressive anxiogenic effect. Surprisingly, when high and fluctuating levels of ovarian hormones were combined with chronic stress, anxiety-like behavior was no longer observed, and a depressive-like state was not detected. Our findings suggest that females subjected to emotional overload induced by repeated ovarian stimulation and chronic stress seem to trigger the elaboration of adaptive coping strategies.

1. Introduction

The relationship among stress, psychological distress, and reproduction, particularly in the context of assisted reproductive technologies (ART), has been extensively investigated (Gameiro et al., 2015; Massarotti et al., 2019; Turner et al., 2013). Stress associated with infertility has been related to several emotional disorders, which have repercussions on marital and social relationships (Rooney and Domar, 2018; Verhaak et al., 2007). The experience of infertility is perceived by the couple as one of the most challenging moments in their lives (Freeman et al., 1985; Slade et al., 2007). Even after seeking specialized treatments, such as ART, symptoms of anxiety and depression are observed in 10% to 50% of women, increasing the probability of withdrawing of treatment (Beutel et al., 1999; Boivin and Takefman, 1995; Crawford et al., 2017; Vahratian et al., 2011; Verhaak et al., 2005). Research on this topic can provide a broad understanding of the infertility experience, aiming for better psychosocial support and quality of life for patients.

* Corresponding author at: Silva Jardim, 133/136 - Vila Mathias, 11015-020 Santos, SP, Brazil.
E-mail address: luciana.maluf@unifesp.br (L. Le Sueur-Maluf).
[1] Present address: Departamento de Morfologia e Genética, Universidade Federal de São Paulo UNIFESP, 04023-900 São Paulo, SP, Brazil.

https://doi.org/10.1016/j.yhbeh.2021.105087
Received 21 July 2021; Received in revised form 24 October 2021; Accepted 14 November 2021
Available online 23 November 2021
0018-506X/

In the biological context, women undergoing ART commonly experience supraphysiological levels of ovarian hormones. Controlled ovarian stimulation induced by exogenous pituitary gonadotropins is employed to stimulate the growth of several ovarian follicles and thereby increase the chances of pregnancy. Consequently, elevated levels of endogenous estradiol and progesterone are generated (Ginsburg and Racowsky, 2013). Collectively, infertility-associated stress and the routine of infertility treatments, have a highly negative impact on women's emotionality (Choi et al., 2005; Gameiro et al., 2008, 2015, 2016; Verhaak et al., 2007).

Women are twice as susceptible as men to develop stress- and anxiety-related psychiatric disorders (Kessler et al., 2009; McLean et al., 2011; Tolin and Foa, 2006), including sex differences in severity, clinical course, and response to treatments (Pigott, 2003). This higher prevalence of affective disturbances in women has been mainly attributed to the cyclical release of female sex hormones, such as estradiol and progesterone (Li and Graham, 2017; Maeng and Milad, 2015). Studies have suggested that, especially during important transitional phases in reproductive life, such as puberty, pregnancy, postpartum, and perimenopause, women are at greater risk of developing affective disorders or exacerbating existing symptoms (Hickey et al., 2012; Li and Graham, 2017; Pigott, 2003; Ross and McLean, 2006; Van Veen et al., 2009). These periods are characterized by drastic hormonal fluctuations, which suggest the potential role of gonadal hormones in the onset and/or recrudescence of emotional disorders in women (Li and Graham, 2017; Maeng and Milad, 2015). Maeng and Milad (2015) also suggest that an elevated risk for anxiety disorders may be more dependent on fluctuations and less on the absolute “low” versus “high” levels of estrogen.

In previous work, we submitted female rats to a single ovarian stimulation (superovulation) and then to short-term psychogenic stress (restraint stress) (Mariotti et al., 2020). Our findings demonstrated anxiolytic-like and possible neuroprotective effects of supraphysiological concentrations of ovarian hormones on the stress response. An activation of inhibitory pathways of the hypothalamic-pituitary-adrenal (HPA) axis, with the participation of the prefrontal cortex, basomedial amygdala, lateral septum, medial preoptic area, dorsomedial and paraventricular hypothalamus, was detected. However, the consequences for female emotionality of multiple cycles of ovarian stimulation associated with chronic stress remain to be elucidated. These constitute most cases found in infertility-associated clinical practice, where usually, various ART cycles treatment may be necessary to achieve pregnancy.

Based on the premise that high and fluctuating levels of gonadal hormones may be related to an emotional imbalance and may modulate the stress response, the present study aimed to investigate the effect of multiple cycles of ovarian stimulation, associated or not with chronic stress, on anxiety-like and depressive-like behaviors in rats. This study in rodents is justified by the possibility of evaluating the effect of repeated ovarian stimulation isolated from the effect of psychogenic stress and, additionally, to investigate the interaction between these variables on emotional behavior, which is not feasible to be performed in humans. This study intends to advance the knowledge about female emotionality in a situation of supraphysiological and oscillating levels of sex hormones associated with chronic stress, a condition commonly experienced by women in ART.

To mimic the context of ART in rodents, female rats were submitted to a chronic stress protocol, and, within this time, repeated cycles of ovarian stimulation were applied. Unpredictable chronic mild stress (UCMS) was used to induce a persistent psychogenic stimulus, which requires interpretation by higher brain structures, with the participation of limbic circuits, and hypothalamic and autonomic activation (Herman and Cullinan, 1997). UCMS is considered a model of psychiatric disorder applied to laboratory animals (rats, mice, and fish) which promotes important behavioral changes in response to chronic exposure to several stressors (Willner, 2016). Changes in sexual behavior and aggression, anhedonia, interrupted sleep patterns, increased corticosterone, decreased locomotor activity and self-care have been reported in the UCMS model (Willner, 2005, 1997). Additionally, superovulation was used to promote ovarian stimulation. This procedure induces the growth of multiple ovarian follicles and, consequently, the production of supraphysiological concentration of endogenous ovarian hormones. Superovulation is a widely known method, used in rodents during the production of transgenic and genetically modified strains, also in research with embryonic stem cells, and in the gnotobiology (Kang et al., 2018; Takeo and Nakagata, 2015). Each ovarian stimulation is achieved through a single injection of pregnant mare serum gonadotropin (PMSG) to stimulate folliculogenesis, followed by a dose of human chorionic gonadotropin (hCG) for induction of final follicular maturation and ovulation (Kang et al., 2018; Takeo and Nakagata, 2015). At the end of the experimental period, anxiety-like and depressive-like behaviors were assessed in a light-dark transition box and splash test, respectively. Biometric parameters such as body mass gain, ovary and adrenal gland mass, quantification of corpora lutea, besides hormonal measures (corticosterone, estradiol, progesterone) were also evaluated.

2. Materials and methods

2.1. Ethics

The experimental protocols were approved by the Committee on Ethics in the Use of Animals (CEUA Protocol n° 3031060616) of the Federal University of São Paulo (UNIFESP), Brazil. The study was developed according to the ethical principles adopted by the Brazilian National Council for the Control of Animal Experimentation (CONCEA) and the more recent Animal Research: Reporting of In Vivo Experiments (ARRIVE) guideline (Percie du Sert et al., 2020).

2.2. Animals

One hundred and six nulliparous female Wistar rats (8 weeks old), weighing about 130–180 g, were obtained from the Center for the Development of Experimental Models for Medicine and Biology (CEDEME) of the UNIFESP. The rats were initially housed in groups of 5 per cage, maintained in acrylic boxes (48.3 cm × 33.7 cm × 26.5 cm) in ventilated racks (Ventilife 25, Alesco Indústria e Comércio Ltda, Brazil), with free access to water and feed, a light/dark cycle of 12 h (started at 7:00 am) and controlled temperature (22 ± 1 °C). After acclimatization for one week, the estrous cycle was monitored (Marcondes et al., 2002) and only rats aged 10 weeks that presented two regular estrous cycles were included in the experimental protocol.

2.3. Unpredictable chronic mild stress (UCMS) procedure

Female rats submitted to UCMS were individually housed in a polypropylene box (32 × 17 × 40 cm) and maintained in a light-dark cycle inversion rack (EB 277; Insight Equipamentos, Pesquisa e Ensino; Brazil). The UCMS protocol was performed according to Dalla et al. (2005), with slight modifications. Briefly, rats were submitted for four weeks to two kinds of daily stressors, randomly changed every 12 h (schedule in Table 1). The stressors were: food and/or water deprivation; stroboscopic illumination (120 flashes/min); intermittent illumination (lights switched on or off every 2 h); paired housing (two animals randomly assigned into one cage); cage tilting (at 45 degrees); and soiled cage (250 ml of tap water into the sawdust bedding) followed by cage cleaning (Supplementary material 1).

2.4. Superovulation

Each ovarian stimulation was induced by a single dose of 150 IU/kg of pregnant mare serum gonadotropin (PMSG; Folligon® Intervet, Brazil) applied via intraperitoneal (IP) at 10:00 am, to stimulate folliculogenesis. After 48 h, 75 IU/kg of human chorionic gonadotropin

Table 1
Schedule of the first week of unpredictable chronic mild stress (UCMS) applied to female rats. Stressors were randomized in the following three weeks.

UCMS protocol		
Weekdays	Period	Stressors
Monday	8:30 am–6:30 pm	Stroboscopic illumination (120 flashes/min) in darkness
	6:30 pm–8:30 am	Food and water deprivation
Tuesday	8:30 am–6:30 pm	Lights switched on or off every 2 h
	6:30 pm–8:30 am	Food deprivation
Wednesday	8:30 am–6:30 pm	Water deprivation
	6:30 pm–8:30 am	Soiled cage
Thursday	8:30 am–6:30 pm	Cage cleaning/stroboscopic illumination in darkness
	6:30 pm–8:30 am	Food deprivation
Friday	8:30 am–6:30 pm	Water deprivation
	6:30 pm–8:30 am	Paired housing
Saturday	8:30 am–6:30 pm	Cages tilted (45° degrees)
	6:30 pm–8:30 am	Cages put in horizontal position/no stress
Sunday	8:30 am–6:30 pm	Lights switched on or off every 2 h
	6:30 pm–8:30 am	Soiled cage

(hCG; Chorulon® Intervet, Brazil) was administered IP to induce ovulation (Kon et al., 2005; Polisseni et al., 2013). Superovulation using PMSG + hCG is the most widely used rodent ovarian stimulation protocol compared to the FSH + LH (or hCG) procedure. In the latter, FSH needs to be administered continuously by an osmotic pump implanted subcutaneously under anesthesia (Agca and Critser, 2006).

2.5. Study design

A schematic representation of the experimental design is shown in Fig. 1. At 10 weeks of age, the rats were randomly distributed into four experimental groups: a) **Repeated Superovulation/UCMS group** (RS/UCMS; n = 26): females were exposed to the UCMS protocol (as previously described) and submitted to three cycles of ovarian stimulation (repeated superovulation) with 8-day intervals among them (corresponding to approximately two estrous cycles). Spontaneous ovulation was allowed 24 h after each hCG injection; b) **Repeated Superovulation/No Stress group** (RS/NS; n = 27): females were maintained in their collective cages and were not submitted to the UCMS stress protocol. Three cycles of superovulation were performed; c) **Saline/UCMS group** (Sal/UCMS; n = 26): females were exposed to the UCMS protocol and submitted to the same manipulation as superovulated animals, but with the administration of 0.9% saline IP (Sal); and d) **Saline/No Stress group** (Sal/NS; n = 27): rats were maintained in their collective cages (not submitted to the UCMS protocol) with the administration of 0.9% saline IP instead of gonadotropins. The body weight of rats was measured once a week on Mondays at 10 am.

Three independent experiments were performed. ***Experiment 1*:** Female rats (n = 8–9 per group) were assigned to the evaluation of the anxiety-like behavior, ovarian hormone measurements, and biometric assessment; ***Experiment 2*:** Female rats (n = 7 per group) were subjected to corticosterone plasma determination, and biometric assessment; ***Experiment 3*:** Based on the results obtained in Experiment 1, a set of rats (n = 10–12 per group) were assigned to the evaluation of the depressive-like behavior.

2.6. Anxiety-like behavior evaluated by the Light-dark transition box (LDB)

The LDB constitutes a rodent model that evaluates aspects of the generalized anxiety disorder found in clinical practice (Tekinay et al., 2009). At the end of the experimental period, animals from Experiment 1 (n = 8–9 per group) in the diestrus phase were submitted to the light-dark transition box (LDB) test (EP 157; Insight Equipamentos, Pesquisa e Ensino; Brazil). The apparatus is divided into two compartments: one light (210 × 450 × 410 mm) and the other dark (210 × 350 × 410 mm), connected by an opening (100 × 100 mm) on the dividing wall (Lopes et al., 2016). After evaluating the latency time to output from the light field, the test lasted for 5 min. Luminosity at the light and dark compartments was 60 and zero lux, respectively. The parameters evaluated were percentage of time in the lit compartment, number of transitions, and number of stretched-attend postures from light to dark compartment. To evaluate the locomotor activity and validate the results obtained in the LDB, the animals were exposed for 5 min to the open field (OF) test (EP 154B; Insight Equipamentos, Pesquisa e Ensino; Brazil). The apparatus is composed of a round arena (90 cm diameter with 50 cm high walls), with the floor divided into 12 areas and surrounded by an acrylic wall. The parameter evaluated was the total number of lines crossed. Luminosity at the center of the apparatus was 60 lux. Both the experimental sessions were recorded on DVDs by a vertically mounted video camera linked to a monitor placed in an adjacent room. The videos were examined by an investigator and by an independent observer (the

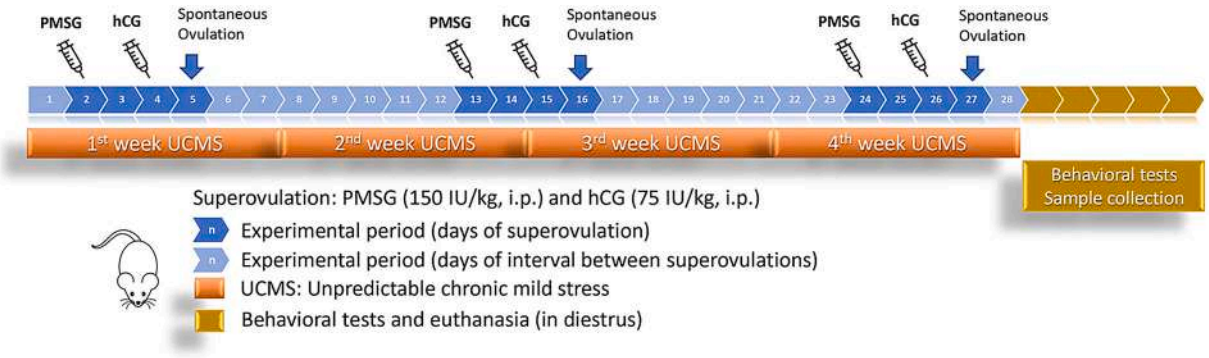

Fig. 1. Timeline containing procedures performed during the experimental period. Female rats were submitted to three cycles of ovarian stimulation (superovulation) with an interval of approximately two estrous cycles (8 days) among them. Each ovarian stimulation consisted of a dose of pregnant mare serum gonadotropin (PMSG) to stimulate folliculogenesis, and after 48 h, the human chorionic gonadotropin (hCG) was administered to promote oocyte maturation and ovulation. A persistent psychogenic stimulus was induced using an unpredictable chronic mild stress (UCMS) protocol applied for 4 weeks. Rats were euthanized in diestrus during the 5th week.

latter did not know the animal codes). For differences of up to 10% between counts, the average was taken, and above 10% the video was re-evaluated by the observers.

2.7. Aspects of depressive-like behavior evaluated by the Splash test

The splash test is a pharmacologically validated test that evaluates motivational parameters considered to parallel some symptoms of depression such as apathetic behavior (Willner, 2005). The test consists of squirting a 10% sucrose solution on the dorsal coat of rodents and, due to its viscosity, the solution adheres to the coat and the rodents start the grooming (self-cleaning) behavior. The rats (Experiment 3) from Sal/NS and RS/NS groups performed the test in an acrylic box, while the rats from Sal/UCMS and RS/UCMS groups carried out the test in a polypropylene box, according to originally housed in this study. Each rat was pre-exposed to the test-box for 5 min and then the sucrose solution was squirted on their dorsal coat (Butelman et al., 2019). The test was recorded on DVD for 5 min with low-intensity lighting (60 lux). After the end of each test, the box was cleaned with a 20% ethanol solution, and the sawdust was changed. The parameters evaluated were latency for first grooming (parameter associated with motivational behavior) and time spent grooming (parameter associated with self-care) (Isingrini et al., 2010; Nouri et al., 2020). The significantly increased latency is indicative of apathy, while decreased time spent on grooming suggests impairment of self-care. To evaluate the locomotor activity and validate the results associated with depressive-like behavior, parameters as time of locomotor activity, distance travelled in the cage and average speed were measured in the same apparatus using Anymaze video-tracking software (Stoelting, USA). The videos were examined by an observer blind to each animal's experimental group.

2.8. Hormone measurements

Immediately following the behavioral test (Experiment 1), the rats were anesthetized with a combination of ketamine (80–90 mg/kg IP; Cetamin® Syntec, Brazil) and xylazine (10 mg/kg IP; Xilasin® Syntec, Brazil), and blood samples were quickly obtained from the left ventricle (4 mL). The samples were centrifuged at 2300 rpm for 15 min at 4 °C, and plasma aliquots were stored at −80 °C until analysis. Plasma 17β-estradiol (E2) and progesterone (P4) concentrations were assessed using the electrochemiluminescence method in an automated way (Atellica, Siemens Healthineers; Erlangen, Germany). For the estradiol, the sensitivity of the assay is 11.8 pg/mL, and inter- and intra-assay variability were 26.86% and 24.4%, respectively. For the progesterone, the sensitivity of the assay is 0.21 ng/mL, and inter- and intra-assay variability were 35% and 22%, respectively.

An independent set of rats (Experiment 2; n = 7 per group) were subjected to corticosterone (CORT) analysis. Blood samples (1 mL) were collected by a cut in the tail and put into heparin-containing tubes, without anesthetic induction. The collection was performed between 7:00 am and 9:00 am (Goel et al., 2014), within a maximum of 8 min, timed from the removal of the animals from their cages in the vivarium (Mariotti et al., 2020). The samples were centrifuged and maintained as described above, and plasma CORT concentrations were assayed using high-performance liquid chromatography-tandem mass spectrometry [HPLC–MS/MS, Shimadzu® WATER model Quattro micro, Micromass®, Kinetex® (50 × 2.10 mm, 2.6 μm)]. Data are presented as absolute quantities and as percent change from baseline (control group) obtained by the equation: % of variation from basal = [(individual CORT value of each treated group) / (mean level of the Sal/NS group)] × 100.

2.9. Evaluation of biometric parameters and euthanasia

At the end of the experimental period (Experiments 1 to 3), the rats were anesthetized as described above and euthanized after collecting blood samples. In order to indirectly evaluate both the efficacy of the repeated superovulation and the HPA axis response to stress, ovaries and adrenal glands from all rats were collected and weighed on a precision analytical balance. Corpora lutea from both ovaries were manually removed one by one using tweezers, and the total number of structures per female was quantified.

2.10. Statistical analysis

To assess the body mass evolution over time, the Generalized Estimated Equation (GEE) method was performed, considering the experimental groups and the time as independent variables. A covariance matrix with an autoregressive one (AR1) structure was used, and data distribution was determined by the Quasi-Information Criteria (QIC) method. For all other parameters, the distribution of data was investigated by the Akaike Information Criteria (AIC) adherence test. The comparison among the groups was performed using a two-way Generalized Linear Model (GzLM), considering the following independent variables: repeated ovarian stimulation (repeated superovulation or saline injections) and chronic stress (submitted, or not, to the UCMS). The main effects of the variables and interactions among them were investigated. Statistical interaction is defined as the combined effects of independent variables on a measure of interest. If an interaction effect is detected, it means that the impact of one variable depends on the level of the other one (Stevens, 1999, 2007). When an interaction between the two independent variables was found, the Sidak *post-hoc* test was performed, and asterisks show significant differences among the groups. Only in the parameters that did not show significant interaction, the main effect analysis of independent variables was considered (Kuehl, 2000). Significant effects of the "repeated ovarian stimulation" are represented by the symbol #, and effects of the "chronic stress" are represented by the symbol &. An alpha level of $p < 0.05$ was considered statistically significant. The results are expressed as mean ± SEM. Cohen's d (d_{Cohen}) was used to estimate the effect of size between subjects for each independent variable, and in the pairwise comparison after interaction (https://www.psychometrica.de/effect_size.html). Statistical analyses and graphs were performed using IBM SPSS Statistics 22 and GraphPadPrism 8.0 software, respectively.

3. Results

3.1. Effects of the repeated ovarian stimulation and chronic stress on biometric parameters

Body mass evolution of female rats was significantly increased during the experimental period ($p < 0.0001$), although without significant difference among the groups over time (Fig. 2A). At the end of the experiment, a significant increase in the relative body mass gain was found in rats undergoing repeated superovulation ($p = 0.003$; $d_{Cohen} = 0.78$), while chronic stress decreased it ($p < 0.0001$; $d_{Cohen} = 0.94$). No interaction between the variables (repeated ovarian stimulation and chronic psychogenic stress) was detected (Fig. 2B).

Macroscopic analysis of reproductive organs showed that superovulated rats (RS/NS and RS/UCMS groups) had larger ovaries than females that did not receive the gonadotropins (Sal/NS and Sal/UCMS groups) (Fig. 2C). Repeated superovulation induced a significant increase in the absolute ($p < 0.0001$; $d_{Cohen} = 1.95$; data not shown) and relative weight of ovaries ($p < 0.0001$; $d_{Cohen} = 1.95$; Fig. 2D) besides an increase in the number of corpora lutea ($p < 0.0001$; $d_{Cohen} = 2.83$; Fig. 2E). Additionally, a significant decrease in the absolute ($p < 0.0001$; $d_{Cohen} = 0.94$; data not shown) and relative weight of adrenal glands ($p < 0.0001$; $d_{Cohen} = 1.21$; Fig. 2F) were found in females submitted to repeated ovarian stimulation. No effects of stress or interaction effects were observed for those parameters.

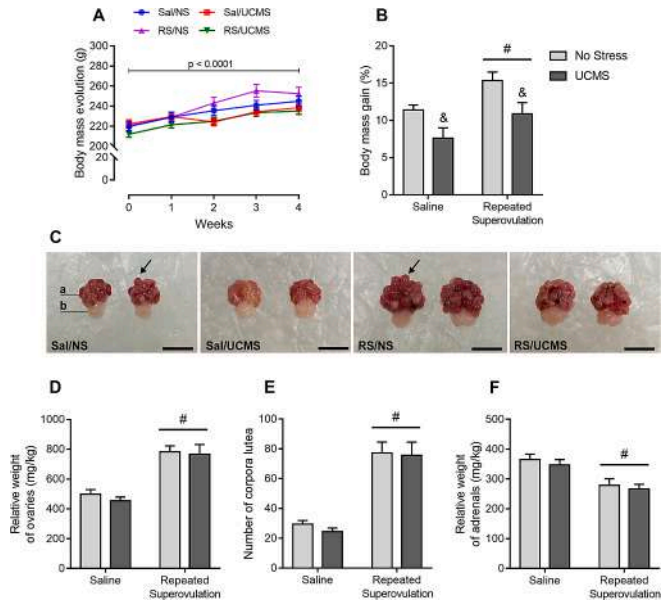

Fig. 2. Effects of chronic stress and repeated ovarian stimulation on biometric parameters of female rats. **A:** body mass was significantly increased over time in all experimental groups ($p < 0.0001$), without significant difference among them (GEE statistical test, with Gamma distribution). **B** and **D–F:** The GzLM statistical test with Linear (B and F) or Gamma (D and E) distribution showed a statistically significant effect ($p < 0.05$) of the repeated ovarian stimulation (#) and/or chronic stress (&). At the end of the experiment, UCMS induced a decrease in relative body mass gain, while repeated superovulation increased it (B). Repeated superovulation also increased both the relative weight of ovaries (D) and the number of corpora lutea (E), besides decreasing the relative weight of adrenal glands (F). Values expressed as mean ± SEM. N = 15 per group. **C:** Representative macroscopic views of reproductive organs from rats in the diestrus phase at the end of the experiment. Note increased ovaries in females submitted to repeated ovarian stimulation (RS/NS and RS/UCMS groups). In a: ovary; b: oviduct; arrows: corpus luteum; Bar: 5 mm. Abbreviations of the independent variables: repeated ovarian stimulation (Sal: saline injection; or RS: repeated superovulation), and chronic stress (NS: no stress; or UCMS: unpredictable chronic mild stress).

3.2. Effects of repeated ovarian stimulation and chronic stress on hormone measurements

Table 2 shows, at the end of the experiment, a significant increase in the progesterone plasma levels ($p < 0.0001$; $d_{Cohen} = 1.55$) in the superovulated groups (RS/NS and RS/UCMS). A significant increase in the CORT plasma levels was found in rats submitted to stress (Sal/UCMS and RS/UCMS groups; $p = 0.003$; $d_{Cohen} = 1.05$), while females undergoing repeated ovarian stimulation significantly decreased it (RS/NS and RS/UCMS groups; $p < 0.0001$; $d_{Cohen} = 0.96$). Similar results were obtained when considering the percentage of CORT from baseline. Increased CORT concentration was found in rats submitted to stress (Sal/UCMS and RS/UCMS groups; $p = 0.003$; $d_{Cohen} = 1.48$), and females undergoing repeated superovulation decreased it (RS/NS and RS/UCMS groups; $p = 0.006$; $d_{Cohen} = 1.37$). No interaction between repeated ovarian stimulation and stress was detected. Additionally, no difference among the groups was observed in the estradiol plasma levels.

3.3. Evaluation of anxiety-like behavior after repeated ovarian stimulation and chronic stress

Our results obtained in the LDB showed that the repeated superovulated groups (RS/NS and RS/UCMS) presented a significant decrease in latency time from light to dark field compared with non-superovulated ones ($p = 0.034$; $d_{Cohen} = 0.75$; Fig. 3A). An interaction between the variables was found in the following parameters: percentage of time in the lit compartment ($p = 0.001$; Fig. 3B), number of transitions ($p = 0.002$; Fig. 3C), and number of stretched-attend postures from dark to light compartment ($p = 0.033$; Fig. 3D).

The Sidak *post-hoc* test demonstrated that rats from RS/NS group showed significantly decreased time in the lit compartment compared

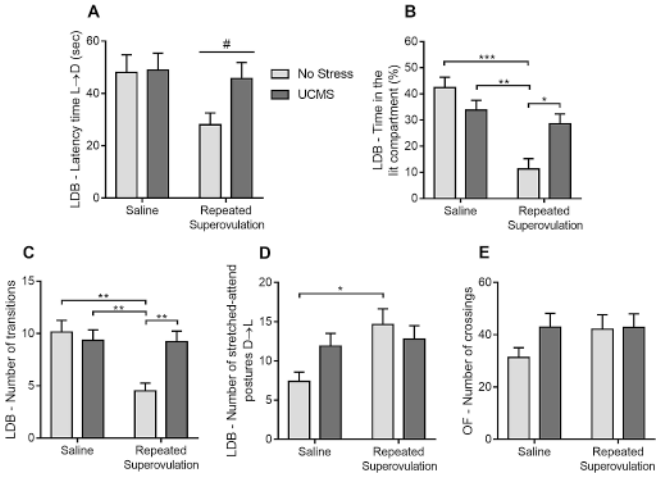

Fig. 3. Evaluation of anxiety-like behavior in female rats submitted to repeated ovarian stimulation and chronic stress. **A–D:** parameters evaluated in the light-dark box (LDB). Data were analyzed using the GzLM test with Gamma (A), Linear (B, C and E) or Tweedie (D) distribution. The statistically significant effect of the repeated ovarian stimulation is represented by the symbol # ($p < 0.05$). Decreased latency time was found in the repeated superovulated groups compared with non-superovulated ones (A). Where a significant interaction effect between chronic stress and repeated superovulation was detected (B–E), the Sidak *post-hoc* test was performed, and asterisks denote significant differences among the groups (* $p < 0.05$; ** $p < 0.01$; and *** $p < 0.0001$). Note that rats submitted only to repeated superovulation (without chronic stress) showed a suggestive anxiety-like behavior (RS/NS group), while rats from the RS/UCMS and Sal/UCMS groups did not exhibit such behavior. **F:** number of lines crossed in the open field (OF) test, performed to evaluate the locomotor integrity, and therefore validate the results obtained in the LDB. No main effect or interaction between the variables was observed in F. Values expressed as mean ± SEM. N = 8–9 per group. L → D: light to dark compartment in the LDB; D → L: dark to light compartment in the LDB. RS: repeated superovulation; NS: no stress; UCMS: unpredictable chronic mild stress.

Table 2
Hormone plasma levels measured at the end of the experiment (5th week) in female rats submitted to repeated ovarian stimulation and chronic stress (UCMS).

	N Per group	Saline No stress	Saline UCMS	Superovulations No stress	Superovulations UCMS
Progesterone (ng/mL)	8	16.80 ± 2.63	18.50 ± 2.77	117.60 ± 30.70$^{\#}$	110.80 ± 35.85$^{\#}$
Estradiol (pg/mL)	8	5.82 ± 0.82	6.73 ± 1.62	5.70 ± 0.40	5.92 ± 0.92
Corticosterone (μg/mL)	7	44.04 ± 9.17	72.67 ± 15.13$^{\&}$	22.02 ± 4.58$^{\#}$	46.62 ± 9.70$^{\&,\#}$
Corticosterone (% from Sal/NS)	7	100.14 ± 20.72	164.86 ± 34.11$^{\&}$	50.43 ± 10.43$^{\#}$	105.71 ± 21.87$^{\&,\#}$

Note: Values expressed as mean ± SEM. GzLM test with Gamma distribution, where #: significant effect of the repeated ovarian stimulation ($p < 0.05$ compared with no superovulated groups); &: significant effect of the chronic stress ($p < 0.05$ compared with no stressed groups). UCMS: unpredictable chronic mild stress. Sal/NS: Saline/No Stress group.

with the groups Sal/NS ($p < 0.0001$; $d_{Cohen} = 2.75$), Sal/UCMS ($p < 0.001$; $d_{Cohen} = 1.97$), and RS/UCMS ($p = 0.009$; $d_{Cohen} = 1.54$). No significant differences were detected between both Sal/NS and Sal/UCMS groups ($p = 0.501$; $d_{Cohen} = 0.78$), and Sal/NS and RS/UCMS groups ($p = 0.072$; $d_{Cohen} = 1.21$). Decreased number of transitions between lit and dark fields was observed in the RS/NS group in comparison with the groups Sal/NS ($p < 0.0001$; $d_{Cohen} = 2.08$), Sal/UCMS ($p = 0.001$; $d_{Cohen} = 1.81$) and RS/UCMS ($p = 0.001$; $d_{Cohen} = 1.77$). Again, no significant differences between both Sal/NC and Sal/UCMS ($p = 0.996$; $d_{Cohen} = 0.25$), and Sal/NC and RS/UCMS ($p = 0.992$; $d_{Cohen} = 0.29$) were detected. Additionally, RS/NS female rats presented a significantly increased number of stretched-attend postures from dark to light compartment when compared with Sal/NS group ($p = 0.012$; $d_{Cohen} = 1.54$). No significant differences among the groups were found in the number of lines crossed in the OF test, used as a locomotor integrity parameter (Fig. 3E).

3.4. Evaluation of depressive-like behavior after repeated ovarian stimulation and chronic stress

Our results obtained by the splash test showed significant interaction between repeated ovarian stimulation and chronic stress in the parameter latency for first grooming ($p = 0.048$; Fig. 4A). The Sidak *post-hoc* test demonstrated that rats from Sal/UCMS group showed significantly increased latency for grooming compared with the groups Sal/NS ($p = 0.045$; $d_{Cohen} = 1.20$), RS/NS ($p = 0.004$; $d_{Cohen} = 1.56$), and RS/UCMS ($p = 0.003$; $d_{Cohen} = 1.54$). No significant differences were detected between both Sal/NS and RS/NS groups ($p = 0.871$; $d_{Cohen} = 0.44$), and Sal/NS and RS/UCMS groups ($p = 0.802$; $d_{Cohen} = 0.51$). No significant differences among the groups were also found in the time spent grooming (Fig. 4B). Additionally, no significant differences among the groups were detected in time spent on locomotor activity, distance travelled in the cage and average speed, all these parameters used to assess the locomotor integrity of rats (Fig. 4C-E).

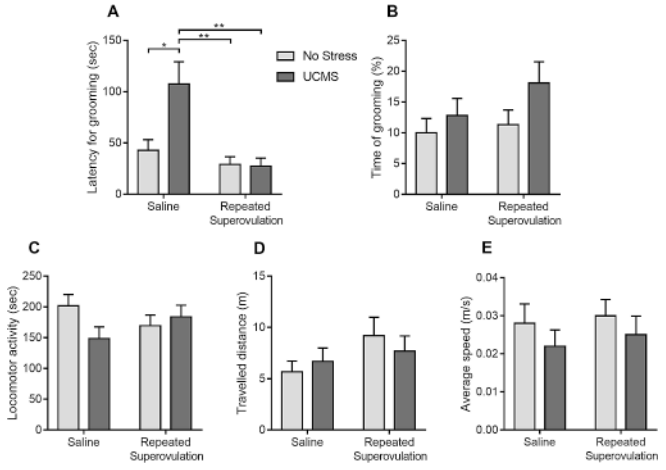

Fig. 4. Evaluation of depressive-like behavior assessed by the splash test in female rats submitted to chronic stress and repeated ovarian stimulation. Data were analyzed using the GzLM statistical test with Tweedie (A), Gamma (B, D and E) or Linear (C) distribution. **A:** a significant interaction between chronic stress and repeated superovulation was detected. The Sidak *post-hoc* test was performed, and asterisks denote significant differences among the groups (* $p < 0.05$ and ** $p < 0.01$). Increased latency for grooming was found in the Sal/UCMS group compared with the other ones, indicating a chronic stress-induced apathetic behavior. Note that rats from the RS/UCMS and RS/NS groups did not exhibit such behavior. No main effect or interaction between the variables was detected in B-E. To validate the results obtained in A and B, locomotor integrity parameters of the rats (C–E) were evaluated. Values expressed as mean ± SEM. N = 10–12 per group. Sal: saline injection; RS: repeated superovulation; UCMS: unpredictable chronic mild stress.

4. Discussion

To our knowledge, this is the first work seeking to study some aspects of the emotional challenge as experienced by women undergoing ART, by using a rodent model. We investigated the effect of repeated ovarian stimulation, associated or not with chronic stress, on the anxiety-like behavior and physiological parameters in rats. To mimic the context of women in ART, female rats were submitted to an unpredictable chronic mild stress paradigm, during which three superovulation procedures were applied with intervals of two estrous cycles between them. Superovulation in rats has been successfully reported in the scientific literature (Kito et al., 2010; Kon et al., 2005, 2014; Mariotti et al., 2020; Polisseni et al., 2013), and results obtained here confirmed the efficacy of superovulation, as demonstrated by the increased ovarian size and weight, a higher number of corpora lutea and increased levels of endogenous progesterone.

The UCMS procedure, applied for four weeks, was able to induce an increase in plasma CORT concentration, indicating glucocorticoid hypersecretion by the adrenal gland, and therefore validating the stress method used here. Elevated CORT levels have been largely demonstrated in female rats and mice from three weeks of UCMS exposure and have been associated with stress-induced activation of the HPA axis (Brooks et al., 2018; Dalla et al., 2005; Palumbo et al., 2020; Xing et al., 2013; Wu et al., 2012). Otherwise, repeated ovarian stimulation induced a significant decrease in CORT concentration, which was accompanied by a reduction in the absolute and relative adrenal gland mass. We did not find in the literature reports about the CORT levels and adrenal gland weight in rodents exposed to repeated superovulation. In general, this is because the main objective of these procedures is to obtain a large number of viable oocytes from donors for fertilization and subsequent implant of the embryos in recipient females. Consequently, biometric and physiological parameters in female oocyte donors are not commonly evaluated.

In previous work, we demonstrated that female rats exposed to a single ovarian stimulation showed an increase in the plasma CORT levels, suggesting a stimulatory effect of supraphysiological levels of sex hormones on the adrenocortical response (Mariotti et al., 2020). We have suggested that such effect may be related to either activation of the HPA axis and/or to peripheral mechanisms (Figueiredo et al., 2007; Heck and Handa, 2019; Herman et al., 2016), that may include an enhanced adrenal sensitivity to adrenocorticotropic hormone (ACTH) (Figueiredo et al., 2007) and/or a direct effect on adrenocortical steroidogenesis (Trejter et al., 2015). Unlike a single ovarian stimulation, repeated superovulation induced a significant decrease in both CORT levels and the adrenal gland weight. In fact, studies carried out by El Etreby and Fath El Bab (1978) and El Etreby (1979) showed that female Beagle dogs treated for eight weeks with high doses of cyproterone acetate (4.0 mg/kg/day orally) and progesterone (42.5 mg/kg/day subcutaneously) presented a decrease in relative mass of adrenal glands, with cortex atrophy and apparent loss of cells in both the fasciculate and reticular cortical regions at histological analysis. The authors attributed these effects to a suppressive action of certain progestogens on CRH-ACTH axis activity, supporting the hypothesis of its anti-glucocorticoid effect, besides indicating that progestogen treatment stimulates a pseudopregnancy-like condition in the adrenal glands (El Etreby, 1979). Additionally, studies have shown that ovariectomized female rats treated with estradiol benzoate (EB) presented an increase in adrenal steroidogenesis with dose-dependent increased plasma prolactin (PRL) and CORT (Lo et al., 2000). In an in vitro study, the same authors demonstrated that PRL stimulates zona fasciculata-reticularis cells from EB-treated rats to produce CORT (Lo et al., 2000).

Consequently, we suggest that decreased both CORT levels and adrenal mass observed in the RS/NS and RS/UCMS groups may be associated with the following: 1) inhibition of the HPA axis by the gonadal hormones, mainly progesterone, which has a chemical structure similar to CORT, with high affinity for glucocorticoid receptors in the

hypothalamus and pituitary gland (Miller et al., 1987; Pedersen et al., 1992); and/or 2) adrenal insufficiency since single superovulation induces increased CORT release and repeated ovarian stimulation may have led to an adrenal overload (Herman et al., 2016); and/or 3) decreased cholesterol bioavailability for adrenocortical steroidogenesis, caused by the increased demand for cholesterol by the ovaries for the synthesis of high levels of gonadal hormones (Miller and Auchus, 2011). As limitations of this study, the evaluation of both ACTH levels and a thorough analysis of the adrenal gland (histological, morphometric, and biochemical evaluations) would have been important for investigating the hypothesis of inhibition of the HPA axis by ovarian hormones after repeated superovulation. A possible bias in CORT concentration values caused by the stress of handling rats during tail vein blood collection should also been considered. Interestingly, rats from the RS/UCMS group showed CORT levels similar to those found in the Sal/NS group, probably due to antagonistic effects of the UCMS (increasing) and repeated superovulation (decreasing) on CORT concentration, despite the reduction in adrenal weight. Further studies are necessary to investigate the mechanisms involved in the repeated superovulation-induced CORT reduction, and also the systemic effect of this CORT decline.

A significant increase in the progesterone plasma levels was found in the superovulated rats, while no difference among the groups was observed in the estradiol plasma concentration. The supraphysiological progesterone levels were consistent with the high number of corpora lutea observed in the ovaries of the repeated superovulated rats (RS/NS and RS/UCMS groups). Studies showing indirect measures, such as elevated number of oocyte retrieval in the repeatedly superovulated mice (Park et al., 2015), indicate enhanced quantities of progesterone-secreting corpora lutea, thus corroborating our findings. The number of corpora lutea and the consequent increase of progesterone observed here after three repeated superovulations were similar to that we found after a single ovarian stimulation (Mariotti et al., 2020). These results suggest that exogenous gonadotropin effects on both ovarian folliculogenesis and steroidogenesis have been preserved after three repeated stimuli, with the reservation that oocyte quality was not assessed as it was not the focus of this study. Regarding estradiol at baseline levels in all experimental groups, this is probably due to euthanasia having occurred in diestrous (stage of the estrous cycle in which estradiol is lower), and also due to exogenous gonadotropins-stimulated follicles having already transformed into progesterone-secreting corpora lutea.

Body mass evolution was increasing overtime in all experimental groups. However, rats submitted to chronic stress (Sal/UCMS and RS/UCMS groups) presented a significantly lower relative body mass gain compared to the unstressed groups, and rats exposed to repeated superovulation showed a significant increase in relative body mass (RS/NS and RS/UCMS groups) compared to the non-superovulated rats. A reduction in the body weight of both female and male rats and mice has been commonly described in the literature from three weeks of UCMS exposure (Prevot et al., 2019; Zhang et al., 2018), even when food deprivation is not part of the set of daily stressors (Nollet et al., 2013; Sahagun et al., 2019). Conversely, studies demonstrating the effect of superovulation on body mass are scarce. Clinical practice shows that gaining weight during ART is a common occurrence reported by patients. Although controversial, increased body mass associated with sex hormones has also been described in some studies as a side effect of the use of contraceptives (Caldwell et al., 2020; Gallo et al., 2014; IQWiG, 2017), and by progestins for the treatment of menopausal symptoms (Liu, 2005). In this work, we were able to reproduce in rodents the increased body mass observed in clinical practice, although the mechanism underlying this effect remains to be elucidated. We suggest that higher weight gain observed in the repeatedly superovulated rats may be associated with either higher food intake or lower energy expenditure, and/or increased water retention resulting from homeostatic alterations of the body fluids (Stachenfeld, 2008). Additionally, reduced CORT levels may also be involved in the higher weight observed in the RS/NS and RS/UCMS groups. Low doses of glucocorticoids have been reported to activate mineralocorticoid receptors with consequent stimulatory effects on fat intake, body weight gain, and fat depots (Devenport et al., 1989; Uchoa et al., 2014). Further studies need to be conducted to investigate the mechanisms involved in the repeated superovulation-induced high weight gain.

Chronic stress constitutes a vulnerability factor for anxiety and depressive disorders and has been widely used to mimic in rodents some aspects of emotionality disorders found in humans. In our experimental conditions, female rats from the Sal/UCMS group did not show significant anxiety-like behavior, despite increased CORT levels. Similar results have been demonstrated in female rats and mice exposed to several UCMS paradigms (Mitra et al., 2005; Borrow et al., 2019; Palumbo et al., 2020) or chronic restraint stress (Herrmann Hibicke et al., 2017). By contrast, an anxiogenic effect has also been found in female rats (Chen et al., 2013) and mice (Zhu et al., 2014) after three or four weeks of UCMS exposure, respectively. Different stress paradigms and rodent strains can be the reason for the variety of results described in the literature. Additionally, the splash test showed that rats in the Sal/UCMS group exhibited apathetic behavior, which composes the myriad of aspects related to depressive-like behavior, widely reported in the UCMS paradigms (Willner, 2005; Planchez et al., 2019; Chevalier et al., 2020).

Rats from the RS/NS group presented a significant increase in the anxiety score but not in the apathetic behavior, both in comparison to the other experimental groups. These results suggest that repeated superovulation-induced fluctuations of high levels of gonadal hormones exert an expressive anxiogenic effect on females. Conversely, in previous work, we demonstrated that a single ovarian stimulation is not able to induce anxiety-like behavior in female rats (Mariotti et al., 2020). Taken together, our findings obtained here and in the previous report (Mariotti et al., 2020) corroborate the hypothesis suggested by Maeng and Milad (2015) that an elevated risk for anxiety disorders may be more dependent on fluctuations than on “low” or “high” absolute levels of gonadal hormones. Marked agitation could also be observed in rats from the RS/NS group throughout the experimental period, such as during the exchange of water and food, evaluation of the estrous cycle phases, and gonadotropin injections. We speculate that both anxiety-like behavior and marked agitation may be associated with repeated superovulation-induced hypocortisolism, as adrenal insufficiency has been shown to be related to a myriad of possible psychiatric disorders (Perry, 2015; Daniels and Sheils, 2017). By contrast to glucocorticoid overproduction, glucocorticoid deficiency represents a delayed consequence of either prolonged stress load or severe stressors, such as childhood abuse and post-traumatic stress disorder (Heim et al., 2000; Prajapati et al., 2020), all of them associated with anxiety disorders. The possible relationship between increased anxiety-like behavior and decreased CORT levels observed in our study needs to be further investigated.

Curiously, the increased anxiety-like behavior observed in the RS/NS rats was not found in the RS/UCMS group. These results suggest that additional stressors may have modulated the repeated superovulation induced-anxiogenic effect, as statistically supported by the interaction effect found between ovarian stimuli and UCMS. Mahmoud et al. (2016) demonstrated that in middle-aged female rats, submitted or not to ovariectomy and exposed to UCMS, ovarian hormones may impart resilience against behavioral and neuroendocrine impairments induced by chronic stress. Studies carried out by Dalla et al. (2005) also showed that after six weeks of UCMS exposure, female rats submitted to strong additional stress, such as forced swim test, had a shorter duration of passive behavior (floating) during the test task, which the authors attributed to a coping strategy. Consequently, the significantly lower anxiety index observed in the RS/UCMS group compared to RS/NS rats suggests that rats may have developed adaptive coping strategies to support the stress added to the anxiogenic context induced by high and oscillating levels of sex hormones. Adaptive coping strategies form the basis of resilience and allow an individual to deal with stressors more effectively, experience less intense symptoms upon exposure, or recover

from stress more quickly (Hammer and Martin, 1988). Evidence suggests that moderate levels of stress exposures may help to develop better coping responses in future stress experiences, shifting an individual's vulnerability inverted U-shaped curve and increasing the range of tolerable stress for the organism (Russo et al., 2012). A possible hypothesis of depressive-like behavior, as a consequence of emotional overload, could also be considered. However, our results obtained in the splash test showed that rats from the RS/UCMS group did not exhibit behaviors suggestive of apathy and/or decreased self-care, indicating the absence of a depressive-like state. In fact, an antidepressant-like effect induced by progesterone and its metabolites has been reported in the scientific literature (Boero et al., 2020; Nouri et al., 2020), and may be associated with the resilience hypothesis suggested here. Both the neurobiological mechanisms involved in a supposed adaptive coping strategy, as well as a possible relationship between the better behavioral response of the RS/UCMS group and the restoration of CORT to baseline level, remain to be further elucidated.

In conclusion, our findings provide evidence that repeated ovarian stimulation exerts by itself an expressive anxiogenic effect on female rats, besides an increase in body weight gain and a decrease in plasma CORT concentration. Supraphysiological and fluctuating levels of ovarian hormones, when combined with adverse situations such as chronic stress, may be able to trigger the elaboration of adaptive coping strategies in face of emotional overload.

Supplementary data to this article can be found online at https://doi.org/10.1016/j.yhbeh.2021.105087.

CRediT authorship contribution statement

BSMG, FFNM, ICC, MBV, LLSM: conceived and designed the study; BSMG, FFNM, GP, MMN, LMC, AM, GSSN: executed the experiments; LLSM: performed the statistical analyses; HKMA, MBV: reviewed the statistical analysis; BSMG, FFNM, MBV, LLSM: interpreted the data; BSMG, LLSM: wrote the manuscript; BSMG, FFNM, GP, MMN, LMC, AM, GSSN, HKMA, ICC, MBV, LLSM: revised the manuscript.

Funding

This study was financed in part by the Coordenação de Aperfeiçoamento de Pessoal de Nível Superior - Brasil (CAPES) - Finance Code 001, and by the Conselho Nacional de Desenvolvimento Científico e Tecnológico – Brasil (CNPq).

Declaration of competing interest

We declare not to have a financial, commercial, political, and personal conflict of interest.

Acknowledgements

We would like to thank Dr. Altay Alves Lino de Souza for statistical classes and Tony Champion for reviewing the English. We also thank the scientific initiation student Giovanna Pimpão, the technicians Carlos Eduardo Sydow, José Simões de Andrade, Gleidinaldo Silva dos Santos and Dr. Karen Maciel de Oliveira, for all the help given during the experimental period.

References

Agca, Y., Critser, J.K., 2006. Assisted reproductive technologies and genetic modifications in rats. In: Suckow, M.A., Weisbroth, S.H., Franklin, C.L. (Eds.), The Laboratory Rat. Elsevier Academic Press, Burlington, pp. 165–189.

Beutel, M., Kupfer, J., Kirchmeyer, P., Kehde, S., Köhn, F.M., Schroeder-Printzen, I., Gips, H., Herrero, H.J., Weidner, W., 1999. Treatment-related stresses and depression in couples undergoing assisted reproductive treatment by IVF or ICSI. Andrologia 31, 27–35.

Boero, G., Porcu, P., Morrow, A.L., 2020. Pleiotropic actions of allopregnanolone underlie therapeutic benefits in stress-related disease. Neurobiol. Stress 12, 100203. https://doi.org/10.1016/j.ynstr.2019.100203.

Boivin, J., Takefman, J.E., 1995. Stress level across stages of in vitro fertilization in subsequently pregnant and nonpregnant women. Fertil. Steril. 64, 802–810. https://doi.org/10.1016/s0015-0282(16)57858-3.

Borrow, A.P., Heck, A.L., Miller, A.M., Sheng, J.A., Stover, S.A., Daniels, R.M., Bales, N. J., Fleury, T.K., Handa, R.J., 2019. Chronic variable stress alters hypothalamic-pituitary-adrenal axis function in the female mouse. Physiol. Behav. 209, 112613 https://doi.org/10.1016/j.physbeh.2019.112613.

Brooks, S.D., Hileman, S.M., Chantler, P.D., Milde, S.A., Lemaster, K.A., Frisbee, S.J., Shoemaker, J.K., Jackson, D.N., Frisbee, J.C., 2018. Protection from vascular dysfunction in female rats with chronic stress and depressive symptoms. Am. J. Physiol. Heart Circ. Physiol. 314, H1070–H1084. https://doi.org/10.1152/ajpheart.00647.2017.

Butelman, E.R., McElroy, B.D., Prisinzano, T.E., Kreek, M.J., 2019. Impact of pharmacological manipulation of the κ-opioid receptor system on self-grooming and anhedonic-like behaviors in male mice. J. Pharmacol. Exp. Ther. 370, 1–8. https://doi.org/10.1124/jpet.119.256354.

Caldwell, A.E., Zaman, A., Ostendorf, D.M., Pan, Z., Swanson, B.B., Phelan, S., Wyatt, H. R., Bessesen, D.H., Melanson, E.L., Catenacci, V.A., 2020. Impact of combined hormonal contraceptive use on weight loss: a secondary analysis of a behavioral weight-loss trial. Obesity (Silver Spring) 28, 1040–1049. https://doi.org/10.1002/oby.22787.

Chen, S., Asakawa, T., Ding, S., Liao, L., Zhang, L., Shen, J., Yu, J., Sugiyama, K., Namba, H., Li, C., 2013. Chaihu-shugan-san administration ameliorates perimenopausal anxiety and depression in rats. PLoS One 8, e72428. https://doi.org/10.1371/journal.pone.0072428.

Choi, S.H., Shapiro, H., Robinson, G.E., Irvine, J., Neuman, J., Rosen, B., Murphy, J., Stewart, D., 2005. Psychological side-effects of clomiphene citrate and human menopausal gonadotrophin. J. Psychosom. Obstet. Gynaecol. 26, 93–100. https://doi.org/10.1080/01443610400022983.

Chevalier, G., Siopi, E., Guenin-Macé, L., Pascal, M., Laval, T., Rifflet, A., Boneca, I.G., Demangel, C., Colsch, B., Pruvost, A., Chu-Van, E., Messager, A., Leulier, F., Lepousez, G., Eberl, G., Lledo, P.M., 2020. Effect of gut microbiota on depressive-like behaviors in mice is mediated by the endocannabinoid system. Nat. Commun. 11, 6363. https://doi.org/10.1038/s41467-020-19931-2.

Crawford, N.M., Hoff, H.S., Mersereau, J.E., 2017. Infertile women who screen positive for depression are less likely to initiate fertility treatments. Human Reprod. 32, 582–587. https://doi.org/10.1093/humrep/dew351.

Dalla, C., Antoniou, K., Drossopoulou, G., Xagoraris, M., Kokras, N., Sfikakis, A., Papadopoulou-Daifoti, Z., 2005. Chronic mild stress impact: are females more vulnerable? Neuroscience 135, 703–714. https://doi.org/10.1016/j.neuroscience.2005.06.068.

Daniels, J., Sheils, E., 2017. A complex interplay: cognitive behavioural therapy for severe health anxiety in Addison's disease to reduce emergency department admissions. Behav. Cogn. Psychother. 45, 419–426. https://doi.org/10.1017/S1352465817000182.

Devenport, L., Knehans, A., Sundstrom, A., Thomas, T., 1989. Corticosterone's dual metabolic actions. Life Sci. 45, 1389–1396. https://doi.org/10.1016/0024-3205(89)90026-x.

El Etreby, M.F., 1979. Effect of cyproterone acetate, levonorgestrel and progesterone on adrenal glands and reproductive organs in the beagle bitch. Cell Tissue Res. 200, 229–243. https://doi.org/10.1007/BF00236416.

El Etreby, M.F., Fath El Bab, M.R., 1978. Effect of cyproterone acetate, d-norgestrel and progesterone on cells of the pars distalis of the adenohypophysis in the beagle bitch. Cell Tissue Res. 191, 205–218. https://doi.org/10.1007/BF00222420.

Figueiredo, H.F., Ulrich-Lai, Y.M., Choi, D.C., Herman, J.P., 2007. Estrogen potentiates adrenocortical responses to stress in female rats. Am. J. Physiol. Endocrinol. Metab. 292, E1173–E1182. https://doi.org/10.1152/ajpendo.00102.2006.

Freeman, E.W., Boxer, A.S., Rickels, K., Tureck, R., Mastroianni Jr., L., 1985. Psychological evaluation and support in a program of in vitro fertilization and embryo transfer. Fertil. Steril. 43, 48–53. https://doi.org/10.1016/s0015-0282(16)48316-0.

Gallo, M.F., Lopez, L.M., Grimes, D.A., Carayon, F., Schulz, K.F., Helmerhorst, F.M., 2014. Combination contraceptives: effects on weight. CD003987. https://doi.org/10.1002/14651858.CD003987.pub5.

Gameiro, S., Silva, S., Canavarro, M.C., 2008. A experiência masculina de infertilidade e de reprodução medicamente assistida. Psicol. Saúde Doenças. 9, 253–270.

Gameiro, S., van den Belt-Dusebout, A.W., Smeenk, J.M., Braat, D.D., van Leeuwen, F.E., Verhaak, C.M., 2016. Women's adjustment trajectories during IVF and impact on mental health 11–17 years later. Hum. Reprod. 31, 1788–1798. https://doi.org/10.1093/humrep/dew131.

Gameiro, S., Boivin, J., Dancet, E., de Klerk, C., Emery, M., Lewis-Jones, C., Thorn, P., Van den Broeck, U., Venetis, C., Verhaak, C.M., Wischmann, T., Vermeulen, N., 2015. ESHRE guideline: routine psychosocial care in infertility and medically assisted reproduction-a guide for fertility staff. Human. Reprod. 30, 2476–2485. https://doi.org/10.1093/humrep/dev177.

Ginsburg, E.S., Racowsky, C., 2013. Assisted reproduction. In: Strauss, J.F., Barbieri, R. (Eds.), Yen & Jaffe's Reproductive Endocrinology: Physiology, Pathophysiology and Clinical Management, 7th ed. Elsevier Saunders, Philadelphia, pp. 734–773.

Goel, N., Workman, J.L., Lee, T.T., Innala, L., Viau, V., 2014. Sex differences in the HPA axis. Comp. Physiol. 4, 1121–1155. https://doi.org/10.1002/cphy.c130054.

Hammer, A.L., Martin, M.S., 1988. Coping Resources Inventory Manual. Consulting Psychologists Press, Palo Alto, California.

Heck, A.L., Handa, R.J., 2019. Sex differences in the hypothalamic-pituitary-adrenal axis response to stress: an important role for gonadal hormones. Neuropsychopharmacology 44, 45–58. https://doi.org/10.1038/s41386-018-0167-9.

Heim, C., Ehlert, U., Hellhammer, D.H., 2000. The potential role of hypocortisolism in the pathophysiology of stress-related bodily disorders. Psychoneuroendocrinology 25, 1–35. https://doi.org/10.1016/s0306-4530(99)00035-9.

Herman, J.P., Cullinan, W.E., 1997. Neurocircuitry of stress: central control of the hypothalamo-pituitary-adrenocortical axis. Trends Neurosci. 20, 78–84. https://doi.org/10.1016/s0166-2236(96)10069-2.

Herman, J.P., McKlveen, J.M., Ghosal, S., Kopp, B., Wulsin, A., Makinson, R., Scheimann, J., Myers, B., 2016. Regulation of the hypothalamic-pituitary-adrenocortical stress response. Compr. Physiol. 6, 603–621. https://doi.org/10.1002/cphy.c150015.

Herrmann Hibicke, M., Graham, M.A., Hayslett, R.L., 2017. Adolescent chronic restraint stress (aCRS) elicits robust depressive-like behavior in freely cycling, adult female rats without increasing anxiety-like behaviors. Exp. Clin. Psychopharmacol. 25, 74–83. https://doi.org/10.1037/pha0000119.

Hickey, M., Bryant, C., Judd, F., 2012. Evaluation and management of depressive and anxiety symptoms in midlife. Climacteric 15, 3–9. https://doi.org/10.3109/13697137.2011.620188.

Institute for Quality and Efficiency in Health Care (IQWiG), 2017. Contraception: Do hormonal contraceptives cause weight gain? https://www.ncbi.nlm.nih.gov/books/NBK441582/. (Accessed 6 October 2021).

Isingrini, E., Camus, V., Le Guisquet, A.M., Pingaud, M., Devers, S., Belzung, C., 2010. Association between repeated unpredictable chronic mild stress (UCMS) procedures with a high fat diet: a model of fluoxetine resistance in mice. PLoS One 5, e10404. https://doi.org/10.1371/journal.pone.0010404.

Kang, Y., Ai, Z., Duan, K., Si, C., Wang, Y., Zheng, Y., He, J., Yin, Y., Zhao, S., Niu, B., Zhu, X., Liu, L., Xiang, L., Zhang, L., Niu, Y., Ji, W., Li, T., 2018. Improving cell survival in injected embryos allows primed pluripotent stem cells to generate chimeric cynomolgus monkeys. Cell Rep. 25, 2563–2576. https://doi.org/10.1016/j.celrep.2018.11.001.

Kessler, R.C., Aguilar-Gaxiola, S., Alonso, J., Chatterji, S., Lee, S., Ormel, J., Ustün, T.B., Wang, P.S., 2009. The global burden of mental disorders: an update from the WHO world mental health (WMH) surveys, 18, 23–33. https://doi.org/10.1017/s1121189x00001421.

Kito, S., Yano, H., Ohta, Y., Tsukamoto, S., 2010. Superovulatory response, oocyte spontaneous activation, and embryo development in WMN/Nrs inbred rats. Exp. Anim. 59, 35–45. https://doi.org/10.1538/expanim.59.35.

Kon, H., Hokao, R., Shinoda, M., 2014. Fertilizability of superovulated eggs by estrous stage-independent PMSG/hCG treatment in adult wistar-imamichi rats. Exp. Anim. 63, 175–182. https://doi.org/10.1538/expanim.63.175.

Kon, H., Tohei, A., Hokao, R., Shinoda, M., 2005. Estrous cycle stage-independent treatment of PMSG and hCG can induce superovulation in adult wistar-imamichi rats. Exp. Anim. 54, 185–187. https://doi.org/10.1538/expanim.54.185.

Kuehl, R.O., 2000. Design of Experiments: Statistical Principles of Research Design and Analysis. Brookes/Cole, Pacific Grove, California.

Li, S.H., Graham, B.M., 2017. Why are women so vulnerable to anxiety, trauma-related and stress-related disorders? The potential role of sex hormones. Lancet Psychiatry 4, 73–82. https://doi.org/10.1016/S2215-0366(16)30358-3.

Liu, J.H., 2005. Therapeutic effects of progestins, androgens, and tibolone for menopausal symptoms. Am. J. Med. 118 (suppl 12B), 88–92. https://doi.org/10.1016/j.amjmed.2005.09.040.

Lo, M.J., Chang, L.L., Wang, P.S., 2000. Effects of estradiol on corticosterone secretion in ovariectomized rats. J. Cell. Biochem. 77, 560–568. https://doi.org/10.1002/(sici)1097-4644(20000615)77:4<560::aid-jcb4>3.0.co;2-d.

Lopes, D.A., Lemes, J.A., Melo-Thomas, L., Schor, H., de Andrade, J.S., Machado, C.M., Horta-Júnior, J.A.C., Céspedes, I.C., Viana, M.B., 2016. Unpredictable chronic mild stress exerts anxiogenic-like effects and activates neurons in the dorsal and caudal region and in the lateral wings of the dorsal raphe nucleus. Behav. Brain Res. 297, 180–186. https://doi.org/10.1016/j.bbr.2015.10.006.

Maeng, L.Y., Milad, M.R., 2015. Sex differences in anxiety disorders: interactions between fear, stress, and gonadal hormones. Horm. Behav. 76, 106–117. https://doi.org/10.1016/j.yhbeh.2015.04.002.

Mahmoud, R., Wainwright, S.R., Chaiton, J.A., Lieblich, S.E., Galea, L., 2016. Ovarian hormones, but not fluoxetine, impart resilience within a chronic unpredictable stress model in middle-aged female rats. Neuropharmacology 107, 278–293. https://doi.org/10.1016/j.neuropharm.2016.01.033.

Marcondes, F.K., Bianchi, F.J., Tanno, A.P., 2002. Determination of the estrous cycle phases of rats: some helpful considerations. Braz. J. Biol. 62, 609–614. https://doi.org/10.1590/s1519-69842002000400008.

Mariotti, F.F.N., Gonçalves, B.S.M., Pimpão, G., Mônico-Neto, M., Antunes, H.K.M., Viana, M.B., Céspedes, I.C., Le Sueur-Maluf, L., 2020. A single ovarian stimulation, as performed in assisted reproductive technologies, can modulate the anxiety-like behavior and neuronal activation in stress-related brain areas in rats. Horm. Behav. 124, 104805 https://doi.org/10.1016/j.yhbeh.2020.104805.

Massarotti, C., Gentile, G., Ferreccio, C., Scaruffi, P., Remorgida, V., Anserini, P., 2019. Impact of infertility and infertility treatments on quality of life and levels of anxiety and depression in women undergoing in vitro fertilization. Gynecol. Endocrinol. 35, 485–489. https://doi.org/10.1080/09513590.2018.1540575.

McLean, C.P., Asnaani, A., Litz, B.T., Hofmann, S.G., 2011. Gender differences in anxiety disorders: prevalence, course of illness, comorbidity and burden of illness. J. Psychiatr. Res. 45, 1027–1035. https://doi.org/10.1016/j.jpsychires.2011.03.006.

Miller, L.K., Kral, J.G., Strain, G.W., Zumoff, B., 1987. Differential binding of dexamethasone to ammonium sulfate precipitates of human adipose tissue cytosols. Steroids 49, 507–522. https://doi.org/10.1016/0039-128x(87)90091-2.

Miller, W.L., Auchus, R.J., 2011. The molecular biology, biochemistry, and physiology of human steroidogenesis and its disorders. Endocr. Rev. 32, 81–151. https://doi.org/10.1210/er.2010-0013.

Mitra, R., Vyas, A., Chatterjee, G., Chattarji, S., 2005. Chronic-stress induced modulation of different states of anxiety-like behavior in female rats. Neurosci. Lett. 383, 278–283. https://doi.org/10.1016/j.neulet.2005.04.037.

Nollet, M., Le Guisquet, A.M., Belzung, C., 2013. Models of depression: unpredictable chronic mild stress in mice. Curr Protoc Pharmacol. https://doi.org/10.1002/0471141755.ph0565s61. Chapter 5: Unit 5.65.

Nouri, A., Hashemzadeh, F., Soltani, A., Saghaei, E., Amini-Khoei, H., 2020. Progesterone exerts antidepressant-like effect in a mouse model of maternal separation stress through mitigation of neuroinflammatory response and oxidative stress. Pharm. Biol. 58, 64–71. https://doi.org/10.1080/13880209.2019.1702704.

Palumbo, M.C., Dominguez, S., Dong, H., 2020. Sex differences in hypothalamic-pituitary-adrenal axis regulation after chronic unpredictable stress. Brain Behav. 10, e01586 https://doi.org/10.1002/brb3.1586.

Park, S.J., Kim, T.S., Kim, J.M., Chang, K.T., Lee, H.S., Lee, D.S., 2015. Repeated superovulation via PMSG/hCG administration induces 2-cys peroxiredoxins expression and overoxidation in the reproductive tracts of female mice. Mol. Cells 38, 1071–1078. https://doi.org/10.14348/molcells.2015.0173.

Planchez, B., Surget, A., Belzung, C., 2019. Animal models of major depression: drawbacks and challenges. J. Neural Transm. 126, 1383–1408. https://doi.org/10.1007/s00702-019-02084-y.

Pedersen, S.B., Borglum, J.D., Moller-Pedersen, T., Richelsen, B., 1992. Characterization of nuclear corticosteroid receptors in rat adipocytes. Regional variations and modulatory effects of hormones. Biochim. Biophys. Acta 1134, 303–308. https://doi.org/10.1016/0167-4889(92)90191-d.

Percie du Sert, N., Ahluwalia, A., Alam, S., Avey, M.T., Baker, M., Browne, W.J., Clark, A., Cuthill, I.C., Dirnagl, U., Emerson, M., Garner, P., Holgate, S.T., Howells, D.W., Hurst, V., Karp, N.A., Lazic, S.E., Lidster, K., MacCallum, C.J., Macleod, M., Pearl, E.J., Petersen, O.H., Rawle, F., Reynolds, P., Rooney, K., Sena, E. S., Silberberg, S.D., Steckler, T., Würbel, H., 2020. Reporting animal research: explanation and elaboration for the ARRIVE guidelines 2.0. PLoS Biol. 18, e3000411 https://doi.org/10.1371/journal.pbio.3000411.

Perry, B.I., 2015. A psychiatric presentation of adrenal insufficiency: a case report. Prim care companion CNS Disord 17. https://doi.org/10.4088/PCC.15l01819.

Pigott, T.A., 2003. Anxiety disorders in women. Psychiatr Clin North Am. 26 https://doi.org/10.1016/s0193-953x(03)00040-6, 621–vii.

Polisseni, J., Grázib, J.G.V., Guerra, M.O., Milen, L.C., Camargo, L.S.A., Peters, V.M., 2013. Impact of the use of gonadotropins on embryonic development - a rat model. JBRA Assist. Reprod. 17, 32–36. https://doi.org/10.5935/1518-0557.20130004. Chapter 5: Unit 5.65.

Prajapati, S.K., Singh, N., Garabadu, D., Krishnamurthy, S., 2020. A novel stress re-stress model: modification of re-stressor cue induces long-lasting post-traumatic stress disorder-like symptoms in rats. Int. J. Neurosci. 130, 941–952. https://doi.org/10.1080/00207454.2019.1711078.

Prevot, T.D., Misquitta, K.A., Fee, C., Newton, D.F., Chatterjee, D., Nikolova, Y.S., Sibille, E., Banasr, M., 2019. Residual avoidance: a new, consistent and repeatable readout of chronic stress-induced conflict anxiety reversible by antidepressant treatment. Neuropharmacology 153, 98–110. https://doi.org/10.1016/j.neuropharm.2019.05.005.

Rooney, K.L., Domar, A.D., 2018. The relationship between stress and infertility. Dialogues Clin. Neurosci. 20, 41–47. https://doi.org/10.31887/DCNS.2018.20.1/klrooney.

Ross, L.E., McLean, L.M., 2006. Anxiety disorders during pregnancy and the postpartum period: a systematic review. J. Clin. Psychiatry. 67, 1285–1298. https://doi.org/10.4088/jcp.v67n0818.

Russo, S.J., Murrough, J.W., Han, M.H., Charney, D.S., Nestler, E.J., 2012. Neurobiology of resilience. Nat. Neurosci. 15, 1475–1484. https://doi.org/10.1038/nn.3234.

Sahagun, E., Ward, L.M., Kinzig, K.P., 2019. Attenuation of stress-induced weight loss with a ketogenic diet. Physiol. Behav. 212, 112654 https://doi.org/10.1016/j.physbeh.2019.112654.

Slade, P., O'Neill, C., Simpson, A.J., Lashen, H., 2007. The relationship between perceived stigma, disclosure patterns, support and distress in new attendees at an infertility clinic. Hum. Reprod. 22, 2309–2317. https://doi.org/10.1093/humrep/dem115.

Stachenfeld, N.S., 2008. Sex hormone effects on body fluid regulation. Exerc. Sport Sci. Rev. 36, 152–159. https://doi.org/10.1097/JES.0b013e31817be928.

Stevens, J., 2007. Routledge, New York.

Stevens, J., 1999. Interaction effects in ANOVA. http://pages.uoregon.edu/stevensj/interaction.pdf. (Accessed 6 November 2021).

Takeo, T., Nakagata, N., 2015. Superovulation using the combined administration of inhibin antiserum and equine chorionic gonadotropin increases the number of ovulated oocytes in C57BL/6 female mice. PloS One 10, e0128330. https://doi.org/10.1371/journal.pone.0128330.

Tekinay, A.B., Nong, Y., Miwa, J.M., Lieberam, I., Ibanez-Tallon, I., Greengard, P., Heintz, N., 2009. A role for LYNX2 in anxiety-related behavior. Proc. Natl. Acad. Sci. U. S. A. 106, 4477–4482. https://doi.org/10.1073/pnas.0813109106.

Tolin, D.F., Foa, E.B., 2006. Sex differences in trauma and posttraumatic stress disorder: a quantitative review of 25 years of research. Psychol. Bull. 132, 959–992. https://doi.org/10.1037/0033-2909.132.6.959.

Trejter, M., Jopek, K., Celichowski, P., Tyczewska, M., Malendowicz, L.K., Rucinski, M., 2015. Expression of estrogen, estrogen related and androgen receptors in adrenal

cortex of intact adult male and female rats. Folia Histochem. Cytobiol. 53, 133–144. https://doi.org/10.5603/FHC.a2015.0012.
Turner, K., Reynolds-May, M.F., Zitek, E.M., Tisdale, R.L., Carlisle, A.B., Westphal, L.M., 2013. Stress and anxiety scores in first and repeat IVF cycles: a pilot study. PloS One 8, e63743. https://doi.org/10.1371/journal.pone.0063743.
Uchoa, E.T., Aguilera, G., Herman, J.P., Fiedler, J.L., Deak, T., de Sousa, M.B., 2014. Novel aspects of glucocorticoid actions. J. Neuroendocrinol. 26, 557–572. https://doi.org/10.1111/jne.12157.
Vahratian, A., Smith, Y.R., Dorman, M., Flynn, H.A., 2011. Longitudinal depressive symptoms and state anxiety among women using assisted reproductive technology. Fertil. Steril. 95, 1192–1194. https://doi.org/10.1016/j.fertnstert.2010.09.063.
van Veen, J.F., Jonker, B.W., van Vliet, I.M., Zitman, F.G., 2009. The effects of female reproductive hormones in generalized social anxiety disorder. Int. J. Psychiatry Med. 39, 283–295. https://doi.org/10.2190/PM.39.3.e.
Verhaak, C.M., Smeenk, J.M., Evers, A.W., Kremer, J.A., Kraaimaat, F.W., Braat, D.D., 2007. Women's emotional adjustment to IVF: a systematic review of 25 years of research. Hum. Reprod. Update 13, 27–36. https://doi.org/10.1093/humupd/dml040.
Verhaak, C.M., Smeenk, J.M., van Minnen, A., Kremer, J.A., Kraaimaat, F.W., 2005. A longitudinal, prospective study on emotional adjustment before, during and after consecutive fertility treatment cycles. Hum. Reprod. 20, 2253–2260. https://doi.org/10.1093/humrep/dei015.
Willner, P., 1997. Validity, reliability and utility of the chronic mild stress model of depression: a 10-year review and evaluation. Psychopharmacology 134, 319–329. https://doi.org/10.1007/s002130050456.
Willner, P., 2005. Chronic mild stress (CMS) revisited: consistency and behavioural-neurobiological concordance in the effects of CMS. Neuropsychobiology 52, 90–110. https://doi.org/10.1159/000087097.
Willner, P., 2016. The chronic mild stress (CMS) model of depression: history, evaluation and usage. Neurobiol. Stress. 6, 78–93. https://doi.org/10.1016/j.ynstr.2016.08.002.
Wu, L.M., Hu, M.H., Tong, X.H., Han, H., Shen, N., Jin, R.T., Wang, W., Zhou, G.X., He, G.P., Liu, Y.S., 2012. Chronic unpredictable stress decreases expression of brain-derived neurotrophic factor (BDNF) in mouse ovaries: relationship to oocytes developmental potential. PloS One 7, e52331. https://doi.org/10.1371/journal.pone.0052331.
Xing, Y., He, J., Hou, J., Lin, F., Tian, J., Kurihara, H., 2013. Gender differences in CMS and the effects of antidepressant venlafaxine in rats. Neurochem. Int. 63, 570–575. https://doi.org/10.1016/j.neuint.2013.09.019.
Zhang, Y., Yuan, S., Pu, J., Yang, L., Zhou, X., Liu, L., Jiang, X., Zhang, H., Teng, T., Tian, L., Xie, P., 2018. Integrated metabolomics and proteomics analysis of hippocampus in a rat model of depression. Neuroscience 371, 207–220. https://doi.org/10.1016/j.neuroscience.2017.12.001.
Zhu, S., Wang, J., Zhang, Y., Li, V., Kong, J., He, J., Li, X.M., 2014. Unpredictable chronic mild stress induces anxiety and depression-like behaviors and inactivates AMP-activated protein kinase in mice. Brain Res. 1576, 81–90. https://doi.org/10.1016/j.brainres.2014.06.002.